GR2008-1

GEOSCIENTIFIC REPORT

Geology of the Rice Lake area, Rice Lake greenstone belt, southeastern Manitoba (parts of NTS 52L13, 52M4)

By
S.D. Anderson

Manitoba

Geoscientific Report GR2008-1

Geology of the Rice Lake area, Rice Lake greenstone belt, southeastern Manitoba (parts of NTS 52L13, 52M4)

by S.D. Anderson

Winnipeg, 2008

Science, Technology, Energy and Mines

Hon. Jim Rondeau
Minister

John Clarkson
Deputy Minister

Mineral Resources Division

John Fox
Assistant Deputy Minister

Manitoba Geological Survey

E.C. Syme
Director

Anderson, S.D. 2008: Geology of the Rice Lake area, Rice Lake greenstone belt, southeastern Manitoba (parts of NTS 52L13, 52M4); Manitoba Science, Technology, Energy and Mines, Manitoba Geological Survey, Geoscientific Report GR2008-1, 97 p.

NTS grid: 52L13, 52M4

Keywords: adakites; Archean; Bidou assemblage; clastic dikes; continental arcs; deformation; fluvial sedimentation; geochronology; gold ores; island arcs; isotopes; Kenoran Orogeny; lithogeochemistry; Manitoba; massive sulphide deposits; mineral deposits, genesis; partitioning; Rice Lake; Rice Lake belt; Rice Lake deposit; rifting; San Antonio assemblage; San Antonio deposit; sanukitoids; Sm/Nd; stratigraphy; structural analysis; subsidence; Superior Province; U/Pb; Uchi Subprovince; volcaniclastics; volcanism

This publication and its accompanying map are also available to download free of charge in Adobe Acrobat PDF from www2.gov.mb.ca/itm-cat/freedownloads.htm.

Published by:
Manitoba Science, Technology, Energy and Mines
Manitoba Geological Survey
360-1395 Ellice Avenue
Winnipeg, Manitoba
R3G 3P2 Canada
Telephone: (800) 223-5215 (General Enquiry)
(204) 945-4154 (Publication Sales)
Fax: (204) 945-8427
E-mail: minesinfo@gov.mb.ca
Website: manitoba.ca/minerals

Cover photo: Rice Lake, looking north toward the headframe of the Rice Lake mine and the town of Bissett, Manitoba.

Abstract

This report presents the results of a comprehensive geoscientific investigation of the Rice Lake area completed under the auspices of the Rice Lake metallogeny project—a multiyear, multidisciplinary initiative by the Manitoba Geological Survey to update the understanding of the geology, metallogeny and tectonic evolution of the Archean Rice Lake greenstone belt. In the Rice Lake area, the crustal-scale Wanipigow Shear Zone separates the Little Beaver assemblage of the Mesoarchean North Caribou Terrane (NCT) on the north from the Neoarchean Bidou assemblage (BA) and San Antonio assemblage (SAA) of the Uchi Subprovince on the south. Detailed bedrock mapping and structural analysis, in conjunction with lithogeochemical, Sm-Nd isotopic and U-Pb geochronological analyses of selected rock types, provide new insight into the stratigraphy, depositional environment, structural evolution and tectonic setting of the BA and SAA in the vicinity of the 2.3 million ounce Rice Lake gold deposit, the largest lode-gold deposit discovered to date in Manitoba.

At Rice Lake, the BA consists of a north-younging stratigraphic succession composed of four distinct lithostratigraphic units. Volcaniclastic and epiclastic rock types in these units record subaqueous deposition on the medial-distal flank of a subaerially exposed, ca. 2747–2715 Ma volcanic complex composed mostly of calacalkalic andesite and dacite, with subordinate tholeiitic basalt. High-field-strength and rare-earth element patterns of the constituent volcanic rocks indicate an affinity to typical volcanic-arc magmas. The lower portion of the succession includes a distinctive association of ca. 2727–2724 Ma basinal marine sedimentary rocks and MORB-like tholeiitic basalt, termed the Rainy Lake Road (RLR) unit, which was deposited in an actively subsiding basin in the hangingwall of a synvolcanic subsidence structure. This structure channelled hydrothermal circulation and base-metal exhalative activity, and controlled emplacement of hypabyssal dike swarms, a thick laccolith of MORB-like tholeiitic gabbro and an apophysis of the ca. 2724 Ma Ross River pluton. The RLR unit records extension and rifting of the volcanic arc, perhaps associated with the initiation of a short-lived back-arc basin. Angular phyllite clasts in clastic dikes preserve the earliest ductile deformation fabric (S_1) in the Rice Lake area, which probably formed in the footwall of extensional faults (D_1 deformation). Adakitic dacite and sanukitoid basalt in the upper portion of the succession point to resurgent volcanic-arc magmatism, possibly with a direct contribution from slab-derived melts. Weak positive initial ε_{Nd} values and Mesoarchean crustal-residence model ages (T_{CR}) indicate minor interaction with older, isotopically evolved crust and thus suggest a continental magmatic-arc setting, likely above a north-verging subduction zone on the south margin of the NCT.

A pronounced angular unconformity separates the BA from overlying fluvial-alluvial conglomerate, arenite and greywacke of the SAA, which were deposited after cessation of arc-magmatism. Detrital zircons in the latter indicate a dominantly Neoarchean (ca. 2730 Ma) source area, with a minor component of Mesoarchean (ca. 3006–2938 Ma) detritus. Early regional tilting of the BA (D_2 deformation), as indicated by the angular unconformity, and deposition of the SAA are attributed to uplift and erosion in response to accretionary processes on the NCT margin. West of Rice Lake, an older-over-younger map pattern between the BA and SAA, coupled with locally preserved bedding-parallel foliation (S_2), are attributed to thrust faulting (D_3 deformation) and tectonic inversion of the San Antonio basin during continued accretion on the NCT margin.

The first regional deformation fabrics (S_3-L_3) were formed at mid-crustal depths in response to northeast-southwest shortening (D_4 deformation) of the Rice Lake belt, perhaps associated with the main collisional stage of the Kenoran Orogeny. During this event, bulk sinistral transpression was strongly partitioned into macroscopic structural domains of sinistral-oblique noncoaxial shearing, upright subhorizontal folding, and bulk flattening and subvertical stretching. Planar fabrics associated with the regional D_5 deformation phase (S_4-S_5-S_6) record a progressive, dextral, transpressional shear deformation in response to northwest-southeast shortening of the Rice Lake belt during the terminal stage of the Kenoran Orogeny.

Gold mineralization in the Rice Lake area is hosted by synkinematic quartz-carbonate veins in brittle-ductile shear zones or complex networks of shear and tensile fractures, which preferentially formed in competent rock types after at least the initial increments of the regional D_4 deformation episode. The style and relative age of this mineralization preclude traditional syngenetic models in favour of epigenetic (i.e., orogenic) models. The results of this study provide a significantly improved geological context for lode-gold exploration in the study area, and indicate a previously unrecognized potential for volcanic-hosted massive sulphide (VHMS) deposits.

TABLE OF CONTENTS

Page

Page

TABLES

FIGURES

MAP

DIGITAL DATA

[1] MGS Data Repository Item DRI2008002, containing the data or other information sources used to compile this report is available online to download free of charge at www2.gov.mb.ca/itm-cat/freedownloads.htm, or on request from minesinfo@gov.mb.ca or Mineral Resources Library, Manitoba Science, Technology, Energy and Mines, 360–1395 Ellice Avenue, Winnipeg, MB R3G 3P2, Canada

Introduction

The Rice Lake area is located 150 km northeast of Winnipeg, Manitoba, in the central portion of the Archean Rice Lake greenstone belt of the western Superior Province. With historic production of 1.77 million ounces of gold from several deposits, the Rice Lake belt is the most prolific Archean lode-gold district in Manitoba. The Rice Lake gold mine (also known as the San Antonio or Bissett mine) is located on the north shore of Rice Lake at Bissett, and is developed on the Rice Lake deposit, a vertically extensive quartz-carbonate vein system hosted by gabbro. This deposit has produced 1.46 million ounces of gold and is reported to host proven and probable reserves of 261 670 ounces within a total resource of 826 920 ounces (George, 2006), making it the largest lode-gold deposit identified to date in Manitoba.

This report documents the lithology, depositional setting, stratigraphy, geochemistry, geochronology and structural geology of Neoarchean supracrustal and intrusive rocks in the vicinity of the Rice Lake deposit, in light of new data collected by the Manitoba Geological Survey as part of the Rice Lake metallogeny project. Initiated in 2002, the objective of this project is to update the understanding of the geology, metallogeny and tectonic evolution of the Rice Lake belt (*see* Anderson, 2002, 2003a, b, 2004, 2005a, b, 2006a, b, 2007). The project goal is an improved geological context and predictive framework for mineral deposits through the application of detailed bedrock mapping and structural analysis, lithogeochemistry, Sm-Nd isotope studies and U-Pb geochronology.

Previous work

The earliest geological investigation of Rice Lake was conducted by E.S. Moore in 1912 (Moore, 1914) to verify reports of the first discovery of gold in Manitoba, which occurred on the Gabrielle claim on the north shore of Rice Lake in 1911. Early follow-up investigations in the Rice Lake area were conducted by Dresser (1917), Cooke (1922) and De Lury (1927). Wright (1923) completed the first geological map of the Rice Lake region, which was published at a scale of 1:63 360 (1 inch to 1 mile) and extended from Wanipigow Lake in the northwest to Manigotagan Lake in the southeast. Wright (1932) also described the geology and mineral occurrences in this area as part of an early regional compilation of southeastern Manitoba geology. In 1936, C.H. Stockwell mapped an area of about 40 km^2 (15 sq. mi.) surrounding the Rice Lake mine, and the resulting report and maps (published at a scale of 1:6000 or 1 inch to 500 feet; Stockwell, 1938, 1940) provide particularly valuable descriptions of the local geology and gold occurrences. The results of this work were incorporated into the regional-scale map of Stockwell (1945), which was published at a scale of 1:63 360 (1 inch to 1 mile) and included marginal notes. Davies (1949, 1950, 1963) remapped the Rice Lake area at a scale of 1:31 680 (1 inch to ½ mile) and also completed a detailed (1:9600 or 1 inch to 800 feet) map of gold occurrences south of Rice Lake (Davies, 1953), in an area adjoining that mapped by Stockwell (1938). During this early period of geological investigations, the geology of the Rice Lake deposit was described by Reid (1931), Bragg (1943), Gibson and Stockwell (1948) and Skerl (1955).

This early mapping was compiled by Weber (1971b) for a belt-scale geological compilation map that was released by the Manitoba Mines Branch as part of Project Pioneer (McRitchie and Weber, 1971a), a multidisciplinary, collaborative study of the Rice Lake region conducted by the Mines Branch and the University of Manitoba from 1966 to 69. Concurrent with this work, Stephenson (1972) examined gold deposits in the Rice Lake area. Under the auspices of the 1984–1989 Canada-Manitoba Mineral Development Agreement (MDA), the immediate area of the Rice Lake mine was remapped at 1:10 000 scale by the Geological Survey of Canada (Poulsen et al., 1986; Poulsen, 1987) in support of detailed volcanological (Tirschmann, 1986), alteration (Ames, 1988; Ames et al., 1991), structural (Lau, 1988; Lau and Brisbin, 1996) and fluid-inclusion (Diamond et al., 1990) studies of the mine and environs. Results of this work were summarized by Poulsen (1989) and Poulsen et al. (1996). Also during the MDA, the Geological Survey of Canada completed a detailed (300 m line spacing) airborne geophysical survey of the Rice Lake area (Geological Survey of Canada, 1986), and Manitoba Energy and Mines documented the area's mineral deposits and occurrences (Fedikow, 1983; Schmidtke, 1984; Theyer, 1983, 1984, 1994; Theyer and Yamada, 1989). Concurrent with the MDA, Whiting (1989) completed a stratigraphic and geochemical study of the hostrocks to the Rice Lake deposit, and Turek et al. (1989) reported U-Pb zircon ages for seven samples from the Rice Lake belt, including a sample from Hares Island on Rice Lake. Most of the present study area was also included in a 1:50 000 scale surficial-geology and drift-geochemistry study of the western portion of the Rice Lake belt (Henderson, 1994).

More recently, Bailes (1998) conducted reconnaissance lithogeochemical sampling of the Rice Lake area as part of the Western Superior NATMAP project; Rhys (2001) described the structural geology of auriferous vein systems in the lower levels of the Rice Lake deposit; and Kremer (2004) examined the basal section of the fluvial-alluvial San Antonio assemblage at Red Rice Lake. Regional compilation maps produced under the auspices of the Western Superior NATMAP project include marginal-note descriptions of the geology, tectonostratigraphic assemblages and regional setting of the Rice Lake area (e.g., Bailes et al., 2003; Lemkow et al., 2006). Results of this project and the concurrent Western Superior LITHOPROBE transects are also presented in a Special Issue of the Canadian Journal of Earth Sciences (Volume 43, Number 7, July 2006).

Methods and scope

In light of the existing comprehensive geological base for the Rice Lake area, the present project was focused on refining the stratigraphic and structural context of gold mineralization through thematic mapping, utilizing modern analytical techniques. To accomplish this, the geology and structure were mapped by the author at 1:20 000 scale during the 2004 field season (Anderson, 2004), with follow-up mapping in the early part of the 2005 season. The provisional results of this work were released as Preliminary Map PMAP2005-1 (Anderson, 2005b), and a revised and expanded version of this map is included herein as Map GR2008-1-1. The study area is bounded on the north mainly by the Wanipigow River and encompasses roughly 90 km^2 centred on Rice Lake. All shoreline outcrops on Rice Lake were accessed via boat from the town of Bissett,

whereas all other areas were accessed by truck or all-terrain vehicle and traverse, using orthorectified aerial photographs and hand-held GPS for field plotting and navigation.

Bedrock outcrops are generally abundant throughout most of the study area; however, with the exception of the recently stripped outcrops along logging roads or near the new tailings impoundment north of Bissett, most are almost completely covered by lichen and moss. The last significant forest fire in the study area occurred more than 50 years ago. In most localities, extensive peeling of moss was required to facilitate detailed geological observations. Southeast of Rice Lake, most outcrops are covered by a very thick growth of moss and juniper, and the quality of exposure was found to be unsuitable for the purposes of this project. For this reason, the detailed geology of Stockwell (1938), which is based on 1:6000 scale mapping of stripped and burnt-over outcrops in 1936, is overlain on Map GR2008-1-1 (with minor modifications) to expand the map coverage in this area.

During the mapping, mesoscopic structural features were examined, described in detail, measured and digitally photographed, and a suite of oriented samples was collected to obtain thin-sections for microstructural analysis. A representative suite of 39 least-altered rock samples was collected and submitted to Activation Laboratories Ltd. for major-, trace- and rare-earth-element data by high-precision inductively coupled plasma–optical emission spectroscopy (ICP-OES) and –mass spectrometry (ICP-MS). For completeness, this report includes an analysis of ICP geochemical data for a suite of 24 rock samples collected by Bailes (1998, 1999) from within the study area (previously released as Data Repository Item DRI2005004 in conjunction with Geoscientific Report GR2005-2; Bailes and Percival, 2005a). A subset of four samples, selected to include both mafic and felsic volcanic rocks from the stratigraphic base and top of the volcanic succession at Rice Lake, was submitted to R.A. Creaser at the University of Alberta Radiogenic Isotope Facility for Sm-Nd isotope analysis. In addition, five samples were submitted for U-Pb dating to L.M. Heaman at the University of Alberta Radiogenic Isotope Facility; these included three samples of felsic magmatic rocks for isotope dilution–thermal ionization mass spectrometry (ID-TIMS) on igneous zircon, and two sandstone samples for laser-ablation, multicollector, inductively coupled plasma–mass spectrometry (LA-MC-ICP-MS) on detrital zircon populations. All of these data are presented herein.

Acknowledgments

A. Carlson, C. Chamale, P. Kremer, L. May and R. Moody provided capable and enthusiastic field assistance. Discussions with A. Bailes, C. Beaumont-Smith, C. Böhm, T. Corkery and L. Heaman helped clarify interpretations presented in this report. M. MacFarlane and P. Lenton provided digital cartographic expertise and B. Lenton drafted many of the figures. R. Boulay, D. Busch, M. Chorm, B. Ferreira, D. Ginn, J. Harvey, R. Jones, A. Kathler, R. Monroe, L. Norquay, R. Pauls, M. Romano, E. Sawitzky, T. Tuba, J. Wong and H. Wynne, are acknowledged for providing fruitful discussion, as well as free access to mineral properties, drillcore and proprietary data. Logistical support was provided by D. Binne and N. Brandson.

Regional geological framework

The Rice Lake greenstone belt is one of several strands of Neoarchean and Mesoarchean supracrustal rocks that, along with the Red Lake and Birch-Uchi belts in Ontario (e.g., Stott and Corfu, 1991), define the western segment of the volcano-plutonic Uchi Subprovince (Card and Ciesielski, 1986) of the western Superior Province (Figure 1). In Manitoba, the Uchi Subprovince is flanked to the north by the mainly plutonic Berens River Subprovince and to the south by metasedimentary rocks and derived gneiss, migmatite and granitoid plutons of the English River Subprovince (Card and Ciesielski, 1986). Thurston et al. (1991) included the Berens River Subprovince and the Mesoarchean portions of the Uchi Subprovince in the continental 'North Caribou Terrane', which has come to be generally regarded as the protocratonic nucleus of the western Superior Province (e.g., Stott and Corfu, 1991; Williams et al., 1992; Skulski et al., 2000; Percival et al., 2002, 2006a; Whalen et al., 2003). The southern boundary of the North Caribou Terrane is defined by the Wanipigow Shear Zone, an east-southeast-trending, subvertical, crustal-scale structure that can be traced along strike for more than 170 km to Red Lake, Ontario. South of the Rice Lake area, the Uchi–English River boundary is defined by the Manigotagan Shear Zone, a similarly oriented structure that can be traced for more than 400 km along strike and is continuous with the Sydney Lake–Lake St. Joseph Fault in Ontario (Figure 1).

Although considerable debate exists regarding the applicability of the modern plate-tectonic paradigm to studies of Archean lithospheric evolution (e.g., de Wit, 1998; Hamilton, 1998, 2003; McCall, 2003; Stern, 2005; Brown, 2006; Furnes et al., 2007), the weight of evidence pertaining to the tectonic evolution of the Superior Province prior to cratonization at ca. 2.6 Ga appears to implicate subduction/accretion processes and the collisional interactions of disparate oceanic and continental terranes (i.e., plate tectonics, *sensu stricto*; e.g., Langford and Morin, 1976; Card, 1990; Stott and Corfu, 1991; Williams et al., 1992; Percival et al., 2006a, b). As described below, a plate-tectonic paradigm offers the most cohesive explanation for the geology of the western Uchi Subprovince, and is thus utilized as the descriptive context for this report.

Stratigraphic nomenclature

Supracrustal rocks in the Rice Lake belt were assigned to the Rice Lake Group and the unconformably overlying San Antonio Formation by Stockwell (1938, 1945). In a revised stratigraphic nomenclature developed during Project Pioneer, the Rice Lake Group was subdivided into the mainly metavolcanic Wallace Lake, Bidou Lake and Gem Lake subgroups (each composed of two or more formations) and the metasedimentary Edmunds Lake Formation (e.g., Campbell, 1971; McRitchie, 1971; Weber, 1971a, b). Subsequent reconnaissance mapping and geochronology at Garner Lake (e.g., Brommecker et al., 1993; Davis, 1994; Poulsen et al., 1994) prompted Poulsen et al. (1996) to propose one additional unit, the mainly metavolcanic Garner Lake subgroup.

Poulsen et al. (1996) also proposed an alternative tectonostratigraphic nomenclature, wherein the supracrustal components of the Rice Lake belt were subdivided into several distinct tectonic 'assemblages' in the sense proposed by Thurston

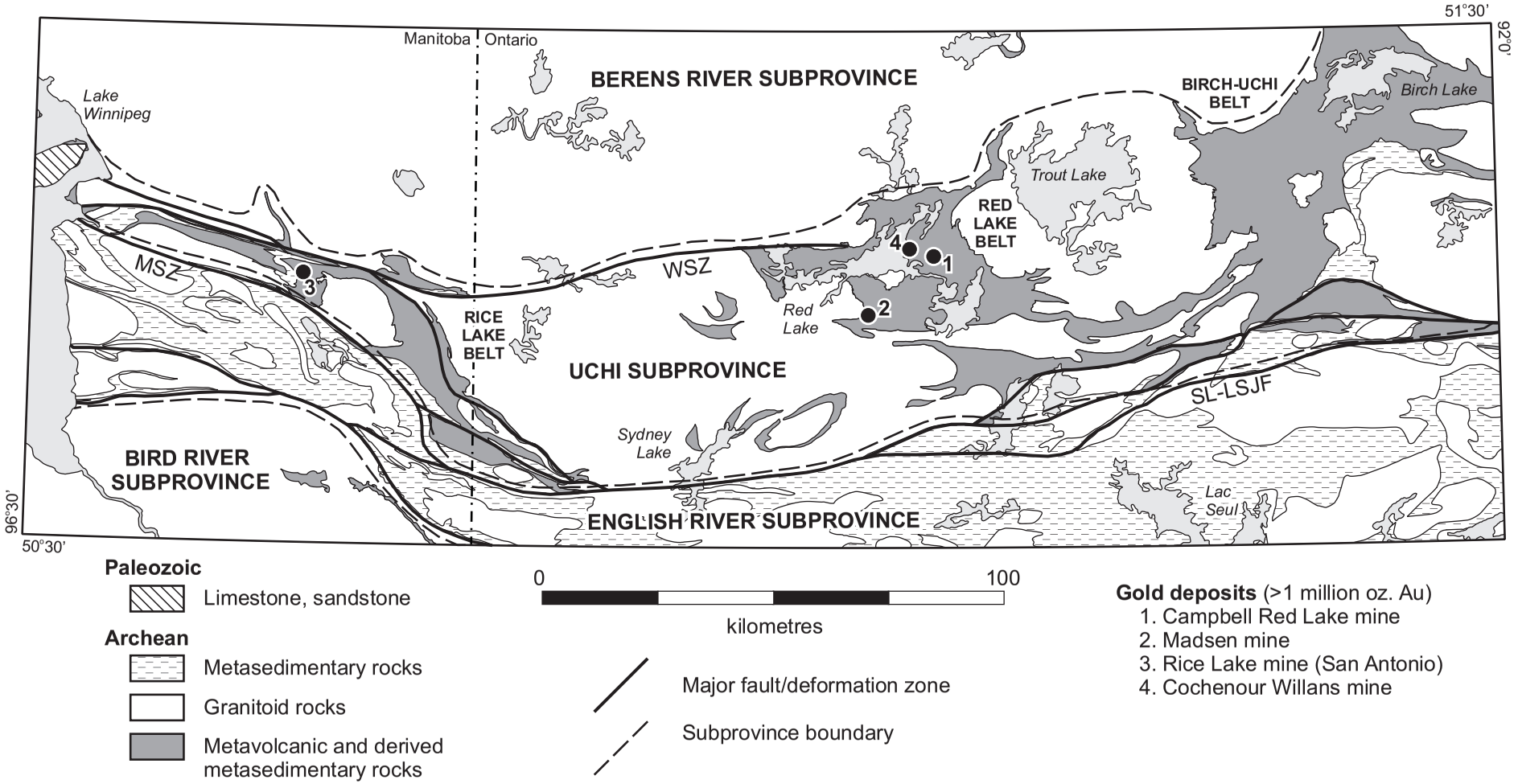

Figure 1: *Regional geological setting of the Rice Lake belt in the western Uchi Subprovince (*modified after *Lemkow et al., 2006). Abbreviations: MSZ, Manigotagan Shear Zone; SL–LSJF, Sydney Lake–Lake St. Joseph Fault; WSZ, Wanipigow Shear Zone.*

et al. (1991) for the northwestern Superior Province in Ontario (i.e., distinct associations of stratified rock types deposited in a common setting in a discrete interval of time; *see also* Williams et al., 1992). In the eastern Rice Lake belt, Poulsen et al. (1996) identified six tectonic assemblages, which included the Mesoarchean Wallace Lake and Garner Lake assemblages, and the Neoarchean Bidou Lake, Gem Lake, Edmunds Lake and San Antonio assemblages (Figure 2). This nomenclature was subsequently adopted and expanded by Bailes et al. (2003), who defined 16 assemblages in the western Uchi Subprovince on the basis of the criteria outlined above, as well as geographic location. In accordance with the nomenclature of Bailes et al. (2003), 'Lake' as been dropped from the assemblage names. As outlined below, these assemblages are interpreted to record rifting, continental- and oceanic-arc magmatism, and synorogenic sedimentation within an interpreted north-verging subduction-accretion complex that developed over a 300 Ma period along the south margin of the North Caribou Terrane (e.g., Stott and Corfu, 1991; Percival et al., 2002, 2006a, b; Bailes et al., 2003). Broadly comparable assemblages in the Red Lake and Birch-Uchi belts in Ontario (*see* Stott and Corfu, 1991; Sanborn-Barrie et al., 2001) provide a basis for regional tectonostratigraphic correlations.

North Caribou Terrane

In Manitoba, the southern margin of the North Caribou continental terrane (Thurston et al., 1991) comprises a basement of ca. 3.01–2.99 Ga, dominantly tonalitic igneous complexes that is nonconformably overlain by locally preserved ca. 2.98–2.92 Ga platform-rift sequences and intruded by ca. 2.94–2.90 and ca. 2.75–2.70 Ga continental-arc plutons collectively referred to as the Wanipigow River plutonic complex (e.g., Bailes and Percival, 2000, 2005a; Percival et al., 2002, 2006a; Bailes et al., 2003; Whalen et al., 2003; Sasseville et al., 2006). The platform-rift sequences, as represented by the Wallace and Lewis-Storey assemblages, consist of basal sections of shallow-water, continental-platform arkose, quartz arenite and pebble conglomerate that contain a single age population of ca. 2.99 Ga detrital zircons (e.g., Davis, 1994; Percival et al., 2006a). The upper sections consist of intercalated iron formation and komatiite that are thought to record ca. 2.98–2.92 Ga plume-related magmatism during continental rifting of the North Caribou Terrane (Percival et al., 2002, 2006a). The Little Beaver assemblage, which is exposed along the southern margin of the North Caribou Terrane north of Rice Lake (Figure 2), comprises a northwest-trending belt of psammitic and semipelitic schist, with minor sulphide-silicate iron formation and gabbro sills. The detrital zircon population from this assemblage defines a cluster between ca. 3.0 and 2.98 Ga (McNicoll and Percival, unpublished data, 2001), suggesting a correlation with the North Caribou platform succession.

Uchi Subprovince

The Uchi Subprovince in Manitoba is defined by the Rice Lake greenstone belt and consists mainly of mafic to intermediate volcanic and volcaniclastic rocks of tholeiitic and

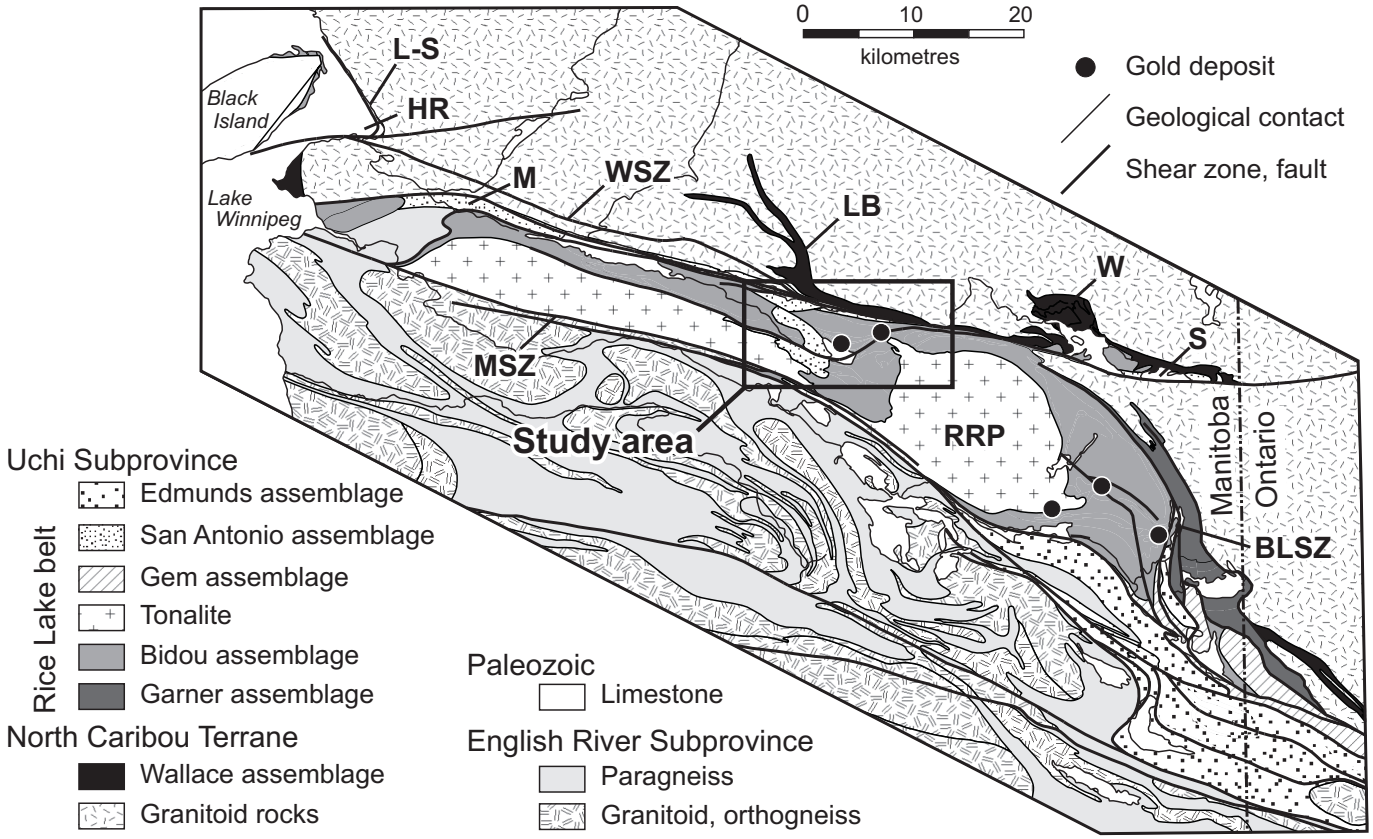

Figure 2: *Simplified geology of the Rice Lake belt, showing the principal lithotectonic assemblages, major gold deposits and location of the study area. Abbreviations: BLSZ, Beresford Lake Shear Zone; HR, Hole River assemblage; LB, Little Beaver assemblage; L-S, Lewis-Storey assemblage; M, Manigotagan assemblage; MSZ, Manigotagan Shear Zone; RRP, Ross River pluton; S, Siderock assemblage; W, Wallace assemblage; WSZ, Wanipigow Shear Zone.*

calcalkalic affinity, intercalated with derived epiclastic rocks and intruded by synvolcanic gabbro sills and tonalite plutons. The exposed portion of the Rice Lake belt trends southeast for a distance of 145 km, from the eastern extent of Paleozoic cover at Lake Winnipeg to just east of the Manitoba-Ontario border, and ranges up to 15 km wide. Regional aeromagnetic patterns indicate that the belt extends at least 150 km to the west beneath Paleozoic cover. The eastern extent of the Rice Lake belt is referred to as the Bee Lake greenstone belt in Ontario, and was recently mapped by Rogers (2001, 2003).

Five distinct tectonostratigraphic assemblages are presently recognized in the eastern portion of the Rice Lake belt, including the Mesoarchean Garner assemblage and the Neoarchean Bidou, Gem, Edmunds and San Antonio assemblages (Poulsen et al., 1996).

Garner assemblage

The Mesoarchean Garner assemblage extends north and southeast of Garner Lake, along the northeastern margin of the Rice Lake belt, and is intruded to the east by granitoid rocks of unknown age and affinity. To the west, the Garner assemblage is juxtaposed with the Neoarchean Bidou, Gem and Edmunds assemblages across the Beresford Lake Shear Zone (Figure 2). The Garner narrows unit, which defines the lower portion of the assemblage, is thought to form a conformable, north-younging stratigraphic succession that is at least 3.0 km thick and consists of heterolithic volcaniclastic and epiclastic rocks at the base, overlain to the north by a thick package of ca. 2.88–2.90 Ga, calcalkalic, intermediate to felsic volcaniclastic rocks of continental-arc affinity, and capped by iron formation (Anderson, 2005a). The Garner narrows unit is intruded by peridotite, pyroxenite and gabbro of the Garner Lake intrusive complex, the latter of which includes dikes and irregular segregation pods of leucogabbro and quartz diorite that have been dated at 2871 Ma (*see* Davis, 1994; Anderson, 2003a). The Garner Lake extrusive complex disconformably overlies the Garner narrows unit and consists of a north-facing succession, more than 3.0 km thick, of subaqueous komatiitic, Mg-tholeiitic and calcalkalic basalt flows, with minor interflow iron formations and related subvolcanic intrusive rocks. The extrusive rocks are interpreted to be comagmatic with the underlying intrusive complex (e.g., Brommecker et al., 1993) and likely record a switch from subduction-related to plume-related magmatism (e.g., Hollings et al., 1999) within a volcanic-arc on, or marginal to, the North Caribou Terrane.

Bidou assemblage

The Neoarchean Bidou assemblage occupies the core of the Rice Lake belt and is intruded by several synvolcanic tonalite and granodiorite plutons, of which the Ross River pluton is the most prominent example (Figure 2). East of the pluton, in the core of a macroscopic anticlinal culmination, the Bidou assemblage is approximately 5.5 km thick and is subdivided into seven conformable formations (Campbell, 1971) that are interpreted to record an upward transition from back-arc to oceanic-arc magmatism (e.g., Poulsen et al., 1996; Bailes et al., 2003; Percival et al., 2006a). The back-arc succession consists of laterally continuous units of massive and pillowed, mid-ocean-ridge (MORB)–like tholeiitic basalt flows (the Unnamed, Tinney Lake and Gunnar formations), which alternate with well-stratified units of feldspathic greywacke and mudstone, with minor intercalations of laminated chert, volcanic conglomerate, iron formation and pillowed basalt (the Stovel Lake, Dove Lake and Stormy Lake formations). The overlying oceanic-arc succession, which is referred to as The Narrows Formation, comprises a 2.5 km thick, coarse volcaniclastic and epiclastic succession composed of calcalkaline porphyritic andesite and dacite. With the apparent exception of the upper portion of The Narrows Formation, all of these units are intruded by tholeiitic gabbro sills. Turek et al. (1989) reported a U-Pb zircon age of 2731 ±3 Ma for The Narrows Formation, as well as overlapping ages of 2728 ±8 Ma and 2731 ±13 Ma for porphyry dikes that intrude the back-arc succession and are presumed to be associated with the Ross River pluton. In addition, Turek and Weber (1991) reported an age of 2733 ±6 Ma for a texturally similar porphyry dike that cuts The Narrows Formation, which indicates that the Ross River pluton and The Narrows Formation are comagmatic.

West of the Ross River pluton at Rice Lake, the Bidou assemblage consists of an upright, homoclinal succession of predominantly intermediate to felsic, subaqueously deposited volcaniclastic and epiclastic rocks that dips moderately north and is at least 7.0 km thick. Between the south shore of Rice Lake and the Wanipigow Shear Zone, Poulsen et al. (1996) subdivided these rocks into a series of informal map units, which include, from south to north, the Hare's Island, Shoreline, Townsite and Round Lake volcanic units. The Hare's Island unit is intruded by a thick gabbro sill, which hosts the Rice Lake gold deposit. Turek et al. (1989) obtained a U-Pb zircon age of 2729 ±3 Ma from the Hare's Island unit at Rice Lake, suggesting a possible correlation with The Narrows Formation east of the Ross River pluton (e.g., Weber, 1971b). These rocks are composed mainly of calcalkalic andesite and dacite, with high-field-strength-element (HFSE) signatures indicative of syncollisional volcanic-arc magmatism (Anderson, 2005a). In the area extending from south of Rice Lake to the Manigotagan Shear Zone, Stockwell (1938) and Davies (1953) mapped a thick package of heterolithic intermediate to felsic volcaniclastic and epiclastic rocks that Weber (1971b) considered part of the younger Gem assemblage. As described below, the rocks south of Rice Lake are herein considered part of the Bidou assemblage, although the geology in this area remains poorly understood.

Gem assemblage

The Neoarchean Gem assemblage overlies The Narrows Formation southeast of the Ross River pluton and consists of a thick succession of mafic to felsic volcanic flows, pyroclastic rocks and derived epiclastic rocks that, at Gem Lake, ranges up to at least 2.0 km thick. Davis (1994) obtained a U-Pb zircon age of 2722 ±2 Ma from quartz-phyric rhyolite breccia at Gem Lake. Portions of the Gem assemblage, as defined by Anderson (2006a, b), were previously assigned to the Banksian Lake Formation (Weber, 1971a), the Manigotagan River Formation (Seneshen and Owens, 1985) and the Garner River unit (Anderson, 2003a). At Gem Lake, the lower portion of the assemblage is defined by a subaerial to shallow subaqueous, rhyolitic vent complex composed of quartz-phyric to aphyric, high-silica

rhyolite flows, coarse flow-lobe breccia units and hypabyssal intrusions (cryptodomes), with minor pumiceous pyroclastic rocks and derived epiclastic rocks. The vent complex is overlain by a thick succession of monolithic to heterolithic volcaniclastic rocks, which includes minor flow-banded to massive dacite and rhyolite flows, gabbro sills, pillowed basalt and basaltic andesite flows and associated coarse fragmental rocks, and well-bedded epiclastic rocks. The top of the Gem assemblage is locally marked by a unit of monolithic volcaniclastic dacite that ranges up to 200 m thick. Felsic flows and pyroclastic rocks in the Gem assemblage classify as FII- and FIIIa-type rhyolite in the scheme of Lesher et al. (1986), with HFSE signatures indicative of extension-related, within-plate volcanism (Anderson, 2005a). The Gem assemblage exhibits many of the hallmarks of extensional tectonic regimes, and was interpreted by Anderson (2005a) to record the initiation of an arc-rift basin within the Bidou oceanic arc (i.e., a possible fore-arc rift; Poulsen et al., 1996).

San Antonio assemblage

The Neoarchean San Antonio assemblage consists of planar- and trough-crossbedded sandstone, deposited in a fluvial-alluvial setting, with subordinate polymictic conglomerate and greywacke-mudstone turbidite. At Rice Lake, these rocks define a 1.2 km thick, broadly S-shaped map unit that trends across the regional strike of the Rice Lake belt (Figure 2). The San Antonio assemblage youngs to the west and overlies the Bidou assemblage along a well-defined angular unconformity (Stockwell, 1938; *see also* Bailes, 1998; Anderson, 2004). Along the south margin of the greenstone belt west of Rice Lake, the San Antonio assemblage nonconformably overlies a tonalite pluton (Stockwell, 1945) that is presumed to be the same age as the Ross River pluton. Toward the west, west-younging volcanic, volcaniclastic and epiclastic rocks of presumed Bidou affinity structurally overlie the San Antonio assemblage along an inferred thrust fault (Anderson, 2004). Detrital zircons in the San Antonio assemblage range in age from ca. 2.98 Ga to 2.705 Ga (Percival et al., 2006a), the latter of which provides the maximum depositional age. Similar rocks occur in discrete, possibly fault-bounded basins at Lake Winnipeg (<2.708 Ga Hole River assemblage; Percival et al., 2006a) and Siderock Lake (<2.709 Ga Siderock assemblage; Sasseville et al., 2006), and as a thin, fault-bounded panel along the Wanipigow Shear Zone (Manigotagan assemblage; Bailes et al., 2003). Collectively, these basins are thought to represent the proximal, subaerial equivalents of the more distal marine turbidites of the ca. 2.70 Ga Edmunds assemblage (*see* below).

Edmunds assemblage

The Neoarchean Edmunds assemblage is at least 2.5 km thick and consists mainly of monotonously bedded greywacke-mudstone turbidites, with subordinate units of polymictic conglomerate, thick-bedded greywacke and discontinuous layers of laminated chert and iron formation. Along the Manigotagan River, the Edmunds assemblage concordantly overlies the Bidou and Gem assemblages along a potentially significant erosional unconformity (Anderson, 2005a, 2006a). The lowermost portion of the assemblage consists of a 1.2 km thick coarsening-upward cycle, suggesting deposition in a progradational submarine fan. South of Gem Lake, the Edmunds assemblage includes thick, laterally continuous units of pillowed basalt flows and dacitic epiclastic rocks that were previously considered part of the Gem Lake subgroup (Weber, 1971a). They are interstratified, however, on a variety of scales (e.g., Weber, 1987) with polymictic conglomerate and quartz greywacke of the Edmunds assemblage, indicating that basin infilling was accompanied by local volcanism (Anderson, 2006a; Anderson, 2007). The youngest detrital zircon obtained from a sample of greywacke turbidite west of Gem Lake yielded a U-Pb age of 2705 ±2 Ma (Davis, 1996). In Ontario, correlative rocks were intruded by calcalkalic plutons at 2698 Ma (Corfu et al., 1995). Deposition of the Edmunds assemblage is thus constrained to ca. 2.70 Ga, coeval with accretion-related orogenesis along the North Caribou Terrane margin (e.g., Percival et al., 2006b).

English River Subprovince

The English River Subprovince, which flanks the Uchi Subprovince to the south and is known as the Manigotagan Gneissic Belt in Manitoba, consists of ca. 2.69 Ga paragneiss, orthogneiss and granitoid plutons that formed during high-T–low-P regional metamorphism of a thick succession of ca. 2.7 Ga marine turbiditic sedimentary rocks (Corfu et al., 1995). The high-grade rocks record tectonic subsidence and regional prograde metamorphism that are interpreted to be related to ca. 2.69 Ga collisional orogenesis of the North Caribou Terrane and Winnipeg River Subprovince (Percival et al., 2006a, b), which culminated prior to the emplacement of late-tectonic granite plutons at ca. 2.66 Ga (Turek et al., 1989). Along the south margin of the Rice Lake belt, high-grade paragneiss is tectonically juxtaposed with lower grade rocks of the Bidou and Edmunds assemblages along a series of greenschist-facies (i.e., retrograde) high-strain zones (e.g., McRitchie and Weber, 1971b), which include the regional-scale Manigotagan Shear Zone and subsidiary structures.

Local geology and stratigraphy

In this report, the supracrustal rocks in the vicinity of Rice Lake are interpreted to comprise the Mesoarchean Little Beaver assemblage and the Neoarchean Bidou and San Antonio assemblages (Figure 3). The Little Beaver assemblage lies in contact to the north with Mesoarchean tonalite and granodiorite of the Wanipigow River plutonic complex and is juxtaposed to the south with Neoarchean supracrustal rocks of the Rice Lake greenstone belt across the Wanipigow Shear Zone (WSZ). The Bidou assemblage is intruded at the base by the synvolcanic Ross River plutonic suite and both are unconformably overlain by the San Antonio assemblage. Thin-bedded greywacke-mudstone turbidites that occur as a fault-bounded panel along the trace of the WSZ were referred to as the Manigotagan assemblage by Bailes et al. (2003) but are herein included in the San Antonio assemblage. All of these units are described in detail below, in general order of decreasing known or apparent age.

Metamorphic mineral assemblages throughout the map area south of the WSZ indicate low to middle greenschist facies regional metamorphism, with the exception of narrow zones along the margins of the larger plutons of the Ross River suite,

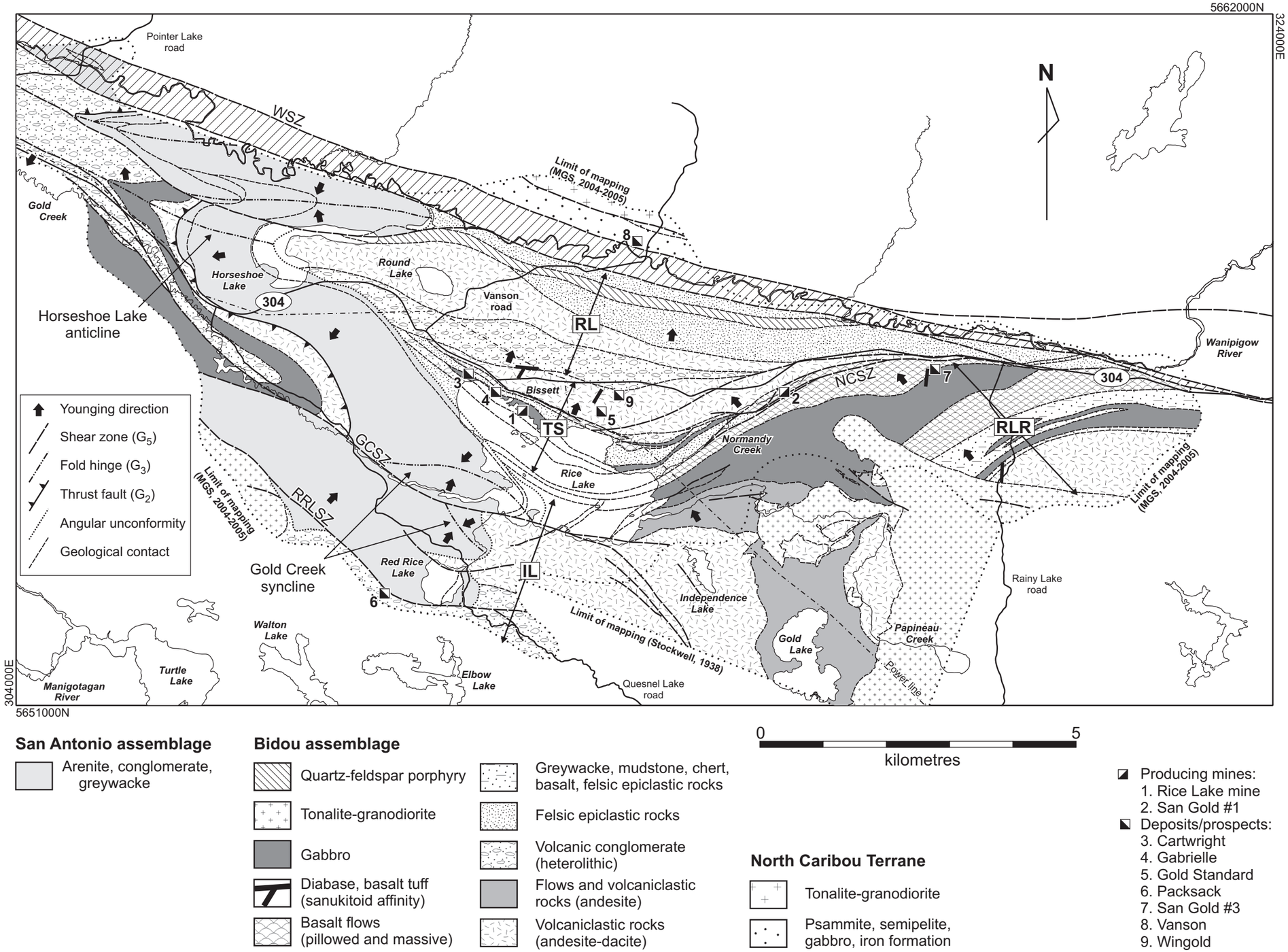

Figure 3: *Geology of the Rice Lake area, simplified after accompanying Map GR2008-1-1 (refer to this map for detailed geology and map unit numbers). The locations of the Independence Lake (IL; map units 4–6), Rainy Lake road (RLR; map units 7–10), Townsite (TS; map units 12–16) and Round Lake (RL; map units 17–21) units are shown for reference. The heavy dotted line shows the outline of the area mapped during the 2004 and 2005 field seasons as part of this study. The geology of the Gold Lake area is modified after Stockwell (1938). Abbreviations: GCSZ, Gold Creek Shear Zone; NCSZ, Normandy Creek Shear Zone; RRLSZ, Red Rice Lake Shear Zone; WSZ, Wanipigow Shear Zone (indicated by hachured pattern).*

which locally contain upper greenschist to lower amphibolite facies assemblages. In the interest of brevity, however, the prefix 'meta' is not utilized in this report and the rocks are described in terms of known or inferred protolith.

Little Beaver assemblage

The Little Beaver assemblage is exposed immediately north of the WSZ, and forms a 300–400 m thick band of supracrustal rocks that strikes west and dips subvertically. The best exposures occur along logging roads that extend to the west and north from the site of the historical Vanson mine, in areas that generally exhibit elevated magnetic intensity (e.g., Geological Survey of Canada, 1986; Assessment File 73689, Manitoba Science, Technology, Energy and Mines, Winnipeg). The Little Beaver assemblage is structurally bounded to the south by the WSZ, and to the north is bounded by felsic plutonic rocks of the Wanipigow River plutonic complex across a narrow zone of chloritic mylonite that obscures a probable intrusive contact. McNicoll and Percival (unpublished data, 2001) determined a maximum age of 2975 Ma for the Little Beaver assemblage, based on U-Pb analysis of detrital zircons from a sample of paragneiss collected approximately 15 km northwest of the study area along strike.

Psammitic and semipelitic schist (unit 1)

This unit is composed mainly of psammitic and semipelitic schist, which forms well-layered intervals up to at least 100 m thick. The psammite weathers light grey to pale green and consists of very fine to fine-grained, equigranular quartz and feldspar with subordinate white mica and zoisite/clinozoisite, and accessory carbonate minerals, pale green chlorite and amphibole, pale pink garnet and pyrite. The garnet forms skeletal porphyroblasts up to 5 mm across (Figure 4a) that typically exhibit prominent mica-depleted reaction haloes. The semipelite weathers green to rusty brown and consists mainly of fine-grained chlorite and white mica, with up to 40% pale pink garnet porphyroblasts that range up to 7 mm across. The metamorphic mineral assemblages are suggestive of calcareous protoliths. Individual layers are typically 2–20 cm thick, but locally range up to more than 2.0 m thick. Intervals of rhythmically alternating psammite and semipelite layers resemble primary turbiditic bedding (Figure 4b). Minor intercalations of gossanous sulphide-silicate– and oxide-facies iron formation (subunit 1a) indicate deposition in a relatively quiescent marine setting. This unit is intruded by dikes of light grey-green, porphyritic tonalite and contain rare sills of dark green to black, medium-grained, equigranular gabbro (subunit 1b) that range up to at least 10 m thick. All of these rocks contain a penetrative and pervasive planar fabric defined by fine-grained foliated micaceous minerals, transposed quartz veins, and a locally prominent gneissosity in the psammite layers. Abundant examples of rootless and isoclinal folds indicate that this unit is strongly transposed.

Chloritic mylonite and tectonite (unit 2)

Chloritic mylonite and tectonite of uncertain precursor and affinity are observed in one location at the contact between the Little Beaver assemblage and the Wanipigow River plutonic complex. Widely spaced outcrops of chloritic mylonite and tectonite are also observed along the trace of the WSZ in the eastern portion of the study area, and are included in the Mesoarchean Little Beaver assemblage because they include minor intercalations of strongly transposed oxide- and sulphide-facies iron formation, and generally coincide with areas of elevated magnetic intensity relative to Neoarchean supracrustal rocks immediately to the south. (It should be noted, however, that these criteria are not necessarily diagnostic, given that oxide-facies iron formation is known to occur in the Neoarchean Edmunds assemblage along the south margin of the Rice Lake belt.) Along strike to the west, the chloritic mylonite and tectonite give way to well-bedded greywacke-mudstone turbidite and polymictic conglomerate that are exposed at Silver Falls on the Wanipigow River, and are included in the Neoarchean San Antonio assemblage on the basis of rock types and detrital zircon U-Pb geochronology data. The contact between the Neoarchean and inferred Mesoarchean rocks is not exposed along the valley of the WSZ, but is presumed to be tectonic.

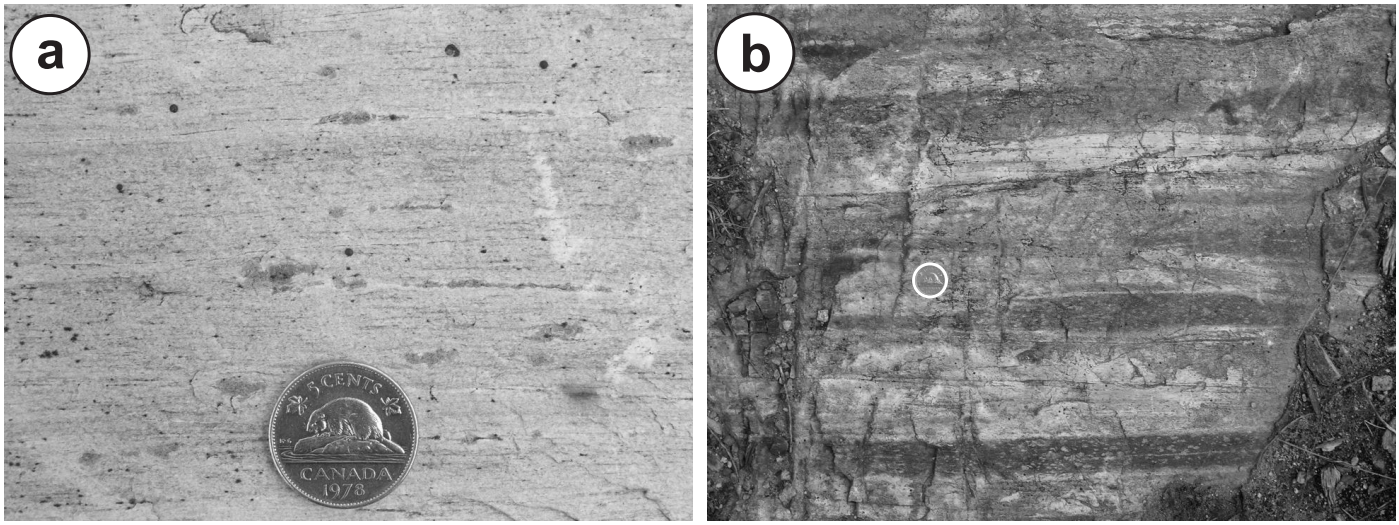

Figure 4: *Outcrop photographs of rock types in map unit 1, northwest of the Vanson mine:* ***a)*** *strongly foliated and garnetiferous psammite (coin is 2.1 cm in diameter);* ***b)*** *rythmically interlayered, light grey psammite and dark grey garnetiferous semipelite (coin for scale, circled).*

Wanipigow River plutonic complex

The Wanipigow River plutonic complex received only limited examination in the present study, but crops out extensively north of the WSZ in the north-central portion of the mapped area. Regional mapping and aeromagnetic data indicate that the examined outcrops define the southern extent of a roughly rectilinear batholith of unseparated granodiorite and tonalite, which has a surface area of approximately 700 km^2. The only available age constraint is provided by a sample of granodiorite collected approximately 12 km to the east of the study area, just north of the northern contact of the Little Beaver assemblage, which returned a U-Pb age of ca. 2.9 Ga (Turek et al., 1989). This contact, which is traced through the northernmost portion of the mapped area, likely represents a tectonized intrusive contact (*see* below).

Biotite tonalite and granodiorite (unit 3)

In the study area, the Wanipigow River plutonic complex is composed of white- to light pink–weathering biotite tonalite and granodiorite. These rocks consist of 80% feldspar, 15–30% quartz and up to 5% fine-grained biotite, and vary in texture from medium grained and equigranular to seriate textured and porphyritic. The porphyritic rocks contain equant, subhedral phenocrysts of plagioclase that range up to 1.0 cm in maximum dimension. Most outcrops are massive and homogeneous, with only minor crosscutting quartz veins or narrow dikes of aplite and pegmatite, and a weak to moderate planar fabric defined by foliated biotite. Along the southern margin of this unit, however, the rocks contain a penetrative and pervasive, locally mylonitic foliation defined by foliated biotite and well-developed quartz ribbons. Enclaves of thin-layered metasedimentary rock were observed in one location along the southern margin, suggesting an intrusive relationship with the Little Beaver assemblage to the south.

Bidou assemblage

In this report, a new stratigraphy is proposed for the Bidou assemblage at Rice Lake, which incorporates the results of mapping and lithogeochemistry conducted by the MGS in 2004 and 2005, and expands upon the preliminary results presented by Anderson (2004, 2005b). This stratigraphy (Figures 3, 5) is subdivided for descriptive purposes into four distinct lithostratigraphic units that trend generally west, dip consistently to the north and are informally termed, from south to north, the Independence Lake (IL), Rainy Lake road (RLR), Townsite (TS) and Round Lake (RL) units. Contact relationships and younging criteria indicate that these units define a north-younging stratigraphic succession.

As described in detail below, the constituent volcanic rocks range in composition from basalt, through basaltic andesite and andesite, to dacite and rhyolite, and are interpreted to record magmatism in an extensional, possibly back-arc portion of a continental-margin magmatic arc. Facies associations indicate a mainly subaqueous depositional setting on the medial to distal flanks of an active volcanic complex. As shown schematically in Figure 5, abrupt lateral and vertical facies transitions, evidence of deep erosional scouring, and the predominance of coarse epiclastic deposits point toward high-energy sedimentation and a very dynamic depositional setting. Most of these deposits are composed of detritus that was significantly reworked in a subaerial to shallow-marine setting prior to final deposition in a moderately deep-water setting. The dominance of coarsely porphyritic dacite detritus and the apparent absence of significant accumulations of primary pyroclastic material indicate a relatively distal volcanic source area that was likely dominated by porphyry effusions and cryptodomes.

The IL unit, at the base of the studied section, consists of epiclastic rocks and intermediate volcanic and volcaniclastic rocks that were likely deposited on the shallow subaqueous, medial flank of an intermediate–felsic volcanic complex. These rocks are the substrate to the RLR unit, which records subaqueous sedimentation and effusive mafic volcanism within a relatively deeper water, restricted basin that is interpreted to have formed in the hangingwall of a synvolcanic subsidence structure (i.e., a synvolcanic fault). Five lines of evidence, which are described in greater detail in the following sections, indicate the existence of this structure:

- On-strike portions of the RLR and IL units exhibit significant differences in lithofacies and geochemical affinity.
- The interface between the on-strike portions of the RLR and IL units is invaded by synvolcanic intrusions and hypabyssal dike swarms, including a major apophysis of the Ross River pluton.
- The RLR-IL interface coincides with occurrences of stringer-style chlorite (Fe-Mg) alteration, laminated sulphidic chert and solid sulphide in the RLR unit, which are indicative of fault-controlled hydrothermal circulation and seafloor discharge.
- The map pattern of an overlapping mafic flow complex indicates a significant change in unit thickness across the RLR-IL interface.
- Facing criteria indicate a pronounced angular discordance between the RLR unit and overlying rocks, which is interpreted to result from syn- to early-post–depositional tilting of the RLR unit in the hangingwall of the subsidence structure.

The Ross River plutonic suite intrudes the IL and RLR units, and may represent the subvolcanic equivalent of the felsic epiclastic rocks at the base of the TS unit (i.e., the Hare's Island rhyolite; *see* Turek et al., 1989). Emplacement of the Ross River pluton may have been, at least in part, controlled by the synvolcanic subsidence structure. The TS and RL units record subaqueous sedimentation and minor volcanism in the medial to distal portion of the mainly volcaniclastic apron that flanked the intermediate–felsic volcanic complex. One additional unit (the Gold Creek unit) comprises a structurally bounded package of intermediate volcanic, volcaniclastic and epiclastic rocks, mafic flows and gabbro sills west of Horseshoe Lake, which is tentatively correlated with the Bidou assemblage on the basis of rock types and geochemistry.

Clastic nomenclature

In the study area, the Bidou assemblage comprises mainly coarse clastic rock types, which apparently developed via a range of volcanic and sedimentary processes. As described by Fisher (1961), it is difficult to devise a simple working classification or nomenclature that incorporates all of the potential processes involved in the generation, transport and deposition

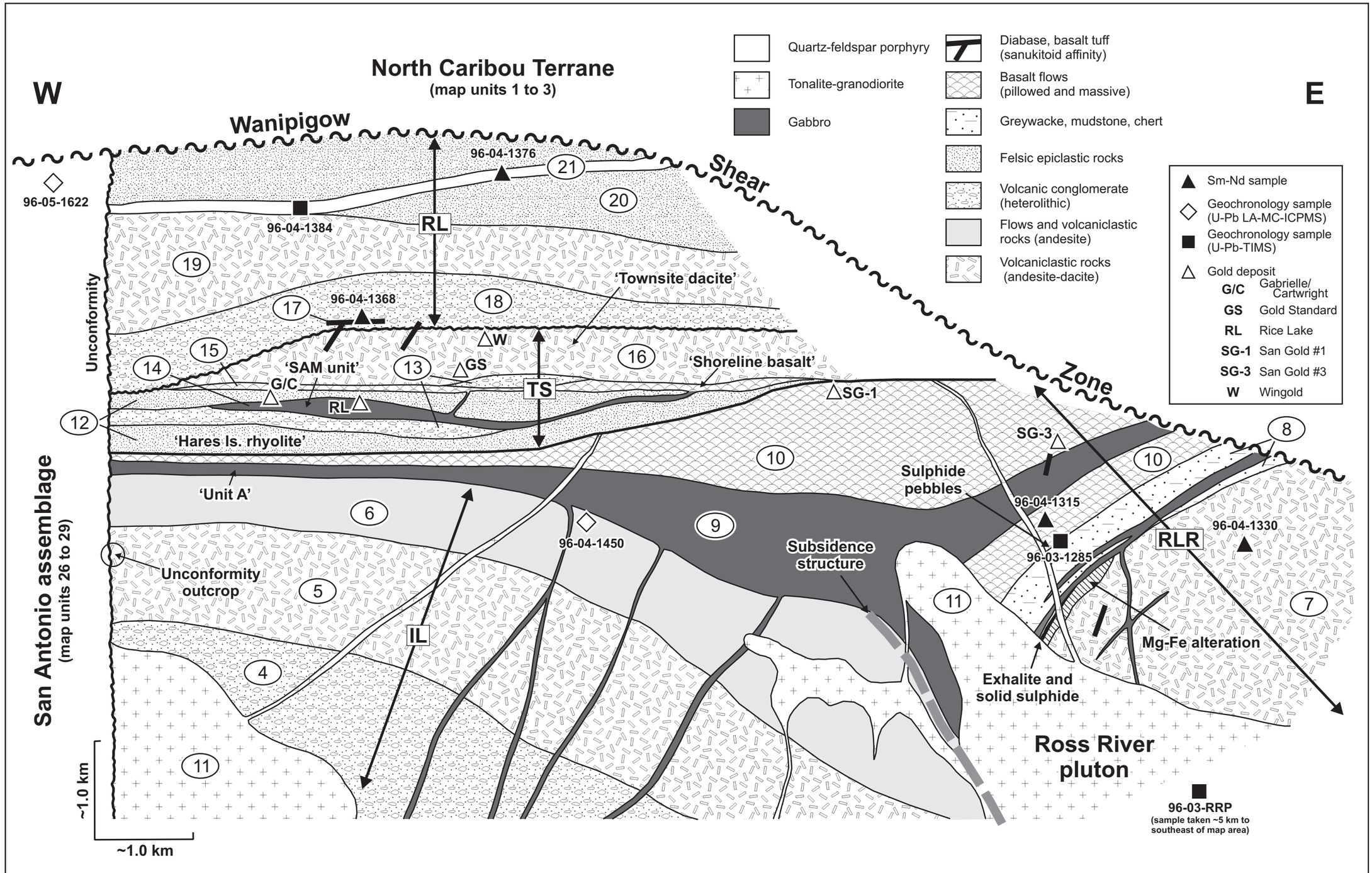

Figure 5: *Schematic lithostratigraphy of the Rice Lake section of the Bidou assemblage (vertical section, looking toward present-day north). For simplicity, the geology north of the Wanipigow Shear Zone and west of the San Antonio assemblage is excluded from this diagram. The numbered ellipses correspond to the map unit numbers in the text. The heavy grey dashed line indicates the approximate location of the subsidence structure that is thought to separate the RLR and IL units east of Rice Lake. The thickness of the exhalite and solid sulphide horizon in the RLR unit is exaggerated. Shown for reference are the known gold deposits and the approximate locations of the samples submitted for isotopic analysis. Abbreviations: IL, Independence Lake unit; RL, Round Lake unit; RLR, Rainy Lake road unit; TS, Townsite unit.*

of clastic material in a volcanic environment (*see also* Fisher, 1966; Cas and Wright, 1987; McPhie et al., 1993; White and Houghton, 2006). Genetic classifications require an understanding of the modes of fragmentation, transport *and* final deposition of the constituent particles, based on detailed observations of primary features at a variety of scales. In the Rice Lake area, however, these features are typically masked by discontinuous and/or poor exposure and the effects of metamorphic recrystallization, penetrative deformation and hydrothermal alteration. Hence, this report utilizes a nomenclature that includes aspects of the classification schemes proposed by Fisher (1961, 1966), Cas and Wright (1987), McPhie et al. (1993) and White and Houghton (2006), yet incorporates some flexibility that takes into account the practicalities of mapping and interpreting these rock types in glaciated greenstone terranes.

In this report, clastic rock types are subdivided into two end members: volcaniclastic and epiclastic (Table 1). The term 'volcaniclastic' is used in a general sense to denote rocks that are composed exclusively of texturally immature fragments of volcanic rock, and for which the process of fragmentation is inferred to be a direct result of volcanism. These rocks are described using the granulometric terms of Fisher (1966), specifically breccia, tuff breccia, lapilli tuff, lapillistone and tuff, but in the nongenetic sense advocated by Gibson et al. (1999); that is, the terms are not strictly applied to lithified primary pyroclastic deposits (e.g., Fisher, 1966; Cas and Wright, 1987). Rocks that are interpreted to be of primary volcaniclastic origin (i.e., pyroclastic, autoclastic, hyaloclastic or peperitic; White and Houghton, 2006) are described using the appropriate genetic modifier (e.g., pyroclastic breccia), whereas rocks interpreted to be resedimented, syneruptive equivalents (*see* McPhie et al., 1993) are denoted with 'reworked' as a genetic modifier (e.g., reworked pyroclastic breccia). Epiclastic rock types, which exhibit textural evidence of weathering and erosion, with deposition by normal sedimentary processes, are described using the standard granulometric terms for sedimentary particles (Wentworth, 1922), and are subdivided into two end members, depending on the provenance of the constituent clasts (Table 1). Epiclastic rock types composed exclusively of volcanic-rock clasts are referred to as 'volcanic' conglomerate, sandstone or mudstone, whereas mixed-provenance clastic rock types are referred to by the same terms, without the 'volcanic' modifier.

Independence Lake unit

The Independence Lake (IL) unit is extensively exposed south of Rice Lake, but clean exposures are largely restricted to the Quesnel Lake road southeast of Red Rice Lake. The IL unit is herein interpreted to extend south from Rice Lake to the Manigotagan Shear Zone; however, only the northernmost portion was examined during the present study. In the area south of Rice Lake, Stockwell (1938) and Davies (1953) mapped a series of generally west-northwest-trending geological units that are variously composed of aphyric to porphyritic, massive to coarsely fragmental, intermediate to felsic volcanic rocks. Although bed forms are extremely rare in this area, the map of Stockwell (1938) shows several bedding symbols that indicate shallow to moderate dips to the north. Stockwell (1938) described two examples of younging criteria, both of which were interpreted to indicate that the rocks are upright. Bed forms observed by the author in two locations trend roughly west, dip steeply north and, in one location, appear to be upright, thereby supporting the interpretation of Stockwell (1938). To the east, in the area of Gold Lake, map patterns

Table 1: Nomenclature for clastic rock types in the Rice Lake area (after Fisher, 1961; Cas and Wright, 1987; McPhie et al., 1993; Gibson et al., 1999; White and Houghton, 2006).

Non-genetic	Volcaniclastic[1]				Epiclastic	
	Primary[2,3]				Volcanic provenance[4]	Mixed provenance[5]
	Pyroclastic	Autoclastic	Hyaloclastic	Peperitic		
Breccia, tuff breccia	Pyroclastic breccia, tuff breccia	Autoclastic breccia, tuff breccia	Hyaloclastic breccia, tuff breccia	Peperitic breccia, tuff breccia	Volcanic boulder or cobble conglomerate	Boulder or cobble conglomerate
Lapillistone	Pyroclastic lapillistone	Autoclastic lapillistone	Hyaloclastic lapillistone	Peperitic lapillistone	Volcanic pebble conglomerate	Pebble conglomerate
Lapilli tuff	Pyroclastic lapilli tuff	Autoclastic lapilli tuff	Hyaloclastic lapilli tuff	Peperitic lapilli tuff	Volcanic pebbly sandstone	Pebbly sandstone
Tuff	Pyroclastic tuff	Autoclastic tuff	Hyaloclastic tuff	Peperitic tuff	Volcanic sandstone or mudstone	Sandstone or mudstone

[1] composed exclusively of texturally immature volcanic-rock clasts, and lacking evidence of significant weathering/erosion, surficial transport, and/or final deposition by 'normal' sedimentary processes

[2] composed exclusively of primary volcanic clasts; clast size and shape unmodified by weathering/erosion; transport and final deposition by volcanic processes

[3] includes resedimented, syneruptive equivalents (i.e., clast size and shape unmodified by weathering/erosion; transport and final deposition by syneruptive sedimentary processes), which are indicated by the prefix 'reworked' (e.g., reworked pyroclastic breccia)

[4] composed exclusively of volcanic-rock clasts; clast size and shape modified by weathering/erosion; transport and final deposition by sedimentary processes

[5] composed of polymictic clasts created and/or extensively modified by weathering/erosion; transport and final deposition by sedimentary processes

become quite irregular and bedding symbols on the map of Stockwell (1938) indicate shallow, locally opposing dips, perhaps indicating the presence of a shallow-plunging antiformal culmination (e.g., Davies, 1953). Unfortunately, bed forms appear to be lacking in the southernmost portion of the IL unit (Davies, 1953); hence, the internal stratigraphy and structural geometry of the IL unit remain poorly understood. As shown on Figure 6, the northern portion of the IL unit is at least 2.5 km thick.

The IL unit is intruded from the west by a tonalite pluton of the Ross River plutonic suite, and is conformably overlain to the north by pillowed flows of MORB-like basalt that define the western extent of the Rainy Lake road (RLR) unit. Here, the contact is intruded by a thick sill of MORB-like gabbro that is also included in the RLR unit, and all of these rocks are overlain to the west by the San Antonio assemblage along a structurally modified angular unconformity. South of Rice Lake, the IL unit is discordantly cut by a swarm of northeast-trending dikes composed of MORB-like diabase that are interpreted to represent feeders to the overlying RLR unit, and are thus taken to indicate a depositional contact relationship. The Ross River pluton intrudes the IL unit from the east and south. Crosscutting dikes of porphyritic granodiorite, which generally have sharp, planar contacts and well-developed chilled margins, are abundant in the IL unit and are interpreted to be comagmatic with the Ross River plutonic suite. The contact between the IL unit and the lower, on-strike portion of the RLR unit to the east is obscured by later intrusions, which include an irregular, northwest-trending apophysis of the Ross River pluton. Significantly different lithofacies characterize the RLR and IL units on either side of the apophysis. Hence, the IL and RLR units are described separately, although it is possible that the IL unit and at least the lowermost portion of the RLR unit are age equivalent.

Heterolithic pebble to boulder volcanic conglomerate (unit 4)

The base of the IL unit consists of a monotonous succession of heterolithic pebble to boulder volcanic conglomerate that is at least 1.0 km thick. On the scale of individual outcrops, the volcanic conglomerate is typically massive, although significant variations in average clast size and proportion of matrix, apparent from outcrop to outcrop, indicate that these rocks are stratified on a macroscopic scale. The conglomerate ranges from matrix to clast supported and is composed of subangular to well-rounded, unsorted, generally equant clasts that range up to 50 cm in maximum dimension, but are typically

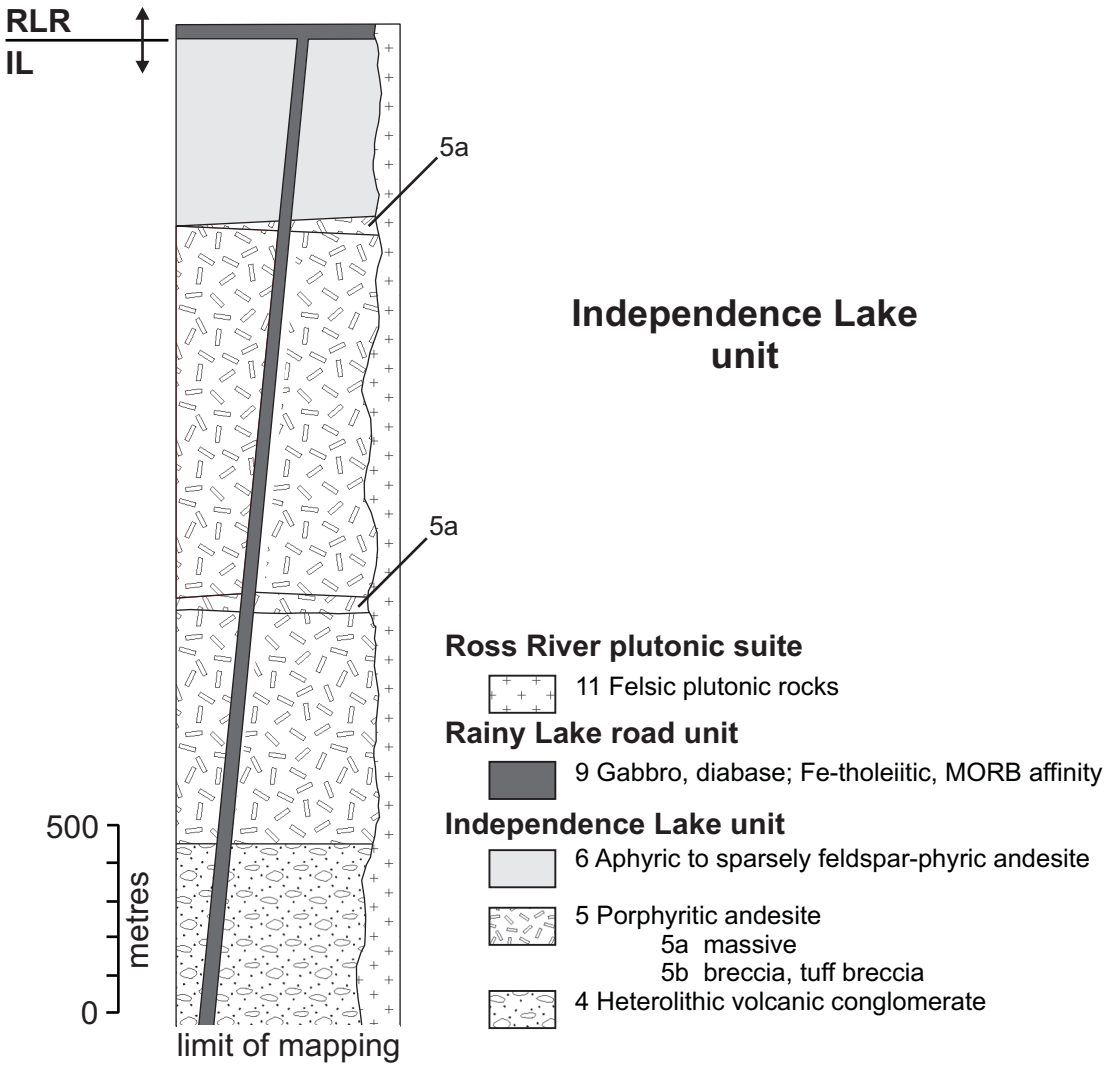

Figure 6: *Schematic stratigraphic column for the Independence Lake (IL) unit. Unit numbers correspond to those in the text and on Map GR2008-1-1.*

2–20 cm across (Figure 7). Slightly elongate clasts define a weak to moderate planar fabric in most outcrops. The majority (~80%) of clasts consist of light grey to buff, feldspar-phyric, intermediate to felsic volcanic material, with subordinate clasts of dark green-brown basalt (up to 5%) and pink-white rhyolite (up to 10%). The matrix consists of dark grey-green, fine- to medium-grained feldspathic sandstone that contains up to 10% fine-grained chlorite and sericite. Visible quartz is rare in both clasts and matrix. Much of this unit was mapped as dacite breccia and crystal tuff by Davies (1963), and was interpreted to be pyroclastic. However, the heterolithic clast populations and abundance of rounded to well-rounded clasts suggest significant subaerial transport. Coupled with the crudely stratified nature, these characteristics are indicative of debris flows deposited in a subaerial or shallow-marine setting on the flank of an intermediate volcanic centre.

Porphyritic andesite (unit 5)

The epiclastic rocks of unit 4 are overlain to the north by a heterogeneous unit of porphyritic andesite that ranges from 1.0 to 2.0 km thick. The contact is presumed to be depositional. The andesite is pale green-grey to buff on weathered surfaces, darker green-grey on fresh surfaces, and typically exhibits a coarse seriate-porphyritic texture (Figure 8a) defined by tabular to equant, white to greenish grey feldspar phenocrysts that range from 1 to 7 mm in length, and are evenly distributed in a darker green-grey aphanitic matrix. The phenocrysts are typically euhedral to subhedral, but include rare examples of well-rounded anhedral crystals, and locally account for up to 40% of the rock (typically 5–15%). In thin section, the phenocrysts are moderately saussuritized and commonly display prominent oscillatory zoning. The matrix consists of very fine grained feldspar, with subordinate chlorite, sericite, carbonate and zoisite.

The porphyritic andesite is subdivided into two textural varieties. Stockwell (1938) mapped several laterally continuous, sill-like bodies of massive porphyritic andesite (subunit 5a) in the area south of Rice Lake, the largest of which are shown on Map GR2008-1-1. He interpreted these rocks as intrusive on the basis of local crosscutting relationships and the presence of chilled margins, and considered them to be the hypabyssal equivalents to associated breccia and tuff breccia (subunit 5b) and composed of texturally similar andesite. These fragmental rocks vary from matrix to clast supported and generally consist of unsorted, angular to subrounded, blocky clasts of porphyritic andesite that are typically 2–30 cm across, but locally range up to 1.0 m (Figure 8b). The matrix is similar in texture and composition to the clasts, but typically exhibits subtle differences in proportion and size of feldspar crystals. Although generally monolithic, some outcrops contain rare subrounded clasts of aphanitic black rhyolite (Figure 8b). The close association of very coarse monolithic breccia units and massive hypabyssal intrusions in this portion of the IL unit is suggestive of block-lava andesite flows, which are described from active intermediate volcanic centres (e.g., Cas and Wright, 1987). Monolithic andesite breccia and tuff breccia in the northwestern portion of this unit locally exhibit a metre-scale stratification defined by variations in the proportion and size of generally more rounded clasts (Figure 8c), suggesting local subaerial reworking. Along the south shoreline of Rice Lake, these rocks are overprinted by a penetrative phyllonitic cleavage that dips steeply north and is defined by fine-grained sericite and chlorite. The resulting phyllonite is about 100 m thick and can be traced along strike for 1.5 km to the west, where it is interpreted to define the trace of the Gold Creek Shear Zone.

Aphyric to sparsely feldspar-phyric andesite (unit 6)

This unit crops out along the western margin of the Ross River pluton in the northeastern portion of the IL unit, and is defined to include two main masses, separated by an irregular intrusion of porphyritic granodiorite (unit 11; Figure 3). Only the northern mass of unit 6 was examined during the present study (subunit 6a), and the observations described below are based on examinations of heavily lichen-covered outcrops along the power line east of Rice Lake, as well as a detailed examination of a single outcrop located 800 m east of Rice Lake on the north side of Papineau Creek. This latter outcrop was stripped, washed and mapped in detail for this study. Although previously mapped as massive to brecciated rhyolite (Stockwell, 1938; Davies, 1963), the field characteristics of this mass are

Figure 7: *Outcrop photograph of volcanic conglomerate of map unit 4, Quesnel Lake access road, southeast of Red Rice Lake: heterolithic, unsorted and clast-supported conglomerate, with subangular to rounded, pebble- and cobble-size clasts.*

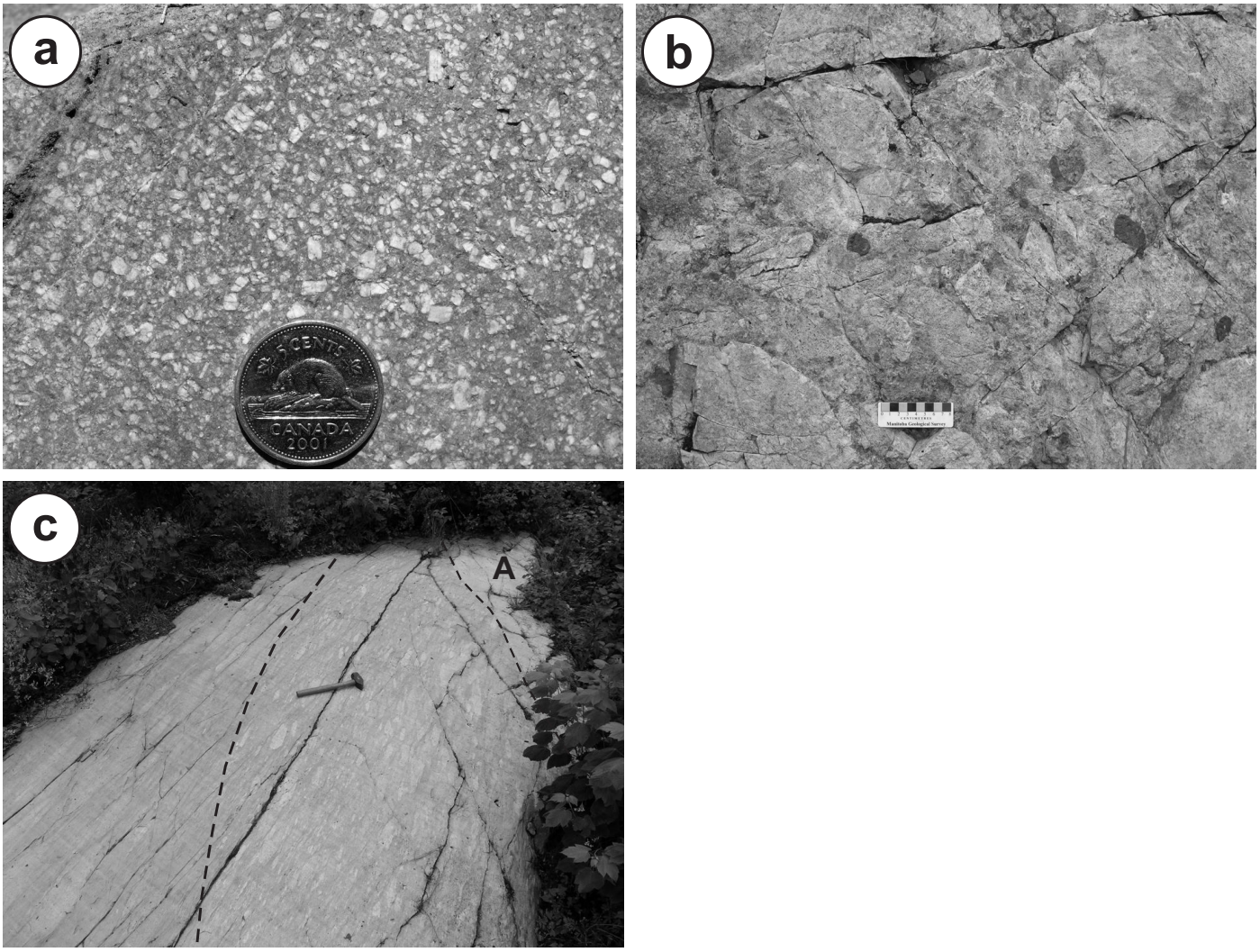

Figure 8: *Outcrop photographs of rock types in map unit 5, northeast of Red Rice Lake:* ***a)*** *massive porphyritic andesite (subunit 5a);* ***b)*** *clast-supported andesite breccia, with minor clasts of black rhyolite (subunit 5b);* ***c)*** *reworked andesite breccia; note faint stratification (indicated by dashed line on left) and discordant andesite dike (A, contact indicated by dashed line at upper right).*

herein considered to be more consistent with rocks of intermediate composition, which have been bleached and altered as a result of contact metamorphism during emplacement of the Ross River pluton. This altered material is characterized by pervasive hackly fracture and, as a result, is typically strongly weathered and rubbly, and was therefore not sampled for geochemical analysis. Stockwell (1938) mapped the southern mass of unit 6 as massive to brecciated porphyritic basalt (subunit 6b) and described contact relationships that appear to be most consistent with a very high-level intrusion. The generally irregular boundaries of this mass and the younger granodiorite intrusions are taken directly from Stockwell's maps, and the interested reader is referred to his report (Stockwell, 1938) for good descriptions of the geology and contact relationships in this area.

The andesite is aphanitic to fine grained, aphyric to sparsely feldspar phyric, and weathers light grey to buff to rusty brown, with dark green fresh surfaces. The porphyritic andesite contains 1–5% euhedral to subhedral feldspar phenocrysts that range up to 3 mm long and are evenly distributed in a darker green, fine-grained matrix of feldspar and chlorite. In places, these rocks contain rare, subhedral to rounded aggregates of chlorite and epidote that range up to 5 mm in maximum dimension and appear to represent either flattened amygdules or pseudomorphic replacements after amphibole or pyroxene phenocrysts. Subunit 6a consists of andesite flows, which vary in texture from massive to brecciated to locally pillowed. The latter contain vague, bun-shaped pillows, up to 50 cm in maximum dimension, with bleached selvages <1 cm thick (Figure 9a). The stripped outcrop along Papineau Creek exposes a massive flow of aphyric andesite that is at least 4 m thick and is overlain to the north by a crudely stratified interval of monolithic andesite breccia and tuff breccia (Figure 9b). The breccia consists of unsorted, very angular to angular, locally shard-like clasts of andesite up to 50 cm across in a dark green to rusty brown, chloritic matrix. On the basis of the high proportion of fine-grained matrix material and the shard-like aspect of the andesite clasts, these rocks are interpreted to represent hyaloclastic breccia and tuff breccia. The flow andesite is discordantly crosscut by a distinctive heterolithic breccia that is interpreted to represent a clastic dike sourced from the overlying TS unit and therefore described in detail with unit 12 of the TS unit. Farther south along the power line, the andesite flows are intercalated with stratified intervals of monolithic to heterolithic breccia, tuff breccia and lapilli tuff composed mainly of

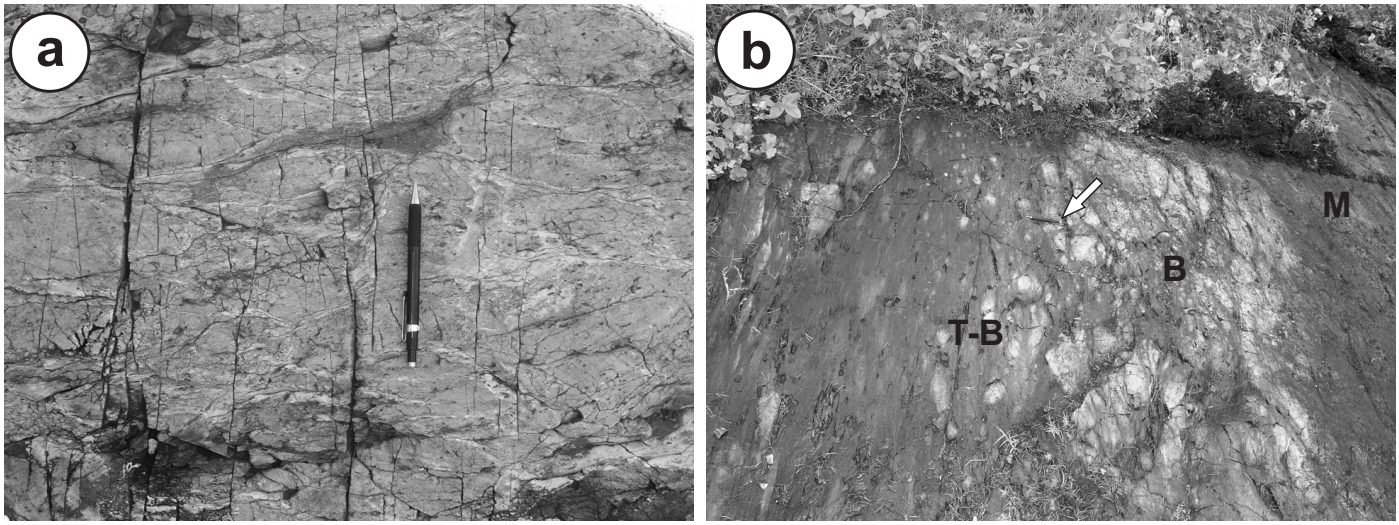

Figure 9: *Outcrop photographs of rock types in map unit 6, east of Rice Lake:* ***a)*** *aphyric andesite with vague pillow-like structures (subunit 6a);* ***b)*** *massive aphyric andesite (M, right) overlain by monolithic andesite breccia (B, middle) and tuff breccia (T-B, left); note pencil for scale (indicated by arrow).*

angular clasts of mafic to intermediate volcanic material. The distinct and apparently abrupt change from the crystal-rich, mainly fragmental andesite of unit 5 to the crystal-poor, mainly flow andesite of unit 6 is in keeping with a fairly dynamic, vent-proximal depositional setting within an evolving andesitic volcanic centre.

Rainy Lake road unit

The Rainy Lake road (RLR) unit is best exposed in clean outcrops along the Rainy Lake logging road, which branches to the south off Provincial Road (PR) 304 approximately 7.5 km east of Bissett (Figure 3). East of Rice Lake, the RLR unit is composed of three distinct packages of supracrustal rocks (units 7, 8 10) that dip moderately to the northwest and are intruded by abundant and voluminous sills of MORB-like gabbro (unit 9). Here, the unit ranges up to at least 2.5 km thick (Figure 10). At Rice Lake, only the uppermost package of supracrustal rocks is exposed, and the unit is less than 200 m thick. Despite its

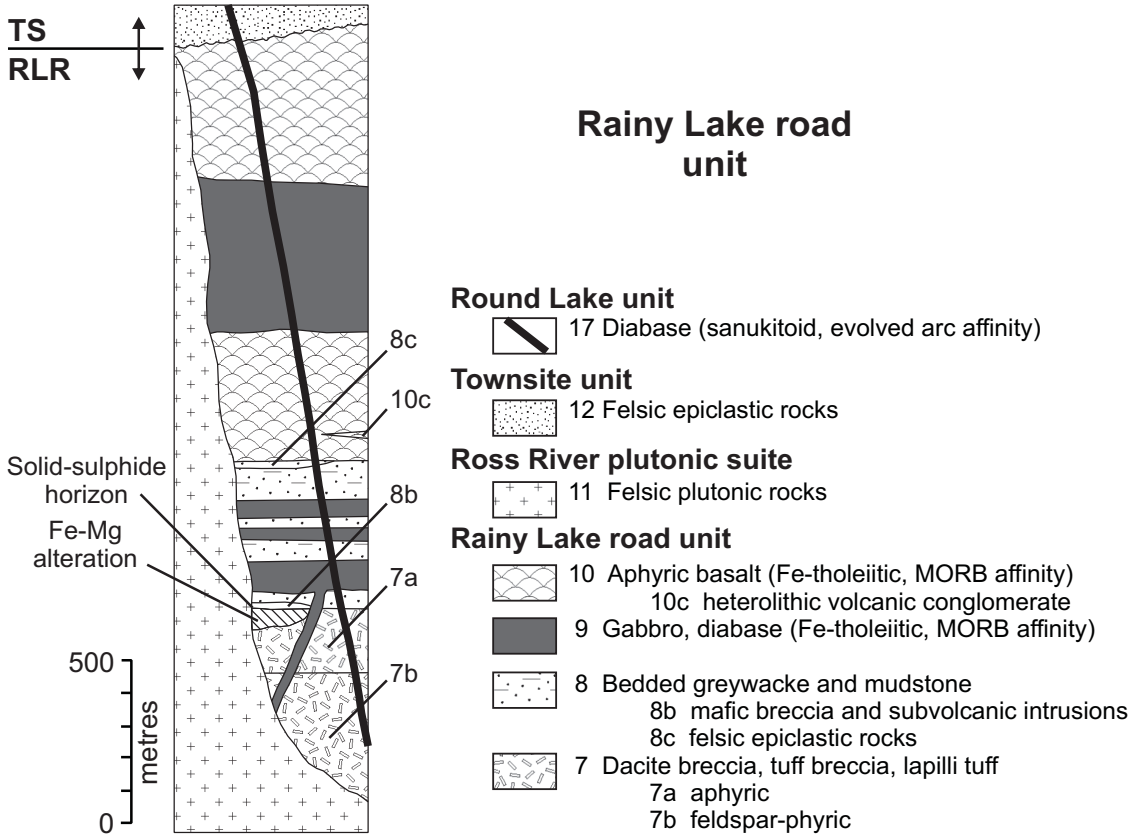

Figure 10: *Schematic stratigraphic column for the Rainly Lake road (RLR) unit. Unit numbers correspond to those in the text and on Map GR2008-1-1.*

proximity to the regional-scale WSZ, the main body of this unit is characterized by an anomalously low state of strain, and thus contains well-preserved primary features. Younging criteria indicate that these rocks are upright.

Supracrustal rocks in the upper portion of RLR unit record subaqueous sedimentation and effusive mafic volcanism within a restricted basin that is interpreted to have formed in the hangingwall of a synvolcanic subsidence structure (*see* below). The lower portion of the RLR unit and the potentially equivalent rocks in the IL unit represent the substrate to this basin. The RLR unit is intruded from the south by the Ross River pluton (unit 11). To the north, the contact with the Townsite (TS) unit coincides with the trace of the Normandy Creek Shear Zone (NCSZ) and is unexposed. Nevertheless, several lines of evidence indicate that these units lie in depositional contact. South and east of Rice Lake, the IL and RLR units contain abundant dikes of porphyritic granodiorite, which range up to 15 m thick and are correlated with the ca. 2.73 Ga Ross River plutonic suite. These dikes are not observed in the overlying TS unit. Instead, the base of the TS unit consists of a thick succession of felsic epiclastic rocks composed of texturally and geochemically similar rhyolite that has been dated at 2729 ±3 Ma (Turek et al., 1989). Likewise, the RLR and TS units contain dikes of sanukitoid-affinity diabase that is geochemically indistinguishable from mafic tuff in the overlying Round Lake unit. These relationships are interpreted to indicate that the RLR, TS and Round Lake units are a stratigraphic succession and are thus separated by depositional contacts.

A pronounced angular discordance between the TS unit and at least the lower portion of the RLR unit is indicated by facing criteria on either side of the NCSZ, where bedding in these units faces in opposite directions on the first regional cleavage, indicating that the angular discordance existed prior to the first regional deformation. Syn- to early-post–depositional tilting of the RLR unit in the hangingwall of a subsidence structure would readily explain this discordance, and is in keeping with the observed lithofacies and basin geometry. Although it is not possible to entirely rule out a fault contact, any such fault would have to be a low-angle structure that predated the basal unconformity of the San Antonio assemblage, which stitches this contact to the west.

Porphyritic to aphyric dacite (unit 7)

The base of the RLR unit consists of a succession of dacitic volcaniclastic and minor epiclastic rocks that is at least 1 km thick. The dacite is light grey or white on weathered surfaces, and dark grey to black on fresh surfaces. In the upper 200 m of the unit, the dacite is generally aphyric or sparsely quartz phyric (subunit 7a; Figure 11a), whereas that in the lower portion is distinctly feldspar phyric and contains 5–20% euhedral feldspar crystals (subunit 7b; Figure 11b). These crystals are typically 0.5–2 mm long, but locally range up to 10 mm, and are evenly distributed in a siliceous, dark grey or black, aphanitic matrix. The dacite typically exhibits coarse fragmental textures and consists predominantly of intercalated breccia and tuff breccia, with minor lapilli tuff. The breccia units are typically monolithic, matrix supported and unsorted, and contain angular to subrounded fragments up to 50 cm across. The fragments range from equant to tabular, and locally exhibit distinctly finer grained, almost vitreous margins and a delicate, shard-like morphology that are suggestive of primary volcanic fragmentation. In most outcrops, the matrix is of very similar texture and composition to the fragments; it is possible that at least some of these rocks are, in fact, massive dacite flows, with 'false' pyroclastic textures (Allen, 1988) produced by the combined effects of devitrification and hydrothermal alteration. The breccia units contain rare intercalations, up to 5 m thick, of well-bedded volcanic sandstone and mudstone, with minor chert (subunit 7c). Individual beds range up to 10 cm thick and locally exhibit normal size grading. The overall characteristics of this unit are interpreted to indicate minor subaerial reworking of primary volcanic material, with final deposition in a shallow subaqueous environment, likely via debris-flow mechanisms. These rocks are similar in some respects to the volcanic conglomerate of the IL unit, and may represent a more proximal age equivalent.

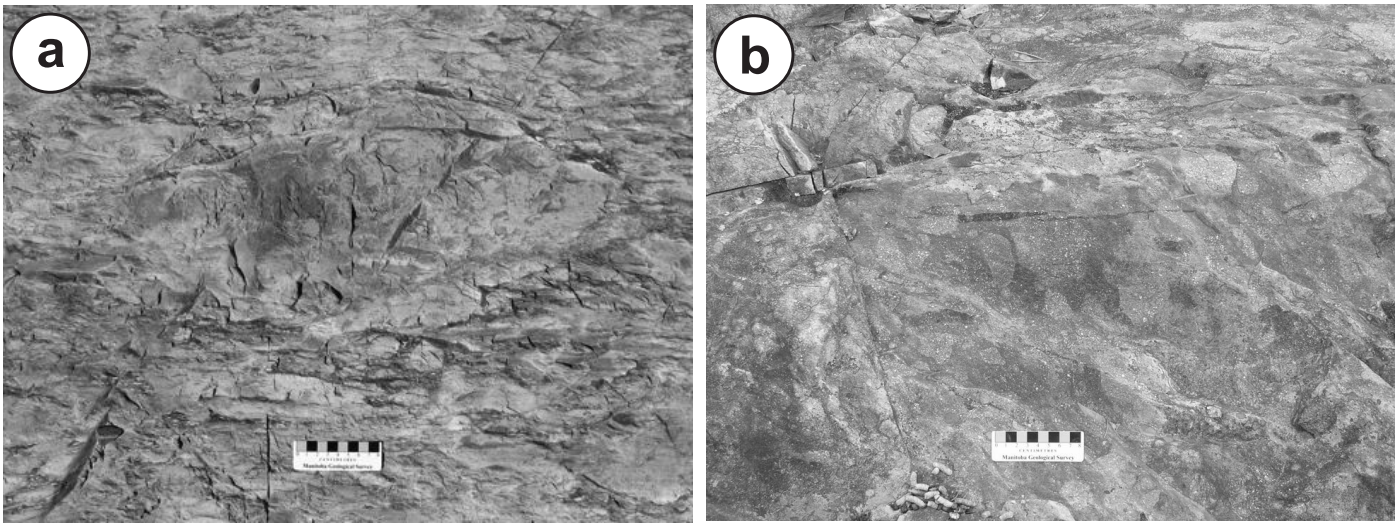

Figure 11: *Outcrop photographs of rock types in map unit 7:* ***a)*** *aphyric dacite breccia, Rainy Lake road;* ***b)*** *porphyritic dacite breccia, north margin of the Ross River pluton, east of the Rainy Lake road.*

Bedded greywacke and mudstone (unit 8)

The dacitic volcaniclastic rocks are overlain to the north by a distinctly heterogeneous, approximately 450 m thick succession that is interpreted to record deposition in an actively subsiding marine basin. The base of this unit is marked by an abrupt change from mainly high-energy, debris-flow sedimentation (unit 7) to mainly density-flow sedimentation in a relatively low-energy subaqueous setting, suggesting that basin infilling may have been preceded by a relatively abrupt subsidence event. Well-bedded greywacke and mudstone (subunit 8a) are the characteristic rock types of the basin fill, and contain subordinate intercalations of sulphidic cherty mudstone, massive to pillowed basalt flows, and felsic epiclastic rocks. The latter appear to include a significant component of resedimented pyroclastic material. Sills and dikes of fine- to medium-grained MORB-like gabbro account for at least 40% of this unit, and range up to 80 m thick.

On the Rainy Lake road, the base of unit 8 is marked by an interval of brecciated basalt (subunit 8b) that is at least 30 m thick and is intruded by abundant hypabyssal sills and dikes of MORB-like basalt (Figure 12a). The breccia consists of angular, blocky, locally interlocking fragments of fine- to medium-grained basalt, which range up to 50 cm across. Up to 5% of the clasts consist of angular fragments of aphyric dacite, which were presumably derived from the underlying dacitic volcaniclastic unit. The matrix typically accounts for less than 10% of the breccia and consists of very fine grained chloritic tuff. Chilled margins are observed on one or more sides of several of the basalt fragments, and the breccia is cut by dikes and sills of texturally similar, though coarser grained, basalt with relatively thick (5–15 cm) chilled margins. The breccia and dikes are interpreted to represent a flow-lobe autoclastic breccia and associated subvolcanic feeders, and indicate that initial basin infilling was accompanied by effusive mafic volcanism.

Moderate to strong, fracture-controlled (i.e., stringer-style) chlorite-garnet alteration is observed in outcrops of aphyric dacite breccia in the immediate footwall of the mafic breccia along the Rainy Lake road (Figure 12b), and is also described in the drill log for diamond-drill hole F-83-04, which was collared a short distance along strike to the southwest to test a stratiform induced-potential anomaly (Assessment File 93163). In this drillhole, the basal contact of unit 8 is marked by a 1.5 m thick layer of faintly layered solid sulphide (pyrite; Figure 12c). Below the contact, the drillhole intersected a 38.65 m interval of moderate to intense chlorite-garnet-pyrite alteration in dacite breccia. Intercepts of unaltered 'feldspar porphyry' in this interval, which most likely correspond to the porphyritic granodiorite dikes described herein (subunit 11d), indicate that the alteration is syngenetic. Above the contact, the solid sulphide is overlain by a 15.53 m interval of laminated, sulphidic (pyrite-chalcopyrite) sedimentary rocks. Assay samples of the mineralized rocks returned negligible Au, Cu and Zn values. Nevertheless, these features indicate that basin subsidence and initial infilling were at least locally accompanied by hydrothermal circulation and discharge (exhalation), and the stringer chlorite alteration is suggestive of close proximity to a fault-controlled discharge site. The localization of these features near the west margin of the basin infill succession supports the inference of a synvolcanic subsidence structure in this location.

North of the mafic breccia, unit 8 consists predominantly of interbedded cherty mudstone and medium- to coarse-grained, pebbly feldspathic greywacke (Figure 12d). These rocks are characterized by well-developed planar bed forms that are typically 5–30 cm thick, but locally range up to 50 cm. The beds generally dip at moderate angles to the northwest. Normal-graded beds, load casts (Figure 12e) and local cross-beds indicate that these rocks are upright. The proportions of mudstone and greywacke are highly variable: some outcrops consist mainly of thin-bedded to laminated cherty mudstone with less than 10% greywacke beds, whereas other intervals consist mainly of greywacke with only minor mudstone. The greywacke typically contains 5–20% subhedral feldspar granules and up to 5% anhedral quartz granules. Individual beds typically show sharp basal contacts, fining-upward grain size and transitional tops. Highly contorted and disrupted bed forms are common and are interpreted to represent slump structures (Figure 12d). Many beds have a basal lag conglomerate composed of tabular rip-up clasts of mudstone and chert, whereas some distinctive beds consist of up to 90% mudstone rip-up clasts in a matrix of coarse-grained feldspathic greywacke. These features are indicative of subaqueous deposition from downslope turbidity flows, most likely in a relatively quiescent setting that was characterized by periodic intervals of sediment starvation.

Pillowed basalt is exposed in two locations near the top of the unit, and occurs as 5–10 m thick flows within intervals of bedded greywacke and mudstone. The basalt is light green-grey to dark brown-green, very fine grained, aphyric and nonamygdaloidal, and forms bun-shaped pillows up to 50 cm across. The pillow selvages are less than 2 cm thick. Interpillow material accounts for up to 5% of the rock and consists of laminated cherty mudstone and carbonate, with minor chloritic hyaloclastic tuff and lapilli tuff

In one location, coarse-grained pebbly greywacke is interstratified with buff to light grey, very fine grained, siliceous sandstone, which occurs as individual beds up to 10 cm thick or is thinly interbedded with grey-black cherty mudstone in discrete intervals up to 1.5 m thick. The siliceous sandstone beds are generally massive, with sharp basal contacts and transitional tops, and have a distinctive powdery appearance that is suggestive of volcanic ash. Local examples of normal size-grading and scour-and-fill structures indicate that these beds were most likely deposited as subaqueous turbidity flows. Locally, the beds contain angular to subrounded pebbles (2–5 mm) of light grey, slightly porous, siliceous material that are concentrated in diffuse lags in the middle to upper portions of otherwise massive beds (Figure 12f). These pebbles were presumably suspended within the primary turbidity flows because of their lower density and larger surface area relative to the matrix material; they are therefore tentatively interpreted as pumice lapilli. If so, the host beds may represent either subaqueous pyroclastic flow deposits or reworked pyroclastic material that was transported and deposited via turbidity flows (i.e., ash turbidites).

A sharp depositional contact, which is well exposed on the Rainy Lake road, separates unit 8 from the overlying pillowed

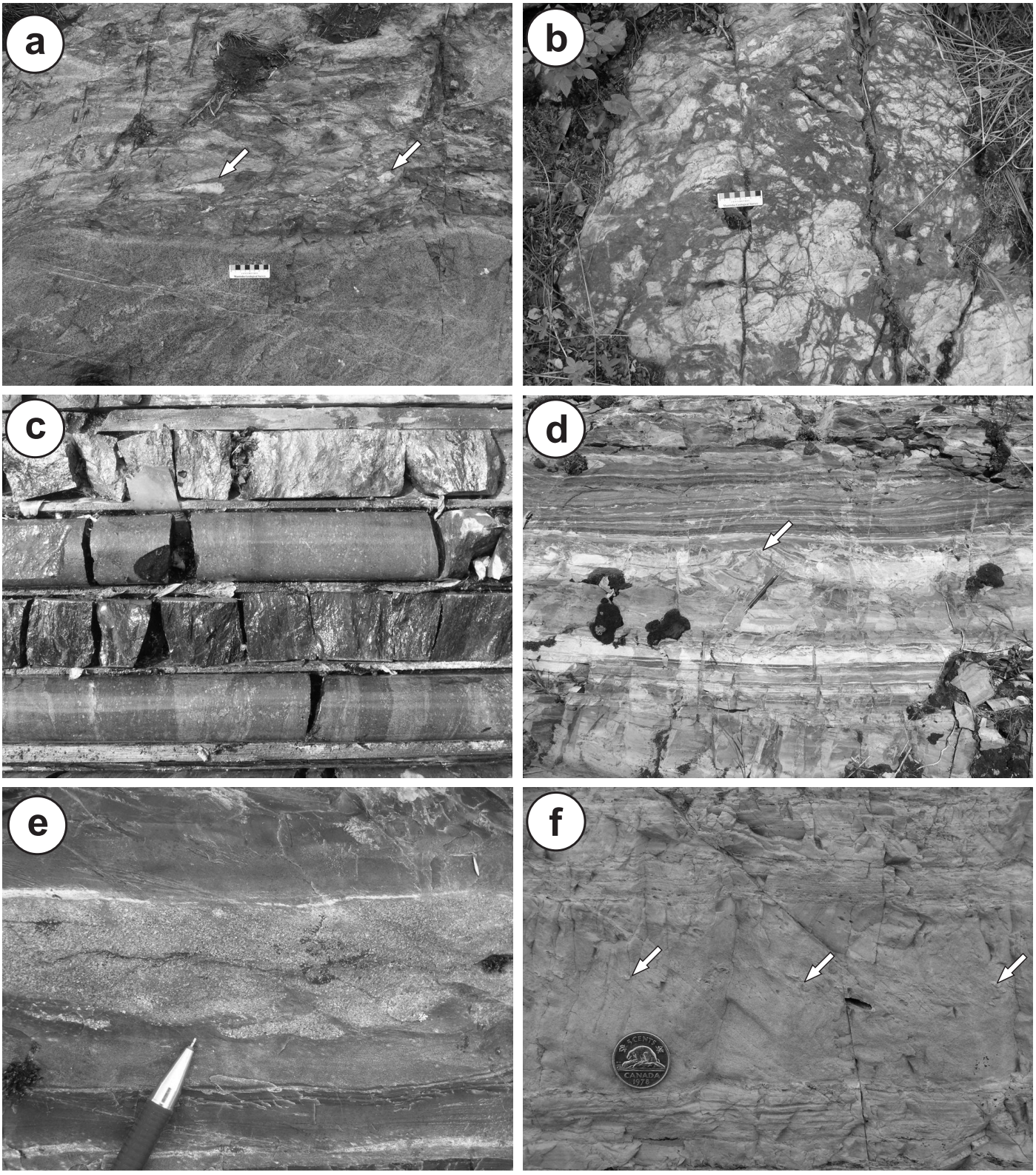

Figure 12: *Outcrop photographs of rock types in map unit 8, Rainy Lake road:* ***a)*** *basalt breccia (top; fragments of aphyric dacite indicated by arrows) cut by texturally similar basalt dike (bottom; note well-developed chilled margin just above scale card);* ***b)*** *fracture-controlled chlorite-garnet alteration in aphyric dacite breccia;* ***c)*** *solid sulphide layer (top) and chlorite-garnet alteration (bottom) in drillcore from diamond-drill hole F-83-04 (drillcore is 3.6 cm in diameter);* ***d)*** *thin-bedded to laminated feldspathic greywacke and cherty mudstone; note prominent slump folds in the light grey layer in the centre of the photograph (arrow; above pencil);* ***e)*** *load structures in thin-bedded greywacke-mudstone turbidites;* ***f)*** *possible concentration of pumice lapilli (arrows) in the upper portion of an otherwise massive bed of very fine grained siliceous sandstone.*

to massive basalt flows of unit 10. In this location, the top of unit 8 is marked by a well-stratified, 25 m thick section of felsic epiclastic rocks (subunit 8c), composed mainly of interbedded buff to pale grey, medium- to coarse-grained, pebbly volcanic sandstone, with subordinate black, laminated, sulphidic mudstone and heterolithic pebble conglomerate. The sandstone beds are typically 1–5 cm thick, but locally range up to 50 cm thick and, in one poorly exposed interval, may be up to 2.5 m thick. Individual beds contain up to 30% of 0.5–2 mm, subhedral feldspar crystals and lithic granules, and vary from massive to crudely stratified to normal size-graded. Local scours indicate that these rocks are upright.

The middle portion of this section contains a crudely graded layer of felsic volcanic conglomerate, which was sampled for U-Pb geochronological analysis to constrain the timing of basin infilling (sample 96-04-1285). This layer is 3.0 m thick and is marked at the base by a sharp undulatory contact that locally cuts down through an underlying bed of laminated black mudstone (Figure 13a). The lower 10 cm of the layer exhibits reverse size-grading, whereas a diffuse normal size-grading is apparent in the upper portion. The conglomerate is matrix supported and poorly sorted, and is composed of angular to subrounded, generally equant clasts that range up to 5 cm in maximum dimension, but are typically 0.2–2.0 cm across (Figure 13b, c). The matrix consists of grey-green, medium- to coarse-grained, crystal-lithic sandstone. The majority (90–95%) of clasts consist of dark grey to buff, feldspar-phyric dacite, with subordinate clasts of porphyritic andesite, aphyric to quartz-phyric rhyolite, felsic tuff (Figure 13d), amygdaloidal basalt, mudstone and solid sulphide. The dacite contains 5–10% euhedral feldspar crystals up to 2 mm long in an aphanitic, siliceous black matrix. The sulphide clasts are subangular to subrounded and consist mainly of massive, fine-grained pyrrhotite, with up to 10% chalcopyrite. Eutaxitic texture is locally developed and is defined by highly elongate, wispy fiamme of dark grey to purple, aphanitic, siliceous material, which may represent collapsed pumice lapilli (Figure 13c). Based on these aspects, this conglomerate is interpreted to represent a proximal,

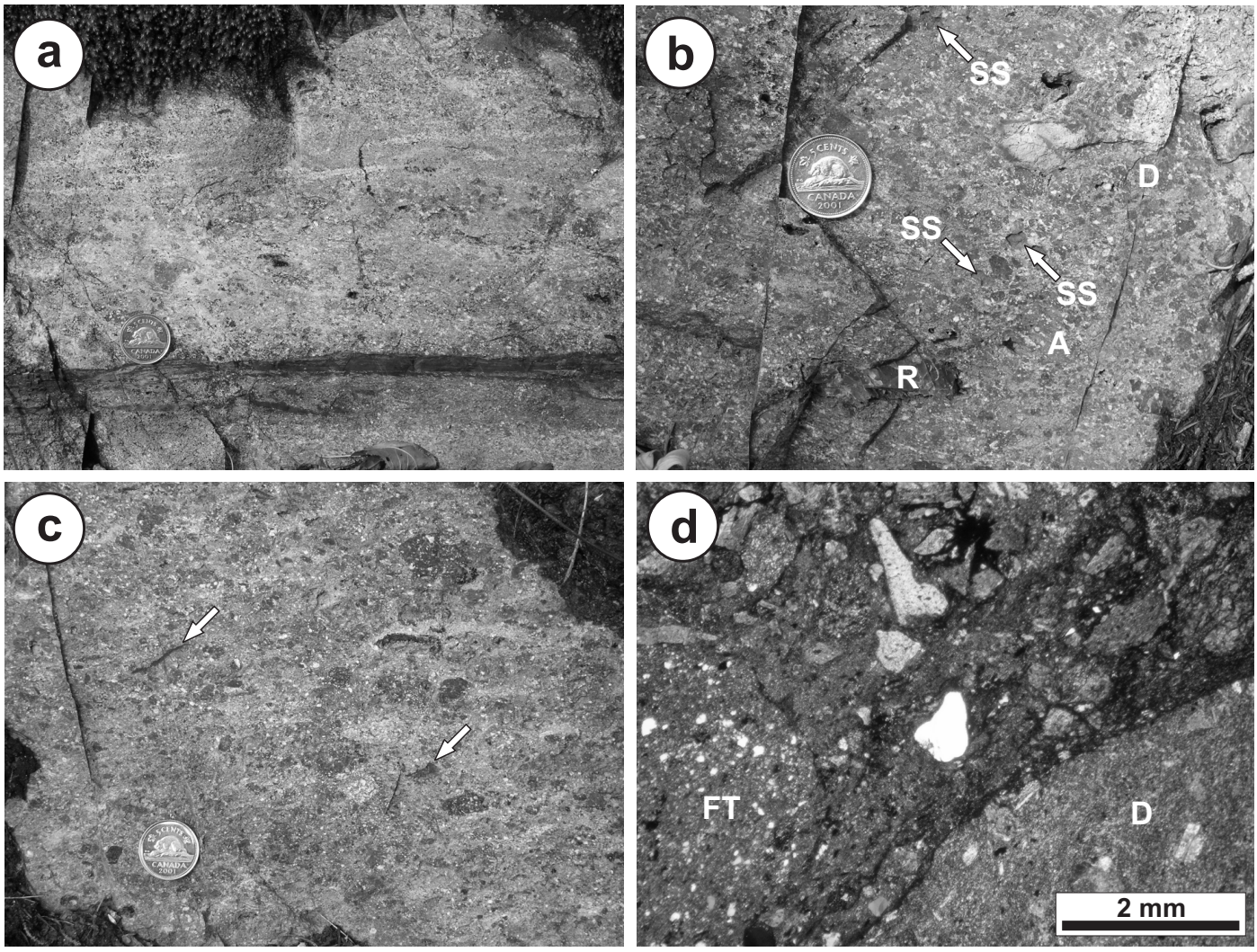

Figure 13: *Outcrop and thin-section photographs of felsic volcanic conglomerate layer at the top of unit 8, Rainy Lake road:* ***a)*** *scoured cherty mudstone layer that defines the base of the conglomerate;* ***b)*** *heterolithic pebble conglomerate composed mainly of porphyritic dacite clasts (D), with subordinate clasts of aphyric rhyolite (R), porphyritic andesite (A) and solid sulphide (SS);* ***c)*** *pebble conglomerate composed mainly of porphyritic dacite clasts, with possible collapsed pumice lapilli indicated by dark purple, siliceous fiamme (arrowed);* ***d)*** *thin-section photograph showing clasts of felsic tuff (FT) and porphyritic dacite (D) in a matrix of coarse-grained, crystal-lithic sandstone (cross-polarized light).*

subaqueous debris flow that includes a significant component of primary pyroclastic detritus. The sulphide clasts indicate coeval exhalative activity and a subaqueous source area for at least some of the detritus.

Gabbro, diabase (unit 9)

Sills and minor dikes composed of MORB-like gabbro (unit 9) are abundant and voluminous throughout the RLR unit, and are interpreted as the subvolcanic equivalents of the associated succession of MORB-like basalt flows (unit 10). Also included in unit 9 is a swarm of northeast-trending dikes composed of MORB-like diabase that cut the underlying IL unit south of Rice Lake. The largest outcrop area of gabbro extends east from Rice Lake and defines a concordant, lenticular intrusion that ranges from 0.1 to 1.2 km thick and is traced along strike for 9.0 km. This intrusion has been referred to as 'unit A' where it is exposed on islands in the south part of Rice Lake (e.g., Theyer, 1983). In the footwall of the thickest portion of this intrusion, Stockwell (1938) mapped a discordant apophysis of gabbro that is approximately 500 m thick and extends toward the southeast for 800 m, where it is cut by the Ross River pluton. As shown in Figure 14, the lenticular gabbro intrusion and discordant apophysis are clearly imaged by high-resolution aeromagnetic survey data (Geological Survey of Canada, 1986; *see also* Assessment File 73689). On the basis of their form, these intrusions are interpreted as a hypabyssal laccolith and feeder dike, the latter of which is interpreted to coincide with the subsidence structure.

The gabbro is typically fine to medium grained, massive and melanocratic, with a brown to green to purple-green weathered surface and a dark green fresh surface (subunit 9a). A subophitic texture is typical, and is defined by closely packed, 0.5–2.0 mm, subhedral, equant crystals of actinolite (after pyroxene) and 0.5–1.5 mm plagioclase laths (Figure 15a, b). In thin-section, remnants of primary pyroxene are observed in the cores of some actinolite crystals (Figure 15c). Most specimens contain 20–50% plagioclase and 1–2% deep blue quartz 'eyes'. Rare exposures of quartz gabbro contain up to 70% plagioclase and 10% blue quartz (subunit 9b). Accessory minerals include titanite, pyrite, pyrrhotite and magnetite, and the quartz gabbro is locally strongly magnetic. In many locations, the gabbro exhibits a seriate porphyritic texture defined by euhedral to subhedral, blocky phenocrysts of actinolite after primary pyroxene, which range from 2 to 7 mm across and impart a distinctive spotted appearance to the rock (Figure 15d). The gabbro also locally contains 5–10% subhedral plagioclase phenocrysts that range up to 2.0 cm long. Plagioclase glomerocrysts up to 2.5 cm across locally characterize the gabbro in the thickest portion of the laccolith (subunit 9c; Figure 15e). The different textural types of gabbro appear to be irregularly distributed, and igneous layering appears to be restricted to relatively narrow, likely composite dikes and sills. In some locations, leucocratic quartz gabbro forms irregular segregation pods or planar dikes in melanocratic gabbro. Where observed, the contacts of gabbro intrusions tend to be sharp and planar, with well-developed chilled margins that range up to 30 cm thick (Figure 15f). Diabase dikes in the IL unit range up to 40 m thick locally and generally have very well

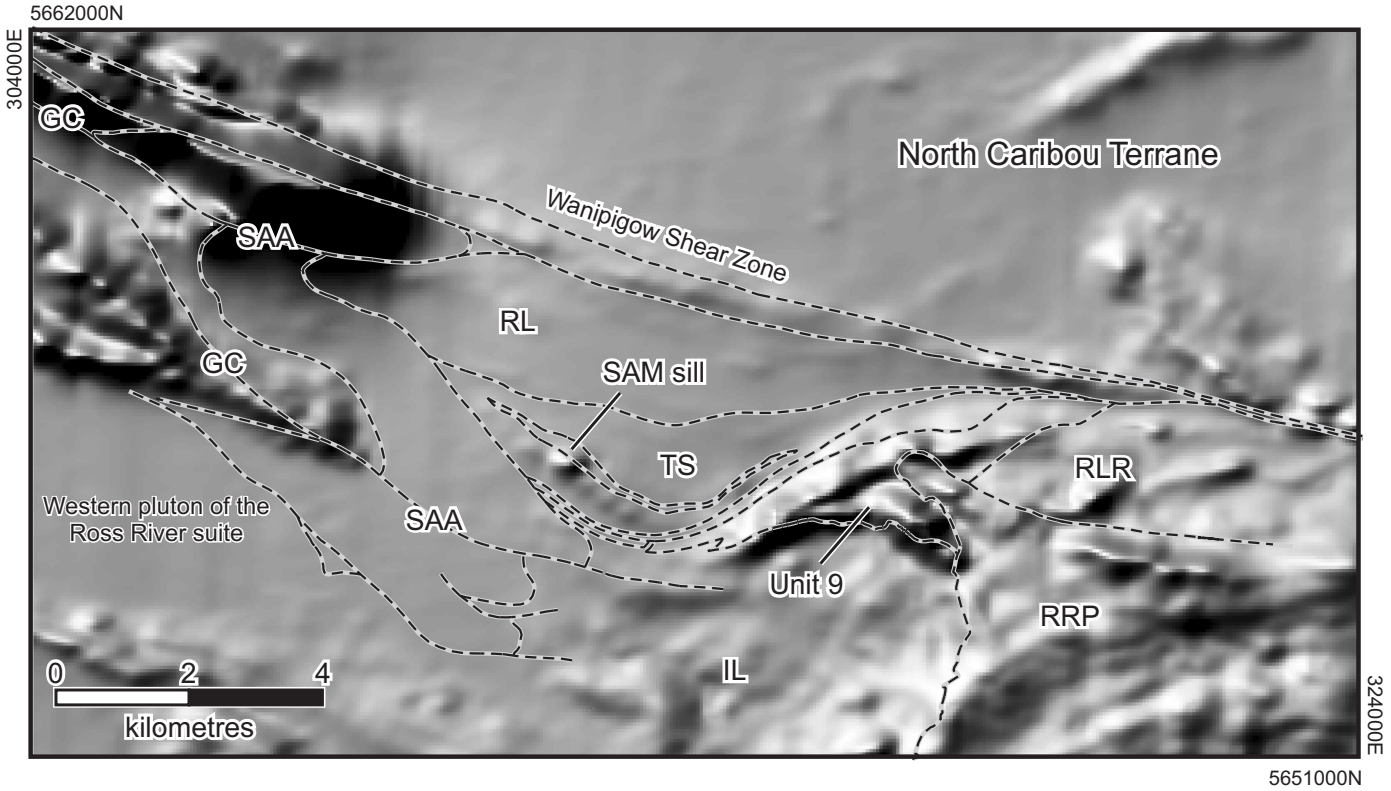

Figure 14: *Aeromagnetic total-field relief map of the Rice Lake area. Data from the Geological Survey of Canada (1986). Simplified contacts and faults shown as thin dashed lines. Abbreviations: GC, Gold Creek unit; IL, Independence Lake unit; RL, Round Lake unit; RLR, Rainy Lake road unit; RRP, Ross River pluton; SAA, San Antonio assemblage; SAM sill, San Antonio mine sill; TS, Townsite unit.*

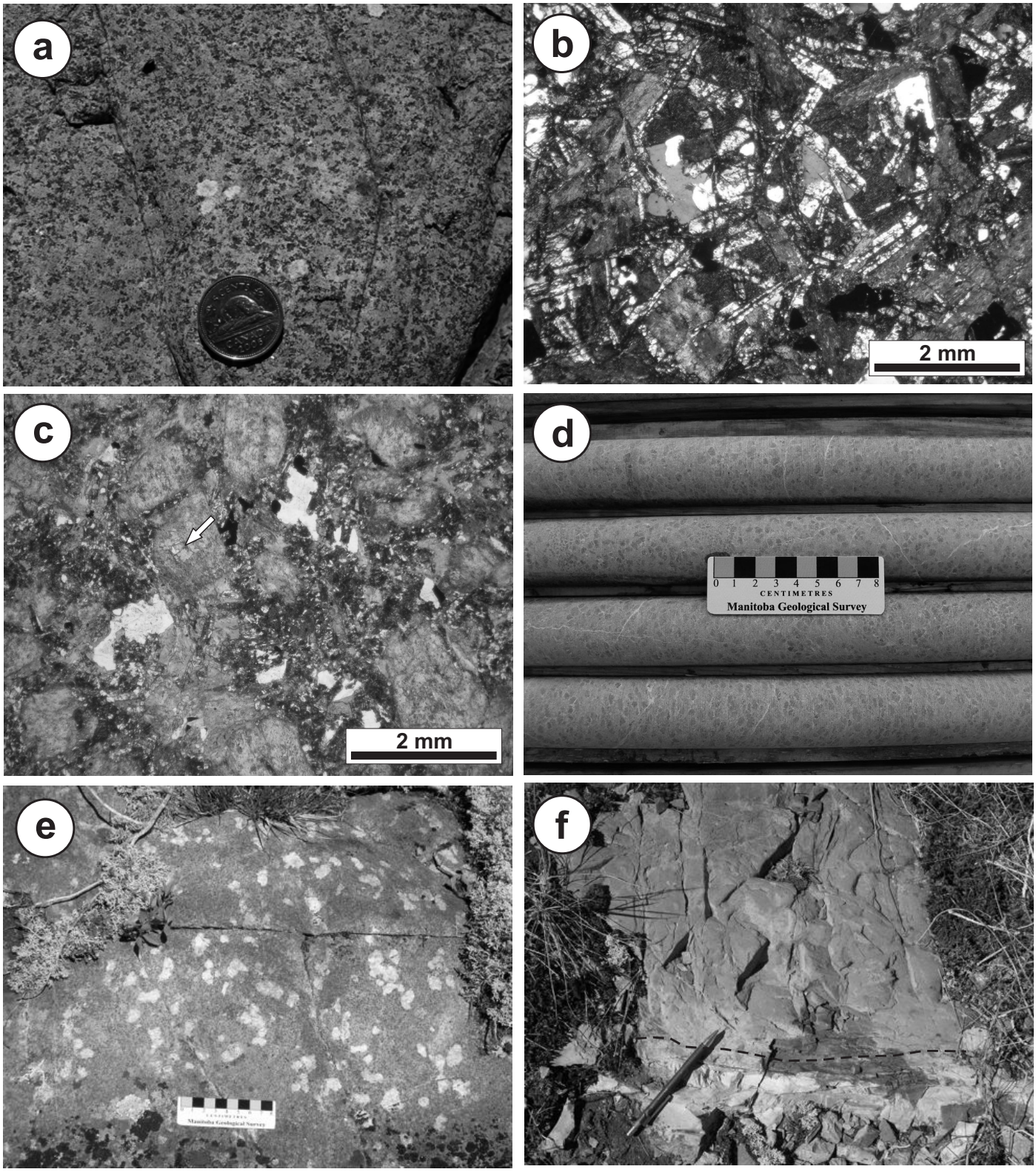

Figure 15: *Outcrop, thin-section and drillcore photographs of rock types in map unit 9, east of Rice Lake:* ***a)*** *subophitic texture in a slightly more leucocratic phase of the gabbro laccolith (note scattered plagioclase phenocrysts);* ***b)*** *equigranular, subophitic texture defined by plagioclase laths (light grey) and actinolite pseudomorphs after primary pyroxene (dark grey); sample contains 1–2% quartz (equant, anhedral white crystals); plane-polarized light;* ***c)*** *actinolite pseudomorphs after primary pyroxene in porphyritic 'spotted' gabbro; relict clinopyroxene indicated by arrow; plane-polarized light;* ***d)*** *porphyritic 'spotted' gabbro from the footwall of the SG-3 deposit (diamond-drill hole SN-03-6);* ***e)*** *glomerophyric gabbro in the lower portion of the gabbro laccolith, Rainy Lake road;* ***f)*** *sharp, planar contact (dashed line) between thin-bedded cherty mudstone (light grey; bottom) and melanocratic gabbro (dark grey; top), showing approximately 25 cm thick chilled margin on the gabbro.*

developed chilled margins, consistent with hypabyssal emplacement. Gabbro and diabase are cut by dikes of porphyritic granodiorite (subunit 11d).

Aphyric basalt (unit 10)

The top of the RLR unit consists of pillowed and massive flows of MORB-like basalt, with minor intercalations of basalt breccia and heterolithic epiclastic rocks. Pillowed basalt flows predominate and define two major flow complexes that are separated by the gabbro laccolith (Figure 3, 10). The lower complex is approximately 450 m thick and conformably overlies stratified epiclastic rocks (unit 8) in the hangingwall of the subsidence structure. The upper complex overlaps the subsidence structure and ranges from 50 to 200 m thick on the west to >600 m thick on the east. This lateral change in unit thickness is interpreted to result from synvolcanic subsidence (i.e., growth-faulting). At the SG-1 deposit, the uppermost portion of the upper flow complex contains minor intercalations of felsic epiclastic rocks that are indistinguishable from those at the base of the TS unit (units 12, 13); due to the very high finite strains recorded in these rocks, it is unclear whether these intercalations are primary (i.e., depositional) or structural. At least 50% of the thickness of this unit is made up of comagmatic gabbro intrusions, consistent with proximity to the subaqueous source vent.

The basalt is generally fine grained and aphyric, with a light green to brown weathered surface and dark green fresh surface. An intergranular texture is defined by acicular plagioclase crystals up to 1.5 mm long and equant aggregates of actinolite, chlorite and epidote after primary pyroxene or olivine (Figure 16a). Most samples contain weak to moderate carbonate alteration. Pillowed basalt (subunit 10a) predominates, and consists of slightly elongate to bun-shaped to amoeboid pillows that are typically 0.3–1.0 m across, but locally range up to 1.5 m (Figure 16b). Pillow cusps in several locations indicate that this unit youngs to the northwest. The pillow selvages are generally less than 2 cm thick and strongly chloritized. Fine-grained interpillow material accounts for 2–5% of the rock, and locally exhibits well-preserved quench-fragmentation textures (i.e., hyaloclastic tuff and lapilli

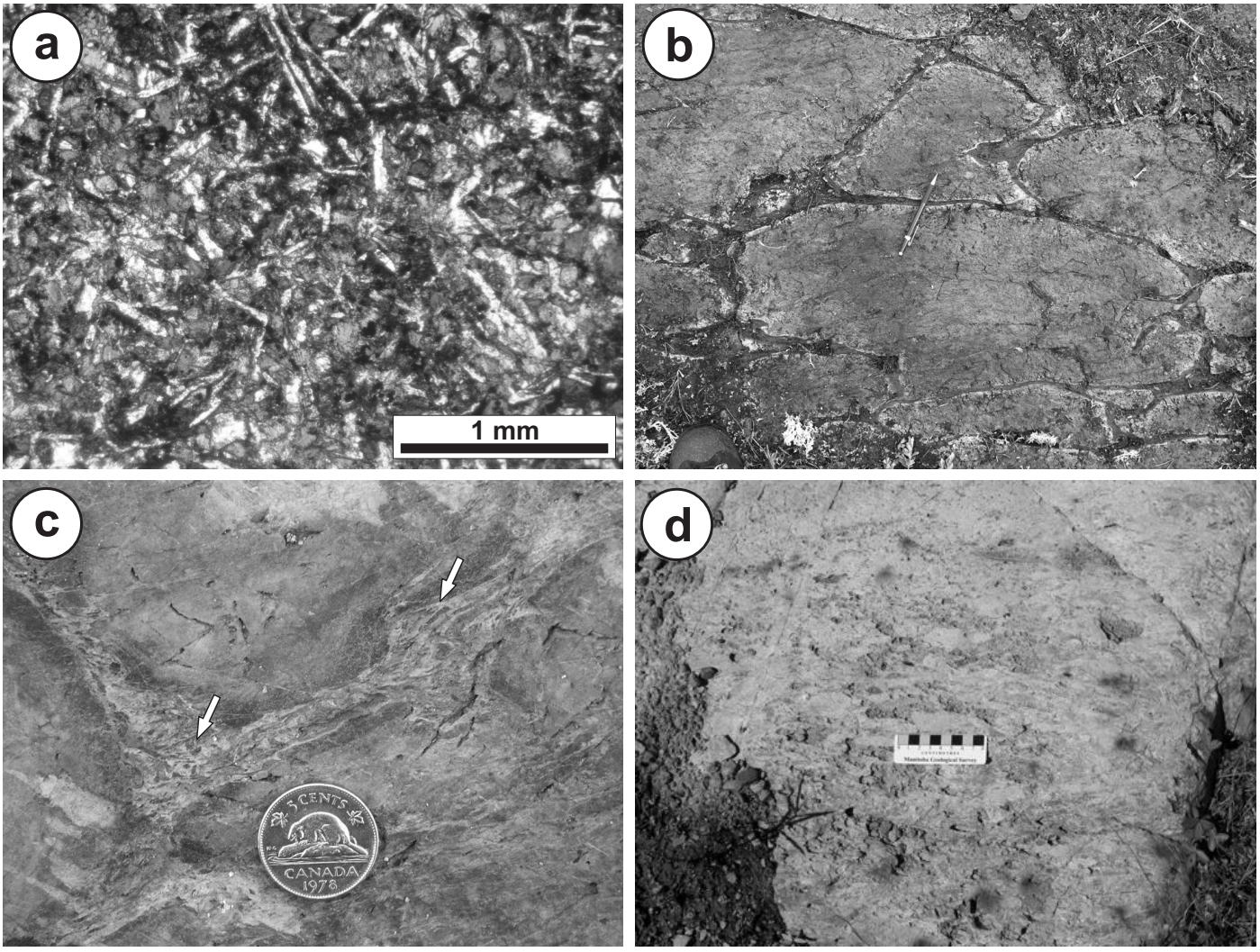

Figure 16: *Outcrop and thin-section photographs of rock types in map unit 10, east of Rice Lake:* ***a)*** *fine-grained intergranular texture defined by plagioclase laths (light grey) and actinolite pseudomorphs after primary pyroxene/olivine (plane-polarized light);* ***b)*** *pillowed basalt flow; cusp on large bun-shaped pillow in centre of photograph indicates tops to the north (north direction indicated by pencil);* ***c)*** *well-preserved interpillow hyaloclastite lapilli tuff (arrows);* ***d)*** *heterolithic pebble conglomerate within the thick succession of pillowed basalt flows exposed along the Rainy Lake road; dark spots on outcrop represent oxidized sulphidic pebbles.*

tuff; Figure 16c). The pillowed basalt is mainly nonamygdaloidal in the west, but the pillow margins in the east commonly contain 5–10% round quartz or calcite amygdules that are typically 2–5 mm in diameter but can range up to 1 cm. Massive flows of sparsely amygdaloidal basalt (subunit 10b) range up to 30 m thick and, in rare locations of continuous exposure, are observed to transition upward into pillowed flows. In general however, exposure is insufficient to determine the organization of these flows. Both flow types contain discontinuous intercalations of monolithic flow breccia. Heterolithic, clast-supported, pebble to cobble conglomerate is exposed in two locations (subunit 10c; Figure 16d). The eastern occurrence is bounded by pillowed basalt flows, whereas the western occurrence appears to form a large raft in the gabbro laccolith. Deformation state generally increases toward a 50–100 m thick zone of steeply dipping chloritic tectonite that defines the northern extent of this unit (i.e., the NCSZ; Figure 3).

Ross River plutonic suite

The Ross River plutonic suite is composed of tonalite and minor granodiorite, mainly disposed in two large plutons that crop out in the extreme southwestern and southeastern portions of the mapped area. Although extensively exposed to the west and east of the study area, only the marginal portions of these plutons were examined in detail by the author. Outside the study area, logging roads provide access to the internal portions, and clean exposures along these roads were briefly examined. The unnamed and undated western pluton is composed of tonalite that is interpreted to intrude the IL unit and, to the northeast, lies in sharp contact with the San Antonio assemblage along a well-exposed nonconformity, which was mapped and described by Stockwell (1945) and Davies (1963). Aeromagnetic data (e.g., Figure 14) indicate a remarkably homogeneous, possibly sheet-like intrusion that ranges from 3 to 6 km thick and is bounded to the south by the Manigotagan Shear Zone. The eastern pluton, which is known as the Ross River pluton (Paulus and Turnock, 1971), crops out over a roughly oval-shaped area of about 200 km^2 and intrudes both the IL and RLR units. Aeromagnetic data and reconnaissance mapping indicate that the Ross River pluton is likely a composite batholith consisting of two nested stocks, each of which is zoned outward from a granodioritic core to a tonalitic margin. Prominent apophyses composed of heterogeneous tonalite extend outwards toward the northwest and southeast, and impart a distinctive sigmoidal shape to the pluton. To the southwest, the pluton is truncated by the Manigotagan Shear Zone.

Felsic plutonic rocks (unit 11)

Biotite granodiorite (subunit 11a) of the Ross River plutonic suite occurs extensively only outside the study area but is described here for the sake of completeness. Outcrops of biotite granodiorite, examined by the author in the central portion of the Ross River pluton, coincide with a prominent oval-shaped area of low magnetic intensity that defines the core of the inner zoned stock. The granodiorite weathers pale pink-white and is light pinkish grey on fresh surfaces. In most outcrops, the granodiorite is massive and homogeneous with a medium-grained, equigranular to sparsely porphyritic texture (Figure 17a). The principal minerals are plagioclase (45–60%), quartz (25–35%), K-feldspar (10–15%) and biotite (5–10%). Biotite forms rare, euhedral to subhedral, locally hexagonal phenocrysts that are 5–10 mm across and, in thin section, are observed to contain delicate lattices of rutile needles. Other accessory minerals include zircon, apatite, titanite and pyrite. Hand specimens of this material are nonmagnetic. Alteration is evidenced by weak to moderate saussuritization of feldspar (Figure 17b) and minor replacement of biotite by epidote and chlorite. Here, the granodiorite lacks xenoliths, crosscutting veins or dikes, and mesoscopic deformation fabrics. A sample of this material was collected for U-Pb geochronological analysis (sample 96-03-RRP).

Biotite-hornblende tonalite, with minor granodiorite (subunit 11b), is the predominate rock type in the western pluton of the Ross River suite and the northwest margin of the Ross River pluton. These rocks weather buff to pale pink-white and are dark grey on fresh surfaces. The principal minerals are plagioclase (55–75%), quartz (15–30%), hornblende (<10%), biotite (<5%) and K-feldspar (<5%). Most outcrops are medium to coarse grained and homogeneous, although the textures range from hypidiomorphic-equigranular to seriate-porphyritic in places, with the latter type containing up to 15% plagioclase phenocrysts that range up to 1.5 cm across (Figure 17c). Subordinate phenocrysts include euhedral, black hornblende crystals up to 1 cm long and euhedral to subhedral (hexagonal) biotite crystals that range from 5 to 10 mm across. The western pluton locally contains 2–3% blue quartz. Accessory minerals include zircon, apatite, titanite and magnetite. Most hand specimens are moderately magnetic, and the tonalitic portions of the Ross River pluton are characterized by high magnetic intensity. Alteration is evidenced by weak to moderate saussuritization of feldspar and minor replacement of biotite and hornblende by epidote and chlorite. This alteration is locally intense along the margins of the plutons or in proximity to discrete ductile-brittle shear zones that locally contain auriferous quartz-carbonate-pyrite veins. Fracture-controlled epidote alteration is also common along the margins of the plutons.

Most outcrops contain a very weak to moderate planar fabric defined by elongate aggregates of mafic minerals. Xenoliths are only common along the north margin of the Ross River pluton (subunit 11c) and include large angular rafts of gabbro and felsic volcaniclastic rocks. The contact in this location is locally marked by a zone of intrusion breccia up to 200 m thick. Crosscutting dikes are very rare in the interior of the plutons and consist of aplite and minor quartz-feldspar porphyry. Along the margin of the Ross River pluton, Stockwell (1938) mapped and described mutual crosscutting relationships with irregular intrusions and dikes of porphyritic (feldspar-quartz±biotite±hornblende) granodiorite (subunit 11d; Figure 17d) that intrude the IL and RLR units south and east of Rice Lake. Stockwell (1938) also described a general northward decrease in number and size of porphyry dikes, with a coincident change from phaneritic to aphanitic matrix textures, and inferred that the dikes were emanating from a plutonic source (or sources) to the south (present co-ordinates). From these relationships, Stockwell (1938) inferred that the pluton and the porphyry intrusions were essentially comagmatic. Samples of the porphyry dikes collected and analyzed for this study were found to be geochemically indistinguishable from the granodioritic

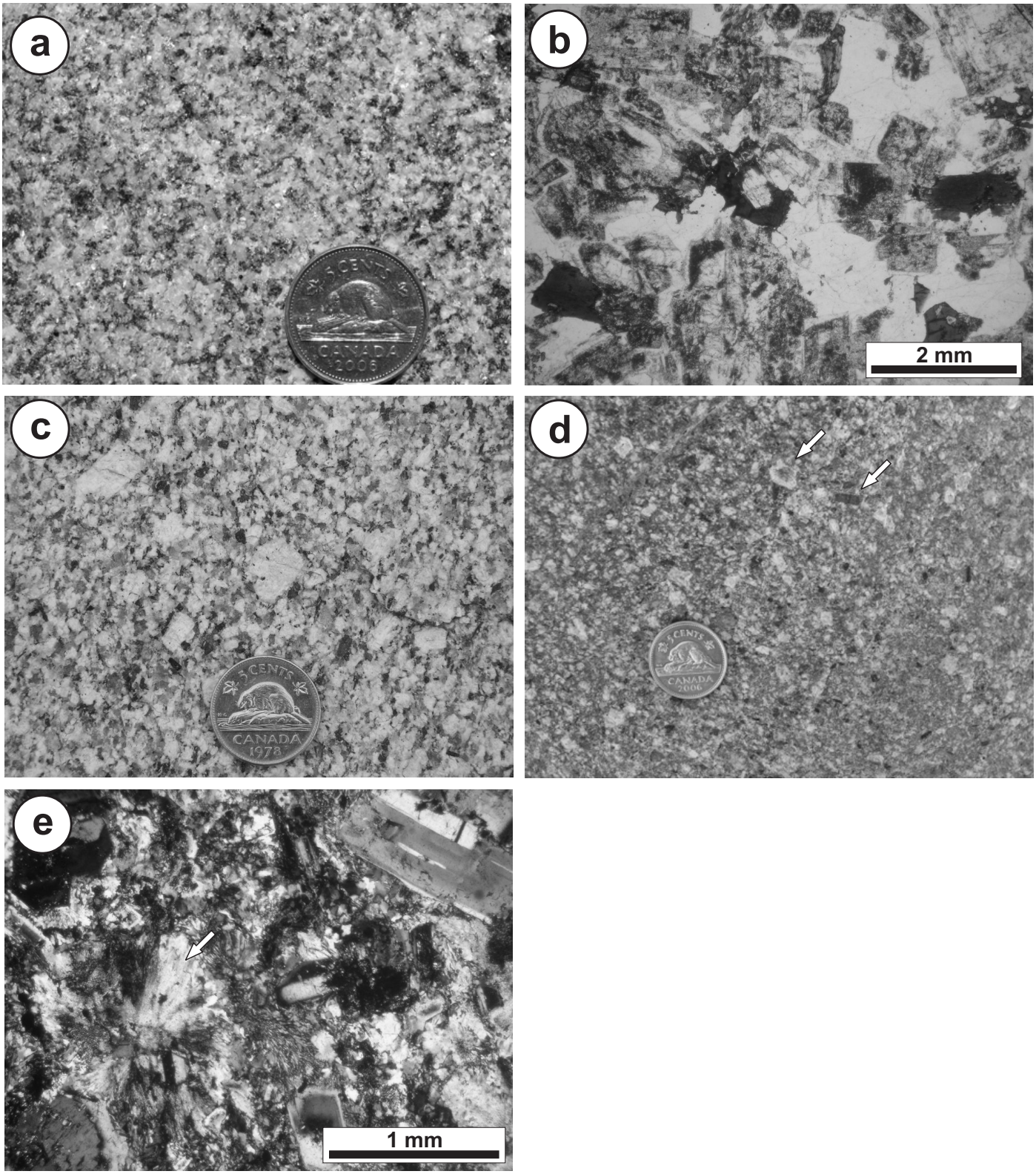

Figure 17: *Thin-section and outcrop photographs of rock types in map unit 11, east of Rice Lake:* ***a)*** *equigranular biotite granodiorite, central portion of Ross River pluton;* ***b)*** *equigranular biotite granodiorite (plane-polarized light), showing moderately saussuritized feldspar (grey) with subordinate quartz (white) and biotite (dark grey), same location as previous;* ***c)*** *porphyritic hornblende-biotite-magnetite tonalite, northern margin of Ross River pluton;* ***d)*** *porphyritic granodiorite dike, Rainy Lake road; note euhedral phenocrysts of hornblende and concentrically zoned feldspar (arrows);* ***e)*** *spherulitic texture (arrow) in the matrix of a porphyritic granodiorite dike (cross-polarized light); Rainy Lake road.*

phases of the Ross River pluton, which would support a comagmatic relationship. Most of the porphyry dikes exhibit sharp planar contacts and well-developed chilled margins, which are indicative of relatively shallow (i.e., hypabyssal) emplacement. Evidence of quench-crystallization, in the form of fan-shaped to subspherical, spherulitic quartz-feldspar intergrowths observed in a thin section (Figure 17e) from a porphyry dike cutting the RLR unit, is consistent with this interpretation. The absence of significant contact metamorphic aureoles adjacent to the associated plutons is also indicative of relatively shallow emplacement; these intrusions are interpreted as hypabyssal equivalents to the felsic epiclastic rocks at the base of the TS unit.

Townsite unit

The Townsite (TS) unit defines a roughly crescent-shaped outcrop area and ranges from moderately northwest dipping in the east to moderately northeast dipping in the west (Figure 3). The unit ranges up to 1.4 km in thickness and consists of felsic volcanic sandstone and heterolithic volcanic conglomerate at the base (units 12 and 13), overlain to the north by mafic flows (unit 15) and a thick package of fragmental rocks of dacitic composition (unit 16; Figures 5, 18). From south to north, these units correspond to, respectively, the Hare's Island, Shoreline and Townsite volcanic units of Poulsen et al. (1996), portions of which have been described in detail by previous workers (e.g., Stockwell, 1938; Theyer, 1983; Tirschmann, 1986; Ames, 1988; Whiting, 1989). The epiclastic rocks are intruded by a thick gabbro sill (unit 14) that hosts the Rice Lake gold deposit and is interpreted as a subvolcanic equivalent to the 'Shoreline' mafic flows (e.g., Ames, 1988). As described previously, the basal contact of the TS unit is unexposed, but field relationships are interpreted to indicate a primary depositional contact with the underlying RLR unit. The western boundary of the TS unit is defined by the angular unconformity at the base of the San Antonio assemblage, which dips steeply northeast and is overturned in this location (i.e., the TS unit and San Antonio assemblage are arranged 'back-to-back'). As described below, the TS unit is overlain to the north by the RL unit along an erosional disconformity.

Felsic volcanic sandstone and pebble conglomerate (unit 12)

Felsic volcanic sandstone, with minor pebble conglomerate, defines two major map units in the lower portion of the TS unit at Rice Lake (Figures 3, 5). These rocks were described as tuff and arkose by Stockwell (1938) and as lithic arenite by Tirschmann (1986); the latter study includes detailed petrographic descriptions. The southern map unit is approximately 300 m thick and is best observed on the small islands located just south of Hare's Island on Rice Lake. East of the lake, this unit is exposed in several small outcrops along the NCSZ, the easternmost of which is located on the southeast side of Normandy Creek in the immediate footwall of the SG-1 deposit. This unit has also been observed by the author on the sixth level of the SG-1 mine and defines the immediate footwall to the mineralized zone. The northern unit is best exposed along the northeastern shoreline of Rice Lake and in outcrops along the power line east of the lake. This unit ranges up to 350 m thick at Rice Lake and thins abruptly to both the east and west.

In both of these units, the felsic volcanic sandstone weathers distinctively white and is typically medium to very

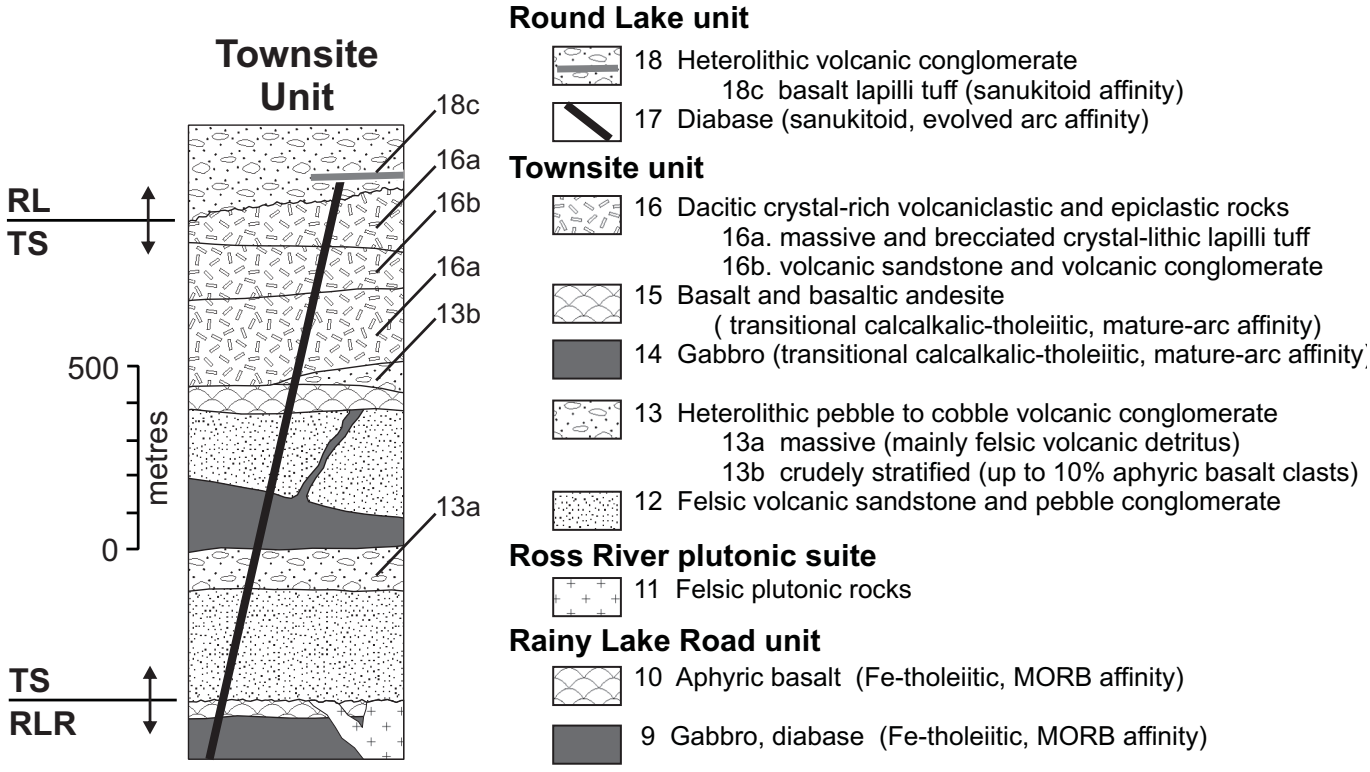

Figure 18: *Schematic stratigraphic column for the Townsite (TS) unit. Unit numbers correspond to those in the text and on Map GR2008-1-1.*

coarse grained (Figure 19a, b). The sandstone contains coarse grains and granules (0.5–4.0 mm) of feldspar (10–40%; euhedral to subhedral) and quartz (1–10%, up to 25% locally; angular to rounded). The feldspar is extensively altered to sericite, clinozoisite and carbonate, and the matrix consists of fine-grained quartz, sericite, carbonate, clinozoisite and chlorite. In most outcrops, the sandstone is massive or very faintly layered (subunit 12a). Well-developed planar bed forms are

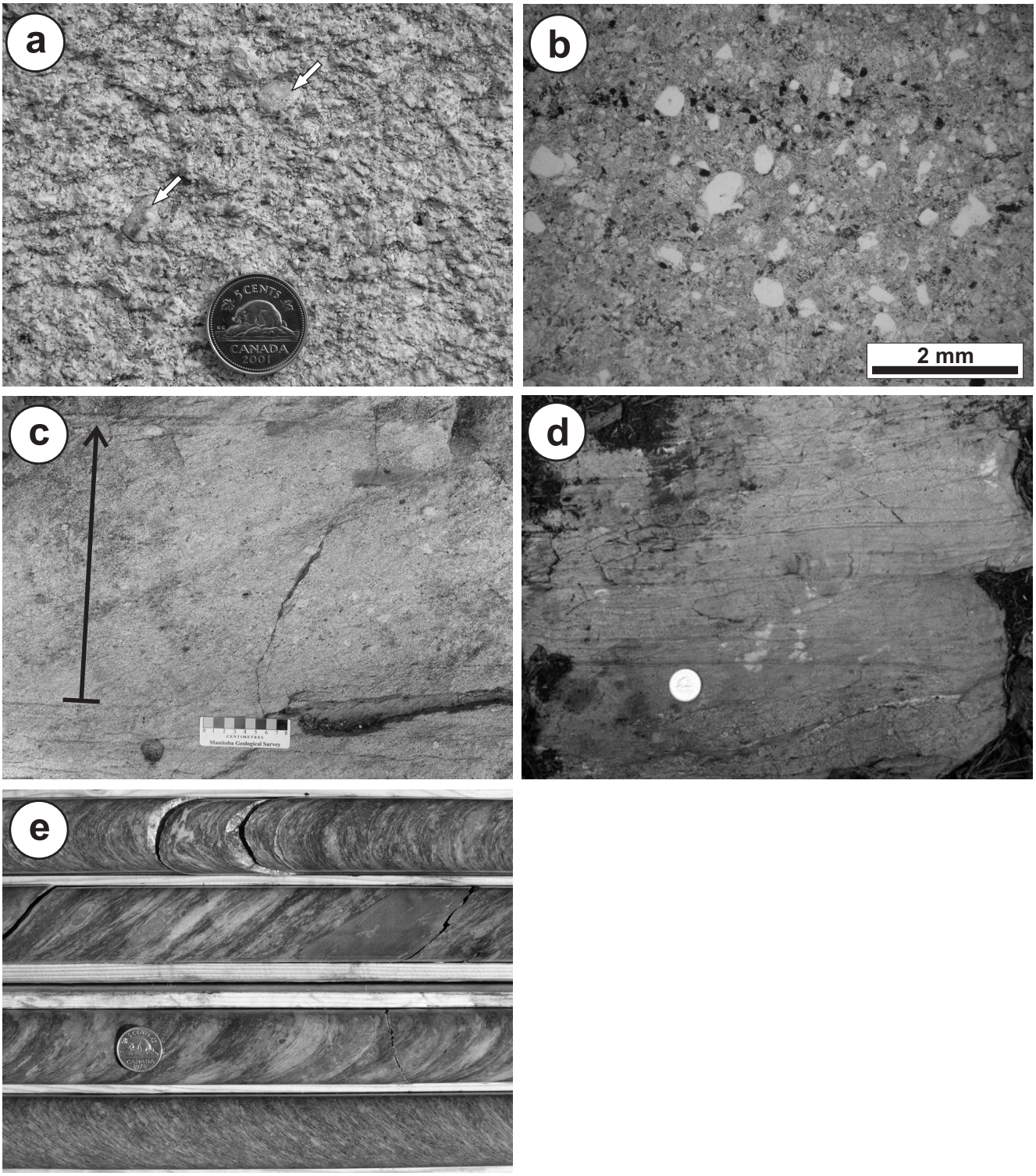

Figure 19: *Outcrop and thin-section photographs of rock types in map unit 12:* ***a)*** *coarse-grained felsic volcanic sandstone containing rounded pebbles of quartz- and feldspar-phyric rhyolite (indicated by arrows), small island south of Hares Island, Rice Lake;* ***b)*** *medium-grained felsic volcanic sandstone, showing angular to rounded quartz grains and diffuse stratification defined by concentration of opaque minerals (plane-polarized light), sample 85-PEA-301, collected in 1985 by H. Poulsen from the east shore of Rice Lake;* ***c)*** *bed of pebbly, coarse-grained, felsic volcanic sandstone showing diffuse reverse (bottom) and normal (top) size-grading, east shore of Rice Lake;* ***d)*** *thin-bedded felsic volcanic sandstone, east of Rice Lake;* ***e)*** *coarse-grained, pebbly volcanic sandstone (bottom core) and pebble volcanic conglomerate in drillcore from the footwall of the SG-1 deposit (diamond-drill hole SG-04-3).*

present locally (e.g., on the south side of Hare's Island and on the north shoreline of the wide, eastern bay of Rice lake) in intervals of thickly interlayered (1–5 m) massive and bedded (<30 cm thick beds) sandstones (subunit 12b; Figure 19c, d). Bedding in these locations dips moderately north, and normal-graded beds and rare scours indicate tops to the north. The lower portions of some beds exhibit reverse grading. At Rice Lake, very coarse grained granule and pebble sandstone occurs in massive layers up to 5 m thick. Subangular to rounded lithic pebbles, composed of pink-white, aphyric to quartz- and/or feldspar-phyric rhyolite, account for up 25% of these layers and also form the dominant clast type in minor lenticular interlayers of massive, unsorted, clast-supported, pebble to cobble volcanic conglomerate (Figure 19e). The northern volcanic sandstone unit is intruded by abundant sills and dikes of fine-grained, sparsely amygdaloidal basalt, which are typically 0.5 m thick and have well-developed chilled margins. These dikes are interpreted as feeders to overlying effusive mafic volcanic rocks (unit 15).

The overall features of this unit are interpreted to indicate deposition via high-density grain and debris flows, likely in a subaerial or shallow-marine setting. Although Tirschmann (1986) favoured a braided stream to braidplain depositional setting for this unit, the apparent absence of features typical of fluvial systems (e.g., channel-lag conglomerate, trough-crossbedded sandstone, overbank deposits, etc.) is herein considered to be more consistent with proximal to medial outwash (i.e., nonchannellized sheet-flood) deposits in a subaerial to shallow-marine fan that formed during rapid denudation of a felsic volcanic edifice. As described by Selley (1988), such deposits are especially characteristic of the fault-proximal deposition in extensional alluvial basins, which would be consistent with the localized occurrence of effusive mafic volcanic rocks (unit 15) in the TS unit.

As noted previously, intermediate flows and volcaniclastic rocks in the upper portion of the IL unit (unit 6) are crosscut in one location by an unusual dike-like body of heterolithic breccia (Figure 20), which is interpreted to represent a sedimentary intrusion (i.e., clastic dike). This dike, which ranges from 2 to 7 m thick over an exposed length of 11 m, trends roughly north and appears to be subvertical, and is thus highly discordant to the west-southwest-trending, subvertical stratification in the hostrocks. The external contacts are very sharp and unaltered (Figure 21a, b), and vary from moderately planar to quite irregular; the opposing contacts are nonparallel. The breccia is heterolithic, unsorted and predominantly matrix supported, although the proportion of matrix to fragments is quite variable (Figure 21c, d); internal stratification is lacking. Most fragments are very angular to subangular, and range in shape from tabular to blocky to distinctly shard like. Evidence of *in situ* fragmentation (i.e., jigsaw texture) is lacking. A small proportion of the fragments is rounded to very well rounded, and some of these are nearly spherical, suggesting significant transport. Aphyric intermediate volcanic material, which is texturally similar to the wallrocks, represents the dominant fragment type; some of these fragments range in size up to 4.0 m, although most others are typically less than 20 cm in maximum dimension. Along the western contact, the breccia cuts a distinctive andesite dike that contains small, round tonalite xenoliths, and fragments of this rock are also found in the breccia. Other fragment types include 1) aphyric, black or buff, felsic volcanic rock; 2) coarsely plagioclase-phyric andesite; 3) well-bedded epiclastic rock; 4) very angular, shard-like fragments of pale yellow-green sericitic phyllite

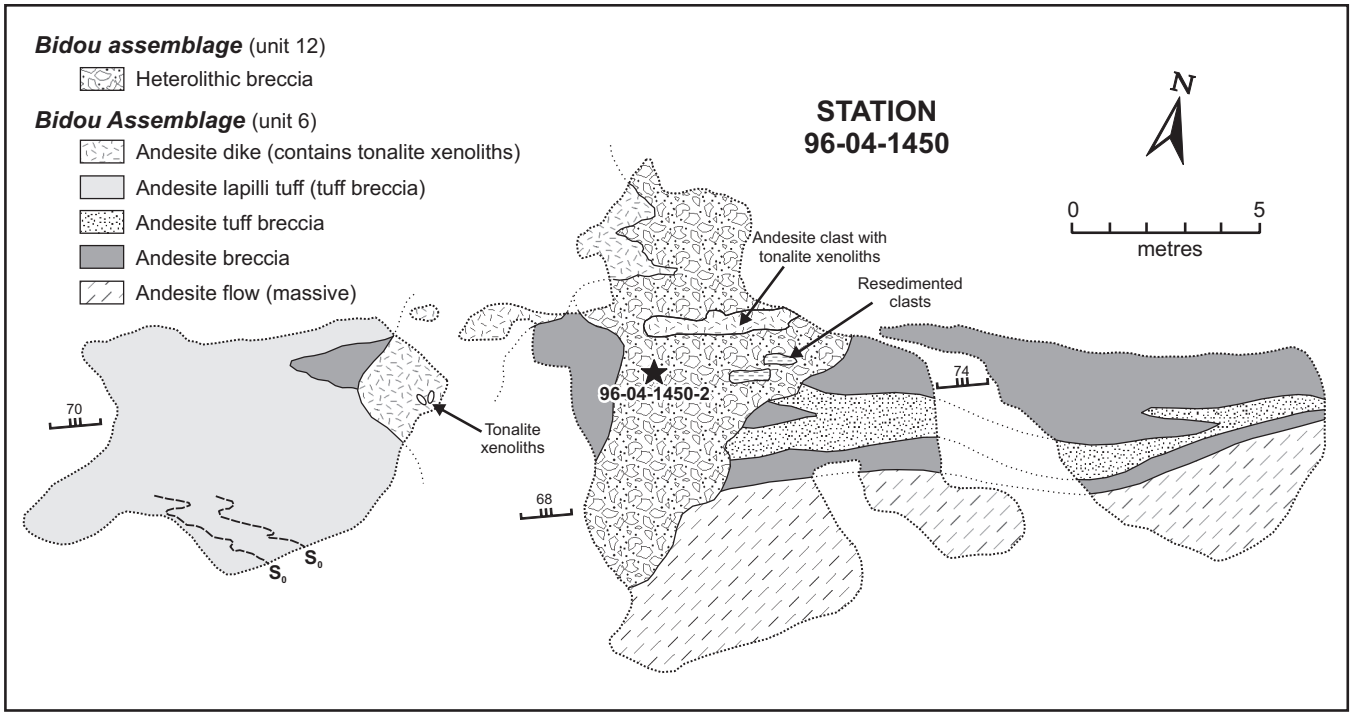

Figure 20: *Detailed outcrop map showing the dike-like body of heterolithic breccia that discordantly cuts intermediate effusive, volcaniclastic and intrusive rocks of map unit 6. Star indicates the location of the sample collected for U-Pb dating of zircon in the sandstone matrix. Structural symbols indicate the orientation of the regional S_3 planar fabric. Outcrop location: 314680E, 5654166N (NAD 83, UTM Zone 15).*

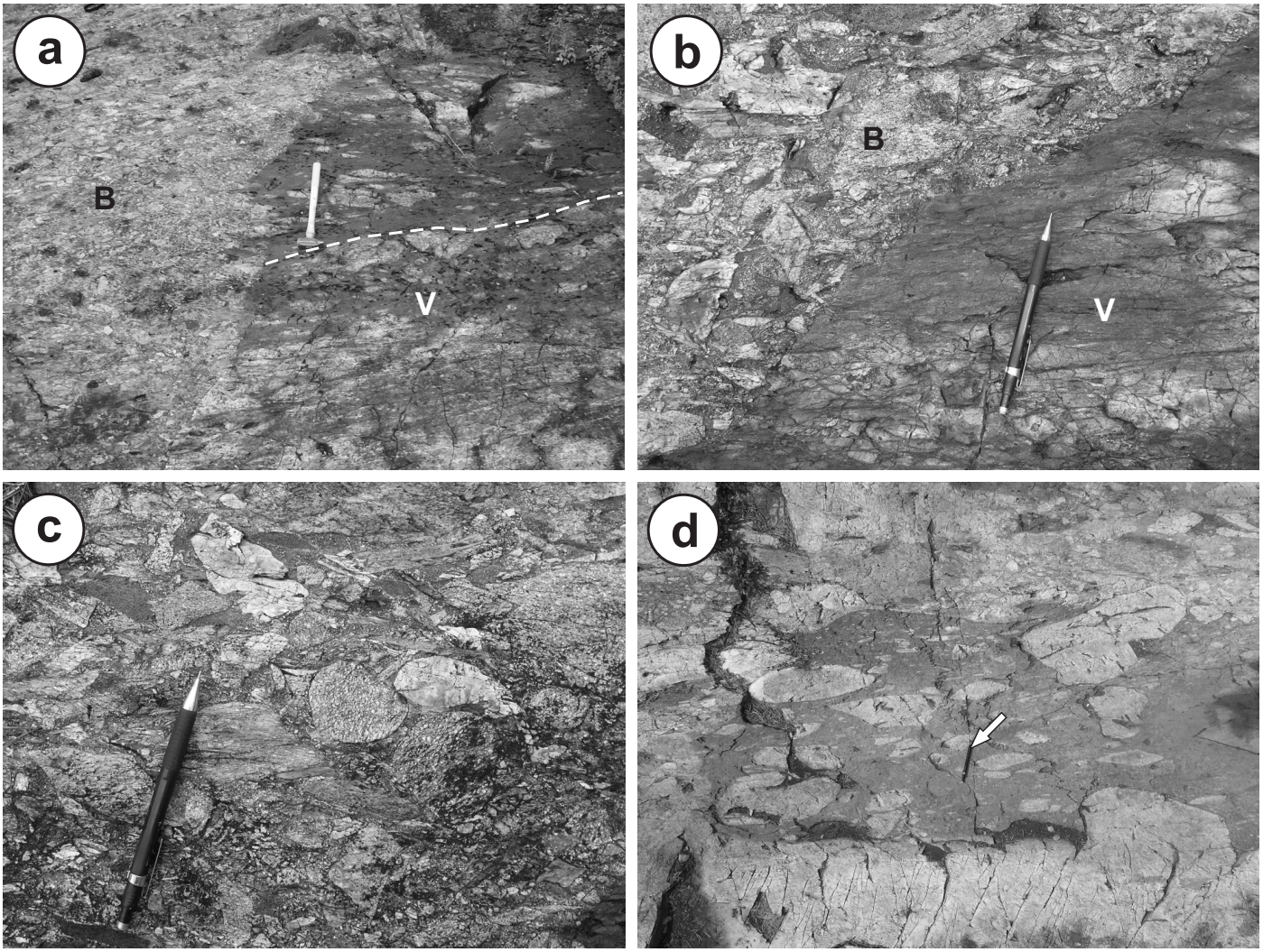

Figure 21: *Outcrop photographs of the heterolithic breccia that forms the dike-like body at 314680E, 5654166N (NAD 83, UTM Zone 15):* ***a)*** *sharp, slightly irregular contact between stratified intermediate volcaniclastic rocks (V) and heterolithic breccia (B); note the highly discordant nature of the contact with respect to the external stratification (dashed line);* ***b)*** *detail of previous photograph, showing sharp, unaltered contact between intermediate volcaniclastic rocks (V) and heterolithic breccia (B);* ***c)*** *detail of fragment-supported breccia, showing heterolithic population of closely packed, very angular to well-rounded fragments;* ***d)*** *detail of matrix-supported breccia, showing generally larger fragments in a coarse-grained muddy sandstone matrix; pencil for scale (arrow).*

(Figure 22a); and 5) rare fragments of fine-grained quartzofeldspathic phyllite. The latter two fragment types contain planar deformation fabrics that predate their entrainment in the breccia (Figure 22b). The breccia matrix consists of rusty brown, hematitic, fine- to coarse-grained sandstone (Figure 22c, d) that is composed of very angular to subrounded feldspar (~40%), quartz (~20%) and lithic (~10%) grains in a chloritic mudstone matrix (~30%). The grain size of the matrix is quite variable and exhibits irregular internal gradations from fine- to very coarse grained pebbly sandstone. In some locations, this gradation occurs over a distance of 1–2 cm (Figures 21c, 22a).

Although breccia can be generated by a variety of geological processes, the features described above are most consistent with a sedimentary intrusion (i.e., clastic dike). The clastic nature of the matrix material, coupled with the heterolithic fragment population, absence of *in situ* fragmentation textures and unaltered nature of the external contacts, collectively rule out brecciation via igneous, hydrothermal, solution/collapse and fault mechanisms. The presence of well-rounded and resedimented clasts, in conjunction with the absence of juvenile volcanic clasts, also rule out emplacement by primary volcanic processes (i.e., volcaniclastic breccia). Impact-related breccia dikes are unlikely to occur in isolation and, since no other dikes or structures of this type are described in the Rice Lake region, this option is also considered highly unlikely. The discordant, sharp and unaltered nature of the breccia contacts are consistent with a sedimentary breccia, such as a gulley-fill or talus deposit, as is the presence of well-rounded and resedimented clasts. More difficult to reconcile, however, is the high abundance of quartz in the matrix relative to the wallrocks and fragment population; this indicates an 'exotic' source for the matrix sand.

Clastic dikes are common in tectonically active settings, where they record fluid overpressuring and fluidization of sediments, triggered by seismic activity and/or applied tectonic stresses (Jolly and Lonergan, 2002). Such dikes are typically sourced in coarse siliciclastic sediments, but can occur in both intra- and extraformational settings. Basement-hosted clastic

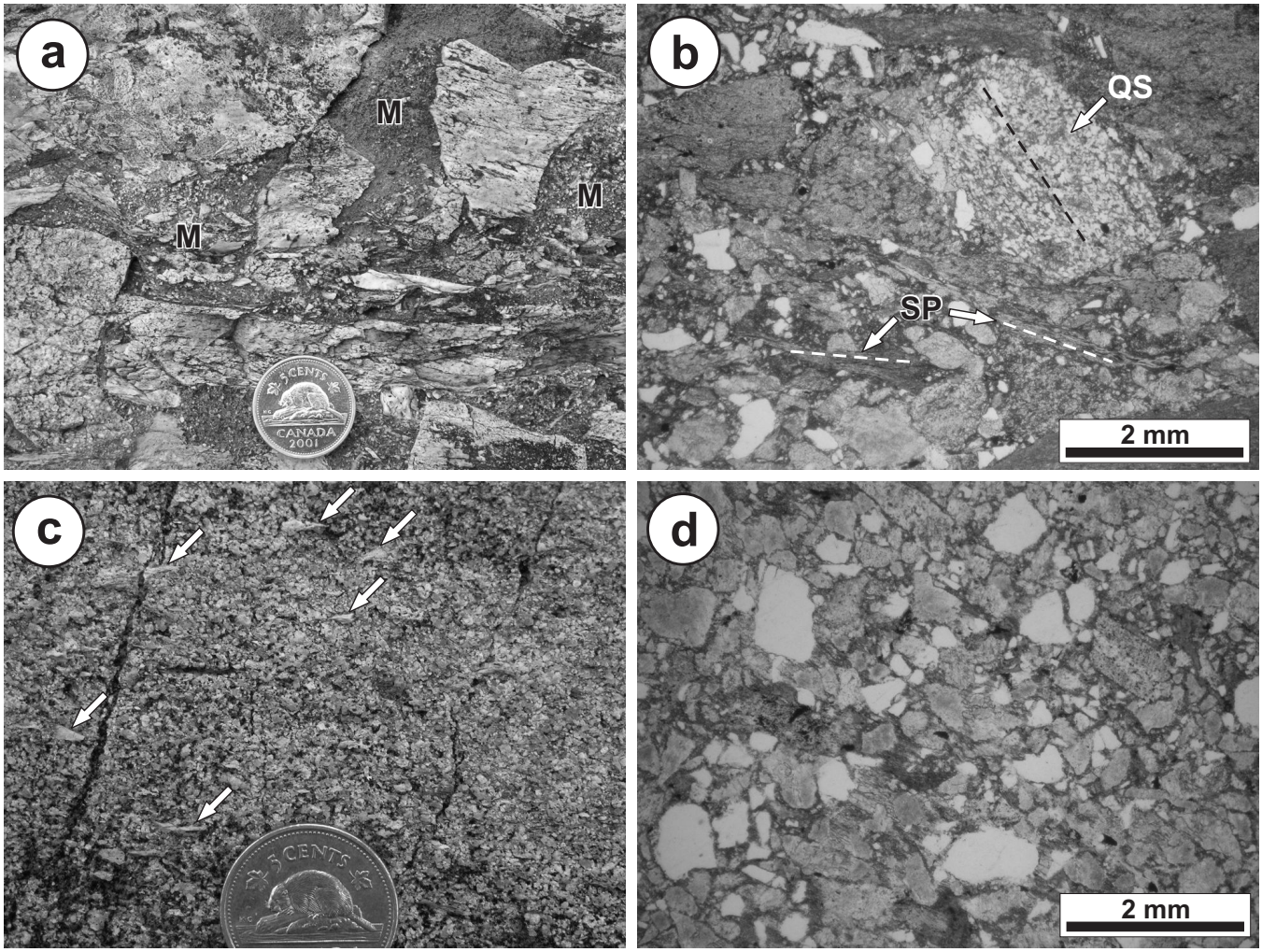

Figure 22: *Outcrop and thin-section photographs showing details of the sandstone matrix of the breccia that forms the dike-like body at 314680E, 5654166N (NAD 83, UTM Zone 15):* ***a)*** *detailed photograph showing significant variations in grain size and lithic content of the matrix (M) over distances of <3 cm; note very angular, shard-like shapes of the lithic fragments, suggesting minimal transport;* ***b)*** *quartzofeldspathic (QS) and sericitic phyllite (SP) granules in the matrix; note that each granule contains pronounced planar fabrics (dashed lines) that do not continue into the chloritic matrix material (plane-polarized light);* ***c)*** *detailed photograph of the coarse-grained greywacke matrix; note the abundant shard-like grains of sericitic phyllite (arrows);* ***d)*** *coarse-grained greywacke composed of very angular to subrounded feldspar, quartz and lithic grains in a chloritic mudstone matrix (plane-polarized light).*

dikes (i.e., dikes of younger sediment cutting older rocks) are documented in several locations (e.g., Beacom et al., 1999; Jonk et al., 2004; Wall and Jenkyns, 2004), where they are interpreted to coincide with extensional tectonic regimes and are generally attributed to gravitational infilling of open fractures from above (i.e., sediment-filled fissures) or forceful downward intrusion of fluidized sediment into new or pre-existing fractures. In the present case, potential nearby sources for the quartz-rich matrix sand appear to be restricted to the coarse felsic volcanic sandstone of the TS unit (unit 12) or the arenite and wacke of the San Antonio assemblage (unit 27 or 28). In order to test these options, a sample of the matrix sandstone was sampled for U-Pb dating of zircons by LA-MC-ICP-MS analysis (sample 96-04-1450-2). The results of this analysis, which are described in detail below, indicate the TS unit as the most likely source.

Heterolithic pebble to cobble volcanic conglomerate (unit 13)

Both the northern and southern map units of felsic volcanic sandstone (unit 12) are capped by discontinuous units of coarse heterolithic volcanic conglomerate (Figures 3, 5). The southern conglomerate unit (subunit 13a) is best observed on the north side of Hare's Island in Rice Lake, where it is homogeneous and massive, and ranges up to 130 m thick. This subunit pinches out 1.4 km to the east along strike and is interpreted to be truncated 2.5 km to the west along strike by the basal unconformity of the San Antonio assemblage. Exposures of this conglomerate 1.6 km below surface in the Rice Lake mine indicate a down-dip extent of at least 2.2 km. Recently stripped outcrops along the haul road to the SG-1 deposit provide the best exposures of the northern unit (subunit 13b), which has a pronounced lenticular shape that ranges up to 150 m thick within a strike length of 1.6 km. The thickest portion separates basalt and basaltic andesite flows (unit 15) on the south from dacitic volcaniclastic rocks (unit 16) on the north; to the east, however, subunit 13b and unit 15 appear to be interstratified.

The conglomerate is typically massive, clast supported and poorly sorted, and is composed of equant, subangular to well-rounded clasts that range up to 30 cm across (typically 0.5–10 cm; Figure 23a, b). Porphyritic dacite and rhyolite are

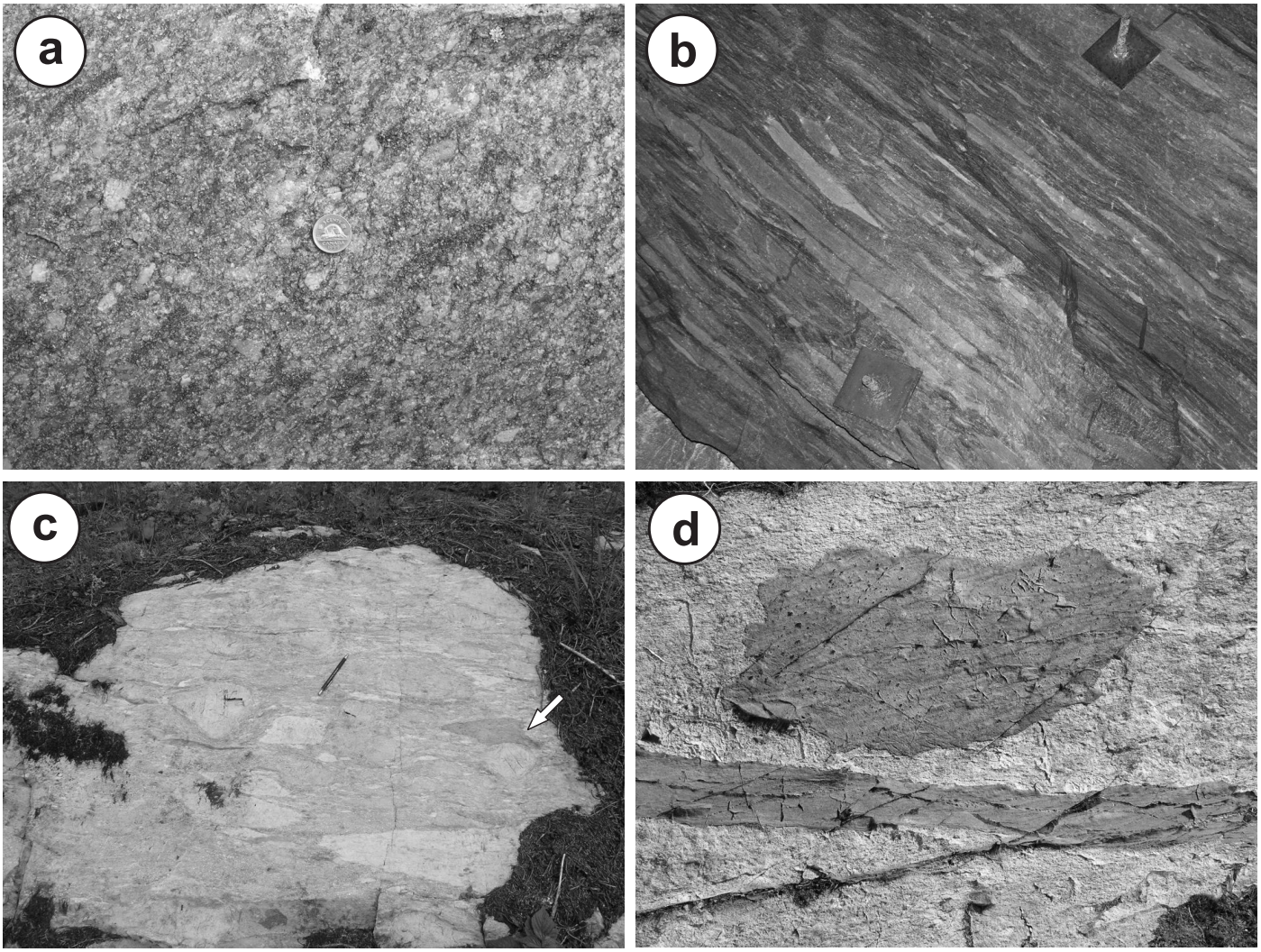

Figure 23: *Outcrop photographs of rock types in map unit 13:* ***a)*** *massive, heterolithic, pebble volcanic conglomerate (subunit 13a), Hares Island, Rice Lake;* ***b)*** *crudely stratified, heterolithic cobble and boulder volcanic conglomerate (subunit 13a), D shaft access drift, level 36, Rice Lake mine (rock-bolt plates are 15 cm square);* ***c)*** *heterolithic cobble and boulder conglomerate (subunit 13b) in the immediate hangingwall of unit 15, 100 m west of the SG-1 portal; note angular basalt clast (arrow);****d)*** *volcanic conglomerate cut by basalt dike and possible lava tube in the immediate hangingwall of unit 15, SG-1 haul road, 1 km east of Rice Lake; lava tube is composed of amygdaloidal basalt that contains minor xenoliths of the adjacent felsic epiclastic rocks; the margins are irregular, sharp and chilled.*

the dominant clast types in subunit 13a. Tirschmann (1986) conducted modal analyses of the clast populations in four etched slabs (~600 points/slab) of pebble conglomerate from Hare's Island, the results of which are summarized as follows: 36–68% porphyritic felsic volcanic; 9–24% porphyritic mafic volcanic; 2–33% aphyric to porphyritic intermediate volcanic; and 0–20% aphyric felsic volcanic. As noted by Tirschmann (1986), the conglomerate on Hare's Island appears to become coarser and more heterolithic toward the north (i.e., up-section). In the immediate footwall to the Rice Lake deposit, this subunit is characterized by intense sericite-ankerite alteration. Subunit 13b is generally more heterogeneous and contains local intercalations of massive, coarse-grained, pebbly volcanic sandstone, and typically contains a significant population of subangular to very angular clasts of aphyric amygdaloidal basalt (Figure 23c). Dikes and sills composed of texturally similar basalt are abundant and range up to 0.5 m thick, with well-developed chilled margins. A possible lava tube, approximately 1.0 m in diameter, is preserved in an outcrop of pebble conglomerate on the north side of the haul road about 2.0 km west of the SG-1 deposit (Figure 23d).

The coarse heterolithic conglomerate that characterizes unit 13 was likely deposited by proximal, high-density debris flows in a subaerial to shallow-marine setting, with the detritus derived from the actively eroding flanks of a mainly felsic volcanic centre. The apparently cyclic repetition of volcanic sandstone (unit 12) and conglomerate (unit 13) is interpreted to represent two depositional cycles within a prograding fan system. Subunit 13b was deposited close to coeval basaltic effusions, perhaps indicating proximity to a basin-bounding fault scarp.

Gabbro (unit 14)

Epiclastic rocks at the base of the TS unit contain two sill-like bodies of gabbro, the larger of which hosts the Rice Lake gold deposit and is informally referred to as the San Antonio mine ('SAM') unit. The SAM unit has traditionally been described as a diabase or gabbro sill (e.g., Reid, 1931;

Stockwell, 1938; Bragg, 1943; Gibson and Stockwell, 1948), and this interpretation is supported by subsequent detailed petrography (Ames, 1988) and underground mapping of the contacts (Rhys, 2001; Anderson, unpublished data, 2007). Although some authors have suggested that the SAM unit is composed of flows and volcaniclastic rocks (e.g., Theyer, 1983; Whiting, 1989), the only evidence cited in support of this interpretation is textural in nature and is not compelling. In marked contrast to chemically similar rocks in the overlying Shoreline volcanic unit (Poulsen et al., 1986; Ames, 1988), which contain abundant and unambiguous evidence of an extrusive origin (*see* below), the present author did not observe any convincing examples of volcanic textures or structures in the SAM unit.

The SAM unit crops out discontinuously over a strike length of 4.5 km, and has been traced by drilling for an additional 700–800 m to the northwest along strike. The eastern portion of the sill is 40–80 m thick and dips steeply to the northwest, whereas the western portion ranges up to 190 m thick and dips moderately to the northeast. In the Rice Lake mine, this unit has been traced over 2.2 km down dip and remains open at depth. The eastern and western extents of the SAM unit appear to represent primary lateral pinch-outs. At Rice Lake, the SAM unit generally appears to be concordant to bedding in the country rocks (i.e., a sill), although Rhys (2001) described local discordant contact relationships at depth in the Rice Lake mine. The hangingwall contact of the gabbro was observed by the present author in two locations on level 29 of the mine (along the D shaft access crosscut and at the east end of the 2998 drift); in each location, irregular dikes and apophyses of gabbro extend outward from the contact into the epiclastic country rocks. Towards to east, the SAM unit is slightly discordant to bedding (Figure 24a) and cuts up-section into the immediate footwall of the Shoreline volcanic unit. In this location, the upper contact is sharp and planar, and separates fine-grained melagabbro from the felsic epiclastic country rocks (Figure 24b). Large rafts and roof pendants of the country rocks near the upper contact of the SAM unit indicate its intrusive nature. A smaller gabbro sill, up to 70 m thick, is discontinuously exposed over a strike length of 1.0 km in the hangingwall of the SAM unit.

The gabbro of unit 14 is separated into three textural and compositional varieties: leucogabbro (subunit 14a), melagabbro (subunit 14b) and layered gabbro (subunit 14c). In most specimens, the primary mineral assemblage is completely replaced by secondary actinolite, chlorite, albite, epidote, carbonate (ankerite and calcite) and quartz, with accessory titanite, magnetite, pyrite and leucoxene (*see* Bragg, 1943; Ames, 1988). A planar fabric defined by foliated chlorite and actinolite is apparent in most specimens. This fabric is generally weakly developed in the thicker western portion of the SAM unit, but is generally penetrative and pervasive to the east in the hangingwall of the NCSZ. At depth in the Rice Lake mine, the SAM unit is strongly foliated and locally contains a penetrative L>S fabric.

Leucogabbro (subunit 14a) weathers light green-grey and is typically medium grained, massive and equigranular, with an ophitic to subophitic texture (Figure 24c) defined by replaced plagioclase laths (0.5–1.5 mm) in a fine-grained matrix of actinolite, chlorite and epidote. The plagioclase, which likely accounted for 50–70% of the primary mineral assemblage, is replaced by very fine grained sericite, zoisite and carbonate. Actinolite and chlorite form pseudomorphic replacements after 1–3 mm, equant, subhedral phenocrysts of primary pyroxene, or perhaps olivine. In most localities, the leucogabbro is strongly magnetic. The melagabbro (subunit 14b) weathers dark green to rusty brown and is dark green on fresh surfaces. This rock typically displays a fine- to medium-grained subophitic texture (Figure 24d) defined by fine (<1.5 mm), stubby, replaced plagioclase laths (20–50% of the primary assemblage). The melagabbro is generally massive and nonmagnetic. Leucogabbro locally forms dikes up to 50 cm thick in the melagabbro (Figure 24e) and is only extensive in the thickest portion of the SAM unit. Here, the leucogabbro ranges up to 130 m thick and the SAM unit is layered on a macroscopic scale from melagabbro at the base to leucogabbro at the top (e.g., Ames, 1988; Rhys, 2001). Ames (1988) interpreted the macroscopic layering to result from *in situ* differentiation of the parent mafic magma. Layered gabbro (subunit 14c) is exposed on a small island in Rice Lake and consists of irregular wisps, clots and discontinuous, contorted layers (2–10 cm thick) of leucogabbro in melagabbro (Figure 24f). This outcrop may be located near the melagabbro-leucogabbro interface, which is described as 'layered' in the Rice Lake mine (e.g., Rhys, 2001). In some layers, the mafic mineral content gradationally decreases toward the north, which is consistent with the *in situ* differentiation model proposed by Ames (1988). In at least the upper levels of the Rice Lake deposit, the upper leucogabbroic portion of the SAM unit preferentially hosts auriferous quartz-carbonate veins. This relationship is less clear at depth, where the SAM sill appears to be texturally heterogeneous and lacks conspicuous igneous layering (J. Harvey, pers. comm., 2008).

Aphyric to sparsely plagioclase-phyric basalt and basaltic andesite (unit 15)

Basalt and basaltic andesite, with associated volcaniclastic and epiclastic rocks, define a laterally continuous map unit (unit 15) in the medial portion of the TS unit. Unit 15 corresponds to the Shoreline volcanic unit of Poulsen et al. (1996) and is typically 40–70 m thick, but locally ranges up to 120 m thick in the area just southwest of the SG-1 portal. A linear, moderate-intensity magnetic anomaly coincides with this unit and is semicontinuous over a strike length of 7.5 km (Assessment File 73689). Unit 15 and is best exposed along the northeast shoreline of Rice Lake, although a good exposure is also present 1.5 km east of the lake along strike, in a large flat outcrop located on the north side of the SG-1 haul road (*see* below). To the east, this unit is interpreted to be structurally truncated in the immediate hangingwall of the SG-1 deposit, whereas the western extent is interpreted to represent a primary stratigraphic pinch-out, although it is also possible that unit 15 is truncated by the erosional disconformity at the base of the Round Lake unit.

The basalt (and basaltic andesite) weathers light green to reddish brown, is dark green on fresh surfaces and is typically aphyric with a very fine grained intergranular texture. Sparsely porphyritic basalt contains 2–10% euhedral to subhedral plagioclase laths that are 1–3 mm in length. The primary mineral assemblage is completely replaced by fine-grained secondary minerals (actinolite-chlorite-epidote-albite-carbonate-quartz). The basalt contains 1–5% finely disseminated magnetite and

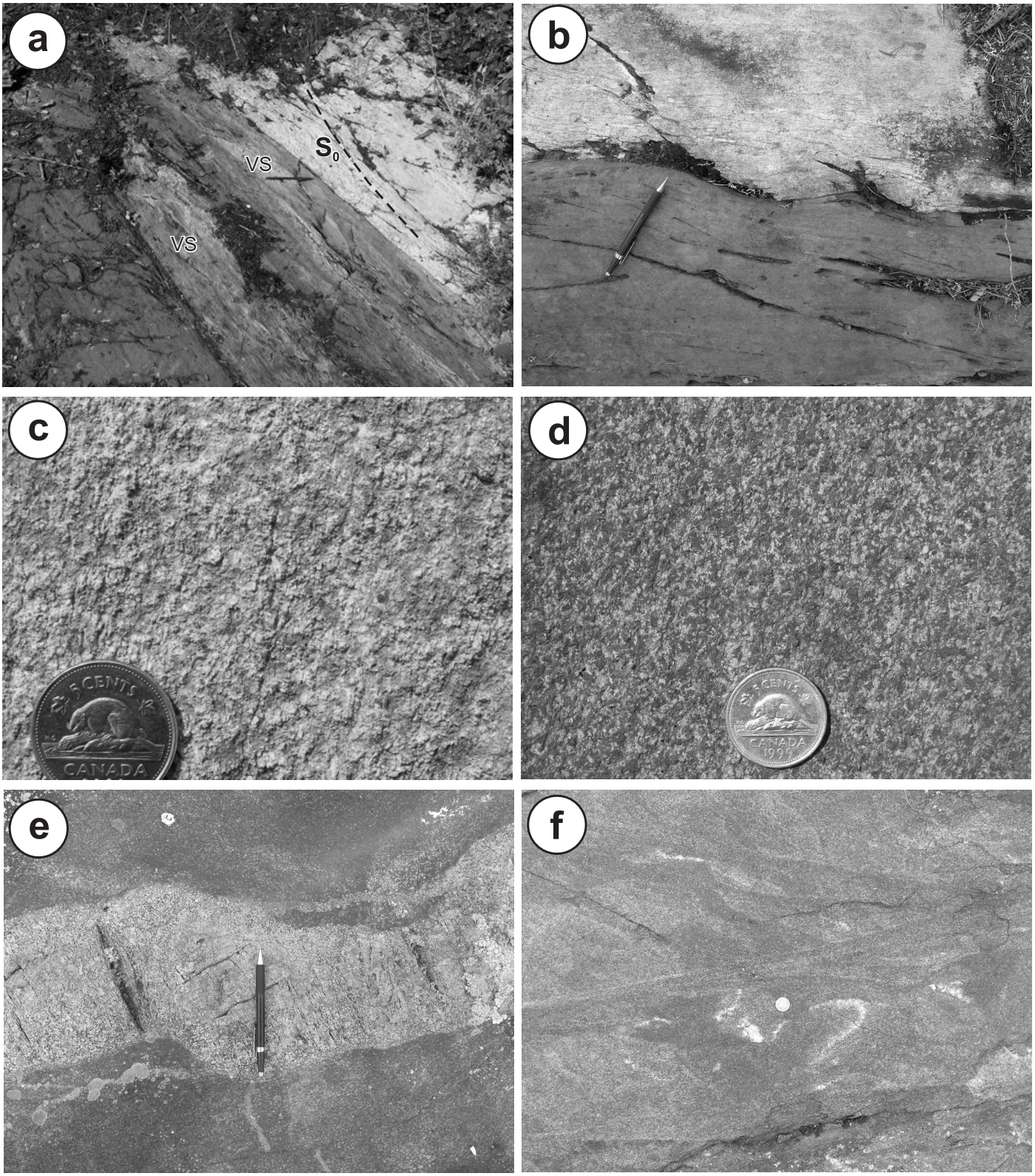

Figure 24: *Outcrop photographs of rock types in the SAM unit of map unit 14:* ***a)*** *upper contact, showing fine-grained melagabbro with partially digested rafts of felsic volcanic sandstone (VS) in contact with thin-bedded volcanic sandstone, east shore of Rice Lake; note slight angular discordance between gabbro contact and bedding (S_0) in the country rocks;* ***b)*** *upper contact, showing very fine grained melagabbro in contact with volcanic conglomerate, 1.5 km east of Rice Lake;* ***c)*** *medium-grained, equigranular leucogabbro, north shore of Rice Lake at the Rice Lake mine headframe;* ***d)*** *fine- to medium-grained, subophitic-textured gabbro, which is transitional in texture and composition between the more typical melagabbro and leucogabbro, east shore Rice Lake;* ***e)*** *medium-grained melagabbro crosscut by dike of coarse-grained leucogabbro, small island in eastern Rice Lake;* ***f)*** *contorted magmatic layering in possible transition zone between leucogabbro and melagabbro, same location as previous.*

is typically weakly to moderately magnetic. The bulk of this unit appears to consist of pillowed basalt with subordinate massive and brecciated basalt (subunit 15a), and minor interlayers of derived epiclastic rocks (subunit 15b). In general, the exposure is insufficient to determine the internal flow organization of unit 15. In the large exposure 1.5 km east of Rice Lake, however, it is possible to demonstrate that at least this portion of the unit is composed of a series of 1–5 m thick, pillowed, massive and brecciated flows, with a cumulative thickness of 45 m. The organization of individual flows locally appears to be comparable to the 'standard sequence' described by Dimroth et al. (1978) for subaqueous basalt flows or, more specifically, the 'compound' flow type described by Bailes and Syme (1989) in the Flin Flon greenstone belt. Unless otherwise indicated, the following description is based on this type locality.

The massive flows range up to at least 4 m thick and are generally fine grained, aphyric and sparsely amygdaloidal. The basal contact of a massive flow is well exposed at the base of unit 15 and shows a very sharp, relatively planar contact with underlying volcanic conglomerate of unit 13 (Figure 25a). The chilled base of the flow ranges from 2 to 10 cm thick and grades upward over 5–20 cm into sparsely amygdaloidal, fine-grained basalt. The upper portion of the flow is also sparsely amygdaloidal, and appears to grade upward over several metres into pillowed basalt. The pillowed flows are composed of bun-shaped pillows 20–50 cm across, with subordinate mattress pillows that range up to 1.5 m in length (Figure 25b). The cores of the pillows are sparsely amygdaloidal, moderately to strongly epidotized, and locally plagioclase phyric. The pillow selvages are typically 0.5–1.5 cm thick and strongly chloritized. Abrupt changes in pillow morphology, locally marked by layers of pillow-fragment breccia and probable hyaloclastite, are indicative of composite flows (Figure 25c). Interpillow hyaloclastic tuff and lapilli tuff account for not more than 5% of the pillowed flows and are remarkably well preserved in places (Figure 25d). On the northeast shoreline of Rice Lake, scattered small exposures indicate that the pillowed basalt flow (or flows) are up to 50 m thick. Here, the pillows contain 5–10% round epidote (±calcite, quartz, or hematite) amygdules up to 5 mm across that, in some cases, are concentrated along the north margins of individual pillows. Pillow cusps in two locations indicate tops to the north. At the type locality, the pillowed basalt is overlain by a poorly exposed unit of brecciated basalt that is at least 8 m thick. The breccia consists of angular to subrounded to very irregular and wispy fragments of epidotized fine-grained basalt. Along strike to the east, chilled margins are locally well preserved on some fragments; however, clear examples of pillow fragments are lacking.

In 2004, the upper contact of unit 15 was exposed in the immediate hangingwall of the SG-1 deposit, in a location now occupied by the mine portal. Here, epidotized pillowed basalt and breccia with wisps of laminated interpillow sedimentary material are overlain to the north by crystal-rich volcaniclastic rocks of unit 16 (Figure 25e). Separating these units is a 2–3 m thick interval of interstratified basalt breccia, crystal-rich pebbly volcanic sandstone, laminated volcanic mudstone, and heterolithic volcanic conglomerate. Bedding dips steeply northwest, and the sandstone beds typically fine to the north and contain angular clasts of the underlying basalt. This contact appears conformable.

On the power line east of Rice Lake, unit 15 includes discontinuous, 1–5 m thick sections of mafic epiclastic rocks, which consist of bedded, fine- to medium-grained volcanic sandstone with minor pebble conglomerate, siltstone and chert. Bedding dips north and fining-upward cycles, up to 1 m thick, indicate that these rocks are upright. The conglomerate is unsorted, matrix supported and monolithic, and contains subrounded to well-rounded clasts up to 15 cm across. These rocks record periodic influxes of significantly reworked mafic detritus, with transport and final deposition via debris and grain flows.

Dacitic crystal-rich volcaniclastic and epiclastic rocks (unit 16)

The uppermost portion of the TS unit is described in detail by Tirschmann (1986) and was referred to as the 'Townsite volcanics' by Poulsen et al. (1996). This unit is well exposed in the large outcrop ridge that extends east from Bissett, and has a pronounced lenticular shape that ranges up to 650 m thick within a strike length of just over 8.0 km. Unit 16 pinches out to the east at the confluence of the NCSZ and WSZ, and is truncated to the west by an apparent erosional scour at the base of the Round Lake unit. Most of this unit is composed of massive crystal-lithic lapilli tuff, of bulk dacitic composition, that contains indistinct layers or irregular bodies (?) of breccia and tuff breccia (subunit 16a). Toward the west, in the upper portion of the unit, these rock types are interstratified with well-bedded volcanic sandstone and heterolithic volcanic conglomerate (subunit 16b) to form a distinctive package of rocks that is approximately 100 m thick and can be traced along strike for over 1.0 km. Dikes of sanukitoid-affinity diabase (unit 17) are common near the upper contact of this unit.

The massive, crystal-lithic lapilli tuff weathers pale green-grey, is dark green on fresh surfaces and characteristically exhibits a seriate-porphyritic texture defined by euhedral to subhedral plagioclase crystals that range up to 1 cm and account for 25–45% of most specimens (Figure 26a). These crystals are evenly distributed in an aphanitic to fine-grained recrystallized matrix of quartz, feldspar, epidote, zoisite/clinozoisite, chlorite, sericite and carbonate. The plagioclase crystals are variably altered to fine-grained sericite, zoisite/clinozoisite and carbonate, and the larger crystals typically display oscillatory zoning. In most specimens, a significant portion (up to 10%) of the plagioclase exhibits distinctly rounded to subrounded, or angular to subangular, broken (locally shard-like) shapes. The crystal component also includes trace to 2% anhedral blue quartz (<5 mm) and trace euhedral hornblende (<3 mm). Possible examples of recrystallized felsic vitriclasts (i.e., clasts that may have originally been composed of felsic volcanic glass) observed in thin section are characterized by wispy lenticular shapes and fine-grained granophyric (quartz-feldspar) textures (Figure 26b, c; *see also* Tirschmann, 1986). Massive lapilli tuff is continuously exposed in intervals up to 10 m thick that exhibit only subtle variations in the size and proportion of plagioclase crystals. Most outcrops contain rare (<2%), angular to subrounded lapilli and blocks of green-brown basalt or andesite up to 10 cm across, which are variably plagioclase porphyritic and locally contain up to 15% round, quartz-filled

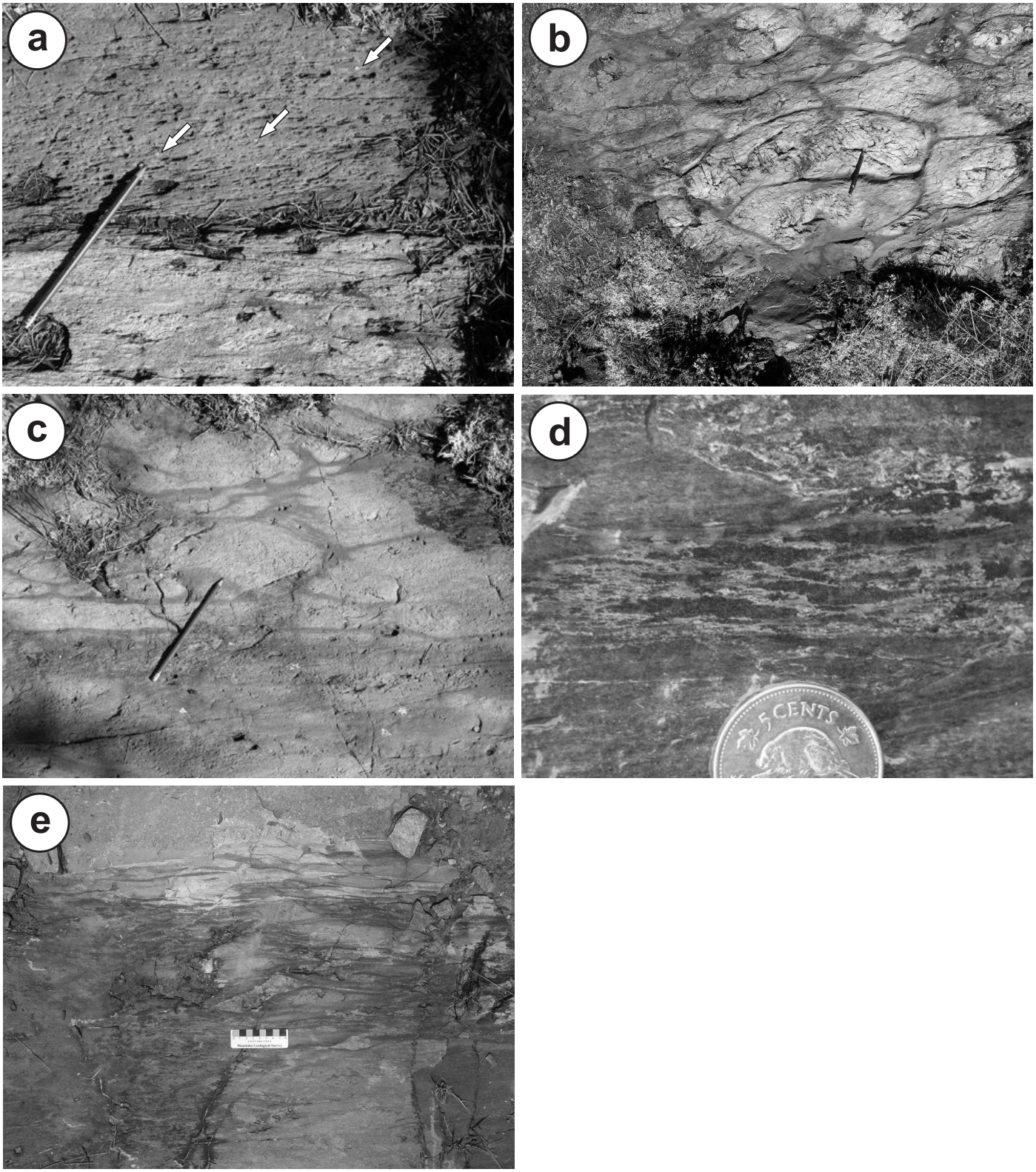

Figure 25: *Outcrop photographs of rock types in map unit 15:* ***a)*** *basal contact of a massive flow at the base of unit 15, showing sparsely amygdaloidal basalt (top; quartz amygdules indicated by arrows) in sharp contact with underlying heterolithic volcanic conglomerate of unit 13 (bottom), 1.5 km east of Rice Lake on the north side of the SG-1 haul road;* ***b)*** *strongly epidotized pillowed basalt, showing bun- to mattress-shaped pillows, same location as previous;* ***c)*** *sharp contact between brecciated basalt and probable hyaloclastite (bottom) and pillowed basalt (top) in the medial portion of unit 15, same location as previous;* ***d)*** *example of well-preserved hyaloclastite lapilli tuff in pillow interstices; approximately 300 m southwest of the SG-1 portal;* ***e)*** *pillowed basalt and basalt breccia (bottom) overlain by crystal-rich volcaniclastic rocks of unit 16 (top); photograph taken in 2004, at the present site of the SG-1 portal.*

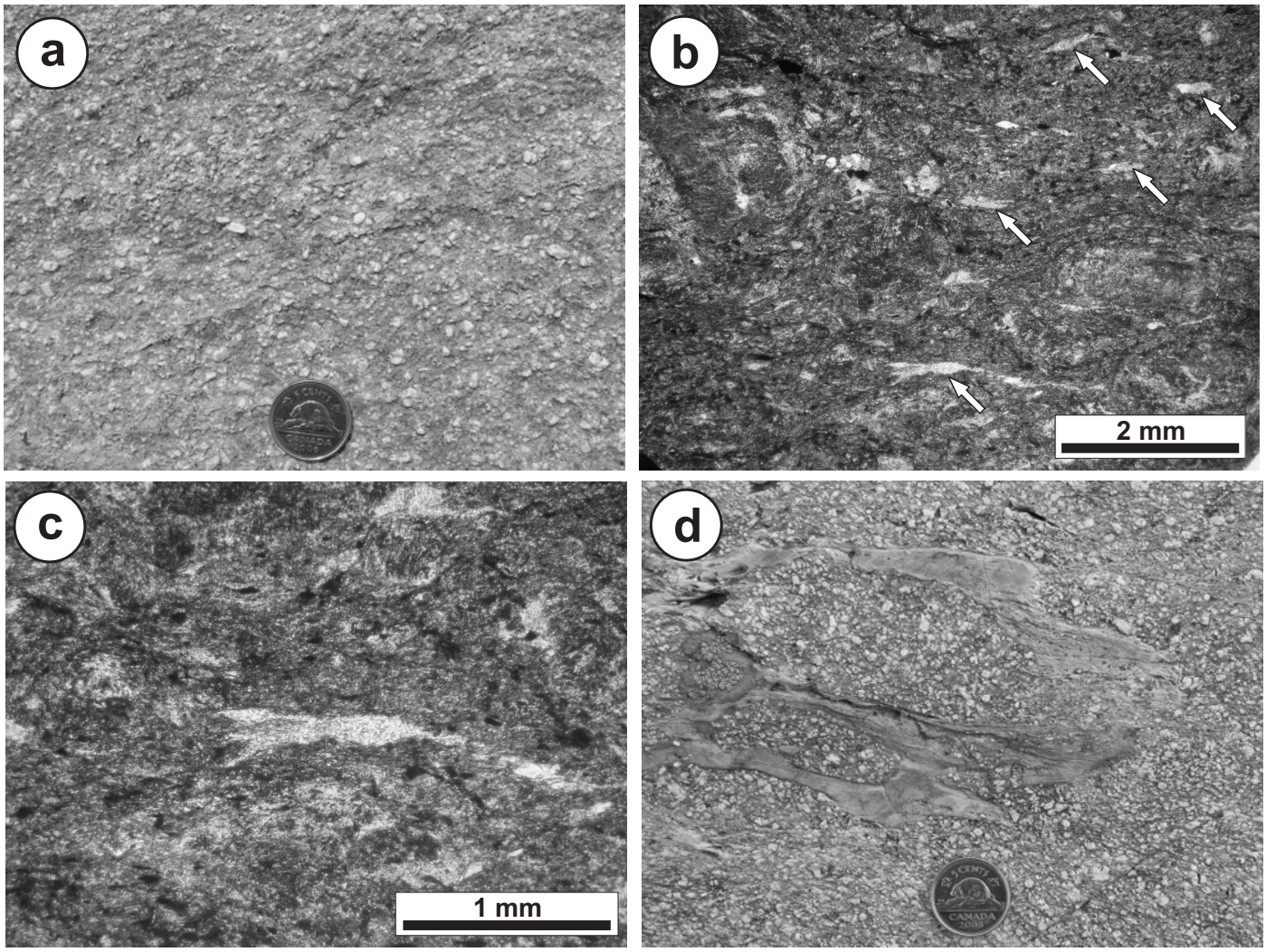

Figure 26: *Outcrop and thin-section photographs of the crystal-lithic lapilli tuff of map unit 16a:* ***a)*** *seriate-porhyritic texture in massive crystal-lithic lapilli tuff; 1 km east of Bissett on the south side of the SG-1 haul road;* ***b)*** *possible examples of collapsed felsic vitriclasts (arrows) showing wispy lenticular shapes, sample 85PEA-309 from P. Tirschmann thesis collection (plane-polarized light); sample location unknown;* ***c)*** *detail of previous, showing ragged outline and fine-grained granophyric texture of possible vitriclast;* ***d)*** *massive crystal-lithic lapilli tuff with a large clast of thin-bedded volcanic sandstone and mudstone that contains outsized clasts with texture similar to that of the enclosing lapilli tuff; 400 m east of the San Antonio Hotel in Bissett.*

amygdules. Other outcrops contain tabular to wispy clasts of thin-bedded volcanic sandstone and mudstone (Figure 26d).

The massive lapilli tuff contains indistinct layers or bodies of derived breccia and tuff breccia (Figure 27a, b). These breccias are monolithic, typically fragment supported and unsorted, and are composed of angular to subangular fragments of the massive lapilli tuff that range in size up to 1.0 m (generally 5–40 cm). The fragment shapes tend to be equant and blocky. Some outcrops are composed of angular interlocking fragments with less than 5% matrix material. Typically, the fragments are more coarsely and densely plagioclase phyric than the matrix, which in some localities contains only sparse plagioclase crystals over 1.0 mm. In other localities, however, the matrix and fragments are texturally similar and indistinct. The margins of individual fragments are generally sharp, although some exhibit diffuse margins that are suggestive of *in situ* disaggregation (Figure 27c). A resedimented origin is indicated by examples of mafic lapilli that are sharply truncated on the margins of some fragments (Figure 27a). In some outcrops, the matrix of the breccia contains scattered fragments of dark green, aphyric andesite or basalt (up to 10%), some of which exhibit wispy lenticular shapes, ragged terminations and vesicular textures, and are interpreted to represent recrystallized and partially collapsed juvenile vitriclasts (i.e., scoria; Figure 27d).

Subunit 16b consists of an approximately 120 m thick package in which the massive and brecciated crystal-lithic lapilli tuff is intercalated with volcanic sandstone and volcanic boulder and cobble conglomerate. The volcanic conglomerate is heterolithic, unsorted and typically matrix supported. Angular to well-rounded clasts range up to 50 cm across and are composed mainly of porphyritic andesite/dacite, with subordinate clasts of aphyric andesite/dacite and amygdaloidal basalt (Figure 28a). The matrix consists of medium-grained sandstone that contains less than 15% feldspar granules. The intercalations of fine- to very coarse grained volcanic sandstone and granule to pebble volcanic conglomerate range up to 5 m thick and exhibit well-developed planar bed forms that range up to 50 cm thick and dip moderately north (Figure 28b, c). Scours and normal size-grading in several locations indicate

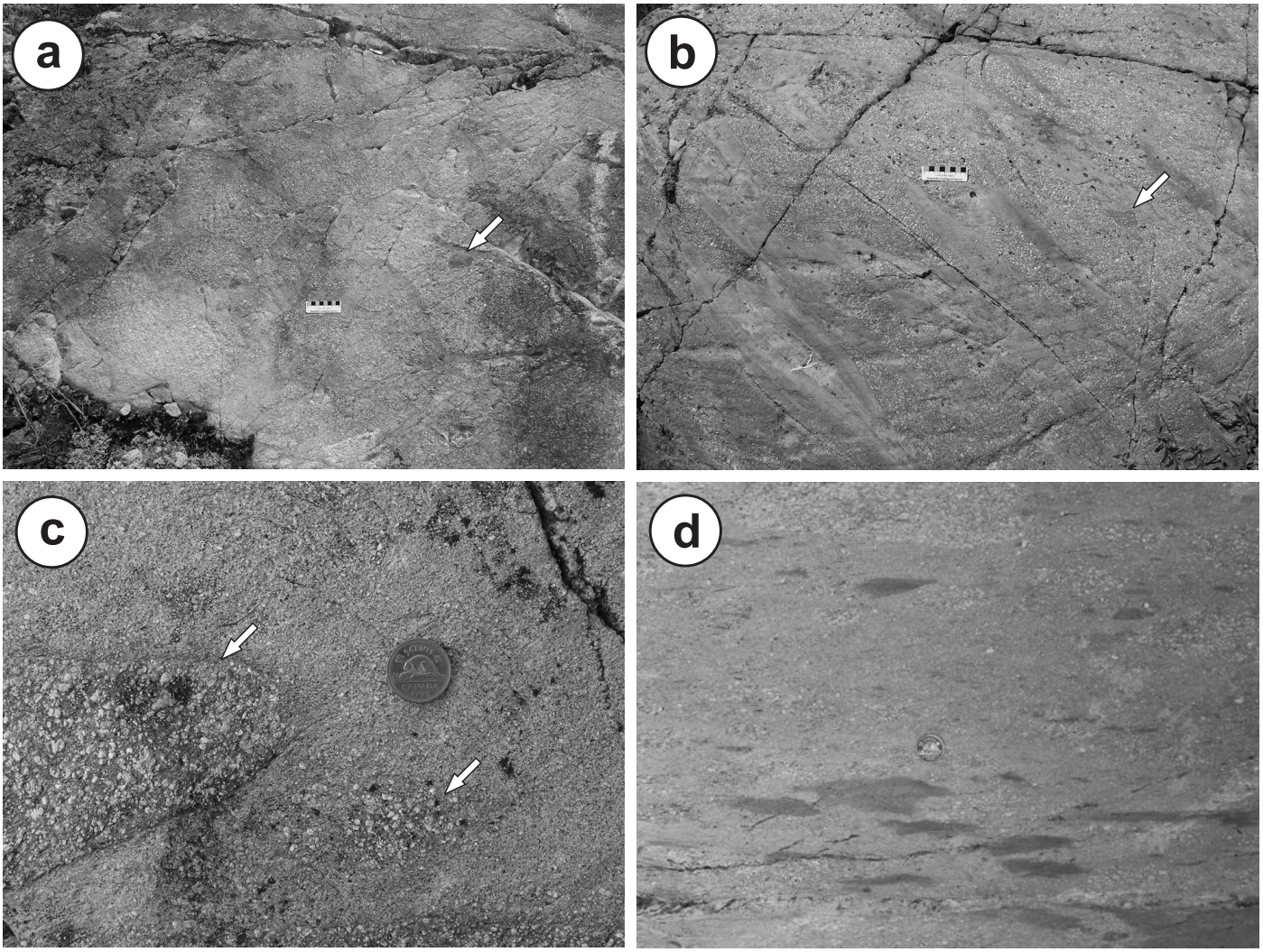

Figure 27: *Outcrop photographs of breccia and tuff breccia of unit 16a, west of Bissett:* ***a)*** *very coarse, fragment-supported breccia composed of plagioclase-phyric fragments in a slightly finer grained matrix; note the sharp truncation of a mafic inclusion on the margin of one block (arrow);* ***b)*** *matrix-supported breccia; note small mafic inclusion in one of the blocks (arrow);* ***c)*** *matrix-supported breccia composed of plagioclase-phyric blocks and lapilli in a finer grained matrix; fragments display both sharp (left) and diffuse (right) margins;* ***d)*** *tuff breccia with wispy, angular fragments of vesicular basalt, interpreted to represent partially collapsed scoria.*

that these rocks are upright (Figure 28b). Load-like structures, developed in one location near the base of subunit 16b, consist of bulbous bodies of crystal-lithic lapilli tuff that disrupt planar bed forms in overlying layers of fine-grained volcanic sandstone (Figure 28d). These features are interpreted to result from compaction-induced fluidization of water-saturated volcaniclastic deposits (*see* below).

The massive and brecciated crystal-rich rock types that characterize unit 16 have been variously described as quartz diorite porphyry (Wright, 1932), porphyritic andesite (Stockwell, 1938), dacitic crystal tuff (Davies, 1963) and porphyritic dacite (Tirschmann, 1986), with postulated modes of emplacement that have varied from intrusive to extrusive (lava flow) to 'glowing avalanche' to pyroclastic flow and surge, respectively. As described above, however, the micro- and meso-scale textures of both the massive and brecciated portions of unit 16 are indicative of a clastic origin and, in conjunction with field relationships, appear to preclude final emplacement as an intrusion or series of lava flows (*see also* Davies, 1963; Tirschmann, 1986). Moreover, the high abundance of euhedral plagioclase crystals, coupled with the significant component of broken crystals and juvenile vitriclasts, indicate that initial fragmentation most likely occurred by explosive eruption of crystal-rich magma. Nevertheless, the apparent absence of features associated with high-temperature emplacement (e.g., welding textures, columnar jointing or gas segregation pipes) argue strongly against explosive pyroclastic processes as the sole means of fragmentation, transport and final deposition.

For this reason, the author favours a resedimented, syneruptive depositional model, wherein the massive lapilli tuff is interpreted to be composed of reworked primary pyroclastic detritus that was redeposited in a shallow subaqueous setting by syneruptive, high-density (i.e., hyperconcentrated) grain flows. A comparable model was proposed by Cas (1979, 1983) for similar crystal-rich volcaniclastic deposits in the Lower Devonian of southeastern Australia. As suggested by Cas (1983), the high concentration of coarse euhedral crystals relative to vitriclasts, coupled with the lack of evidence for significant reworking, appear to implicate syneruptive elutriation processes as the mechanism of producing unusually crystal-rich

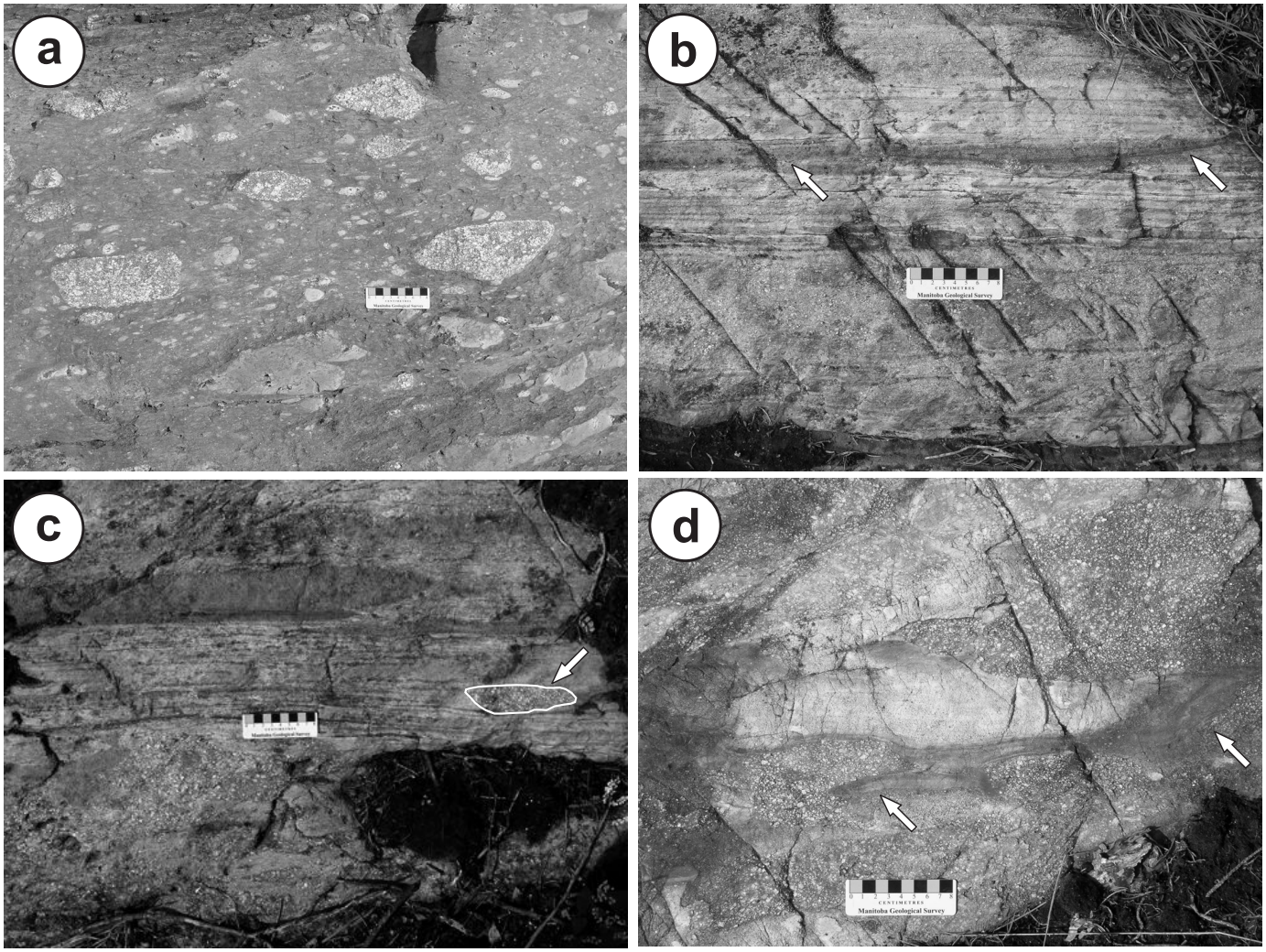

Figure 28: *Outcrop photographs of rock types in map unit 16b, west of Bissett:* ***a)*** *matrix-supported volcanic conglomerate composed of unsorted, angular to subrounded pebbles and cobbles of plagioclase-phyric and aphyric andesite;* ***b)*** *bedded volcanic sandstone with low-angle scour surface (arrows) that indicates tops to the north (top of photograph);* ***c)*** *pebble to cobble volcanic conglomerate (bottom) overlain by thin-bedded volcanic sandstone (top) that contains outsized clasts of crystal-lithic lapilli tuff (outlined); this type of layer likely represents the source of the clasts shown in Figure 26d;* ***d)*** *bedded volcanic sandstone disrupted (arrows) by bulbous bodies of plagioclase-phyric material, interpreted to result from compaction-induced fluidization.*

volcaniclastic deposits. The brecciated portions of subunit 16a, which are composed of angular to subangular, locally interlocking fragments of the massive lapilli tuff (some of which exhibit textural evidence of *in situ* disaggregation), are interpreted to represent secondary mass flows generated by gravitational instability of the partially consolidated grain-flow deposits. The minor intercalations of well-stratified volcanic sandstone and heterolithic volcanic conglomerate (subunit 16b) indicate periodic influxes of more highly reworked (epiclastic) detritus, which was likewise deposited in a shallow subaqueous setting by high-density grain and mass flows.

Round Lake unit

The Round Lake (RL) unit consists of a basal heterolithic volcanic conglomerate unit (unit 18), overlain to the north by a succession of volcanic, volcaniclastic and epiclastic rocks that, up section, exhibit increasingly felsic bulk compositions, from andesitic (unit 19) through dacitic (unit 20) to rhyolitic (unit 21; Figures 3, 5, 29). The basal conglomerate includes minor layers of sanukitoid-affinity basalt tuff, which are geochemically similar to hypabyssal diabase dikes in the underlying RLR and TS units (unit 17). Unlike the underlying IL, RLR and TS units, mafic intrusions are apparently absent in all but the lowermost portion of the RL unit (e.g., Stockwell, 1938), and the constituent volcanic rocks are, in places, distinctly hornblende phyric. The RL unit trends west, dips moderately north and ranges up to 1.7 km thick. This unit is truncated to the north and east by the WSZ, and is unconformably overlain to the west by west-facing rocks of the San Antonio assemblage. Apparent finite strain generally increases toward the east in this unit, and the aspect ratios of deformed clasts in horizontal outcrop surfaces near the confluence of the NCSZ and WSZ locally exceed 100:1 (some of these rocks were previously mapped as bedded rhyolitic tuff; e.g., Davies, 1963, Plate 3). The high finite strain likely accounts for the progressive eastward decrease in thickness, and local pinching out, of the RL unit.

Diabase (unit 17)

Diabase of unit 17 is characterized by a distinctive sanukitoid-affinity geochemical signature and, on this basis, has

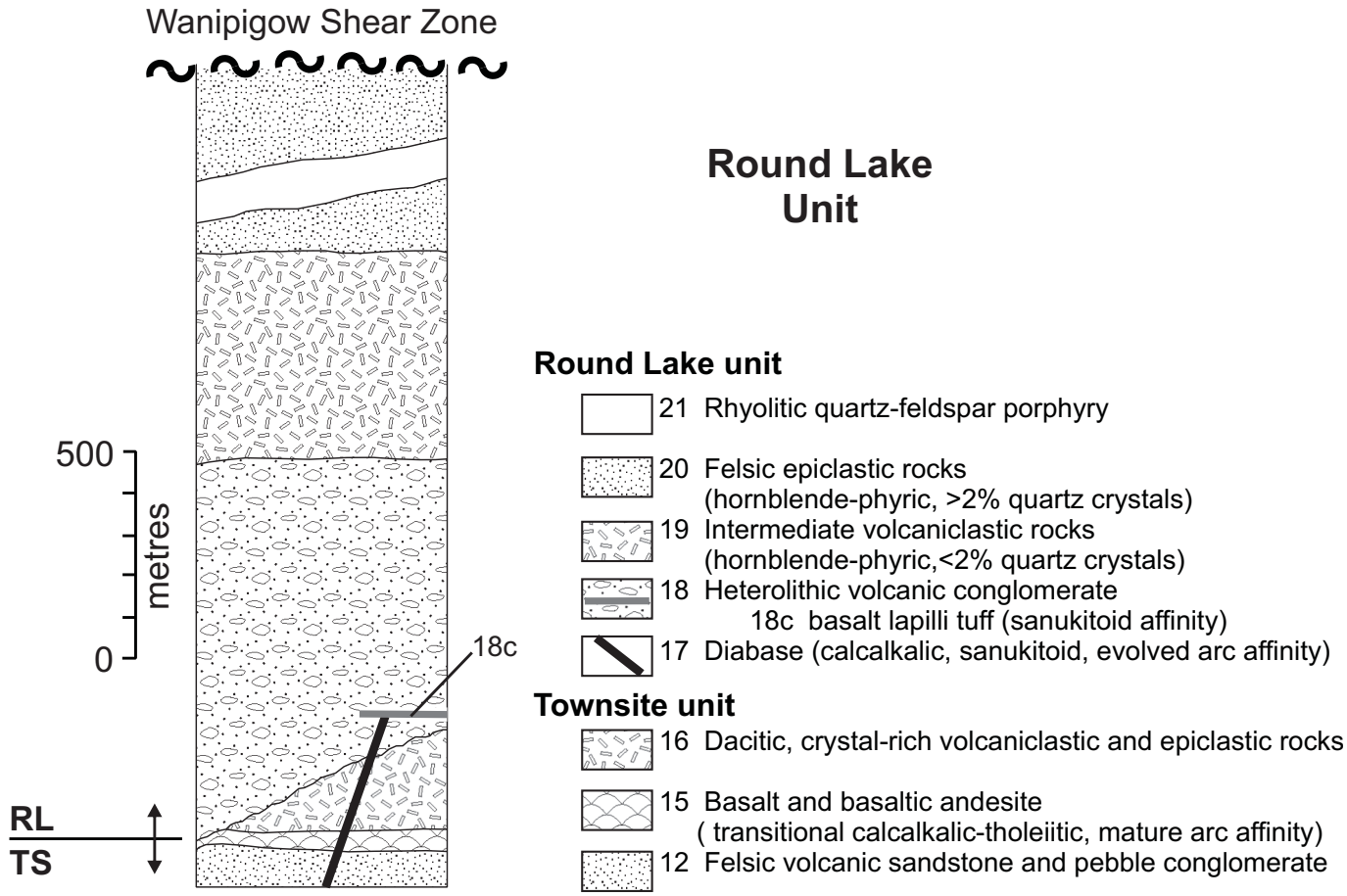

Figure 29: *Schematic stratigraphic column for the Round Lake (RL) unit. Unit numbers correspond to those in the text and on Map GR2008-1-1.*

been identified as intrusive dikes and sills in two locations in the RLR unit (hosted by units 7 and 10) and in one location in the TS unit (unit 16). The largest of these intrusions ranges up to about 3 m thick and is thus not mappable at 1:20 000 scale. Included in this unit are planar to irregular dikes and sills of texturally similar diabase that locally define swarms at the top of the TS unit and are not observed north of the upper contact. These intrusions, which are shown as 'meta-diabase' on the maps of Stockwell (1938), are best observed along the south slope of the large outcrop ridge just north of the trailer park in Bissett.

The diabase weathers light green and is dark green on fresh surfaces. In most outcrops, the diabase is characterized by a very fine to medium-grained, equigranular subophitic texture. Most specimens are strongly altered, and fine-grained chlorite, epidote, sericite and carbonate replace the primary mineral assemblage. The cores of some intrusions contain 2–3% subhedral actinolite (after pyroxene) phenocrysts (2–5 mm across; Figure 30a). In others intrusions, the cores contain up to 5% subhedral plagioclase phenocrysts (2–4 mm). Most of these intrusions have planar and sharp contacts with well-developed, typically 5–10 cm thick chilled margins (Figure 30b). One of the dikes sampled for geochemistry is composite, with evidence of at least three injection phases. Other dikes, particularly near the upper contact of unit 16, are highly irregular and amoeboid (Figure 30c), suggesting emplacement into unconsolidated volcaniclastic material.

Heterolithic volcanic conglomerate (unit 18)

Heterolithic volcanic conglomerate at the base of the RL unit defines a distinct map unit that ranges up to 650 m thick and is well exposed in the large outcrop ridge just north of PR 304 between Bissett and the Vanson road turn-off. Good exposures of this unit are also found along the south side of the tailings impoundment northeast of Bissett. The volcanic conglomerate is typically crudely stratified, matrix supported and poorly sorted (Figure 31a), and contains very well rounded to subangular clasts that range up to 2.5 m across (typically 0.5–30 cm). Individual clasts range in shape from tabular to nearly spherical. Many clasts exhibit narrow (<2 cm) bleached margins, possibly as a result of predepositional weathering. In general, the dominant clast type is buff to light grey, aphanitic to fine-grained, aphyric to sparsely feldspar-phyric andesite, which is similar in appearance to unit 6 of the IL unit. Near the base of this unit, however, clasts of crystal-lithic lapilli tuff from the underlying TS unit predominate, and the conglomerate locally contains distinct, 1–3 m thick layers in which these clasts constitute up to 90% of the clast population (subunit 18b). Resedimented clasts are present in most outcrops and include examples of thin-bedded volcanic sandstone. The matrix consists of green-grey, fine- to coarse-grained feldspathic sandstone that generally lacks coarse detrital quartz. Crudely stratified intervals, defined by subtle changes in the proportion of clasts and matrix on a 1–10 m scale, characterize the base of this unit and include minor interlayers of thin-bedded, medium- to coarse-grained

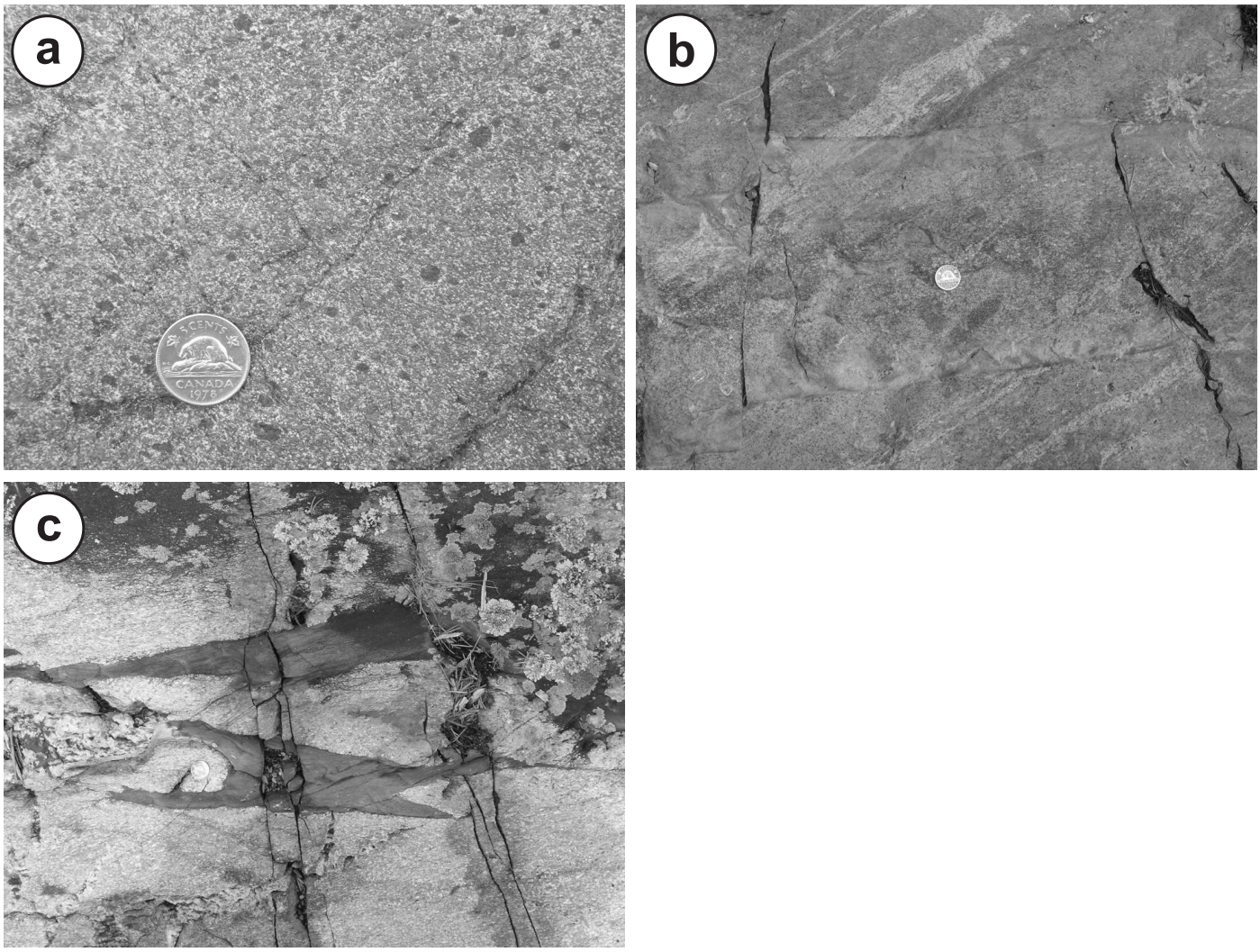

Figure 30: *Photographs of sanukitoid-affinity diabase dikes of map unit 17:* ***a)*** *pyroxene-phyric diabase dike hosted by aphyric dacite breccia of unit 7, Rainy Lake road;* ***b)*** *well-developed chilled margins on thin diabse dike hosted by massive gabbro of unit 9 in the footwall of the SG-3 deposit;* ***c)*** *thin, irregular diabase dikes in the uppermost portion of unit 16, Provincial Road 304, northeast of Bissett.*

volcanic sandstone up to 50 cm thick (subunit 18a). The beds dip moderately to the north, and a scour in one location indicates these rocks are upright. The heterolithic clast population and high degree of rounding, coupled with the possible presence of weathered rinds on some clasts, suggest significant subaerial transport, with final deposition in a high-energy fan setting.

The contact with the underlying TS unit is well exposed in several large outcrops immediately north of the new trailer park in Bissett, and is clearly depositional (Stockwell, 1938; Davies, 1963; Tirschmann, 1986). Here, the top of the TS unit is marked by 2–3 m of reworked crystal-rich volcaniclastic material, overlain to the north by 35–40 m of heterolithic conglomerate in which the proportion of crystal-lithic lapilli tuff clasts decreases northward from 90% to less than 20%. In this location, the TS unit is crosscut by dikes and sills of fine-grained diabase (unit 17; sanukitoid-affinity), which have well-developed chilled margins. These dikes were not observed north of the contact. Instead, the conglomerate contains texturally similar fragments of pale green basalt (Figure 31b) that locally constitute up to 80% of the clast population. These fragments, which range up to 20 cm across, are very angular to subangular and commonly exhibit delicate cuspate shapes. Several fragments have distinctly finer grained, dark green rims that are suggestive of chilled margins, and are thus interpreted to result from primary fragmentation of proximal lava flows, by either autoclastic or hyaloclastic processes. In one location, approximately 35 m above the basal contact, the conglomerate also contains a 15 m thick layer of pale green–weathering mafic tuff that appears to coincide with the northernmost of a series of sill-like 'meta-diabase' bodies mapped by Stockwell (1938). Two samples of this layer collected for lithogeochemical analysis indicate it is composed of sanukitoid-affinity basalt (subunit 18c) that is chemically indistinguishable from the underlying diabase dikes. Lapilli of aphanitic black basalt (2–3%; 0.5–40 mm) are evenly distributed throughout the layer and range in shape from very angular and shard like to wispy and lenticular with ragged terminations (Figure 31c). These fragments are interpreted to represent altered and collapsed juvenile pyroclasts (i.e., scoria). The tuff also contains rare subhedral feldspar crystals that range from 1 to 3 mm. The basal contact of the tuff layer, exposed in one location, is sharp and slightly undulose, and appears to be depositional (Figure 31d). On the basis of these features, the basalt tuff is interpreted to represent a distal scoria-fall deposit that accompanied

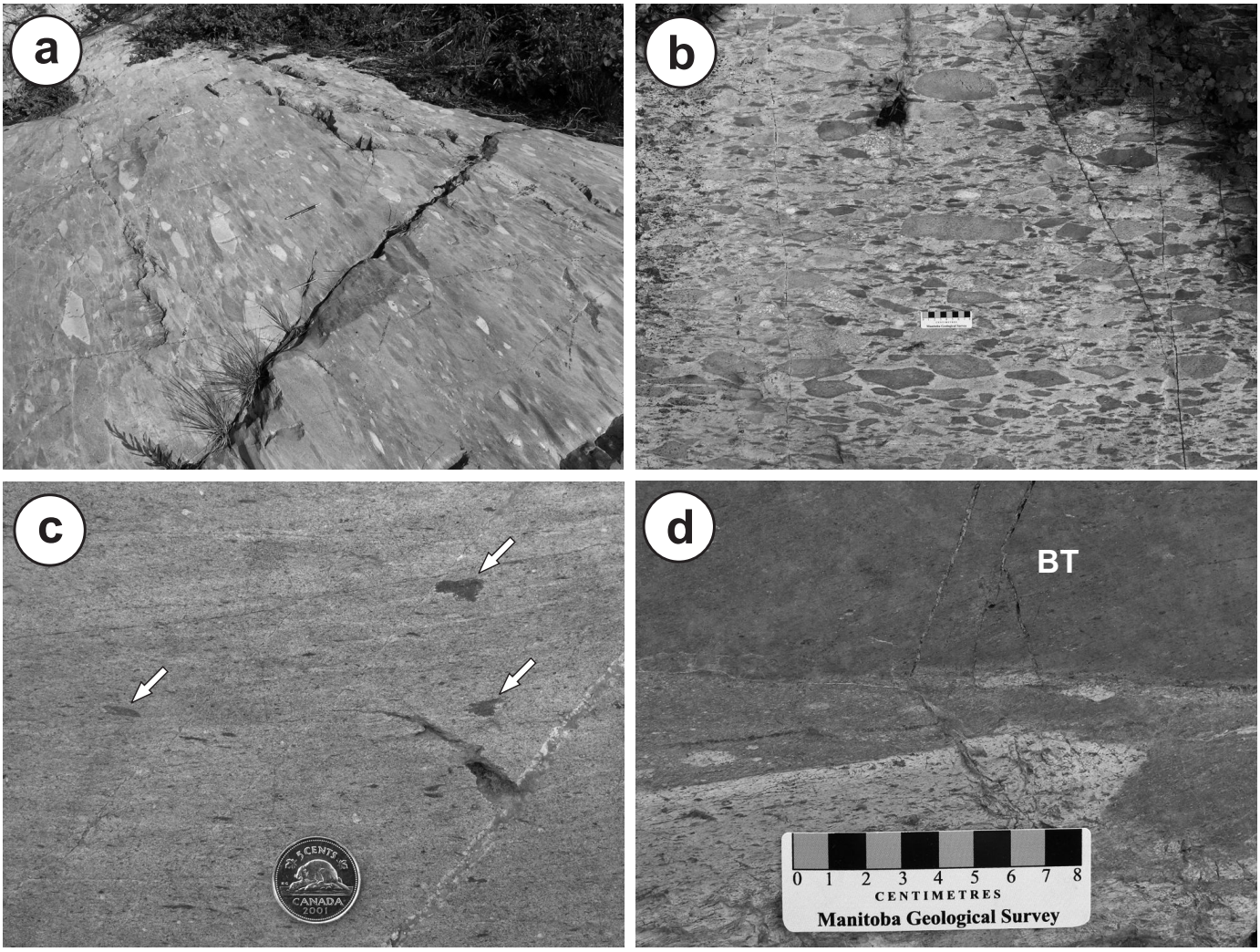

Figure 31: *Outcrop photographs of rock types in map unit 18, north of Bissett:* ***a)*** *moderately well stratified, matrix-supported volcanic conglomerate, composed of subangular to rounded pebbles, cobbles and boulders of various volcanic, volcaniclastic and epiclastic rock types;* ***b)*** *crudely stratified, heterolithic, pebble and cobble volcanic conglomerate; note the abundance of angular to subangular clasts of dark grey basalt, particularly in the lower portion of the photograph;* ***c)*** *angular to wispy basalt lapilli (arrows), interpreted to represent partially collapsed scoria, in the massive basalt tuff layer at the base of unit 18;* ***d)*** *base of the basalt tuff layer (BT), showing sharp and slightly undulose contact.*

emplacement of hypabyssal dikes and local lava effusions composed of sanukitoid-affinity diabase and basalt.

Intermediate volcaniclastic rocks (unit 19)

The medial portion of the Round Lake unit contains a poorly exposed unit of intermediate volcaniclastic rocks that ranges up to 1.1 km thick. The best outcrops of this unit occur along the western and northern margins of the tailings impoundment north of Bissett. The upper and lower contacts of this unit appear to be conformable and gradational. The dominant rock type is massive to faintly layered crystal-lapilli tuff (subunit 19a; Figure 32a) of andesitic composition that weathers pale green-grey to buff-brown and is dark green or grey on fresh surfaces. The lapilli tuff contains 10–25% plagioclase crystals that range in size up to 8 mm and are evenly distributed in a very fine grained matrix of feldspar, quartz, sericite, chlorite and epidote. Euhedral to subhedral plagioclase crystals typically predominate, although some samples contain subequal amounts of angular broken crystals (Figure 32b). In some outcrops, the lapilli tuff contains subordinate (1–5%) euhedral to subhedral hornblende crystals that range in size from 1 to 5 mm. Anhedral quartz crystals (<2 mm) are also locally observed but do not exceed 2% of the rock. Most outcrops contain rare, angular to rounded lithic lapilli composed of dark green, aphyric to feldspar-phyric andesite or basalt. Subtle variations in the proportion and size of the plagioclase crystals define diffuse, laterally continuous (>20 m) layers up to 50 cm thick; intervals of layered lapilli tuff range up to 15 m thick. The crystal-lapilli tuff is interlayered in some outcrops with intermediate tuff breccia and breccia (subunit 19b). The tuff breccia is massive, unsorted, matrix supported and typically monolithic, although heterolithic breccia is common near the base of the unit. The angular to subrounded fragments, which range up to 1 m across (generally 5–40 cm), are typically texturally similar to the crystal tuff, although often more densely plagioclase phyric. In some cases, the clasts also contain a higher abundance of hornblende crystals as compared to the matrix. Rare lithic lapilli within the fragments indicate a resedimented origin (Figure 32c). Dikes of feldspar-hornblende–porphyritic andesite (subunit 19c) that cut the San Antonio mine (SAM) unit at

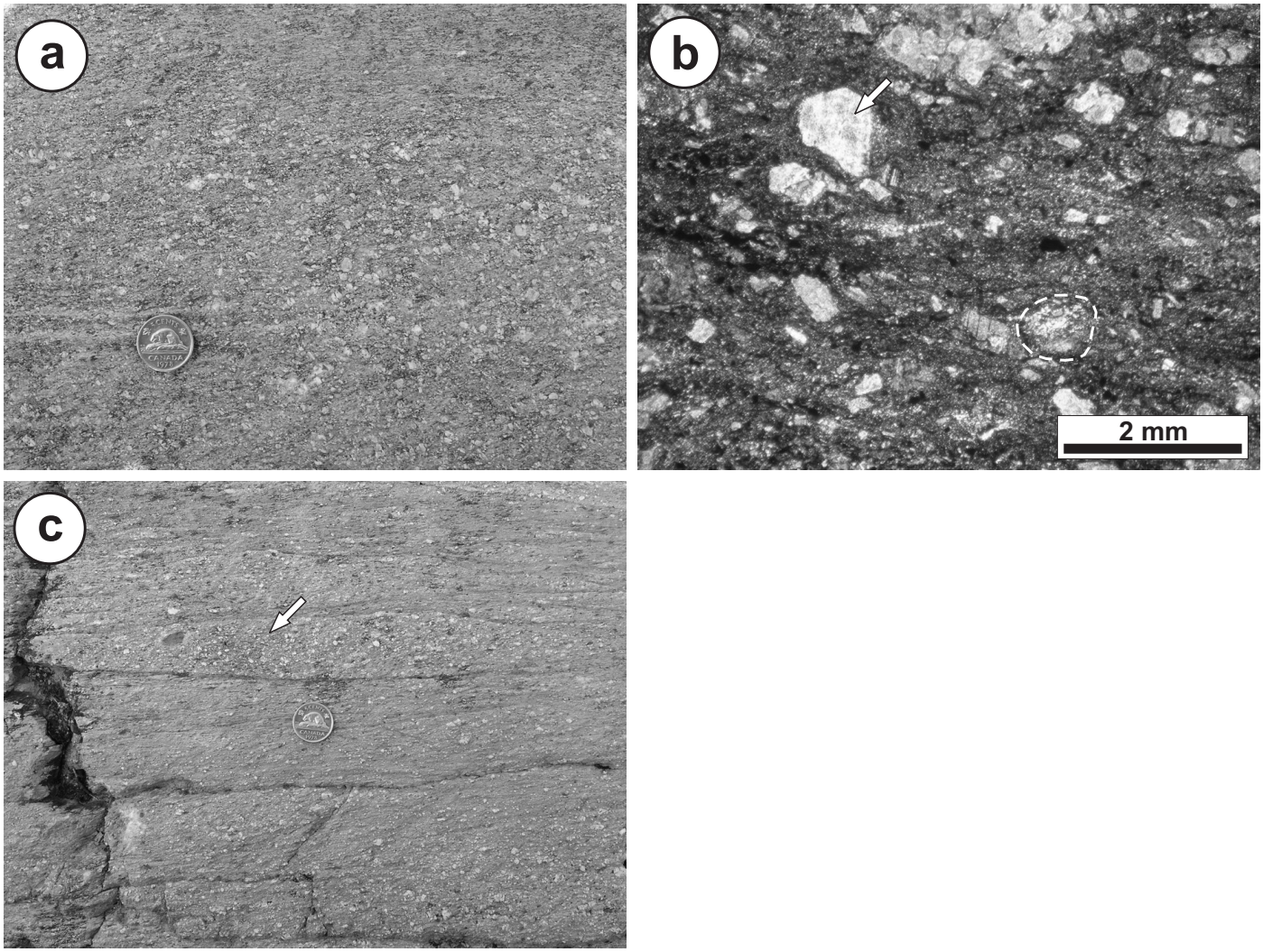

Figure 32: *Outcrop and thin-section photographs of rock types in map unit 19; northern edge of the new tailings impoundment, north of Bissett:* ***a)*** *faintly stratified example of andesitic crystal-lapilli tuff (subunit 19a);* ***b)*** *broken plagioclase crystal (arrow) and lithic clast (outlined) in crystal-lithic lapilli tuff (cross-polarized light);* ***c)*** *block of redeposited crystal-lithic lapilli tuff (arrow) in andesitic tuff breccia (subunit 19b).*

Rice Lake are included in unit 19 on the basis of their similar texture and composition. Unit 19 is similar in many respects to unit 16 of the TS unit, and is likewise interpreted to be composed mainly of reworked pyroclastic material, with final deposition by subaqueous high-density grain flows.

Felsic epiclastic rocks (unit 20)

The upper portion of the RL unit consists of a 400–450 m thick succession of felsic epiclastic rocks that is extensively exposed north and northeast of Bissett, in the prominent outcrop ridge along the south margin of the Wanipigow Shear Zone. The cleanest exposures of these rocks are found along the Vanson road and in the cleared area north of the town dump, as well as in the large rock quarry 5 km east of Bissett on the north side of PR 304. This unit consists mainly of intercalated pebble to cobble volcanic conglomerate and volcanic sandstone (Figure 33a, b), with minor interbeds of volcanic mudstone (subunit 20a). The conglomerate is heterolithic, unsorted to poorly sorted and matrix supported, and contains subangular to well-rounded clasts that are typically 1–10 cm across but locally range up to 1 m. Buff- to light grey–weathering, sparsely quartz- and feldspar-phyric dacite is the dominant clast type throughout this unit and typically contains up to 5% anhedral quartz 'eyes' and 5–20% subhedral feldspar phenocrysts, which normally do not exceed 3 mm. In general, the quartz-crystal component of the dacite clasts and matrix becomes coarser and more abundant up-section. Subordinate clast types include coarsely feldspar-phyric andesite, quartz-phyric pink-white rhyolite and minor aphyric basalt. The conglomerate layers range up to 10 m thick and are massive to moderately graded; some layers exhibit reverse-graded bottoms and normal-graded tops. Normal-graded layers are capped by bedded intervals (beds <30 cm thick) of fine- to very coarse grained, pebbly volcanic sandstone and mudstone that range up to several metres thick. Normal-graded beds and scours in four locations indicate tops to the north. In the field, the contact with the underlying intermediate volcaniclastic rocks of unit 19 is generally gradational over 30–50 m, and was defined on the basis of the first appearance of significant (>2%) coarse quartz as granules in the matrix or as phenocrysts in clasts. The contact relationships with unit 21 are described below. The overall characteristics of this unit indicate significant reworking and transport of detritus

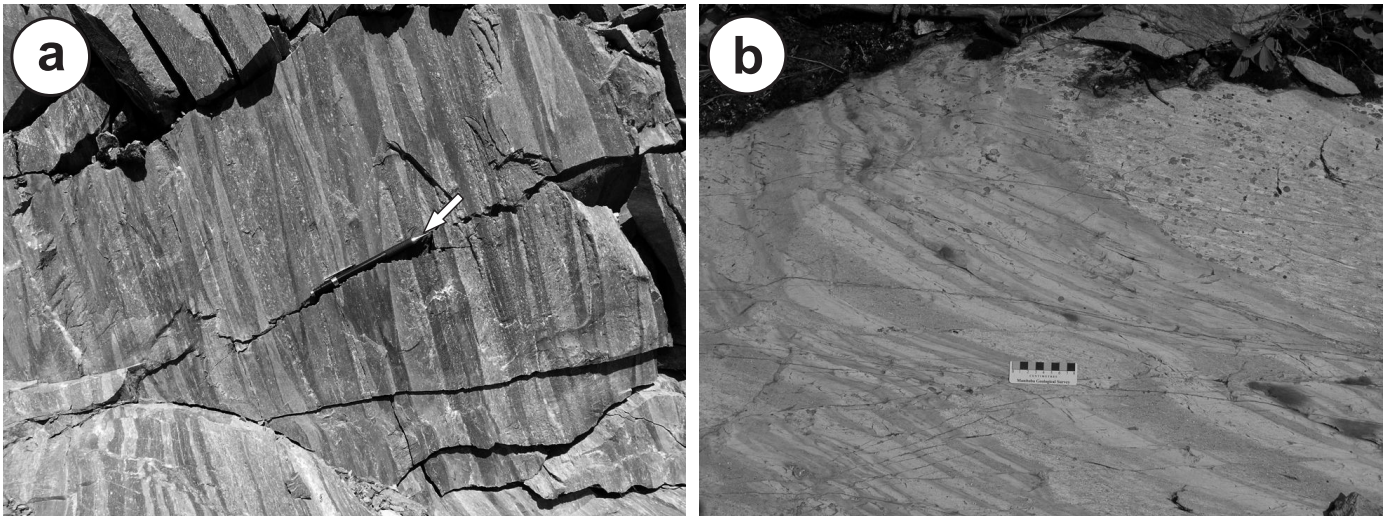

Figure 33: *Outcrop photographs of rock types in map unit 20:* ***a)*** *volcanic conglomerate composed mostly of subrounded cobbles of variably quartz- and/or feldspar-porphyritic dacite (pencil for scale indicated by arrow), rock quarry north of Provincial Road 304, 5 km east of Bissett;* ***b)*** *bedded volcanic sandstone and pebble conglomerate, Vanson mine road.*

that was likely sourced from a dacitic vent complex, with final deposition via subaqueous low-density debris and grain flows.

Rhyolitic quartz-feldspar porphyry (unit 21)

The felsic epiclastic rocks at the top of the RL unit contain a distinctive unit of massive quartz-feldspar porphyry that ranges from 100 to 150 m thick and is traced continuously along strike for more than 7.0 km. Previous authors have variously described this porphyry as intrusive (Stockwell, 1945; Davies, 1963), intrusive and extrusive (Poulsen et al., 1986) or extrusive (Bailes, 1998). The porphyry weathers buff or light grey and typically exhibits a seriate-porphyritic texture defined by phenocrysts of feldspar (10–30%) and quartz (2–5%), which range in size up to 10 mm and are evenly distributed in an aphanitic to very fine grained matrix of feldspar, quartz, sericite and carbonate (Figure 34a). Locally, this rock also contains up to 2% euhedral hornblende crystals. The feldspar crystals are typically euhedral to subhedral and concentrically zoned. The quartz crystals are slightly blue-grey and typically euhedral to subhedral. In thin section, the quartz crystal component includes abundant examples of embayed crystals, which range in shape from spherical to highly amoeboid and delicate (Figure 34b, c). In places, the porphyry contains up to 5% subangular to subrounded inclusions of aphanitic green-grey andesite that range up to 5 cm across. Although generally very massive and homogeneous, variations in the proportion of feldspar crystals in one location define very subtle, diffuse layers that are concordant with the trend of the unit. Toward the west, the porphyry cuts discordantly down through bedded felsic epiclastic rocks of unit 20 and lies in contact to the south with the more massive intermediate volcaniclastic rocks of unit 19. On the basis of this discordant map pattern, as well as the common preservation of delicately embayed, presumably magmatic, quartz crystals, unit 21 is herein interpreted to represent a very high level hypabyssal intrusion. A sample of this material (sample 96-04-1384) was collected for U-Pb geochronological analysis to establish the age of what appears to represent the youngest Neoarchean magmatism in the Rice Lake section of the Bidou assemblage.

Gold Creek unit

The Gold Creek (GC) unit consists of an intensely transposed package of intermediate volcaniclastic rocks (unit 22), basalt flows and gabbro (unit 23), a thick succession of intermediate epiclastic and effusive volcanic rocks (unit 24), and minor dikes and sills of quartz-feldspar porphyry (unit 25). These rocks are best exposed in the area west of Horseshoe Lake, between PR 304 and the Wanipigow River. Also included in the GC unit are sparse outcrops of pillowed basalt flows and gabbro that occur south of PR 304 along the wide drift-filled valley of Gold Creek. On the basis of comparable rock types and chemistry, the GC unit is tentatively correlated with the upper portion of the Bidou assemblage at Rice Lake. Due to the intense transposition and generally poor exposure, however, the internal contact relationships and stratigraphy of the GC unit remain poorly constrained.

To the east, the GC unit lies in contact with west-facing sedimentary rocks of the San Antonio assemblage, which are inferred to be younger on the basis of regional geological and geochronological constraints, and the conspicuous absence of crosscutting intrusions (e.g., Stockwell, 1938, 1945; Davies, 1953, 1963). The map patterns of these assemblages define a macroscopic train of tight upright folds, the most prominent examples of which are the Horseshoe Lake anticline and Gold Creek syncline (Figure 3). Facing criteria in packets of intensely transposed epiclastic rocks in the hinge of the Horseshoe Lake anticline indicate that the GC unit also faces west and thus describes an older-over-younger relationship with the San Antonio assemblage. For this reason, the basal contact of the GC unit is here interpreted as a thrust fault, along which the GC unit was emplaced atop the San Antonio assemblage prior to regional folding. To the north, the GC unit is tectonically juxtaposed with a fault-bounded panel of the San Antonio assemblage along the Wanipigow Shear Zone. To the south, the contact with tonalite of the Ross River plutonic suite is presumed to represent the westward continuation of the basal thrust. Hence, the GC unit is structurally bounded to the north, east and south, but remains ‘open’ to the west beyond the limits of this project.

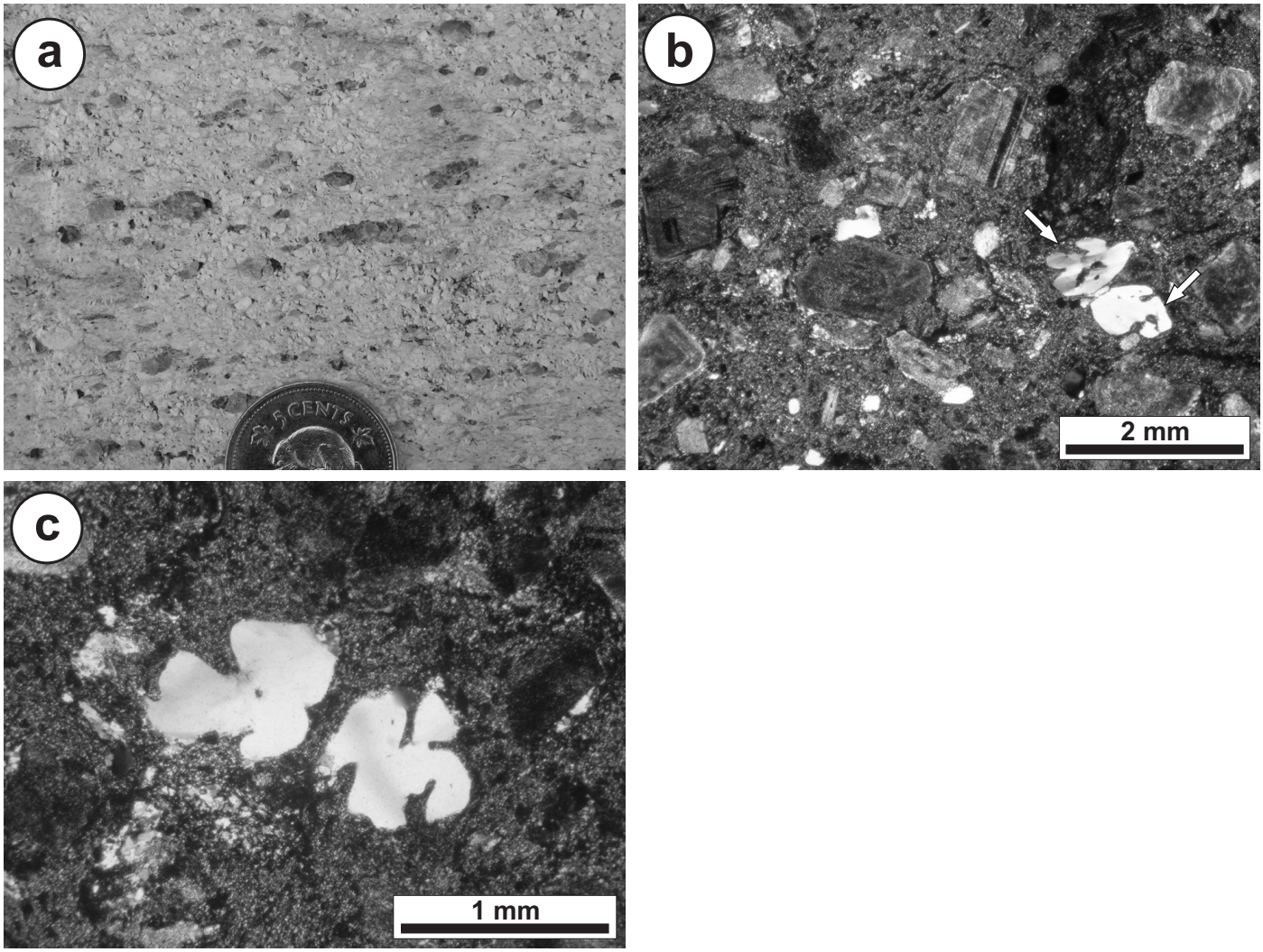

Figure 34: *Outcrop and thin-section photographs of rock types in map unit 21:* ***a)*** *massive quartz-feldspar porphyry, Vanson mine road;* ***b)*** *porphyritic texture defined by euhedral plagioclase and resorbed quartz (arrows) phenocrysts in a fine-grained quartzofeldspathic matrix (cross-polarized light), north of Bissett;* ***c)*** *strongly resorbed, 'amoeboid' quartz phenocrysts (cross-polarized light), north of Bissett.*

Intermediate volcaniclastic rocks (unit 22)

Two outcrops in the hinge of the Horseshoe Lake anticline are composed of a coarsely porphyritic rock that is interpreted to define the base of the GC unit in this location. This rock weathers green to brown, is green on fresh surfaces and exhibits a massive seriate-porphyritic texture defined by up to 40% subhedral plagioclase crystals (<10 mm) in a fine-grained matrix of feldspar, quartz, epidote and chlorite. A vague fragmental texture is locally defined by equant to irregularly shaped, lapilli-sized fragments that are more coarsely and densely porphyritic than the matrix. Locally, this rock also contains 1–2% subhedral quartz crystals. Although poorly exposed, this rock type closely resembles the intermediate volcaniclastic rocks of the RL unit (i.e., unit 19), and is thus tentatively interpreted to be of similar origin.

Basalt and gabbro (unit 23)

Outcrops of mafic intrusive and extrusive rocks define an approximately 300 m thick map unit in the core of the Horseshoe Lake anticline. Similar rocks exposed in widely scattered outcrops in the hinge and on the south limb of the Gold Creek syncline are interpreted to represent the southern continuation of this unit. Pillowed basalt flows (subunit 23a) are best exposed in the hinges of both the Horseshoe Lake anticline and the Gold Creek syncline. The basalt weathers pale green to grey and is dark green on fresh surfaces. Most specimens are aphyric and nonamygdaloidal, with a subophitic texture defined by fine laths of plagioclase (40–50%) in an aphanitic to fine-grained matrix of actinolite, chlorite, epidote and carbonate. The pillows range from bun shaped to amoeboid and are typically highly flattened (Figure 35a, b), with chloritic selvages that range up to 5 cm thick (typically less than 2 cm). Interpillow material generally accounts for less than 5% of individual outcrops and appears to consist of strongly altered (chlorite calcsilicate) hyaloclastite (Figure 35c). In the hinge of the Horseshoe Lake anticline, the interpillow material is locally tourmalinized (Figure 35d) and, in some outcrops, the pillow cores contain patchy, pale brown-pink calcsilicate alteration and up to 5% calcsilicate veins (Figure 35e). These outcrops also contain localized swarms of quartz-feldspar porphyry dikes (Figure 35f), which are possibly correlative with unit 25. The pillowed flows contain minor intercalations of pillow-fragment breccia that range up to 15 m

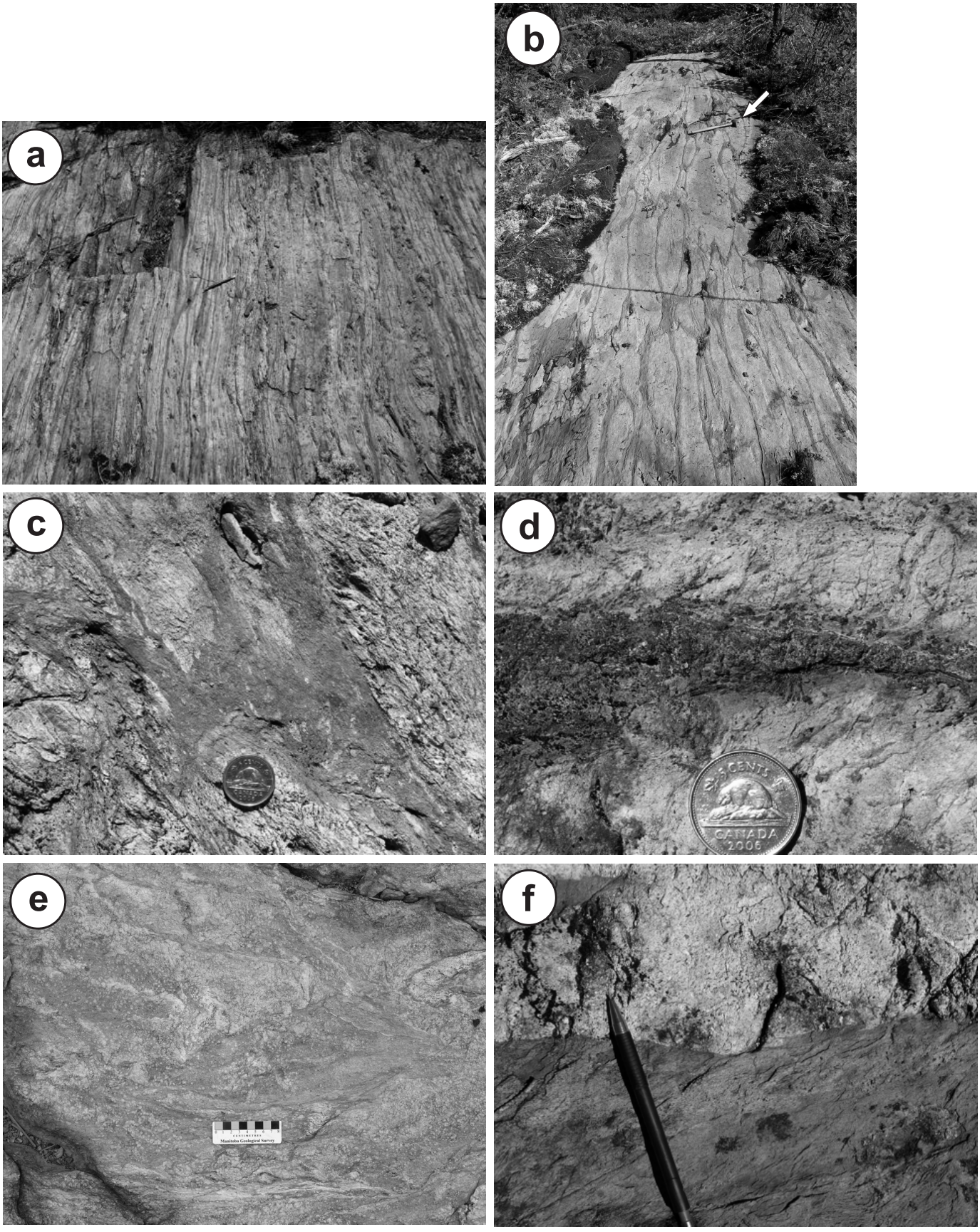

Figure 35: *Outcrop photographs of rock types in map unit 23:* ***a)*** *strongly flattened pillowed basalt in the hinge of the Horseshoe Lake anticline, west of Horseshoe Lake;* ***b)*** *pillowed aphyric basalt, south of Horseshoe Lake;* ***c)*** *well-preserved interpillow hyaloclastite, west of Horseshoe Lake;* ***d)*** *tourmaline-epidote-magnetite alteration in pillow intersticies, same location as previous;* ***e)*** *patchy to veinlet-controlled calcsilicate alteration in pillowed basalt, west of Horseshoe Lake;* ***f)*** *sharp contact between basalt and crosscutting quartz-feldspar porphyry dike, west of Horseshoe Lake.*

thick and are composed of angular to wispy, closely packed fragments of basalt that locally display well-developed chilled margins.

The pillowed basalt flows are associated with sill-like bodies of gabbro and/or massive basalt flows that range up to at least 50 m thick (subunit 23b). These rocks weather light green-grey to brown and are dark green on fresh surfaces. Most are massive and leucocratic, with a fine- to medium-grained subophitic texture defined by lath-shaped plagioclase crystals (60–80%) in a fine-grained matrix of chlorite, actinolite, epidote and carbonate (20–40%), with up to 3% magnetite. In some specimens, equant to tabular aggregates (1–5 mm) of actinolite, chlorite, biotite and epidote, which likely replace primary pyroxene, define a porphyritic texture. Most samples are moderately to strongly epidotized and contain 2–3% epidote veins. Up to 5% quartz is present in rare pods of coarse-grained to pegmatitic gabbro. Although the nature of the contact relationship with the associated pillowed basalt flows remains unknown, the close spatial association and chemical similarity of these rock types are interpreted to indicate a comagmatic relationship.

Intermediate epiclastic and effusive volcanic rocks (unit 24)

The upper portion of the GC unit is best exposed on the north limb of the Horseshoe Lake anticline, where it ranges up to at least 900 m thick. This unit consists mainly of intermediate volcanic conglomerate (subunit 24a) and sandstone (subunit 24b), with minor andesite flows and associated volcaniclastic rocks (subunit 24c). Massive to faintly stratified volcanic conglomerate predominates in the upper portion of this unit. This conglomerate weathers light green-grey to reddish brown and is heterolithic, unsorted to poorly sorted and generally matrix supported (Figure 36a). Variations in the size and proportion of clasts define sharp to diffuse bed forms in some outcrops, although the exposure is generally insufficient to determine the internal organization of individual beds. Angular to rounded clasts of variably feldspar-phyric, intermediate to felsic volcanic rock predominate, and range up to 75 cm in maximum dimension (typically 5–40 cm). Subordinate clast types include white aphyric rhyolite, dark green aphyric basalt and epidosite. This conglomerate is interpreted to record deposition from high-density debris flows in a shallow subaqueous setting.

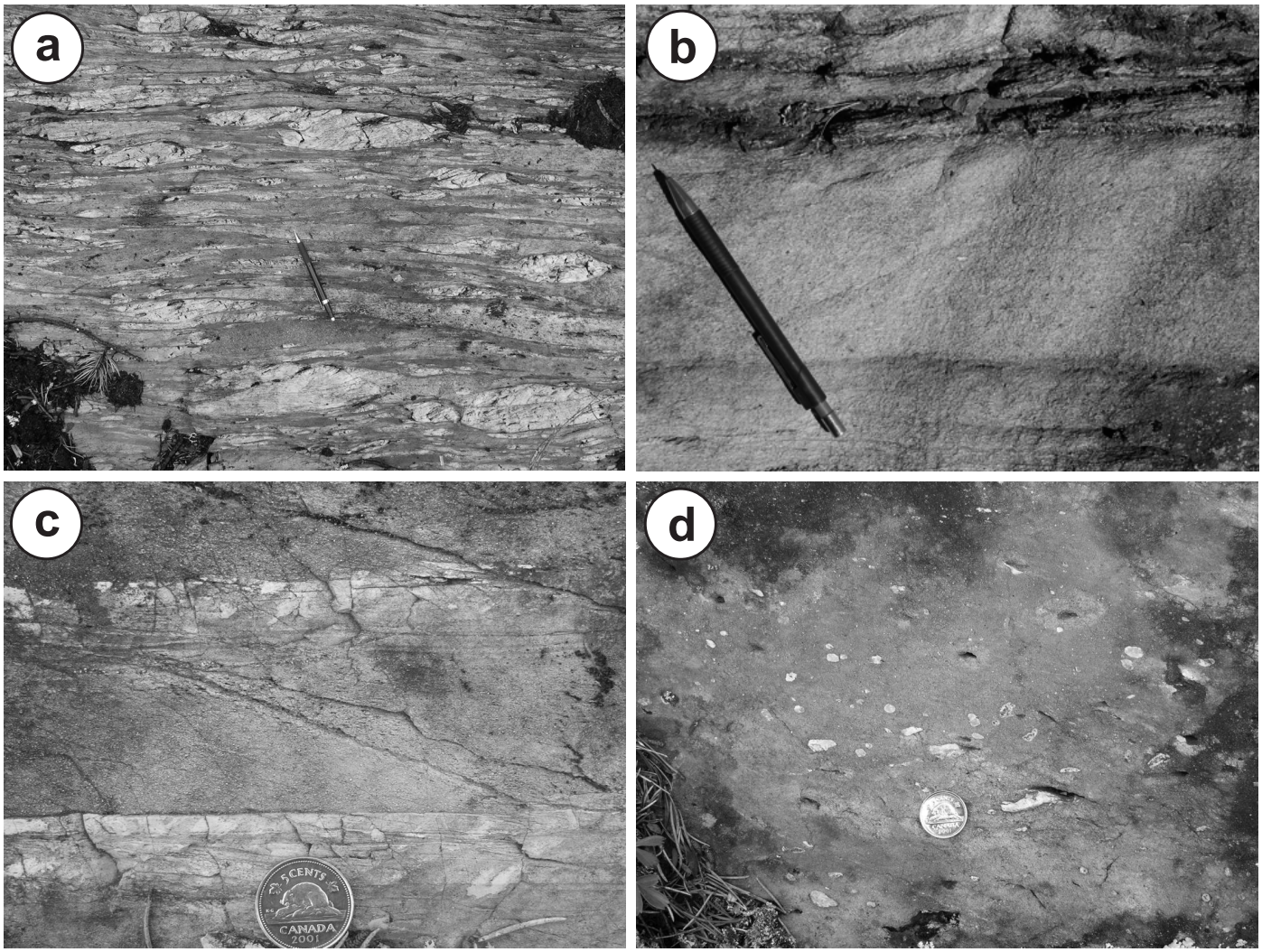

Figure 36: *Outcrop photographs of rock types in map unit 24, west of Horseshoe Lake:* ***a)*** *massive, heterolithic volcanic conglomerate;* ***b)*** *bedded intermediate volcanic sandstone;* ***c)*** *thin-bedded intermediate volcanic sandstone and mudstone; normal-graded beds indicating tops to the north in this location, north limb of the Horseshoe Lake anticline;* ***d)*** *quartz amygdules in otherwise massive aphyric andesite flow.*

Toward the base of this unit, the volcanic conglomerate is intercalated with subequal intervals of intermediate volcanic sandstone. This sandstone weathers light green to buff to rusty brown and is light green on fresh surfaces. Most specimens are fine to medium grained and contain 5–25% subhedral plagioclase and trace to 2% anhedral quartz grains that do not exceed 2.0 mm and are supported in a very fine grained chloritic matrix. The sandstone ranges from massive to faintly stratified to well bedded (Figure 36b) in individual outcrops. Intervals of massive or very faintly stratified sandstone range up to at least 40 m thick in some locations. In the bedded intervals, individual sandstone beds are typically planar, normal graded and up to 1.5 m thick, and are capped by 1–5 cm thick beds of pale yellow-brown mudstone (Figure 36c). Angular mudstone rip-up clasts are locally concentrated at the base of the graded beds. These features, coupled with rare examples of load structures, indicate deposition via low-density subaqueous grain flows, likely during intervals of relative quiescence on the associated volcanic centre.

In two locations, the epiclastic rocks are intercalated with amygdaloidal andesite flows and associated coarse, monolithic to heterolithic volcaniclastic rocks. The andesite weathers buff to light grey-green and is medium green-grey on fresh surfaces. Most specimens are fine grained and aphyric, with up to 5% elongate to round quartz amygdules that range up to 1.5 cm in maximum dimension (Figure 36d). In one location, the size and abundance of the amygdules appears to increase up section within an otherwise massive flow that is approximately 10 m thick. Some portions of these flows are sparsely plagioclase phyric and contain up to 3% euhedral plagioclase phenocrysts up to 1.5 mm. The associated volcaniclastic rocks consist of lapilli tuff, tuff breccia and breccia that contain closely packed angular clasts of variably amygdaloidal and plagioclase-phyric andesite. Given the close spatial association to andesite flows, these rocks are interpreted to be composed of primary and slightly reworked autoclastic debris.

Quartz-feldspar porphyry (unit 25)

The mafic intrusive and extrusive rocks on the north and south limbs of the Gold Creek syncline are intruded by quartz-feldspar porphyry dikes that range up to 20 m in thickness. These dikes weather light grey to pink and are pink-grey on fresh surfaces. The porphyry contains 5–10% euhedral to subhedral, pink-white feldspar phenocrysts that range up to 3 mm across and are evenly distributed in an aphanitic siliceous matrix. Most specimens also contain 1–2% each of anhedral, slightly blue-grey quartz and acicular green amphibole phenocrysts, which range up to 5 mm in maximum dimension. These rocks are texturally similar to the rhyolitic quartz-feldspar porphyry in the RL unit (unit 21).

San Antonio assemblage

The San Antonio assemblage (<2.705 Ga; Percival et al., 2006a) consists mainly of unseparated arenite and wacke (unit 27), with subordinate intervals of conglomerate (unit 26), quartz wacke (unit 28) and rhythmically interbedded greywacke

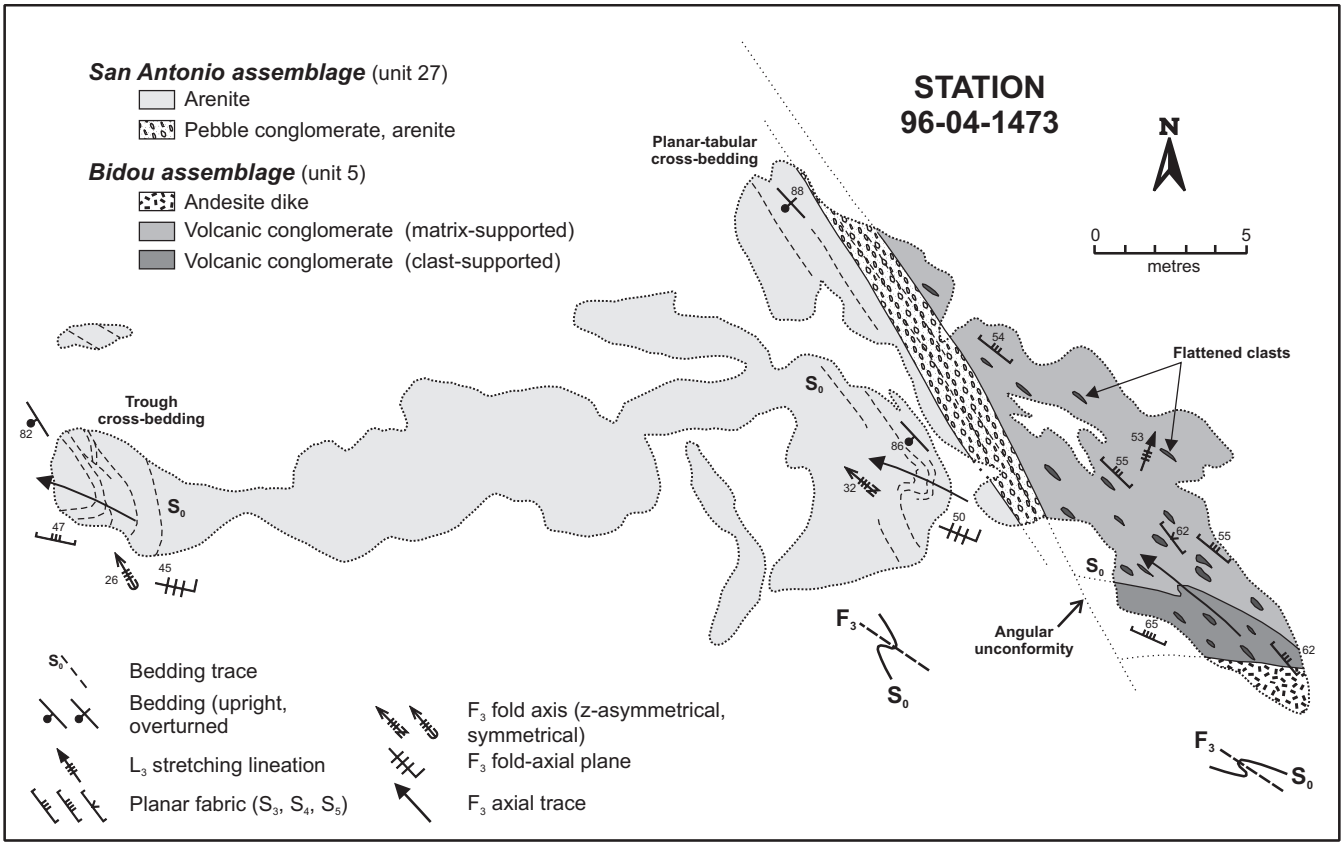

Figure 37: *Detailed outcrop map showing the angular unconformity at the base of the San Antonio assemblage. This locality, 600 m northeast of Red Rice Lake, was originally mapped and described by Stockwell (1938). The change in fold vergence across the contact in this location indicates the angular nature of the unconformity. Outcrop location: 311498mE, 5653786mN (NAD 83, UTM Zone 15).*

and mudstone (unit 29). These rocks define a 1.2 km thick succession that is well exposed west of Bissett, between Red Rice Lake and Horseshoe Lake, and describes a broadly S-shaped map pattern that cuts across the regional strike of the Rice Lake belt (Figure 3). Younging criteria are abundant and well preserved, and consistently face west on the main regional cleavage, which is axial planar to the Horseshoe Lake anticline and Gold Creek syncline. The San Antonio assemblage overlies the Bidou assemblage along a pronounced angular unconformity that is exposed approximately 600 m northeast of Red Rice Lake (Stockwell, 1938; *see also* Poulsen et al., 1996). In this location (Figure 37), crudely stratified intermediate volcaniclastic rocks of the IL unit, which dip and young to the north-northeast, are discordantly overlain by crossbedded arenite that dips and youngs to the southwest. The contact is marked by a 1–2 m thick unit of interstratified arenite and pebble conglomerate, the latter of which is mainly composed of intermediate volcanic detritus of apparently local derivation, with rare quartz pebbles up to 1.5 cm in size. Changes in younging direction and fold vergence across the contact indicate the angular nature of the unconformity.

In marked contrast to adjacent rocks of the Bidou assemblage, no intrusions are known to cut the San Antonio assemblage (e.g., Stockwell, 1938; Davies, 1953, 1963). Along the south margin of the greenstone belt west of Rice Lake, beyond the limits of the present mapping project, the San Antonio assemblage overlies tonalite of the Ross River plutonic suite along a well-exposed nonconformity that is described in detail by Stockwell (1945) and Davies (1963). A thin, fault-bounded panel of greywacke, mudstone and conglomerate along the Wanipigow Shear Zone, referred to as the Manigotagan assemblage by Bailes et al. (2003), is herein included in the San Antonio assemblage, and is interpreted to lie in fault contact to the north with the Mesoarchean Little Beaver assemblage. As described previously, the west-facing San Antonio assemblage is structurally overlain to the west by west-facing rocks of the Bidou assemblage, and this contact is inferred to represent an early thrust fault (Anderson, 2004).

Conglomerate (unit 26)

Conglomerate defines lenticular map units in several locations along the upper and lower contacts of the San Antonio assemblage; two subunits are distinguished on the basis of clast populations. Monolithic conglomerate (subunit 26a) occurs in two locations along the southern part of the San Antonio assemblage, close to the western pluton of the Ross River suite, and ranges up to 300 m thick in exposures along the southeast shoreline of Red Rice Lake. This conglomerate is very crudely stratified, unsorted and clast supported, and consists almost exclusively of subangular to well-rounded cobbles and boulders of tonalite (Figure 38a), the latter of which range up to several metres across. In most outcrops, the conglomerate contains less than 10% matrix material, which typically consists of fine-grained, pebbly feldspathic wacke and mudstone. At Red Rice Lake, the southern extent of this unit was mapped as a quartz diorite intrusion by Stockwell (1945) and Davies (1953, 1963). However, freshly peeled portions of these outcrops show medium- to coarse-grained tonalite that contains irregular seams (up to 20 cm thick) of fine-grained greywacke, mudstone and pebble conglomerate (Figure 38b). These seams, which locally account for up to 5% of the outcrops, are interpreted to represent the matrix to metre-scale blocks and boulders in a particularly coarse facies of the monolithic conglomerate. Rare examples of aplite dikes, which are sharply truncated at the margins of individual boulders, do not extend into the matrix, and are not observed in adjacent clasts, indicate at least some transport. To the east, this conglomerate is underlain by a strongly transposed package (at least 50 m thick) of thin- to thick-bedded, medium- to very coarse grained, pebbly feldspathic wacke (tonalite grit) and sericitic mudstone (Figure 38c), with minor intercalations of monolithic (tonalite) or polymictic pebble conglomerate. The overall features of this subunit indicate deposition at an abrupt topographic break, such as a fault scarp or steep-sided erosional feature, very close to a tonalitic source area. The low abundance and relatively fine grained nature of the matrix component imply deposition by either debris-flow or rock-fall (i.e., avalanche) mechanisms. This conglomerate was referred as a 'landslide facies' by Weber (1969).

Polymictic cobble conglomerate (subunit 26b) defines markedly lenticular map units along the upper and lower contacts of the main body of the San Antonio assemblage, and is also exposed just north of Silver Falls, in the fault-bounded panel along the Wanipigow Shear Zone. This conglomerate is clast supported and poorly sorted (Figure 38d), and contains subangular to well-rounded clasts composed mainly of intermediate to felsic volcanic material. Well-rounded pebbles of bull quartz (up to 5%) are characteristic (Figure 38e) and readily distinguish this conglomerate from similar rocks in the underlying Bidou assemblage. Subordinate clast types include quartzite, aplitic granite, tonalite, sericitic mudstone, iron formation and chert. The lower (basal?) conglomerate is at least 50 m thick on the prominent point on the south shore of Rice Lake and, in this location, exhibits an upward transition from massive boulder conglomerate to crudely stratified cobble conglomerate (Figure 38f) to well-stratified pebble-cobble conglomerate and very coarse grained pebbly sandstone. The conglomerate beds (1–10 m thick) exhibit crude normal size-grading and are locally capped by 30–40 cm thick, normal-graded beds of medium- to coarse-grained sandstone. These rocks are overlain by a thick succession of trough-crossbedded, medium- to very coarse grained pebbly sandstone (unit 27, described below). A strongly sheared chloritic conglomerate that contains abundant clasts of magnetite-jasper-chert iron formation is also exposed at the base of the assemblage near the east end of Horseshoe Lake. The upper conglomerate, which ranges up to 150 m thick and is distinctively hematitic, is exposed in two locations west and northwest of Horseshoe Lake. These conglomerate lenses range up to 150 m thick and are generally massive with rare interbeds of coarse-grained pebbly sandstone up to 0.5 m thick. The lenticular aspect of this conglomerate, coupled with its association with trough-crossbedded sandstone, are indicative of channel-fill deposits in a braided fluvial system.

Unseparated arenite and wacke (unit 27)

Unseparated arenite and wacke constitute the bulk of the San Antonio assemblage, and exhibit features characteristic of channel-fill deposits in braided fluvial systems. These rocks weather buff to pale pink to light grey and are typically

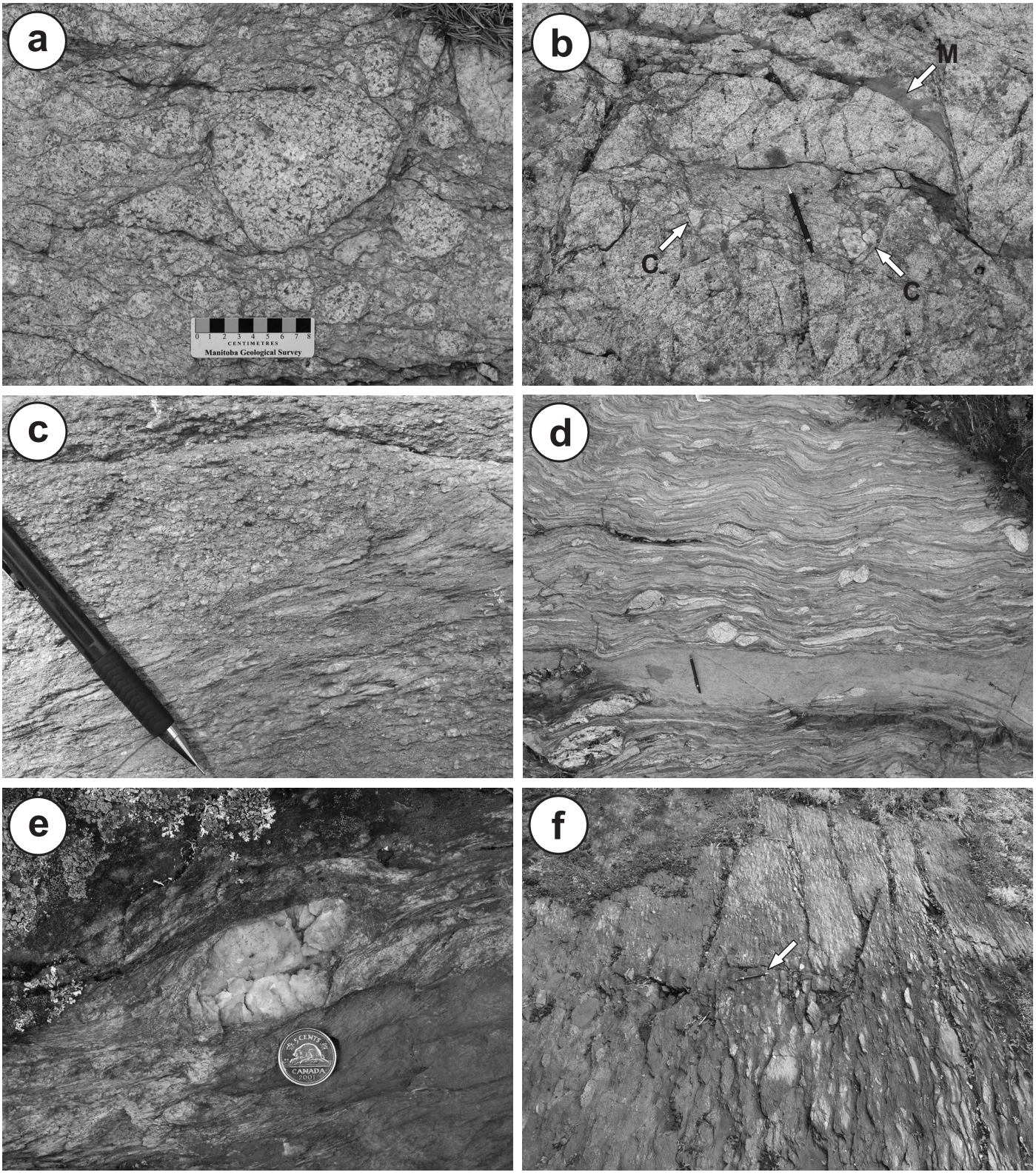

Figure 38: *Outcrop photographs of rock types in map unit 26:* ***a)*** *monolithic tonalite conglomerate, south shore of Red Rice Lake;* ***b)*** *monolithic tonalite conglomerate, south shore of Red Rice Lake; note thin irregular seams of pebble conglomerate (C) and mudstone (M);* ***c)*** *bedded coarse-grained tonalitic sandstone (grit) and mudstone; south shore of Red Rice Lake;* ***d)*** *polymictic cobble conglomerate with distinct bed of coarse-grained sandstone, north of Silver Falls, Wanipigow River; this conglomerate contains abundant tonalite cobbles;* ***e)*** *quartz pebble in polymictic conglomerate, northwest of Horseshoe Lake;* ***f)*** *stratified cobble (bottom) and pebble (top) conglomerate (pencil for scale, indicated by arrow) in the hinge of the Gold Creek syncline, south shore of Rice Lake; note near-orthogonal relationship between bedding and the regional flattening fabric; graded beds in this location indicate tops to the west.*

grey-green on fresh surfaces. The typical specimen is medium to coarse grained and composed of angular to subrounded quartz (50–75%), feldspar (5–30%) and lithic (<10%) grains in a sericitic mudstone matrix (<20%; Figure 39a); most classify as subarkosic arenite in the scheme of Pettijohn (1975). Lithic clasts (1–5%; <10 cm) are ubiquitous and range from very angular and tabular to well rounded and nearly spherical (Figure 39b, c). Clast types include sericitic mudstone, vein quartz, aplitic granite, quartzite, quartz-phyric rhyolite, variably sulphidic chert, and fuchsitic schist. Fuchsite is also present as fine grains and flakes in the mudstone matrix. Individual outcrops range from crossbedded (subunit 27a) to planar-bedded (subunit 27b) to massive. The crossbedded arenite is prevalent in the lower portion of the assemblage, southwest of Rice Lake, and characteristically contains trough-crossbeds (Figure 39d) with subordinate planar-tabular cross-sets. The scoured bottomsets of individual cross-sets are marked by diffuse pebble-lag deposits (Figure 39e), and the foresets typically grade upward from very coarse grained, pebbly sandstone to medium-grained sandstone. Individual sets and cosets are also locally separated by discontinuous (scoured) bottomsets composed of light brown mudstone. Massive, medium- to very coarse grained, pebbly arenite is particularly common in the area of Horseshoe Lake and ranges up to several metres thick. Here, the arenite contains minor occurrences of fracture-controlled and disseminated pitchblende (Assessment File 92536). Intervals of planar-bedded arenite occur in association with both the massive and crossbedded arenite, and consist of massive to normal-graded, medium- to coarse-grained, pebbly arenite beds that range up to 50 cm thick and are separated by discontinuous beds (<10 cm thick) of light brown or grey-black mudstone. Some of these beds are capped by sets of ripple crosslaminated sandstone <10 cm thick (Figure 39f).

Quartz wacke (unit 28)

Relatively clean quartz wacke defines two lenticular map units just below the upper contact of the San Antonio assemblage, in the area northwest of Horseshoe Lake. The quartz wacke is white to pale grey or green on both weathered and fresh surfaces, and is composed of more than 90% quartz. This rock is typically medium to coarse grained and consists of texturally immature, angular to subrounded quartz grains (~45%; 0.1–1.0 mm) of poor sphericity, which are supported in a very fine grained matrix of quartz and sericite (Figure 40a). Most of the quartz grains are monocrystalline; coarse feldspar is absent. Accessory minerals observed in outcrop and thin-section include pyrite, tourmaline and rounded, apparently detrital, opaque grains. Some beds contain up to 5% subrounded quartz granules and pebbles up to 3 cm across. Massive, tabular-planar beds of quartz wacke range up to several metres thick and are separated by minor interbeds (<5 cm thick) of darker green feldspathic wacke (Figure 40b). In contrast to the underlying sandstone, crossbeds and scour structures are not apparent in these intervals. As described by Pettijohn (1975) and Selley (1988), quartz wacke is an uncommon rock type (chemically mature, yet texturally immature) that is usually derived from pre-existing sediments and deposited in fanglomerate and alluvial facies of proximal continental deposits.

Greywacke and mudstone (unit 29)

Rhythmically interbedded greywacke and mudstone define a mappable unit in the lower portion of the San Antonio assemblage in the area of Horseshoe Lake (subunit 29a). A similar rock type (subunit 29b) is present in the fault-bounded panel along the trace of the Wanipigow Shear Zone, and is best exposed in heavily lichen-covered outcrops at Silver Falls on the Wanipigow River. Here, the section is at least 200 m thick and consists of rhythmically interlayered grey-brown greywacke and dark grey mudstone (Figure 41a). The typical greywacke specimen is medium to very coarse grained and composed of angular to subrounded quartz (15–20%), feldspar (~10%) and lithic (<10%) grains in a sericitic mudstone matrix (55–60%). This rock classifies as feldspathic greywacke in the scheme of Pettijohn (1975). Polycrystalline grains are abundant and include examples of coarse-grained quartz-feldspar aggregates of plutonic derivation (Figure 41b). Some beds contain up to 15% coarse sand– to granule-size grains of blue quartz, which is likewise consistent with a plutonic source area. Individual greywacke beds range up to 30 cm thick and vary from massive to well-graded, whereas the mudstone beds range up to 10 cm thick. The graded beds generally fine toward the north. These rocks are interpreted to represent A-E turbidites that were deposited in a relatively distal marine fan setting. A sample of this material (sample 96-05-1622) was collected for U-Pb dating of the detrital zircon population by LA-MC-ICP-MS analysis.

South of the Wanipigow Shear Zone, rhythmically interlayered greywacke and mudstone are exposed in several large outcrops located approximately 800 m northwest of Horseshoe Lake. These outcrops define a map unit at least 300 m thick that is interpreted to continue through the topographically low area to the east, along the base of the San Antonio assemblage. These rocks weather light green-grey to brown and are medium green on fresh surfaces. The greywacke is fine to medium grained and generally lacks coarse detrital quartz. Most specimens consist of angular to subrounded feldspar and quartz grains (<1 mm; 10–30%) in a sericitic mudstone matrix (50%). The greywacke beds range up 40 cm thick and are rhythmically interlayered with beds of brown mudstone up to 5 cm thick (Figure 41c). The thicker greywacke beds generally have sharp scoured bottoms and normal-graded tops; some beds are also reverse-graded at the base. Some outcrops contain minor beds of more quartz-rich (up to 40%) wacke and pebble conglomerate, which contain up to 5% quartz granules and pebbles. The upper portion of this unit contains distinctive intervals, up to 1.0 m thick, of rhythmically interlayered, very thin bedded to laminated, fine-grained greywacke and mudstone (Figure 41d). These characteristics are indicative of density-flow sedimentation in a relatively low-energy setting within the braided fluvial system; hence, these rocks are interpreted to represent abandoned channel-fill or overbank deposits.

Lithogeochemistry and Sm-Nd isotope geochemistry

In order to establish the composition of volcanic and plutonic rock types in the Rice Lake area, a suite of representative geochemical samples, including most of the principal map units, was collected for lithogeochemical analysis. In this

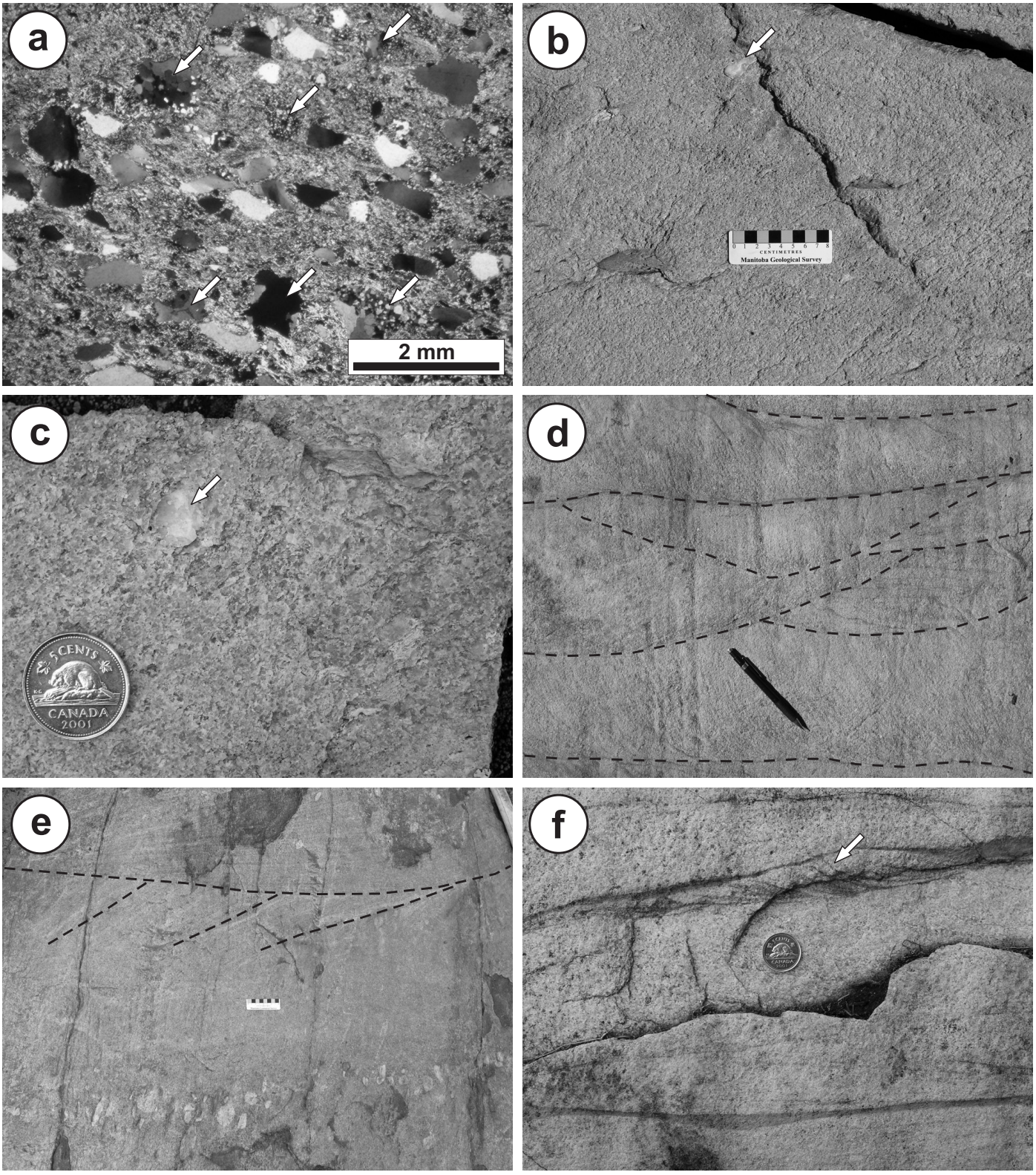

Figure 39: *Outcrop and thin-section photographs of rock types in map unit 27:* ***a)*** *medium-grained feldspathic greywacke composed of angular to subrounded quartz and lithic (arrows) grains in a fine-grained, sericitic mudstone matrix (cross-polarized light), west of Red Rice Lake;* ***b)*** *massive, coarse-grained subarkosic arenite with scattered pebbles of quartz (arrow) and mudstone, south of Horseshoe Lake;* ***c)*** *very coarse grained subarkosic arenite with abundant mudstone and lesser quartz (arrow) pebbles, northwest of Horseshoe Lake;* ***d)*** *trough-crossbedded subarkosic arenite, northeast of Red Rice Lake; scoured bottomset of each cross-set indicated by dashed lines;* ***e)*** *tabular-planar cross-set in coarse-grained subarkosic arenite in the hinge of the Horseshoe Lake anticline, southwest of Horseshoe Lake; note near orthogonal relationship between bedding and the regional flattening fabric defined by elongate pebbles; scoured bottomset is marked by pebble lag-deposit along bottom edge of photograph; bottomset of succeeding cross-set indicated by horizontal dashed line; tops to the west;* ***f)*** *ripple crosslaminations (arrow) in quartz-rich arenite, northeast of Red Rice Lake.*

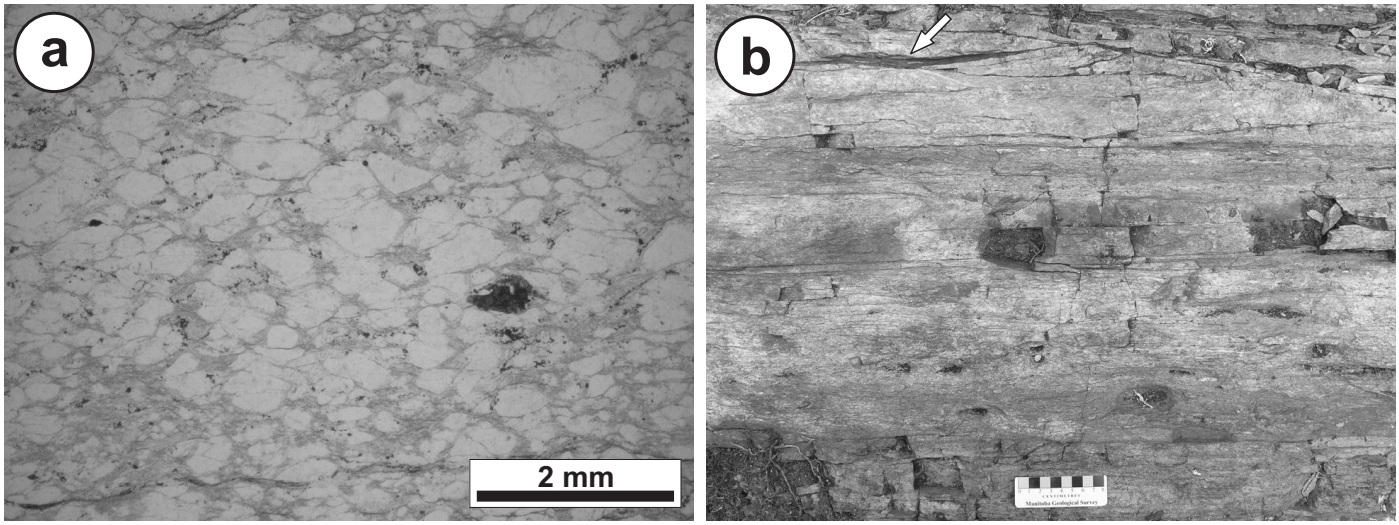

Figure 40: *Thin-section and outcrop photographs of quartz wacke of map unit 28, northwest of Horseshoe Lake:* ***a)*** *closely packed, angular to subrounded quartz grains in a fine-grained sericitic mudstone matrix (plane-polarized light);* ***b)*** *planar-bedded, coarse-grained quartz wacke with lenticular mudstone interbed (arrow).*

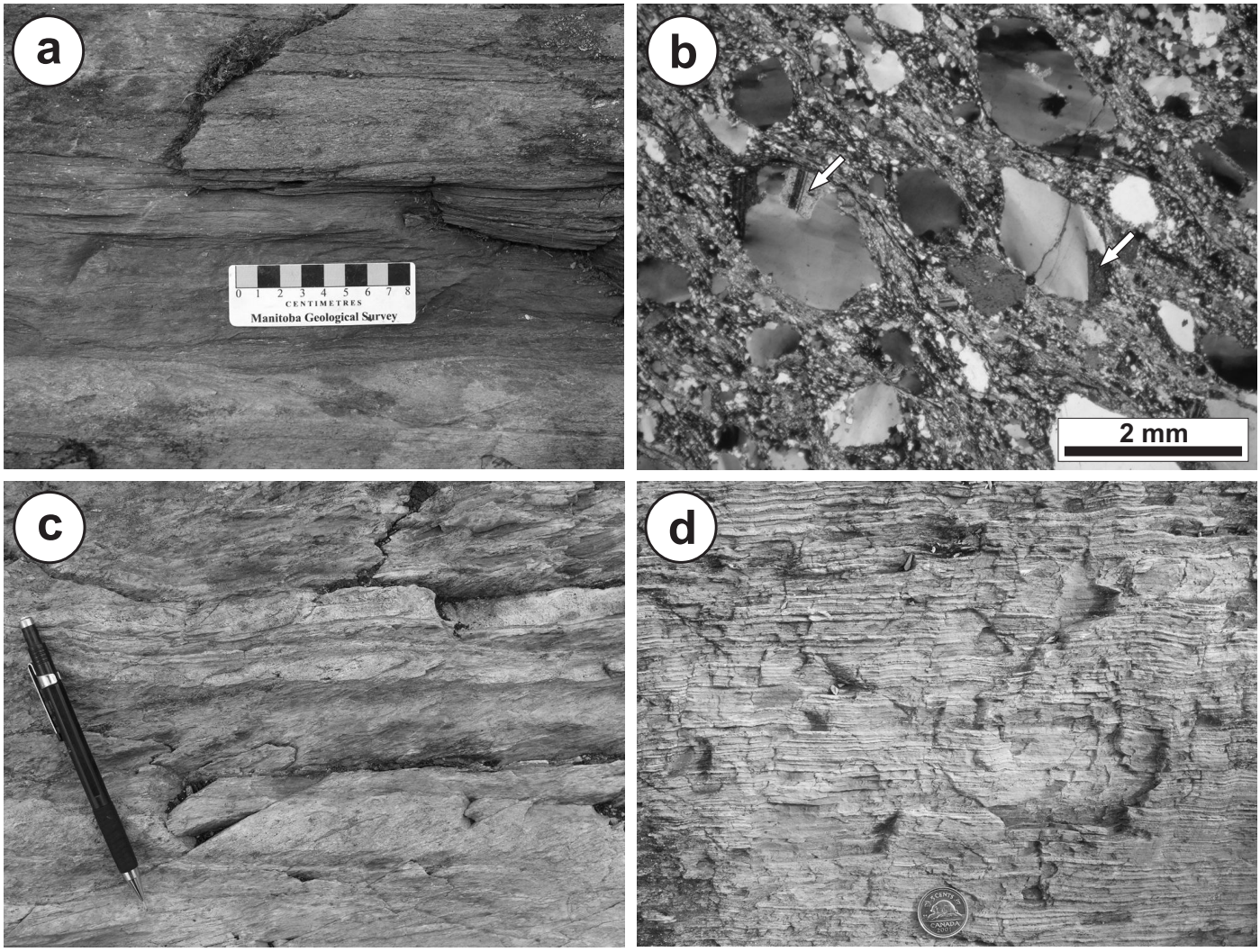

Figure 41: *Outcrop and thin-section photographs of rock types in map unit 29:* ***a)*** *planar-bedded, coarse-grained greywacke and mudstone, Silver Falls, Wanipigow River;* ***b)*** *quartz-feldspar aggregates (arrrows) of probable plutonic derivation in coarse-grained greywacke (cross-polarized light), Silver Falls, Wanipigow River;* ***c)*** *thin-bedded, fine-grained feldspathic greywacke and mudstone, northwest of Horseshoe Lake;* ***d)*** *laminated feldspathic greywacke and mudstone, northwest of Horseshoe Lake.*

section, the geochemical attributes of these samples are described and the variations in major and trace-element chemistry and Nd isotopic compositions are examined in detail to provide insight into the geochemical evolution and potential tectonic setting of magmatism in the Rice Lake area. For completeness, this report includes an analysis of geochemical data for a suite of 24 samples that collected in the study area by Bailes (1998, 1999) under the auspices of the Western Superior NATMAP project. These samples were included in Data Repository Item DRI2005004 Bailes and Percival, 2005b), which was published in conjunction with Geoscientific Report GR2005-2 (Bailes and Percival, 2005a). Sampling procedures and analytical methods, which are described below, were identical for all samples.

Sampling procedures and analytical methods

The representative suite of 39 geochemical samples was collected during the bedrock mapping component of this study. Each sample consisted of 1–2 kg of least-altered, homogeneous rock that was collected by hammer or rock-saw from bedrock and manually trimmed in the field to remove all weathered surfaces, veins, altered fractures or other inhomogeneities. Samples of pillowed basalt flows were obtained from the least-altered cores of single pillows. With the exception of sample 96-04-1285-2, which consists of heterolithic volcanic conglomerate, all of the volcaniclastic rock types collected for analysis consist of monolithic and homogeneous fragmental aggregates that are characterized by textural similarity of fragments and matrix. In the MGS rock-preparation facility, the clean rock chips obtained in the field were crushed in a steel jaw-crusher to <5 mm and pulverized in a steel swing mill. The powders were homogenized by rolling and then splitting to obtain approximately 55 g of analytical material. A minimum of one internal standard and one blind duplicate was inserted into each sample batch for analytical quality control.

The samples were submitted to Activation Laboratories Ltd. in Ancaster, Ontario and analyzed using the '4Litho' analytical package, which employs a lithium metaborate/tetraborate fusion technique, followed by nitric-acid digestion and analysis by inductively coupled plasma–optical emission spectroscopy (ICP-OES) for the major elements and select trace elements (Ba, Sc, Sr, V, Y, Zr), and by inductively coupled plasma–mass spectrometry (ICP-MS) for the remainder of the trace elements and the rare-earth elements. The resulting high-precision geochemical data exhibit very consistent and coherent intra- and intersample elemental behaviour, particularly for the high-field-strength elements (HFSE) and rare-earth elements (REE). Hence, despite evidence of secondary chemical modification in some samples in the form of higher loss-on-ignition values (LOI ≥3.5 wt. %), the HFSE and REE variations are considered to reflect primary igneous processes.

Representative analyses of the principal map units are presented in Table 2, and all of the major, trace and REE data are included in Data Repository Item DRI2008002[2]. In the data tables, analytical results below detection limits were arbitrarily assigned a value of 50% of the detection limit.

A subset of four samples, selected to include mafic and felsic volcanic rocks from the Rainy Lake road (RLR) and Round Lake (RL) units of the Bidou assemblage, were submitted for Sm-Nd isotope geochemical analysis to the University of Alberta Radiogenic Isotope Facility in Edmonton, Alberta. Samarium-neodymium isotopic data can provide important insights into the possible contributions of crust- and mantle-derived melts during magma petrogenesis. The rock sampling and initial processing procedures followed were the same as those for the lithogeochemistry samples. The samples were processed and analyzed for Sm-Nd isotopes following the chromatographic and mass spectrometry procedures described by Unterschutz et al. (2002) and Schmidberger et al. (2007). Samarium and neodymium isotopic compositions were determined by multicollector ICP-MS, for which an in-house Nd isotope standard was used (Schmidberger et al., 2007). Chemical processing blanks were <200 pg for Nd and Sm. The Nd isotope data are presented relative to a $^{143}Nd/^{144}Nd$ value of 0.511850 for the La Jolla standard, and crustal residence model ages (T_{CR}) were calculated based on the model of Goldstein et al. (1984), which assumes a linear evolution of isotopic ratios in the depleted mantle, using present day depleted-mantle values of $^{143}Nd/^{144}Nd = 0.513160$ and $^{147}Sm/^{144}Nd = 0.2141$. The Sm–Nd isotopic data are presented in Table 3.

Samples with 1000-series numbers (31 samples) were collected by the author in 2004 and 2005 from bedrock outcrops in the study area. Sample RRP consists of granodiorite from the central portion of the Ross River pluton southeast of the study area and was collected by the author in 2003. Sample 2287-1, collected by the author in 2007, is from south of Wanipigow Lake in the central portion of the large unnamed pluton of the Ross River Plutonic suite. Samples SG1-1 and L6E-1 were also collected by the author in 2007, from diamond-drill core and underground workings, respectively, on the sixth level of the SG-1 mine. The four samples with the suffix 'DL' were collected by D. Lewis in 2005 from an outcrop in the immediate footwall of the SG-3 deposit (station 96-04-1343). The twenty-four bedrock samples collected by Bailes (1998, 1999) are indicated by the sample numbers with three numerals. Universal Transverse Mercator (UTM) co-ordinates (NAD 83, Zone 15) are provided for all samples in Data Repository Item DRI2008002.

Major-, trace- and rare-earth–element geochemistry

Volcanic and plutonic rock types in the Rice Lake area exhibit a distinct bimodality of bulk compositions and are divided for descriptive purposes into mafic (SiO_2 ≤56 wt. %, Fe_2O_3+MgO ≥15 wt. %; anhydrous) and felsic (SiO_2 ≥62 wt. %, Fe_2O_3+MgO <10 wt. %; anhydrous) sample suites (Figure 42a). Only one sample (an andesite from the Gold Creek [GC] unit) plots outside of the limits specified above, and is not included in the following analysis.

Mafic volcanic and plutonic rocks

Mafic volcanic and plutonic rocks in the Rice Lake area are subalkaline and plot as basalt and basaltic andesite on the SiO_2

[2] Available online to download free of charge at www2.gov.mb.ca/itm-cat/freedownloads.htm, or on request from minesinfo@gov.mb.ca or Mineral Resources Library, Manitoba Science, Technology, Energy and Mines, 360–1395 Ellice Avenue, Winnipeg, MB R3G 3P2, Canada

Table 2: Lithogeochemical data for representative rock samples of the principal map units in the Rice Lake area.

	Mafic sills and dikes						Mafic flows			Mafic volcaniclastic		Felsic volcanic/volcaniclastic					Felsic plutonic		
SAMPLE	1381-1	1345-1	1631-1	1697-1	1282-1	1533-1	1315-1	64-1-1	1746-1	1368-1	1611-1	21-1-1	1679-1	1330-2	1741-1	1379-1	RRP	1330-1	1376-1
Unit code	1	9	9	14	17	23	10	15	23	18	24	4	5	7	16	19	11	11	21
Rock-type	GS	GS	DD	GS	DD	GS	PF	PF	MF	LT	LT	DC	MF(?)	BX	XLTF	LT	GD	QFP	QFP
(wt.%)																			
SiO_2	49.96	49.40	47.87	48.36	47.10	48.53	50.47	50.05	49.04	50.85	56.05	64.99	64.41	65.95	61.66	63.73	68.12	67.46	69.03
TiO_2	0.67	1.52	1.07	0.84	0.88	0.95	1.26	0.94	1.99	0.77	0.91	0.52	0.40	0.43	0.48	0.52	0.43	0.42	0.32
Al_2O_3	14.36	12.63	13.97	14.92	13.98	17.28	13.47	15.28	13.93	14.02	14.46	16.42	15.79	16.57	16.37	15.65	15.50	15.82	15.25
Fe_2O_3	10.77	17.65	14.33	12.54	10.77	12.81	14.81	11.47	18.97	8.77	8.49	4.03	4.33	5.03	5.44	4.63	3.82	3.92	2.69
MnO	0.17	0.26	0.20	0.18	0.18	0.17	0.21	0.24	0.22	0.13	0.11	0.06	0.05	0.05	0.08	0.07	0.05	0.06	0.04
MgO	8.57	4.21	6.60	6.63	10.49	4.47	5.93	3.07	4.77	8.29	3.96	1.55	2.11	1.10	2.36	2.37	1.56	1.59	0.91
CaO	11.53	8.35	10.38	8.87	9.91	8.01	8.34	9.61	7.74	8.61	6.05	4.81	3.51	4.79	5.95	4.71	3.47	3.93	3.46
Na_2O	2.15	2.28	1.91	2.67	2.05	3.97	3.33	3.48	2.84	3.67	3.74	4.13	5.18	4.06	4.18	4.16	4.53	4.52	4.53
K_2O	0.25	0.21	0.01	0.01	0.89	0.10	0.26	0.14	0.08	0.89	0.03	1.53	0.70	1.19	0.77	1.76	1.51	1.54	1.81
P_2O_5	0.06	0.11	0.08	0.09	0.28	0.08	0.11	0.12	0.16	0.54	0.14	0.14	0.19	0.11	0.09	0.14	0.11	0.10	0.09
LOI	1.00	2.38	2.60	3.89	2.48	3.00	0.97	6.33	0.67	2.45	5.14	1.68	2.73	0.60	2.63	1.91	0.92	0.58	1.26
TOTAL	99.48	99.00	99.00	98.98	99.02	99.38	99.16	100.74	99.06	98.99	99.07	99.87	99.40	99.87	100.01	99.66	100.01	99.92	99.38
Mg#	61	32	48	51	66	41	44	35	33	65	48	43	49	30	46	50	45	45	40
(ppm)																			
Cr	328	10	110	150	264	209	47	230	107	352	90	44	30	75	108	65	10	10	10
Co	52	58	49	43	34	41	33	36	59	40	25	11	12	16	18	15	10	7	7
Ni	174	21	80	140	402	40	56	103	39	163	100	39	40	66	38	44	21	21	10
Cu	155	156	60	100	110	104	118	61	98	66	70	5	40	16	31	29	19	28	19
Zn	83	127	70	80	100	94	117	94	127	108	70	57	60	36	55	69	76	62	47
Sc	39	41	39	30	27	38	39	39	44	22	19	11	8	10	9	10	7	7	5
V	248	391	276	201	198	266	266	216	454	173	160	68	56	68	101	83	50	52	34
Ga	18	25	18	19	16	24	17	18	26	22	18	21	18	24	25	22	19	17	23
Y	15	27	24	21	15	24	26	21	48	17	17	9	8	8	9	8	5	6	5
Zr	35	83	65	44	84	57	95	77	117	130	103	151	115	126	91	110	142	91	106
Nb	4.6	4.1	4.0	2.0	2.4	2.3	6.1	1.8	5.1	3.4	5.0	5.9	4.0	4.9	3.7	2.7	5.5	3.4	3.2
Hf	1.2	2.5	2.0	1.6	2.3	1.7	2.8	1.7	3.4	3.1	2.9	3.4	3.1	3.4	2.7	3.0	3.7	2.6	2.9
Ta	0.1	0.3	0.2	0.1	0.1	0.2	0.4	0.1	0.3	0.2	0.3	0.5	0.4	0.6	0.3	0.2	0.3	0.3	0.4
Th	0.2	0.5	0.5	1.6	6.7	0.7	0.8	1.8	0.7	13.3	1.8	3.1	2.5	2.4	2.6	3.7	2.1	3.2	2.9
U	0.1	0.1	0.1	0.3	1.4	0.2	0.2	0.3	0.2	2.8	0.5	0.6	0.7	0.4	0.7	0.9	0.8	0.9	0.9
Ba	26	45	44	26	386	86	52	20	31	874	29	248	272	234	198	460	364	382	536
Rb	3	2	1	1	22	1	4	1	1	13	1	30	16	37	20	40	43	33	48
Sr	83	126	180	359	691	249	199	652	150	831	322	290	300	285	429	460	346	340	442
La	1.7	6.9	4.9	8.8	41.1	7.2	7.9	10.4	7.3	100.1	10.6	18.9	14.2	18.5	13.7	22.8	13.8	14.8	15.4
Ce	5.4	16.7	12.3	20.8	90.8	15.8	19.9	24.7	19.2	208.1	23.8	37.5	28.7	34.9	26.8	46.9	26.2	29.1	28.9
Pr	0.9	2.4	1.8	2.9	11.0	2.0	2.7	3.1	2.9	25.4	3.0	3.8	3.4	3.8	3.0	5.4	3.0	3.1	3.1
Nd	5.1	12.1	8.6	12.0	42.4	9.3	13.5	13.8	14.7	96.7	12.0	16.1	12.2	14.0	11.2	20.0	11.7	10.7	10.6
Sm	1.7	3.5	2.6	2.8	7.6	2.5	3.9	2.8	4.6	15.4	2.7	2.8	2.2	2.5	2.1	3.6	2.2	2.0	1.8
Eu	0.7	1.3	1.0	1.0	2.0	1.0	1.1	0.9	1.5	3.8	0.9	0.9	0.7	0.8	0.7	1.0	0.6	0.6	0.6
Gd	2.3	4.3	3.2	2.8	4.9	3.2	4.5	3.0	5.5	8.6	2.8	2.3	1.8	2.1	1.8	2.6	1.8	1.5	1.4
Tb	0.5	0.8	0.6	0.5	0.6	0.7	0.8	0.5	1.1	0.9	0.5	0.3	0.3	0.3	0.3	0.4	0.2	0.2	0.2
Dy	3.0	5.6	3.7	3.3	3.1	4.4	4.9	3.3	7.1	4.0	2.7	1.7	1.4	1.7	1.5	1.8	1.0	1.2	1.0
Ho	0.7	1.2	0.8	0.7	0.6	0.9	1.1	0.8	1.5	0.6	0.5	0.3	0.2	0.3	0.3	0.3	0.2	0.2	0.2
Er	1.9	3.4	2.4	2.2	1.7	2.8	3.2	2.3	4.7	1.6	1.6	0.9	0.7	0.8	0.9	0.9	0.5	0.7	0.5
Tm	0.3	0.5	0.4	0.3	0.2	0.4	0.5	0.4	0.7	0.2	0.3	0.1	0.1	0.1	0.1	0.1	0.1	0.1	0.1
Yb	1.8	3.1	2.3	2.2	1.5	2.7	2.9	2.3	4.6	1.3	1.5	0.9	0.6	0.7	0.8	0.8	0.5	0.6	0.4
Lu	0.3	0.5	0.3	0.3	0.2	0.4	0.4	0.4	0.7	0.2	0.2	0.1	0.1	0.1	0.1	0.1	0.1	0.1	0.1
Sr/Y	5.4	4.6	7.5	17.1	45.5	10.3	7.7	30.4	3.2	48.5	18.9	30.6	37.5	36.3	47.1	55.0	63.7	56.4	95.4
Zr/Y	2.3	3.0	2.7	2.1	5.5	2.4	3.7	3.6	2.5	7.6	6.1	16.0	14.4	16.1	10.0	13.1	26.2	15.0	22.8
Eu/Eu*	1.0	1.1	1.0	1.0	1.0	1.0	0.8	1.0	0.9	1.0	1.0	1.1	1.1	1.1	1.0	1.0	0.9	1.1	1.1
$(La/Yb)_N$	0.7	1.6	1.5	2.9	20.2	1.9	1.9	3.3	1.1	53.2	5.1	16.0	17.0	18.9	12.6	20.7	21.1	18.0	25.7
$(La/Sm)_N$	0.7	1.3	1.2	2.0	3.5	1.9	1.3	2.4	1.0	4.2	2.5	4.3	4.2	4.7	4.1	4.1	4.1	4.8	5.4
$(Gd/Yb)_N$	1.1	1.1	1.2	1.1	2.8	1.0	1.3	1.1	1.0	5.2	1.5	2.2	2.5	2.4	1.9	2.8	3.2	2.1	2.6
$(Th/Nb)_{PM}$	0.3	1.0	1.0	6.7	24.0	2.6	1.1	8.4	1.1	33.1	3.0	4.4	5.2	4.2	6.0	11.5	3.2	8.1	7.6
$(Nb/La)_{PM}$	2.6	0.6	0.8	0.2	0.1	0.3	0.7	0.2	0.7	0.0	0.5	0.3	0.3	0.3	0.3	0.1	0.4	0.2	0.2

Abbreviations: BX, breccia; DC, dacite clast; DD, diabase dike; GD, granodiorite; GS, gabbro sill; LT, lapilli tuff; MF massive flow; PF, pillowed flow; QFP, quartz-feldspar porphyry; XLTF, crystal tuff

Table 3: Sm-Nd isotopic data from the Rice Lake section of the Bidou assemblage. Also provided in Data Repository Item DRI2008002.

Sample number	Rock type	Map unit	Sm (ppm)	Nd (ppm)	$^{147}Sm/^{144}Nd$[1]	$^{143}Nd/^{144}Nd$[2]	εNd[3] (2.715 Ga)	εNd[3] (2.73 Ga)	T_{CR}[4] (Ga)
96-04-1330-2	Dacite breccia	7	2.21	11.78	0.113	0.511153(8)	–	0.3	3.03
96-04-1315-1	Pillowed basalt	10	3.67	12.95	0.171	0.512252(6)	–	1.4	–
96-04-1368-1	Basalt lapilli tuff	18	14.09	91.86	0.093	0.510835(6)	1.2	–	2.91
96-04-1376-1	Quartz-feldspar porphyry rhyolite	21	1.84	10.82	0.103	0.511011(5)	1.1	–	2.94

[1] estimated error is better than 0.5%

[2] normalized to $^{146}Nd/^{144}Nd = 0.7219$; external precision based on repeat La Jolla Nd standard runs; numbers in parentheses are the 2σ errors x 10^{-6}

[3] εNd values at 2.715 Ga and 2.73 Ga calculated using present-day chondritic ratios of $^{143}Nd/^{144}Nd = 0.512638$ and $^{147}Sm/^{144}Nd = 0.1967$

[4] crustal residence Nd model ages (T_{CR}) calculated according to the model of Goldstein et al. (1984)

vs. total alkali discrimination diagram of Le Bas et al. (1986) and the immobile trace-element (Nb/Y vs. Zr/TiO_2) diagram of Pearce (1996; *modified after* Winchester and Floyd, 1977; Figure 42b, c). On the plots of Barrett and MacLean (1994), Irvine and Baragar (1971) and Jensen (1976), these rocks exhibit a somewhat continuous variation from tholeiitic to transitional to calcalkalic geochemical affinity (Figure 42d, e, f). The basalt–basaltic andesite samples are subdivided into three distinct subsuites according to their differing geochemical attributes (Table 4), as described below.

MORB-like tholeiitic basalt

This subsuite has been identified in the Independence Lake (IL) unit as diabase dikes (2 samples); in the RLR unit as massive, pillowed and brecciated basalt flows (10 samples), gabbro sills (6 samples) and basalt dikes (1 sample); and in the GC unit as a massive basalt flow (1 sample). This subsuite consists predominantly of Fe-tholeiitic basalt, with minor tholeiitic basalt and Mg-tholeiitic basalt (Figure 43a), which exhibit a range of SiO_2 of 46–51 wt. %, TiO_2 of 0.7–2.0 wt. % and Fe_2O_3 of 11–19 wt. % over an Mg# range of 32–57. The basalt exhibits relatively flat profiles on extended-element plots (Figure 44c, d, i, j) normalized to normal mid-ocean-ridge basalt (NMORB) and primitive-mantle (PM; $La/Yb_N = 1.0–2.6$), typically with weakly fractionated light REE ($La/Sm_N = 0.9–1.5$) and heavy REE ($Gd/Yb_N = 1.0–1.5$), and weak negative Nb anomalies ($Th/Nb_{PM} = 0.8–1.4$). In relation to NMORB, the light REE (LREE) are generally weakly enriched, whereas the heavy REE (HREE) are mostly depleted, and most samples exhibit evidence of weak Zr depletion. Chromium values range from less than detection limit (<DL) to 355 ppm (average 124 ppm) and Ni values from <DL to 102 ppm (average 70 ppm). Ternary plots of Th–Hf/3–Ta (Wood, 1980) and La/10–Y/15–Nb/8 (Cabanis and Lecolle, 1989) indicate that these basalts are transitional between arc-tholeiite and mildly enriched NMORB, and most closely resemble modern back-arc basin basalt (Figure 43b, c). On the Th/Yb vs. Nb/Yb diagram of Pearce and Peate (1995), these rocks exhibit a within-plate enrichment trend, with evidence of a minor subduction component (Figure 43d). A sample of pillowed basalt in the RLR unit (sample 1315-1) has an initial ε_{Nd} of 1.4 (at 2.73 Ga), suggesting minor interaction with isotopically evolved (i.e., older) crust (Table 3).

One sample collected from a gabbro sill in the Little Beaver assemblage north of the Wanipigow Shear Zone exhibits 50 wt. % SiO_2, 0.67 wt. % TiO_2, 11 wt. % Fe_2O_3 and an Mg# of 61, and plots in the field of Fe-tholeiitic basalt (Figure 43a). The gabbro exhibits relatively flat profiles on NMORB and PM-normalized extended-element plots ($La/Yb_N = 0.7$; $La/Sm_N = 0.7$; $Gd/Yb_N = 1.1$), with weak negative Zr and Ti anomalies, strong positive Nb anomalies ($Th/Nb_{PM} = 0.3$), and variable positive (NMORB) or negative (PM) Th anomalies (Figure 44a, b). With the exception of Th and Nb, the HFSE and REE are depleted in relation to NMORB; Cr and Ni values are 328 and 174 ppm, respectively. Ternary plots of Th–Hf/3–Ta (Wood, 1980) and La/10–Y/15–Nb/8 (Cabanis and Lecolle, 1989) indicate that the gabbro is transitional between arc tholeiite and mildly enriched NMORB, and thus exhibits an affinity to back-arc basin basalt (Figure 43b, c). On the Th/Yb vs. Nb/Yb diagram of Pearce and Peate (1995), the gabbro exhibits evidence of a minor subduction component (Figure 43d).

Arc-like tholeiitic basalt

This subsuite has been identified in the Townsite (TS) unit as massive, pillowed and brecciated basalt flows (3 samples) and gabbro sills (4 samples), and in the GC unit as gabbro sills (2 samples). The subsuite consists predominantly of tholeiitic basalt, with minor Fe- and Mg-tholeiitic basalt (Figure 43a), which exhibit a range of SiO_2 of 44–53 wt. %, TiO_2 of 0.5–1.5 wt. % and Fe_2O_3 of 10–15 wt. % over an Mg# range of 31–57. The basalt exhibits weakly to moderately sloped profiles on NMORB- and PM-normalized extended-element plots ($La/Yb_N = 1.7–11.1$), with moderately enriched and fractionated LREE ($La/Sm_N = 1.4–3.4$), generally unfractionated HREE ($Gd/Yb_N = 0.9–2.0$), prominent negative Nb anomalies ($Th/Nb_{PM} = 2.6–10.9$) and weak negative Zr and Ti anomalies (Figure 44e, f, i, j). Chromium values range from less than detection limit (<DL) to 435 ppm (average 193 ppm) and Ni values from <DL to 250 ppm (average 92 ppm). Ternary plots of Th–Hf/3–Ta (Wood, 1980) and La/10–Y/15–Nb/8 (Cabanis and Lecolle, 1989) indicate that these basalts are transitional between typical calcalkalic and tholeiitic arc-basalts (Figure 43b, c). On the Th/Yb vs. Nb/Yb diagram of Pearce and Peate (1995), these rocks exhibit a possible within-plate enrichment

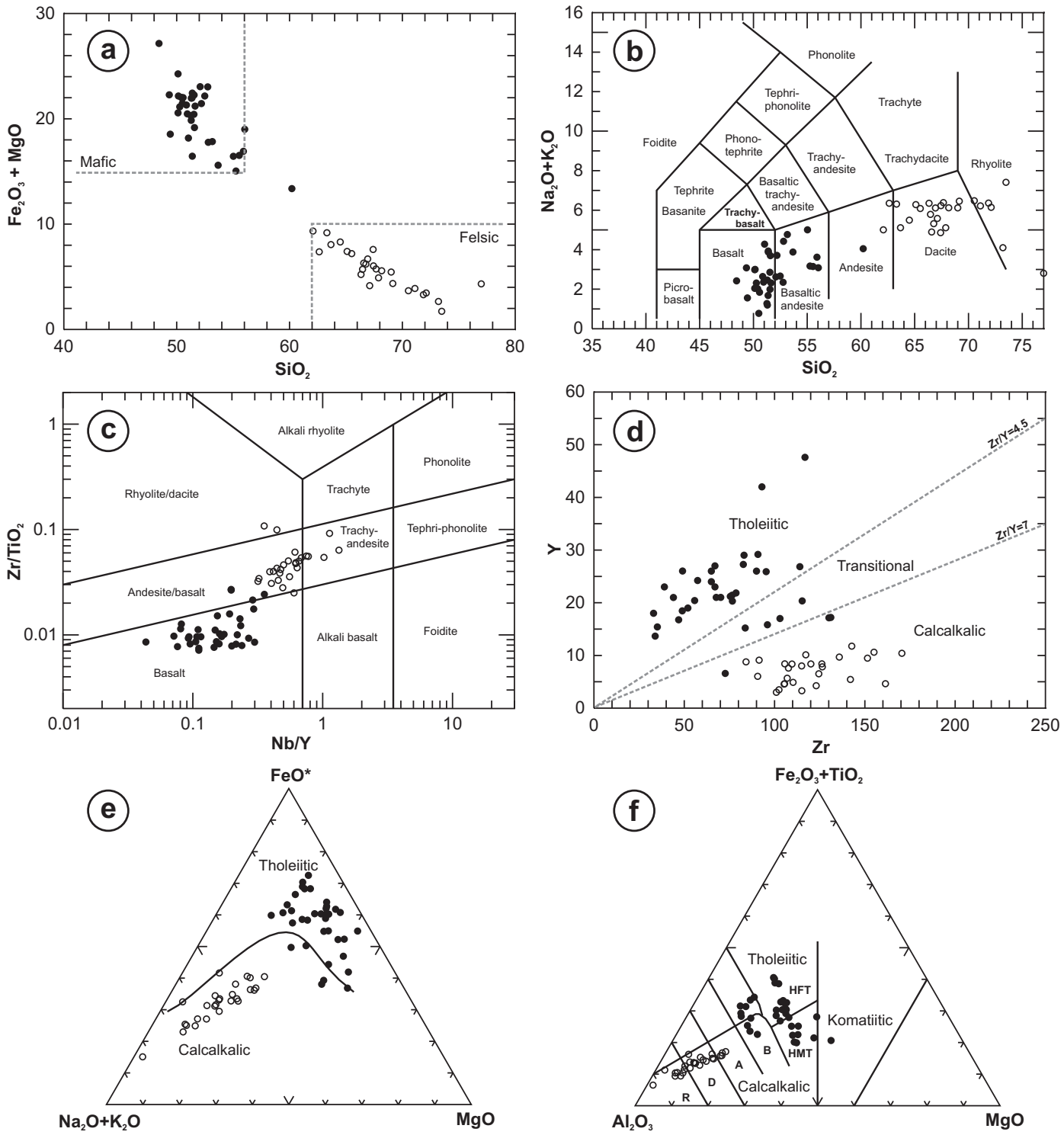

Figure 42: *Discrimmination diagrams showing the compositions of mafic (filled circles) and felsic (open circles) volcanic and plutonic rocks from the Rice Lake area:* ***a)*** *SiO_2 vs. Fe_2O_3+MgO plot, showing the essentially bimodal nature of the magmatism;* ***b)*** *SiO_2 vs. total alkali diagram of Le Bas et al. (1986);* ***c)*** *Nb/Y vs. Zr/TiO_2 diagram of Pearce (1996;* modified after *Winchester and Floyd, 1977);* ***d)*** *Zr vs. Y diagram of Barrett and MacLean (1994);* ***e)*** *AFM diagram of Irvine and Baragar (1971);* ***f)*** *Al_2O_3 vs. Fe_2O_3+TiO_2 vs. MgO diagram of Jensen (1976). Abbreviations: A, andesite; B, basalt; D, dacite; HFT, high-Fe tholeiite; HMT, high-Mg tholeiite; R, rhyolite.*

trend, with evidence of a significant subduction component (Figure 43d). The Nb/Yb ratios indicate an affinity to either oceanic or continental-arc magmatism. One sample from the SAM gabbro sill (sample 9-1-1) exhibits strongly depleted and fractionated HREE, suggesting derivation from a strongly depleted source.

Sanukitoid-like transitional basalt and basaltic andesite

This subsuite has been identified in the RLR and TS units as diabase dikes (3 samples) and in the RL unit as a 15 m thick layer of lapilli tuff (2 samples), which is interpreted as a proximal scoria deposit. The subsuite consists of basalt and basaltic andesite of transitional tholeiitic–calcalkalic affinity,

Table 4: Salient geochemical characteristics of mafic volcanic and plutonic rocks in the Rice Lake area.

	SiO_2 (wt. %)	TiO_2 (wt. %)	Fe_2O_3 (wt. %)	Mg#	Cr (ppm)	Ni (ppm)	$(La/Yb)_N$	$(La/Sm)_N$	$(Gd/Yb)_N$	$(Th/Nb)_{PM}$
MORB-like (N = 20):										
Range	45.9–50.6	0.7–2.0	10.6–19.0	32–57	<DL–355	<DL–102	1.0–2.6	0.9–1.5	1.0–1.5	0.8–1.4
Average	48.6	1.2	14.3	44	124	70	1.7	1.2	1.2	1.1
Arc-like (N = 9):										
Range	44.4–53.0	0.5–1.5	10.3–15.4	31–57	<DL–435	<DL–250	1.7–11.1	1.4–3.4	0.9–2.0	2.6–10.9
Average	49.2	0.9	12.7	42	193	92	3.6	2.3	1.1	6.6
Sanukitoid-like (N = 5):										
Range	45.3–50.9	0.8–1.0	8.8–10.8	61–70	231–408	101–402	20.2–55.8	3.2–4.2	2.8–5.6	9.4–33.9
Average	48.5	0.8	9.5	65	322	233	36.7	3.6	4.4	23.5

Abbreviations: N, chondrite-normalized; PM, primitive-mantle–normalized (values *from* Sun and McDonough, 1989)

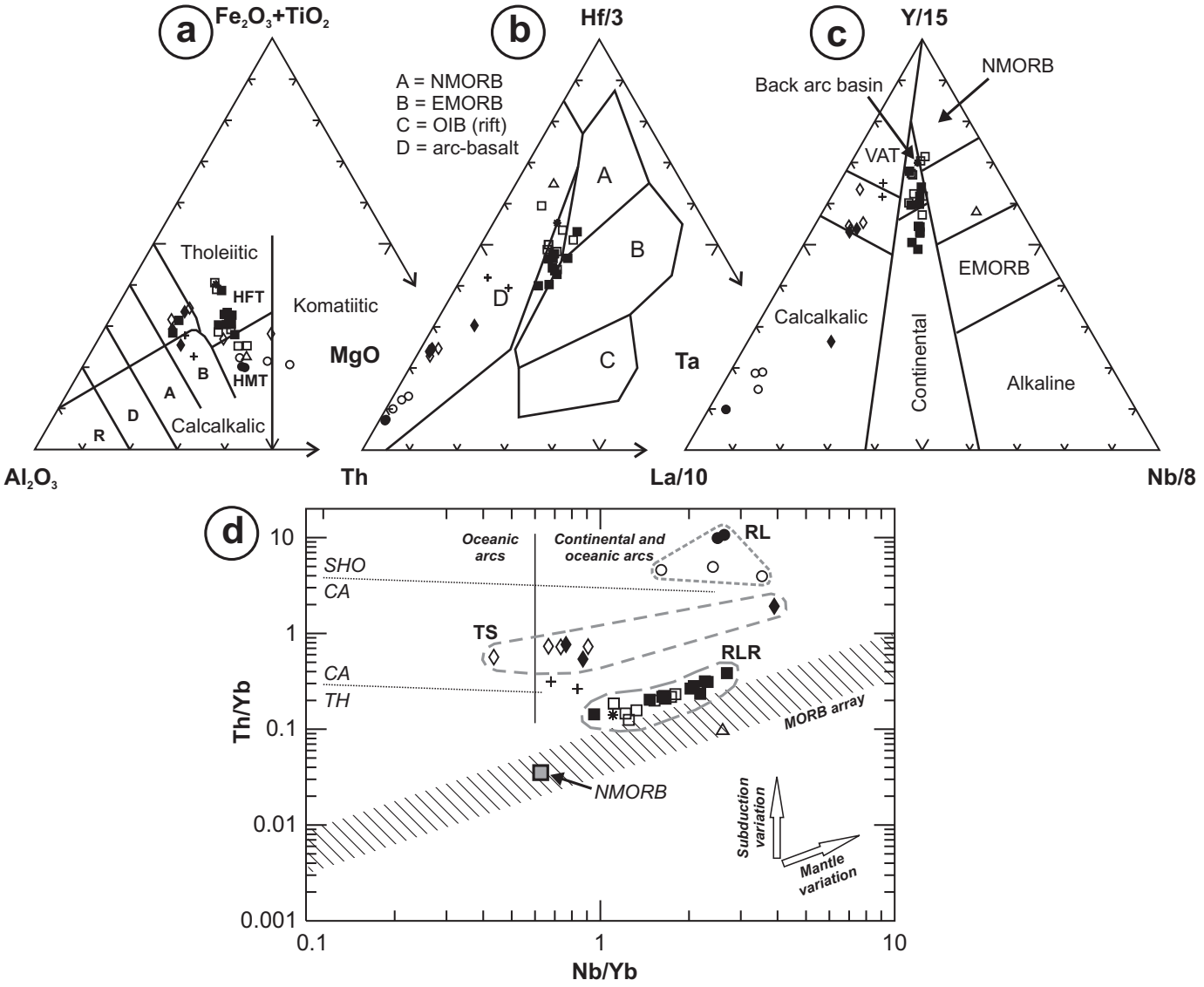

Figure 43: *Discrimmination diagrams showing the compositions of mafic volcanic and plutonic rocks from the Rice Lake area:* ***a)*** *Al_2O_3 vs. Fe_2O_3+TiO_2 vs. MgO diagram of Jensen (1976); A, andesite; B, basalt; D, dacite; HFT, high-Fe tholeiite; HMT, high-Mg tholeiite; R, rhyolite;* ***b)*** *Th vs. Hf/3 vs. Ta diagram of Wood (1980);* ***c)*** *La/10 vs. Y/15 vs. Nb/8 diagram of Cabanis and Lecolle (1989); VAT, volcanic-arc tholeiite;* ***d)*** *Nb/Yb vs. Th/Yb diagram (*after *Pearce and Peate, 1995); CA, calcalkalic; SHO, shoshonitic; TH, tholeiitic. Abbreviations: EMORB, enriched mid-ocean-ridge basalt; NMORB, normal mid-ocean-ridge basalt; OIB, ocean-island basalt. See Figure 44 for symbol definitions.*

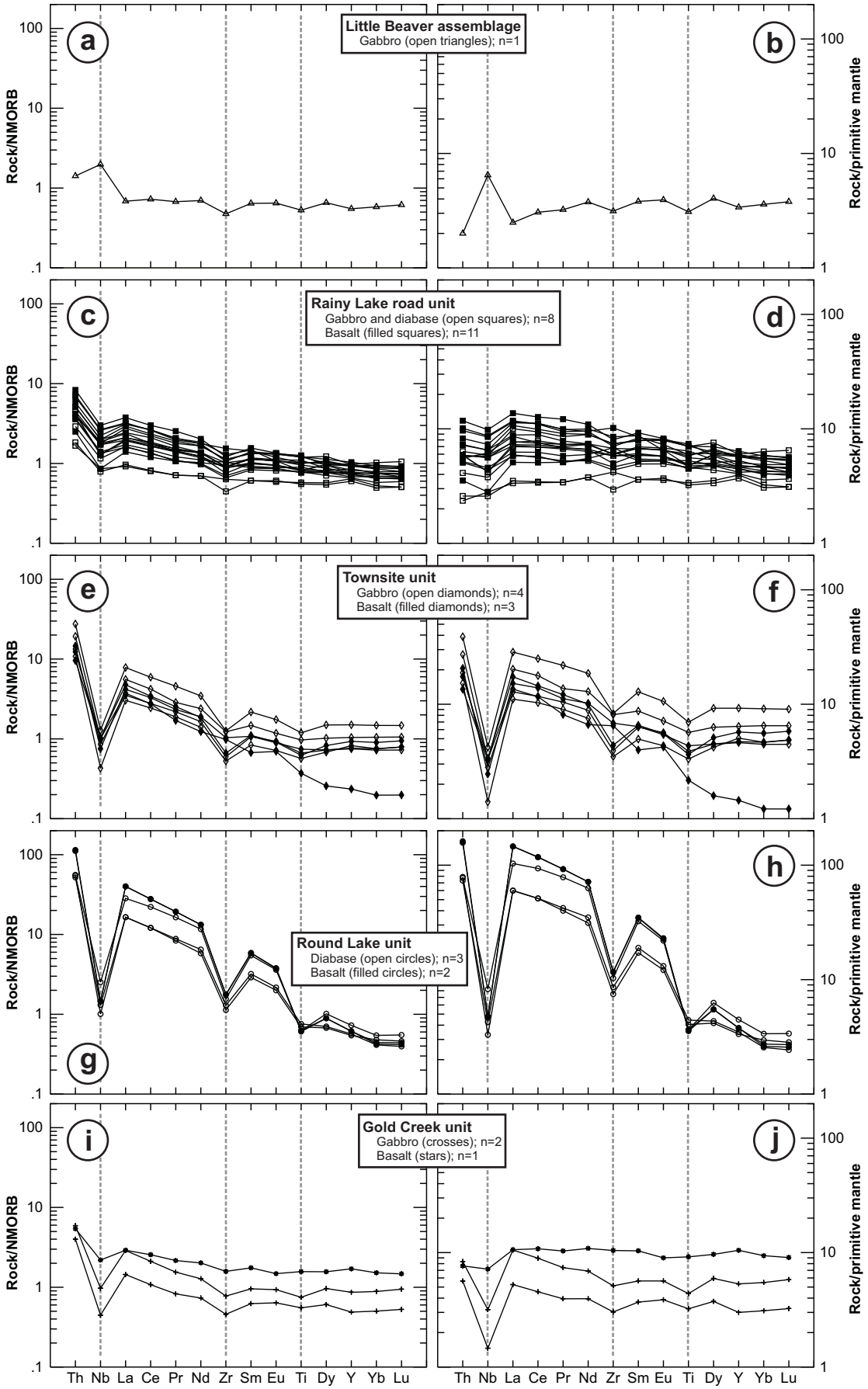

Figure 44: *Normal mid-ocean-ridge basalt (NMORB; left column)– and primitive-mantle–normalized (right column) extended-element plots for mafic volcanic and plutonic rocks from the Rice Lake area. Normalizing values are from Sun and McDonough (1989).*

which exhibit a range of SiO_2 of 45–51 wt. %, TiO_2 of 0.8–1.0 wt. % and Fe_2O_3 of 9–11 wt. % over an Mg# range of 61–70. These rocks exhibit steeply sloped profiles on NMORB- and PM-normalized extended-element plots, with extreme La/Yb_N ratios of 20.2–55.8, given the high Mg# values. The profiles are characterized by strongly enriched and fractionated LREE (La/Sm_N = 3.2–4.2), depleted and fractionated HREE (Gd/Yb_N = 2.8–5.6) and very pronounced negative Nb (Th/Nb_{PM} = 9.4–33.9), Zr and Ti anomalies (Figure 44g, h). Chromium and nickel values are highly elevated and range from 231 to 408 ppm (average 322 ppm) and from 101 to 402 ppm (average 233 ppm), respectively. Ternary plots of Th–Hf/3–Ta (Wood, 1980) and La/10–Y/15–Nb/8 (Cabanis and Lecolle, 1989) indicate an affinity to highly evolved calcalkalic arc-basalt (Figure 43b, c). On the Th/Yb vs. Nb/Yb diagram of Pearce and Peate (1995), these rocks exhibit evidence of a significant subduction component (Figure 43d). A sample of the scoria layer in the RL unit (sample 1368-1) has an initial ε_{Nd} value of 1.2 (at 2.715 Ga) and a crustal-residence model age (T_{CR}) of 2.91 Ga, suggesting derivation from melts that interacted with older, isotopically evolved crust (Table 3).

The high Mg# values, extreme LREE enrichment, steeply fractionated REE profiles and strongly enriched Cr, Ni and large-ion lithophile element (LILE; e.g., Sr, Ba) contents (Figure 45) distinguish these rocks from the other mafic volcanic and plutonic rocks in the Rice Lake area. As shown in Table 5, with the exception of Ba in the diabase samples, the average compositions exhibited by the sanukitoid-like subsuite in the Rice Lake area compare favourably with the late-Archean sanukitoid suite, first identified in the Superior Province by Shirey and Hanson (1984). As summarized by Martin et al. (2005), the sanukitoid suite represents a magmatic series that, at SiO_2 contents of <60 wt. %, is characterized by MgO>6 wt. %, Mg# >0.60, Cr and Ni each >100 ppm, Sr and Ba each >500 ppm, and strongly enriched LREE and corresponding high La/Yb ratios (Table 5; *see also* Shirey and Hansen, 1984; Stern, 1989; Stern et al., 1989; Smithies and Champion, 2000). The petrogenetic and paleotectonic significance of the sanukitoid-like rocks are described below.

Felsic volcanic and plutonic rocks

Felsic samples plot mainly as dacite on the SiO_2 vs. total alkalis discrimination diagram of Le Bas et al. (1986) in Figure 42b. Most samples appear to exhibit elevated Ti in relation to Zr, and thus plot toward more mafic compositions on the immobile trace-element diagram of Pearce (1996; modified

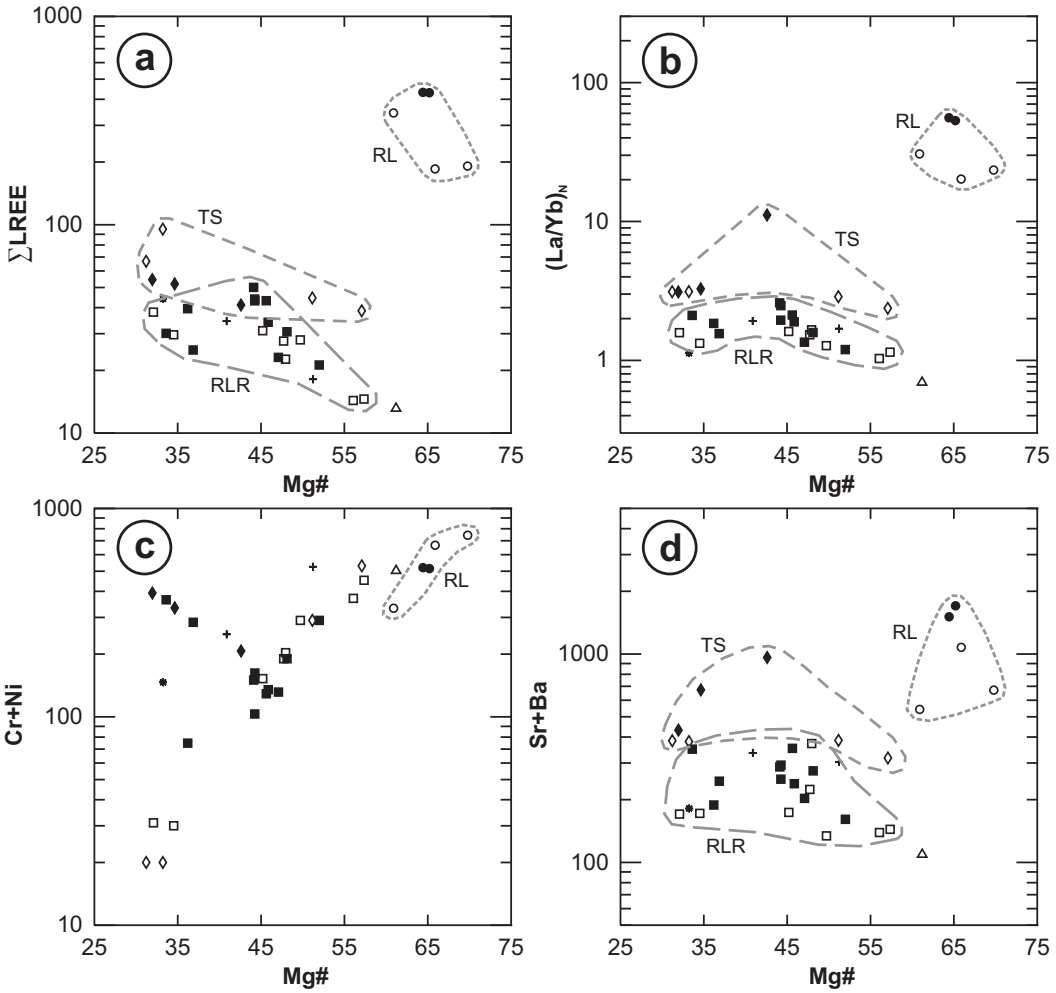

Figure 45: *Variation of specified REE and trace elements with Mg# for the sanukitoid-like subsuite in the Rice Lake area:* ***a)*** *Mg# vs. ∑LREE (La, Ce, Pr, Nd);* ***b)*** *Mg# vs. chondrite-normalized La/Yb (normalizing values* from *Sun and McDonough, 1989);* ***c)*** *Mg# vs. Cr+Ni;* ***d)*** *Mg# vs. Sr+Ba. Abbreviations: LREE, light rare-earth element(s); RL, Round Lake unit; RLR, Rainy Lake road unit; TS, Townsite unit. See text for discussion.*

Table 5: Salient geochemical characteristics of sanukitoids as compared to the sanukitoid-like subsuite in the Rice Lake area.

	SiO_2 (wt. %)	MgO (wt. %)	Mg#	Cr (ppm)	Ni (ppm)	Ba (ppm)	Sr (ppm)	$(La/Yb)_N$ [1]
Sanukitoid[2]	<60	>6	>0.60	>100	>100	>500	>500	>10
Unit 17 (n = 3)								
Range	45.3–48.6	7.4–11.4	0.61–0.70	231–408	101–402	16–386	326–691	20.2–30.7
Mean	47	9.8	0.66	301	280	249	515	24.8
Unit 18c (n = 2)								
Range	50.7–50.9	8.2–8.3	0.64–0.65	352–358	162–163	399–874	831–1110	53.2–55.8
Mean	50.8	8.3	0.65	355	163	637	971	54.5

[1] subscript 'N' refers to chondrite normalization using the values of Sun and McDonough (1989)

[2] *after* Martin et al. (2005), and references therein

after Winchester and Floyd, 1977) in Figure 42c; most of these samples plot as rhyodacite and dacite on the original Winchester and Floyd (1977) diagram. Although most are subalkaline, some samples also appear to exhibit elevated Nb in relation to Y, suggesting a mildly alkaline affinity. The plots of Barrett and MacLean (1994), Irvine and Baragar (1971) and Jensen (1976) indicate a calcalkalic geochemical affinity (Figure 42d, e, f). All samples exhibit broadly similar HFSE and REE contents, as evidenced by the roughly parallel chondrite-normalized and primitive-mantle–normalized extended-element profiles in Figure 46, and are thus described together.

The felsic samples exhibit smoothly sloping chondrite-normalized extended-element profiles (Figure 47), with strongly enriched and fractionated LREE (La/Yb_N = 9.4–57.8; La/Sm_N = 3.3–6.3) and weakly to moderately fractionated HREE (Gd/Yb_N = 1.7–6.9); negative Eu anomalies are lacking (Eu/Eu* = 0.9–1.5). All samples exhibit strong negative Nb anomalies on primitive mantle–normalized profiles (Th/Nb_{PM} = 3.0–15.9), with generally weak positive Zr and weak negative Ti (Figure 46b). On the Nb vs. Y diagram of Pearce et al. (1984), these rocks plot with the field of volcanic-arc and syncollisional granites (Figure 48a). High La/Yb_N (9.4–57.8) and Zr/Y (9.6–35.0) ratios, correspondingly low Yb (0.2–1.2 ppm) and Y (3.0–11.8 ppm) and lack of negative Eu anomalies all indicate an affinity to 'FI' felsic volcanic rocks (Figure 48b; Lesher et al., 1986; Hart et al., 2004). A sample of brecciated dacite in the RLR unit (sample 1330-2) has an initial ε_{Nd} of 0.3 (at 2.73 Ga) and a crustal-residence model age (T_{CR}) of 3.03 Ga, whereas a sample of quartz-feldspar porphyry (QFP) rhyolite in the RL unit (sample 1376-1) has an initial ε_{Nd} of 1.1 (at 2.715 Ga) and a crustal-residence model age (T_{CR}) of 2.94 Ga, both of which are consistent with derivation from melts that interacted with older, isotopically evolved crust (Table 3).

A subset of the felsic igneous samples, consisting of coarsely porphyritic (feldspar±hornblende±quartz) volcaniclastic rocks of andesite–dacite composition in the TS and RL units (units 16 and 19, respectively), is characterized by relatively high Mg# values, high contents of Cr, Ni and Sr, anomalously low contents of Y and Yb, strongly fractionated REE patterns and correspondingly high Sr/Y and $(La/Yb)_N$ ratios (Table 6). These chemical attributes indicate a close chemical affinity to Cenozoic adakite, which are a distinctive suite of high-silica igneous rocks associated with oceanic and continental-arc settings. Compared to typical calcalkalic andesite and dacite in these settings, adakite with an SiO_2 content above 56 wt. % is characterized by high Mg# (~0.5), Sr (≥400 ppm), Ni (≥20 ppm) and Cr (≥30 ppm), very low Y (≤18 ppm) and Yb (≤ 1.9 ppm), and strongly fractionated REE, and are identified on the basis of their characteristically high Sr/Y (≥20) and $(La/Yb)_N$ (≥20) ratios (Defant and Drummond, 1990; Martin, 1999; Martin

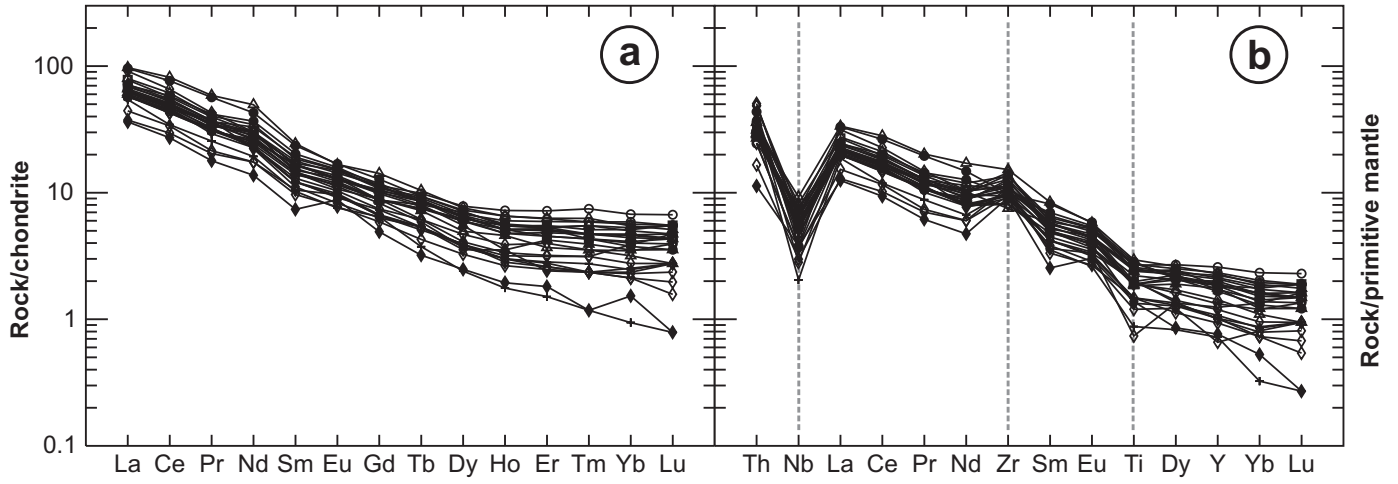

Figure 46: *Chondrite-normalized* ***(a)*** *and primitive-mantle–normalized* ***(b)*** *extended-element plots for felsic volcanic and plutonic rocks from the Rice Lake area. Normalizing values are from Sun and McDonough (1989).*

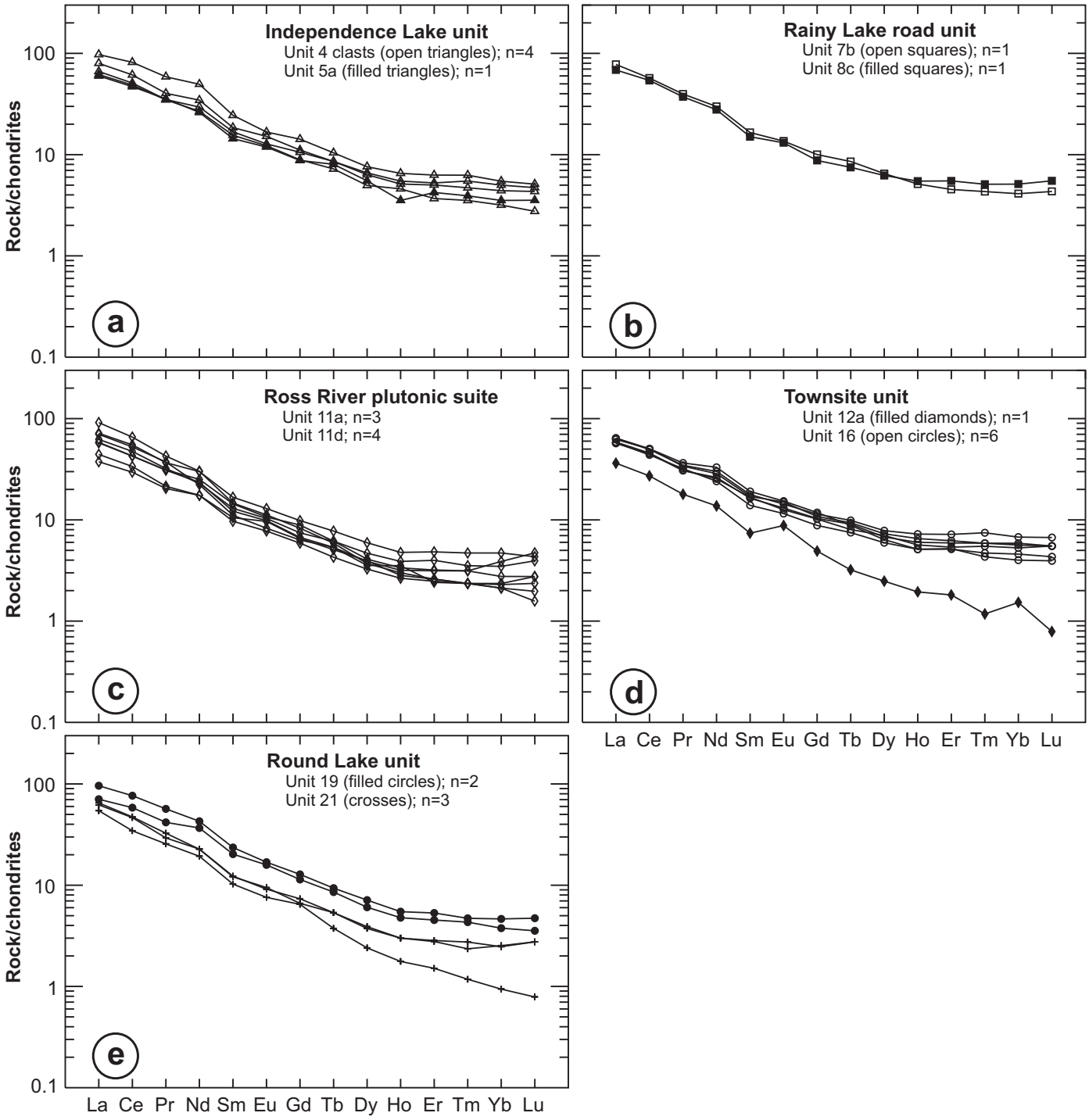

Figure 47: *Chondrite-normalized extended-element plots for felsic volcanic and plutonic rocks from the Rice Lake area. Normalizing values are from Sun and McDonough (1989).*

et al., 2005; Richards and Kerrich, 2007). The petrogenetic and paleotectonic significance of the adakite-like rocks are described below.

Petrogenesis and paleotectonic significance

Felsic volcaniclastic rock types and their subvolcanic equivalents dominate the stratigraphic succession in the Rice Lake area, and are composed mainly of calcalkaline dacite, with subordinate andesite and rhyolite. The predominance of coarse epiclastic deposits containing rounded volcanic-rock clasts, coupled with the apparent absence of significant accumulations of primary felsic pyroclastic material or felsic flows, suggest deposition in the medial–distal portion of a volcaniclastic apron on the flanks of a subaerially exposed volcanic complex. The dominance of coarsely porphyritic dacite detritus indicates a volcanic source area dominated by porphyry effusions and cryptodomes.

The HFSE and REE concentrations of the constituent felsic volcanic and plutonic rocks indicate a close chemical affinity to the 'FI' felsic volcanic rocks described by Lesher et al. (1986), which are generally interpreted to be derived from low-degree partial melting of metasomatized mantle-wedge

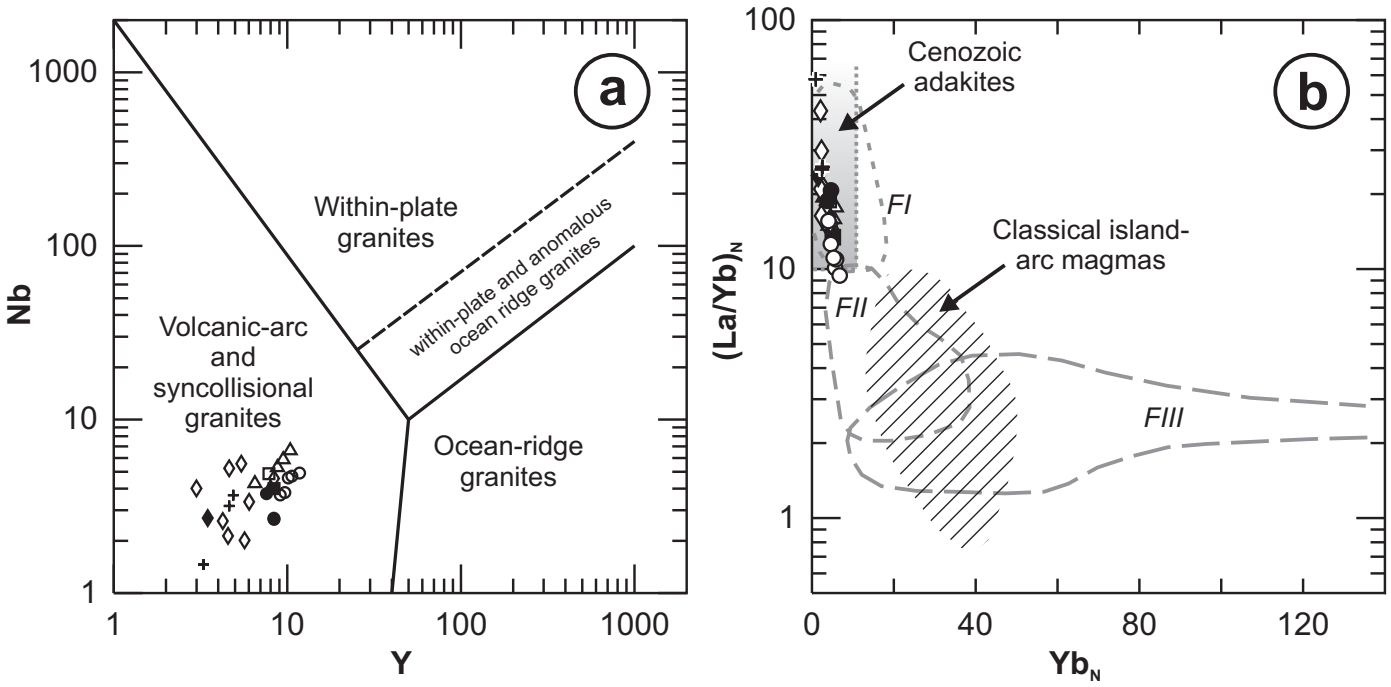

Figure 48: *Discrimmination diagrams showing the compositions of felsic volcanic and plutonic rocks from the Rice Lake area:* ***a)*** *Y vs. Nb diagram of Pearce et al. (1984);* ***b)*** *Yb_N vs. La/Yb_N diagram, showing the fields for FI, FII and FIII felsic metavolcanic rocks in the Superior Province (*after *Lesher et al., 1986); field for Cenozoic adakites is from Martin et al. (2005); field for classical island-arc magmas is from Drummond and Defant (1990). See Figure 47 for symbol definitions.*

Table 6: Salient geochemical characteristics of adakite and adakite-like rocks from units 16 and 19, Rice Lake area.

	SiO_2 (wt. %)	Na_2O (wt. %)	K_2O/Na_2O	Mg#	Ni (ppm)	Cr (ppm)	Sr (ppm)	Yb (ppm)	Y (ppm)	Sr/Y	La/Yb
Adakite[(1)]	≥56	≥3.5	~0.42	~0.5	≥20	≥30	≥400	≤1.9	≤18	≥20	≥20
Unit 16 (n = 6)											
Range	59.6–64.0	4.07–5.47	0.12–0.42	0.40–0.52	38–57	25–108	222–929	0.68–1.15	8.39–11.76	22.0–110.7	13.1–21.7
Mean	61	4.5	0.23	0.48	43	46	644	0.91	9.95	65.8	16.2
Unit 19 (n = 2)											
Range	62.9–63.7	4.16–4.79	0.27–0.42	0.50–0.52	38–44	33–65	460–837	0.64–0.79	7.59–8.36	55.0–110.3	26.2–28.8
Mean	63	4.5	0.35	0.51	41	49	649	0.72	7.98	82.7	27.5

(1) *after* Richards and Kerrich (2007), and references therein

peridotite, with variable contamination by crustal material, in suprasubduction-zone settings (Barrie et al., 1993). Some of these rocks also exhibit a chemical affinity to modern adakite, which is widely considered to be the direct product of partial melting of subducting slabs of young, hot oceanic lithosphere (e.g., Kay, 1978; Defant and Drummond, 1990; Martin et al., 2005). More recently, however, other authors have suggested that adakite-like rock compositions can also be produced from mantle-wedge–derived magmas by simple fractionation and contamination processes in the upper plate, without direct contributions from slab melts (e.g., Richards and Kerrich, 2007).

Regardless of petrogenetic model, the presence of adakite-like rocks at Rice Lake strongly implies the operation of subduction processes and is thus interpreted to indicate a supra-subduction zone setting for the felsic magmatism in the Bidou assemblage. Similar models have been proposed for Late Archean adakite-like rocks identified in the Uchi (Hollings and Kerrich, 2000) and Wawa subprovinces (Polat and Kerrich, 2001) of the Superior Province. Initial ε_{Nd} values and crustal-residence model ages (T_{CR}) indicate derivation from melts that interacted with older, isotopically evolved crust, perhaps suggesting that the Bidou volcanic arc formed on or close to the south margin of the Mesoarchean North Caribou Terrane.

In the Rice Lake area, the felsic volcaniclastic rocks are intercalated with three distinct geochemical suites of mafic volcanic and intrusive rocks. Iron-tholeiitic basalt forms thick successions of pillowed and massive flows (unit 10) and synvolcanic sills (unit 9) in the RLR unit, as well as diabase dikes cutting felsic volcanic and volcaniclastic rocks in the underlying IL unit. Facies associations and stratigraphic relationships indicate that this mafic magmatism is associated with the development of a restricted marine basin that formed in

the hangingwall of a synvolcanic subsidence structure in the IL unit. In keeping with this setting, the HFSE and REE abundances in the Fe-tholeiitic basalt indicate a chemical affinity to modern back-arc basin basalt, which is generally interpreted to result from partial melting of a depleted mantle source that interacted with a slab-derived aqueous fluid and/or melt component (e.g., Sinton and Fryer, 1987). Hence, both the stratigraphic and chemical attributes the RLR unit are compatible with an extensional geodynamic setting, perhaps associated with the initiation of a back-arc basin within the Bidou volcanic arc. With the exception of a slight enrichment in LREE, slightly higher Th and Nb, and slightly lower ε_{Nd}, the RLR basalt is similar to the Grey Point basalt of the Black Island assemblage at Lake Winnipeg, which likewise exhibits a chemical similarity to modern back-arc basin basalt and has been attributed to a back-arc magmatic setting (Bailes and Percival, 2005a). As noted by these authors, similar chemical features also characterize the Unnamed, Tinney and Gunnar basalt units, which dominate the lower portion of the Bidou assemblage east of the Ross River pluton.

Basalt and basaltic andesite of tholeiitic affinity define a pillowed and massive flow unit (unit 15) hosted by felsic epiclastic rocks (units 12 and 13) of the overlying TS unit. The epiclastic rocks are interpreted to record deposition in a subaerial to shallow-marine alluvial fan on the flanks of a subaerially exposed volcanic complex, and are cut by dikes and thick sills of tholeiitic gabbro (unit 14) that are interpreted to represent subvolcanic feeders to the overlying effusive rocks. The HFSE and REE contents of the basalt and gabbro are most similar to modern volcanic-arc basalt and are thus interpreted to indicate a resurgence of arc-magmatism subsequent to the initiation of back-arc spreading. The petrogenesis of modern volcanic-arc basalt is generally thought to involve partial melting of the mantle wedge above a subducting slab of oceanic lithosphere, with contributions of slab-derived aqueous fluid and/or melt (e.g., Pearce and Peate, 1995).

Adakite-like volcaniclastic rocks (unit 16) overlie unit 15 and are cut by irregular dikes of magnesian basalt and basaltic andesite (unit 17) that exhibit transitional calcalkalic–tholeiitic affinities. Compositionally similar basalt also defines a thin fragmental unit, interpreted to represent a proximal scoria-fall deposit, in the heterolithic conglomerate (unit 18) that defines the base of the RL unit. The unique chemistry of the mafic volcanic rocks in the RL unit (high Mg#, Cr and Ni, with strongly enriched LREE and LILE) indicates an affinity to the Late Archean sanukitoid suite. As described by Shirey and Hanson (1984), the petrogenesis of these rocks is generally thought to involve partial melting of sub-arc mantle peridotite that was extensively metasomatized by slab-derived fluids (*see also* Stern, 1989; Stern et al., 1989). At Rice Lake, these rocks are interpreted to signal a change toward more evolved magmatism in the advanced stages of the Bidou volcanic arc.

The distinctive geochemical association of volcanic-arc–like basalt and adakite-like dacite with the sanukitoid-like basalt in the TS and RL units further implicates subduction processes in their petrogenesis and a suprasubduction zone paleotectonic setting for at least this portion of the Bidou assemblage. The weakly positive initial ε_{Nd} values and Nd model ages of ca. 2.9–3.0 Ga are most consistent with a continental-margin setting for the magmatism, presumably in proximity to the margin of the ca. 3.0 Ga North Caribou continental terrane.

U-Pb zircon geochronology

In order to better constrain the timing of volcanism, plutonism and sedimentation in the Rice Lake area, five samples from the various lithostratigraphic units in the study area were collected for U-Pb zircon geochronological analysis. Igneous zircons were obtained from felsic plutonic rocks of the Ross River plutonic suite (map unit 11a; sample 96-03-RRP) and the RL unit (map unit 21; sample 96-04-1384), and a single sample of sulphide-clast–bearing felsic volcanic conglomerate from the RLR unit (map unit 8c; sample 96-03-1285). Detrital zircons were also obtained from the fault-bounded panel of the San Antonio assemblage along the Wanipigow Shear Zone (map unit 29a; sample 96-05-1622-1) and from the unusual discordant body of heterolithic breccia (map unit 12; sample 96-04-1450-2) that cuts intermediate volcanic and volcaniclastic rocks of the IL unit.

Methodology

Each sample consisted of 10–15 kg of least-altered, omogeneous and representative rock, which was collected by hammer or rock-saw from bedrock and was manually trimmed in the field to remove all weathered surfaces, veins, altered fractures or other inhomogeneities. The resulting clean rock-chips were triple bagged, sealed in a plastic rock-pail, and shipped to the University of Alberta Radiogenic Isotope Facility in Edmonton, Alberta, for mineral separation, processing and analysis.

The igneous zircons separated from the volcanic and plutonic rock samples underwent conventional U-Pb dating by isotope dilution–thermal ionization mass spectrometry (ID-TIMS), which generally followed the procedures outlined in Heaman et al. (2002). All analyses were performed on a VG354 mass spectrometer operated in single Faraday or Daly (analogue) collector peak-hopping mode, and were corrected for mass discrimination based on replicate measurement of the NBS981 and U500 standards. In addition, all measurements obtained with the Daly photomultiplier detector were adjusted for detector bias. The isotopic composition of common Pb in excess of analytical blank (2 pg of Pb) was calculated using the two-stage model of Stacey and Kramers (1975). The resulting U-Pb isotopic data are listed in Table 7 and plotted as concordia diagrams in Figure 49. All errors reported in Table 7 are quoted at 1σ and were calculated by numerical propagation of all known sources of uncertainty. The concordia diagrams were generated using the Isoplot version 3.0 application of Ludwig (2003), and the error ellipses on these diagrams are shown at 2σ.

The detrital zircons separated from the siliciclastic rock samples underwent U-Pb dating by laser-ablation, multicollector, inductively coupled plasma–mass spectrometry (LA-MC-ICP-MS), which generally followed the procedures outlined by Simonetti et al. (2005). The mineral separation techniques were identical to those for the ID-TIMS samples and the resulting zircons were hand picked, mounted in epoxy and polished to half-section thickness for analysis. All analyses were performed on a Nu Plasma MC-ICP-MS coupled to a frequency

Table 7: U-Pb isotope dilution thermal ionization mass spectrometry (ID-TIMS) analytical data for igneous zircons from felsic volcanic and plutonic rock samples in the Rice Lake area. Also provided in Data Repository Item DRI2008002.

									Isotopic ratios[2]			Age (Ma)[2]			
Sample/ fraction	Description[1]	Weight (mg)	U (ppm)	Th (ppm)	Pb (ppm)	Model Th/U	^{204}Pb (pg)	^{206}Pb/ ^{204}Pb	^{206}Pb/ ^{238}U	^{207}Pb/ ^{235}U	^{207}Pb/ ^{206}Pb	^{206}Pb/ ^{238}U	^{207}Pb/ ^{235}U	^{207}Pb/ ^{206}Pb	Disc. (%)
96-03-1285: RLR unit, volcanic pebble conglomerate (map unit 8c); UTM (NAD83, Z15) 319690mE, 5655510mN															
1z	2°NM col pr (1)	12.0	48.1	25.7	29.1	0.54	3.1	6085	0.52192 ±0.00061	13.5829 ±0.0160	0.18875 ±0.00005	2707.3 ±3.0	2721.1 ±1.0	2731.3 ±0.4	1.1
2z	2°NM col pr (1)	13.0	79.7	31.1	47.3	0.39	4.0	8571	0.52905 ±0.00062	13.7333 ±0.0171	0.18827 ±0.00009	2737.4 ±3.0	2731.5 ±1.0	2727.1 ±0.8	-0.5
3z	2°NM col pr (1)	13.0	64.6	35.7	41.0	0.55	21.1	1323	0.52972 ±0.00103	13.9219 ±0.0633	0.19061 ±0.00067	2740.3 ±4.0	2744.4 ±4.0	2747.4 ±5.7	0.3
4z	2°NM pink pr (1)	7.2	72.7	35.1	44.1	0.48	16.4	1036	0.50974 ±0.00110	13.2345 ±0.0363	0.18830 ±0.00032	2655.5 ±4.7	2696.5 ±2.6	2727.4 ±2.8	3.2
5z	2°NM pink pr (5)	8.8	79.2	46.8	49.8	0.59	23.3	977	0.51499 ±0.00072	13.4473 ±0.0220	0.18938 ±0.00014	2677.9 ±3.1	2711.6 ±1.5	2736.8 ±1.3	2.6
96-03-RRP: Ross River pluton, biotite granodiorite (map unit 11a); UTM (NAD83, Z15) 320712mE, 5647567mN															
1z	0°M pink frag (1)	7.7	47.8	33.4	31.3	0.70	19.2	630	0.51341 ±0.00085	13.2952 ±0.0283	0.18782 ±0.00023	2671.2 ±3.6	2700.8 ±2.4	2723.1 ±2.0	2.3
2z	0°M pink frag (1)	8.3	73.4	37.9	40.9	0.52	9.4	1933	0.47484 ±0.00056	12.3074 ±0.0155	0.18798 ±0.00008	2504.7 ±2.5	2628.1 ±1.3	2724.6 ±0.7	9.7
3z	0°M pink euh pr (2:1 to 3:1) (16)	27.9	79.9	39.9	41.7	0.50	12.8	4930	0.45148 ±0.00051	11.6581 ±0.0126	0.18728 ±0.00008	2401.8 ±2.2	2577.3 ±1.1	2718.4 ±0.7	13.9
4z	0°M eq euh rd pink (3)	9.3	34.7	17.8	19.1	0.51	3.2	3038	0.47544 ±0.00073	12.3135 ±0.0190	0.18784 ±0.00009	2507.4 ±3.2	2628.6 ±1.5	2723.3 ±0.8	9.6
5z	0°M pink sl (>5:1) pr (11)	16.6	44.0	26.3	23.0	0.60	8.1	2499	0.43970 ±0.00051	11.3485 ±0.0137	0.18719 ±0.00006	2349.3 ±2.3	2552.2 ±1.1	2717.6 ±0.5	16.1
7z	0°M euh pink pr (8)	17.0	212.8	102.6	109.5	0.48	62.5	1598	0.43765 ±0.00062	11.2581 ±0.0165	0.18657 ±0.00013	2340.1 ±3.0	2544.7 ±2.0	2712.1 ±1.2	16.3
8z	0°M euh pink pr (7)	10.0	91.8	55.3	61.9	0.60	249.3	97	0.36939 ±0.00115	9.4023 ±0.0705	0.18461 ±0.00113	2026.5 ±5.0	2378.1 ±9.0	2694.7 ±10.1	28.8
9z	0°M col eq; TA-CA (6hr) (1)	6.0	91.7	40.9	53.5	0.45	6.7	2638	0.50895 ±0.00070	13.1054 ±0.0171	0.18676 ±0.00012	2652.1 ±2.8	2687.3 ±1.2	2713.8 ±1.1	2.8
12z	0°M col rd eq; TA-CA (6hr) (1)	3.6	79.0	41.0	53.0	0.51	39.0	232	0.47648 ±0.00122	12.4206 ±0.0877	0.18906 ±0.00102	2511.9 ±5.3	2636.7 ±6.6	2734.0 ±8.9	9.8
96-04-1384: RL unit, rhyolitic quartz-feldspar porphyry (map unit 21); UTM (NAD83, Z15) 312102mE, 5657942mN															
1z	pink euh pr (3)	11.0	131.1	55.7	77.6	0.43	11.8	4082	0.52078 ±0.00062	13.4228 ±0.0180	0.18693 ±0.00012	2702.5 ±3.0	2709.9 ±1.0	2715.4 ±1.1	0.6
2z	pink larger euh pr (2)	12.0	156.2	68.5	92.6	0.44	11.4	5442	0.52094 ±0.00132	13.4596 ±0.0356	0.18739 ±0.00015	2703.2 ±6.0	2712.5 ±3.0	2719.4 ±1.3	0.7
3z	tan-pink euh pr (4)	12.0	148.5	66.7	74.1	0.45	8.5	5677	0.43645 ±0.00081	11.3439 ±0.0210	0.18851 ±0.00008	2334.7 ±4.0	2551.8 ±2.0	2729.2 ±1.0	17.2

[1] magnetic susceptibility of zircons is indicated by M (magnetic) or NM (non-magnetic), prefaced by the inclination of the Frantz isodynamic separator; number in parentheses indicates number of grains included in analysis

[2] isotopic ratios and ages are corrected for fractionation, blank, spike and initial common lead (Stacey and Kramers, 1975)

Abbreviations: col, colourless; eq, equant; euh, euhedral; frag, fragment; pr, prism; rd, round; sl, slender; TA-CA, thermal annealing and chemical abrasion

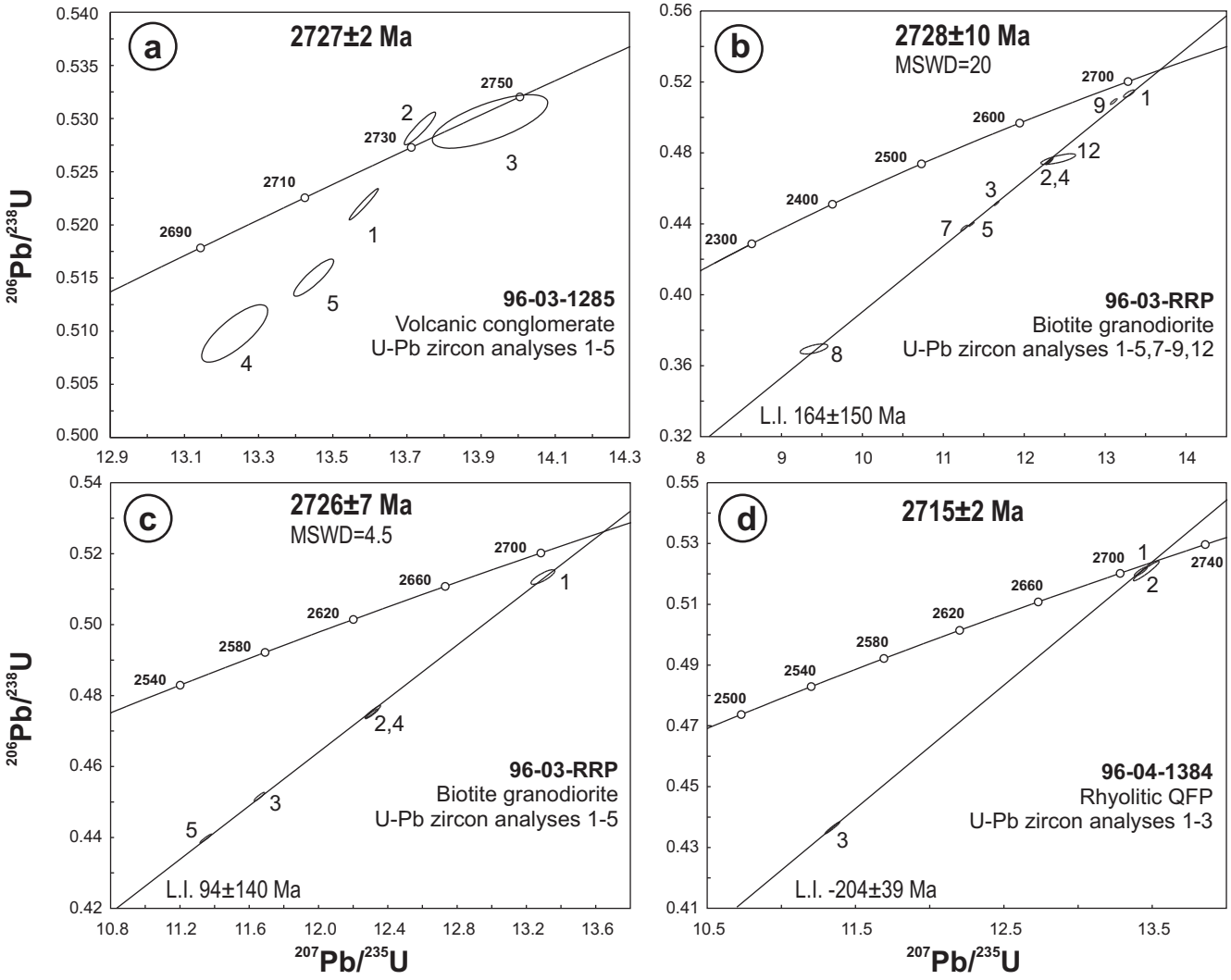

Figure 49: *U-Pb concordia diagrams for igneous zircons from felsic volcanic and plutonic rock samples in the Rice Lake area:* ***a)*** *volcanic conglomerate of the RLR unit (sample 96-03-1285, showing all data);* ***b)*** *biotite granodiorite of the Ross River pluton (sample 96-03-RRP, showing all data);* ***c)*** *sample 96-03-RRP, showing only analyses 1–5;* ***d)*** *rhyolitic quartz-feldspar porphyry (QFP) of the Round Lake (RL) unit (sample 96-04-1384, showing all data). Abbreviations: L.I., lower intercept; MSWD, mean square of weighted deviates. Refer to text for a discussion of the preferred interpretation and geological significance of the U-Pb analytical data.*

quintupled Nd:YAG laser-ablation system. Ion-counting detectors were used to measure ^{207}Pb, ^{206}Pb and ^{204}Pb, whereas U was measured on Faraday collectors. The procedures for determining the Faraday ion-counter factor and the Faraday multiplier calibration, and correcting the measured Pb isotope ratios for instrumental mass bias, are described by Simonetti et al. (2005). Common Pb corrections utilized the projected age of the zircon and the corresponding initial Pb isotopic compositions from the two-stage evolution model of Stacey and Kramers (1975). The resulting U-Pb isotopic data are listed in Table 8 and plotted as concordia diagrams (Figure 50). All errors reported in Table 8 are quoted at 1σ and were calculated by numerical propagation of all known sources of uncertainty. The concordia diagrams were generated using the Isoplot version 3.0 application of Ludwig (2003), and the error ellipses on the diagrams in Figure 50 are shown at 2σ. Figure 51 shows the same data using a combination of binned frequency histograms and probability density distribution curves, which were generated using the AgeDisplay application of Sircombe (2004). For the purposes of interpretation, the results were filtered to include only the most concordant (≥90%) and precise (1σ analytical errors ≤20 Ma) $^{207}Pb/^{206}$ ages. Table 9 summarizes the preferred interpretation and geological significance of the U-Pb zircon analyses.

Results

Sample 96-03-1285, felsic volcanic conglomerate (unit 8c)

Sample 96-03-1285 is from a well-stratified section of felsic epiclastic rocks at the top of unit 8 of the RLR unit, and was collected from an outcrop approximately 1 km south of PR 304 on the Rainy Lake logging road. The sample was collected from a crudely graded layer of matrix-supported and poorly sorted felsic volcanic conglomerate (~3.0 m thick) that is interpreted to represent a proximal, subaqueous debris-flow. The conglomerate contains mostly angular to subrounded, generally equant clasts (typically 0.2–2.0 cm across) of dark grey to buff, feldspar-phyric dacite, with subordinate clasts of porphyritic andesite, aphyric to quartz-phyric rhyolite, felsic

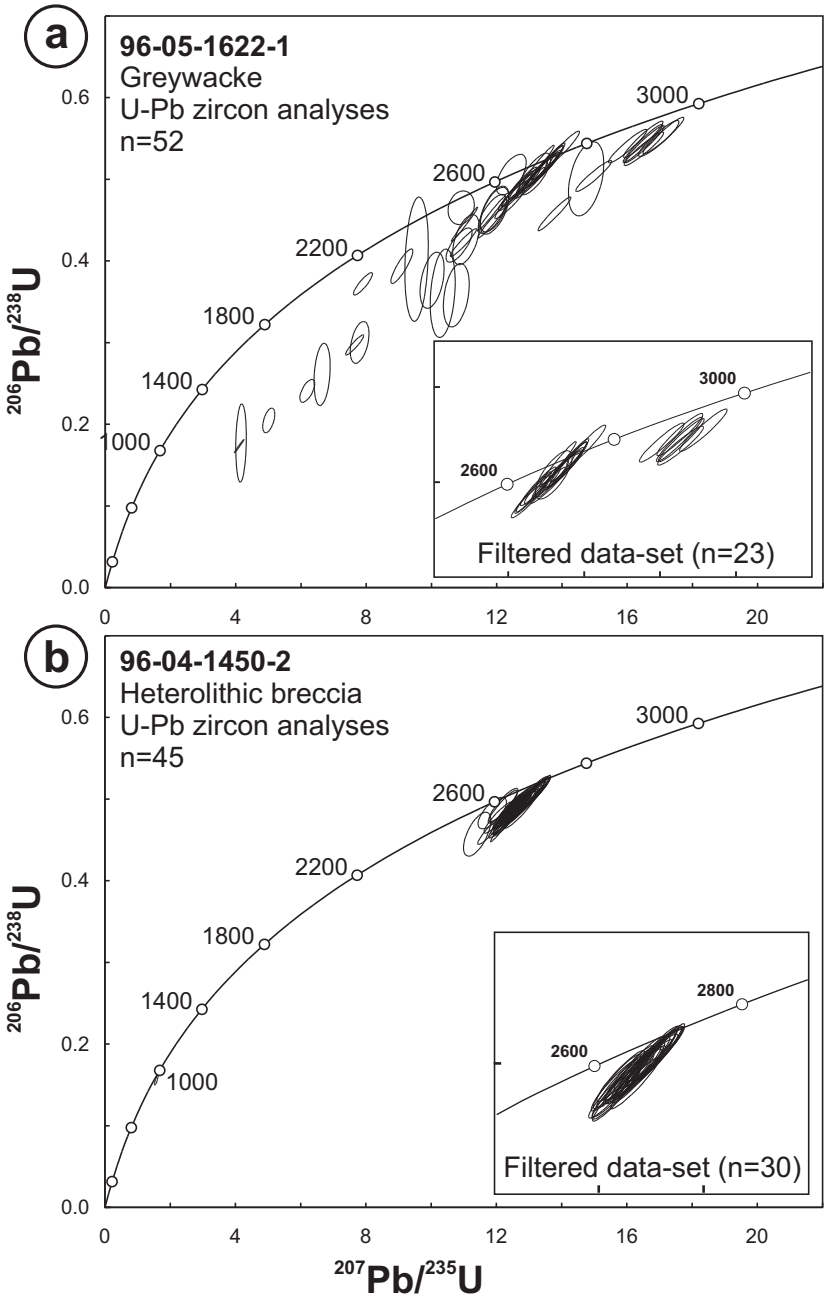

Figure 50: *U-Pb concordia diagrams for detrital zircons from siliciclastic rock samples in the Rice Lake area:* ***a)*** *feldspathic greywacke (unit 29a; sample 96-05-1622-1);* ***b)*** *heterolithic breccia (unit 12; sample 96-04-1450-2). Inset diagrams show the filtered data set for each sample (analyses ≥90% concordant, with 1σ errors ≤20 Ma). Refer to text for a discussion of the preferred interpretation and geological significance of the U-Pb analytical data.*

tuff, amygdaloidal basalt, mudstone, solid sulphide and possible collapsed pumice.

The sample yielded colourless to light pink, slender to stubby prismatic zircons. Four single zircon crystals of fairly homogeneous size (200–300 µm) and composition (48.1–79.7 ppm U; 25.7–35.7 ppm Th; 29.1–47.3 ppm Pb; Table 7), and one five-grain zircon fraction, were selected for analysis. The four single zircon crystals yielded one concordant analysis (3z) with a $^{207}Pb/^{206}Pb$ age of 2747.4 ±5.7 Ma, and one near-concordant (–0.5%) analysis with a $^{207}Pb/^{206}Pb$ age of 2727.1 ±0.8 Ma (2z; Table 7; Figure 49a). Two other single zircon crystals gave slightly discordant analyses with $^{207}Pb/^{206}Pb$ ages of 2731.3 ±0.4 Ma (1z; 1.1% discordant) and 2727.4 ±2.8 Ma (4z; 3.2% discordant), whereas the multigrain fraction (5z) gave a slightly discordant analysis (2.6%) with a $^{207}Pb/^{206}Pb$ age of 2736.8 ±1.3 Ma. The essentially identical ca. 2727 Ma $^{207}Pb/^{206}Pb$ ages of analyses 2z and 4z give a weighted-average age of 2727.1 ±1.5 Ma, which is interpreted to represent the maximum depositional age of the volcanic conglomerate. Based on the U-Pb results from sample 96-03-RRP, this age is also considered to closely approximate the age of deposition. In keeping with the heterolithic nature of the conglomerate, the slightly older $^{207}Pb/^{206}Pb$ ages (2731, 2737 and 2747 Ma) are interpreted to indicate the presence of slightly older detrital or inherited components, perhaps derived from the underlying IL unit.

Table 8: U-Pb laser-ablation, multicollector, inductively coupled plasma–mass spectrometry (LA-MC-ICP-MS) analytical data for detrital zircons from siliciclastic rock samples in the Rice Lake area. Also provided in Data Repository Item DRI2008002.

		Isotopic ratios							Age (Ma)						
Sample/analysis number	^{206}Pb (cps)	^{206}Pb/^{238}U	± (1σ)	^{207}Pb/^{235}U	± (1σ)	^{207}Pb/^{206}Pb	± (1σ)	rho	^{206}Pb/^{238}U	± (1σ)	^{207}Pb/^{235}U	± (1σ)	^{207}Pb/^{206}Pb	± (1σ)	Disc. (%)
96-05-1622-1: San Antonio assemblage, greywacke (map unit 29); UTM (NAD83, Z15) 304993mE, 5661211mN															
96-05-1622-1-1	827	0.520	0.007	13.562	0.170	0.189	0.000	0.952	2701.0	71.6	2719.6	28.0	2733.1	16.5	1.4
96-05-1622-1-2	46115	0.402	0.061	9.545	1.738	0.171	0.004	0.199	2179.3	279.6	2391.9	27.8	2572.1	46.4	18.0
96-05-1622-1-3	490	0.537	0.004	16.510	0.128	0.222	0.000	0.945	2772.4	69.8	2906.8	28.3	2998.5	16.4	9.3
96-05-1622-1-4	144	0.543	0.009	16.528	0.251	0.221	0.001	0.957	2796.0	77.2	2907.9	28.3	2985.2	16.5	7.8
96-05-1622-1-5	718	0.518	0.011	13.544	0.255	0.189	0.000	0.974	2691.2	80.5	2718.4	28.0	2731.6	16.8	1.8
96-05-1622-1-6	821	0.462	0.019	11.931	0.479	0.187	0.000	0.592	2446.3	102.6	2599.0	27.8	2719.0	16.6	12.0
96-05-1622-1-7	1288	0.464	0.018	11.931	0.475	0.187	0.000	0.609	2455.7	100.0	2599.0	27.8	2711.5	16.6	11.3
96-05-1622-1-8	2652	0.518	0.012	13.274	0.337	0.186	0.001	0.978	2689.9	82.3	2699.3	28.0	2705.1	17.2	0.7
96-05-1622-1-9	558	0.538	0.007	14.025	0.175	0.189	0.000	0.952	2773.4	72.9	2751.4	28.0	2734.5	16.5	-1.8
96-05-1622-1-10	340	0.494	0.008	12.760	0.159	0.187	0.001	0.954	2589.8	71.5	2662.1	27.9	2712.8	17.1	5.5
96-05-1622-1-11	2387	0.504	0.004	14.973	0.115	0.215	0.000	0.946	2630.9	66.3	2813.5	28.2	2943.2	16.3	12.9
96-05-1622-1-12	471	0.544	0.010	16.481	0.273	0.219	0.001	0.963	2799.9	79.5	2905.1	28.3	2972.6	16.5	7.2
96-05-1622-1-13	3608	0.445	0.011	11.015	0.274	0.179	0.000	0.990	2372.5	76.6	2524.4	27.6	2647.8	16.7	12.4
96-05-1622-1-14	681	0.486	0.007	12.602	0.173	0.189	0.000	0.956	2552.6	70.1	2650.4	27.8	2729.1	16.5	7.8
96-05-1622-1-15	49690	0.465	0.009	10.910	0.882	0.184	0.009	0.167	2462.6	73.5	2515.5	27.6	2689.9	83.8	10.2
96-05-1622-1-16	392	0.515	0.007	13.477	0.176	0.190	0.000	0.953	2676.2	72.1	2713.7	28.0	2741.2	16.7	2.9
96-05-1622-1-17	5340	0.300	0.019	7.798	0.468	0.188	0.001	0.431	1692.6	103.0	2207.9	26.7	2724.8	19.1	42.9
96-05-1622-1-18	249	0.470	0.004	12.395	0.108	0.191	0.000	0.946	2482.7	64.2	2634.8	27.8	2752.1	16.8	11.8
96-05-1622-1-19	2853	0.549	0.008	16.491	0.205	0.217	0.001	0.947	2820.9	75.2	2905.7	28.3	2960.3	17.4	5.8
96-05-1622-1-20	623	0.502	0.006	13.080	0.160	0.190	0.000	0.950	2621.2	69.5	2685.5	27.9	2739.5	16.7	5.3
96-05-1622-1-21	810	0.376	0.026	10.019	0.722	0.190	0.001	0.403	2059.0	130.5	2436.6	27.4	2741.9	17.4	29.0
96-05-1622-1-22	785	0.448	0.010	11.862	0.231	0.192	0.001	0.972	2387.8	73.0	2593.6	27.7	2756.5	17.0	16.0
96-05-1622-1-23	840	0.496	0.004	13.022	0.128	0.191	0.000	0.946	2594.8	66.6	2681.3	27.9	2747.0	16.7	6.7
96-05-1622-1-24	709	0.458	0.011	11.841	0.277	0.187	0.000	0.987	2431.2	77.6	2591.9	27.7	2717.6	16.8	12.6
96-05-1622-1-25	8088	0.177	0.039	4.162	1.108	0.160	0.006	0.142	1051.1	210.6	1666.5	25.4	2460.3	63.9	61.9
96-05-1622-1-26	852	0.458	0.014	11.868	0.351	0.188	0.000	0.706	2429.2	85.5	2594.1	27.7	2722.6	16.7	12.9
96-05-1622-1-27	1366	0.422	0.006	10.977	0.155	0.188	0.000	0.952	2271.5	63.0	2521.1	27.5	2725.9	16.8	19.7
96-05-1622-1-28	635	0.489	0.009	12.645	0.231	0.187	0.000	0.967	2565.2	74.8	2653.6	27.9	2719.0	16.6	6.8
96-05-1622-1-29	6181	0.372	0.001	7.901	0.079	0.154	0.002	0.878	2038.6	52.5	2219.8	26.7	2386.9	25.3	17.0
96-05-1622-1-30	1127	0.507	0.014	13.171	0.336	0.189	0.001	0.735	2641.9	87.9	2692.0	27.9	2731.6	17.2	4.0
96-05-1622-1-31	1598	0.513	0.005	13.433	0.173	0.190	0.001	0.945	2669.2	69.2	2710.6	28.0	2744.4	17.1	3.3
96-05-1622-1-32	559	0.511	0.006	13.400	0.148	0.190	0.000	0.950	2660.4	70.4	2708.2	28.0	2738.9	16.7	3.5
96-05-1622-1-33	940	0.501	0.034	14.741	1.019	0.213	0.001	0.406	2616.5	157.4	2798.6	28.2	2930.6	16.9	13.0
96-05-1622-1-34	1029	0.541	0.004	16.016	0.111	0.214	0.000	0.945	2786.1	69.8	2877.8	28.3	2937.8	16.4	6.4
96-05-1622-1-35	3140	0.522	0.010	13.595	0.256	0.189	0.000	0.969	2706.8	78.9	2721.9	28.0	2731.3	16.6	1.1
96-05-1622-1-36	860	0.495	0.005	12.870	0.110	0.188	0.001	0.942	2592.9	67.3	2670.2	27.9	2727.3	17.5	6.0
96-05-1622-1-37	2064	0.360	0.043	10.345	1.312	0.208	0.001	0.247	1984.1	206.4	2466.1	27.7	2889.9	19.1	36.3
96-05-1622-1-38	2997	0.480	0.004	12.506	0.104	0.189	0.000	0.945	2526.3	64.9	2643.2	27.8	2731.7	16.8	9.1
96-05-1622-1-39	7199	0.297	0.005	7.645	0.143	0.187	0.002	0.929	1677.0	50.3	2190.1	26.6	2715.0	21.1	43.3
96-05-1622-1-40	1252	0.458	0.010	13.770	0.378	0.217	0.001	0.962	2429.2	74.4	2734.0	28.0	2959.6	18.5	21.5
96-05-1622-1-41	637	0.506	0.011	13.250	0.291	0.190	0.000	0.977	2640.9	80.0	2697.6	27.9	2738.8	16.6	4.4
96-05-1622-1-42	5681	0.241	0.009	6.193	0.235	0.186	0.001	0.629	1391.4	59.5	2003.4	25.9	2708.5	17.5	53.9
96-05-1622-1-43	1052	0.554	0.008	17.113	0.248	0.223	0.001	0.951	2840.0	75.4	2941.2	28.4	3005.5	16.6	6.8
96-05-1622-1-44	8365	0.506	0.013	12.448	0.660	0.175	0.005	0.609	2638.5	86.2	2638.8	27.8	2608.1	53.8	-1.4
96-05-1622-1-45	40510	0.394	0.013	9.094	0.508	0.168	0.004	0.868	2139.6	79.3	2347.5	27.1	2532.8	38.9	18.2
96-05-1622-1-46	4090	0.205	0.011	5.012	0.238	0.179	0.002	0.502	1200.4	65.3	1821.3	25.1	2645.8	22.1	59.7
96-05-1622-1-47	2866	0.426	0.022	11.057	0.549	0.188	0.000	0.512	2287.4	112.2	2527.9	27.6	2726.3	17.0	19.1
96-05-1622-1-48	4305	0.358	0.030	10.759	0.805	0.222	0.003	0.340	1973.1	148.9	2502.6	27.6	2994.5	25.0	39.4
96-05-1622-1-49	14513	0.261	0.030	6.647	0.727	0.185	0.003	0.254	1495.3	157.3	2065.6	26.4	2699.5	30.7	49.8

Table 8: U-Pb laser-ablation, multicollector, inductively coupled plasma–mass spectrometry (LA-MC-ICP-MS) analytical data for detrital zircons from siliciclastic rock samples in the Rice Lake area. Also provided in Data Repository Item DRI2008002. *(continued)*

		Isotopic ratios							Age (Ma)						
Sample/analysis number	^{206}Pb (cps)	^{206}Pb/^{238}U	± (1σ)	^{207}Pb/^{235}U	± (1σ)	^{207}Pb/^{206}Pb	± (1σ)	rho	^{206}Pb/^{238}U	± (1σ)	^{207}Pb/^{235}U	± (1σ)	^{207}Pb/^{206}Pb	± (1σ)	Disc. (%)
96-05-1622-1-50	11947	0.173	0.004	4.105	0.105	0.172	0.000	0.990	1029.8	37.0	1655.3	24.2	2575.3	17.0	64.7
96-05-1622-1-51	2623	0.550	0.007	16.970	0.183	0.224	0.002	0.920	2825.4	74.6	2933.1	28.4	3006.9	20.7	7.5
96-05-1622-1-52	1578	0.419	0.012	10.846	0.326	0.187	0.001	0.736	2258.0	77.3	2510.1	27.5	2719.9	17.6	20.1
96-04-1450-2: Heterolithic breccia (map unit 12); UTM (NAD83, Z15) 314678mE, 5654168mN															
96-04-1450-2-1	157161	0.476	0.007	12.346	0.125	0.188	0.001	0.935	2508.8	69.0	2631.1	27.8	2726.4	19.6	9.6
96-04-1450-2-2	80850	0.490	0.006	12.562	0.129	0.186	0.002	0.917	2571.3	68.2	2647.4	27.8	2710.8	21.2	6.2
96-04-1450-2-3	129507	0.500	0.007	12.972	0.176	0.187	0.001	0.926	2613.2	71.4	2677.6	27.9	2720.0	20.9	4.8
96-04-1450-2-4	190872	0.477	0.006	12.350	0.135	0.187	0.001	0.941	2513.7	67.1	2631.4	27.8	2720.3	18.1	9.2
96-04-1450-2-5	100607	0.482	0.007	12.331	0.167	0.186	0.001	0.937	2537.0	69.5	2630.0	27.8	2706.2	19.3	7.6
96-04-1450-2-6	57651	0.483	0.006	11.872	0.221	0.181	0.004	0.692	2539.7	68.1	2594.4	27.7	2658.4	40.9	5.4
96-04-1450-2-7	123027	0.473	0.009	12.212	0.186	0.187	0.001	0.945	2497.2	74.0	2620.8	27.8	2717.2	20.5	9.8
96-04-1450-2-8	199169	0.500	0.006	12.909	0.109	0.188	0.001	0.937	2613.0	69.5	2673.1	27.9	2723.1	18.8	4.9
96-04-1450-2-9	170787	0.487	0.005	12.580	0.096	0.187	0.001	0.931	2559.5	67.3	2648.8	27.8	2719.3	19.3	7.1
96-04-1450-2-10	248830	0.493	0.006	12.831	0.141	0.189	0.001	0.946	2584.0	68.0	2667.3	27.9	2731.6	17.1	6.6
96-04-1450-2-11	114008	0.464	0.007	11.865	0.133	0.186	0.001	0.939	2456.3	69.2	2593.8	27.7	2702.9	19.5	11.0
96-04-1450-2-12	267975	0.484	0.007	12.719	0.140	0.190	0.001	0.949	2544.3	69.3	2659.1	27.9	2743.5	17.3	8.8
96-04-1450-2-13	154125	0.476	0.006	12.283	0.122	0.187	0.001	0.941	2511.0	67.4	2626.3	27.8	2717.0	18.3	9.1
96-04-1450-2-14	275114	0.475	0.008	12.360	0.150	0.189	0.001	0.951	2504.0	70.7	2632.1	27.8	2730.2	17.9	10.0
96-04-1450-2-15	85894	0.477	0.006	12.064	0.122	0.184	0.002	0.915	2515.8	67.8	2609.4	27.8	2688.3	21.8	7.7
96-04-1450-2-16	109418	0.489	0.006	12.442	0.132	0.186	0.001	0.934	2567.0	68.5	2638.4	27.8	2705.8	19.1	6.2
96-04-1450-2-17	100135	0.490	0.006	12.726	0.091	0.188	0.002	0.908	2572.7	68.6	2659.6	27.9	2724.9	22.5	6.8
96-04-1450-2-18	151734	0.486	0.006	12.489	0.106	0.186	0.003	0.855	2552.8	68.8	2641.9	27.8	2706.2	28.2	6.9
96-04-1450-2-19	93601	0.488	0.006	12.616	0.120	0.188	0.001	0.933	2560.4	68.9	2651.4	27.8	2722.6	19.5	7.2
96-04-1450-2-20	89644	0.485	0.009	12.372	0.154	0.184	0.001	0.939	2549.6	72.8	2633.0	27.8	2691.2	20.2	6.4
96-04-1450-2-21	167524	0.495	0.007	12.816	0.138	0.188	0.001	0.944	2591.4	70.9	2666.2	27.9	2724.5	18.4	5.9
96-04-1450-2-22	423558	0.504	0.009	13.136	0.215	0.190	0.000	0.959	2630.4	73.9	2689.5	27.9	2738.5	16.9	4.8
96-04-1450-2-23	132373	0.503	0.008	13.036	0.128	0.188	0.001	0.946	2627.8	73.8	2682.2	27.9	2725.6	18.9	4.4
96-04-1450-2-24	202517	0.502	0.008	13.005	0.159	0.188	0.001	0.951	2621.9	72.1	2680.0	27.9	2722.9	17.5	4.5
96-04-1450-2-25	184761	0.502	0.009	13.014	0.192	0.188	0.002	0.928	2622.0	74.1	2680.7	27.9	2722.8	21.5	4.5
96-04-1450-2-26	259852	0.508	0.009	13.183	0.198	0.188	0.001	0.956	2645.9	75.5	2692.8	27.9	2726.3	17.8	3.6
96-04-1450-2-27	262997	0.507	0.008	13.135	0.171	0.188	0.001	0.947	2642.9	72.2	2689.4	27.9	2725.6	18.0	3.7
96-04-1450-2-28	248545	0.506	0.008	13.148	0.164	0.188	0.001	0.952	2637.5	73.5	2690.4	27.9	2725.0	17.8	3.9
96-04-1450-2-29	199018	0.492	0.008	12.610	0.236	0.187	0.001	0.945	2578.5	72.6	2651.0	27.8	2712.4	19.0	6.0
96-04-1450-2-30	247300	0.457	0.017	11.411	0.483	0.180	0.001	0.626	2426.2	96.4	2557.3	27.7	2655.5	18.4	10.3
96-04-1450-2-31	182032	0.492	0.006	12.745	0.132	0.188	0.001	0.947	2580.9	68.9	2661.0	27.9	2723.1	17.4	6.3
96-04-1450-2-32	69414	0.493	0.008	12.216	0.175	0.180	0.002	0.880	2582.8	71.6	2621.2	27.8	2655.5	26.7	3.3
96-04-1450-2-33	218764	0.490	0.008	12.604	0.165	0.187	0.001	0.953	2571.7	71.6	2650.5	27.8	2720.2	17.3	6.6
96-04-1450-2-34	251888	0.497	0.007	12.946	0.173	0.189	0.001	0.951	2599.8	71.1	2675.7	27.9	2733.5	17.2	5.9
96-04-1450-2-35	301332	0.502	0.004	13.053	0.085	0.189	0.001	0.938	2623.1	66.6	2683.5	27.9	2731.9	17.7	4.8
96-04-1450-2-36	103343	0.494	0.008	12.666	0.158	0.186	0.002	0.921	2589.8	72.2	2655.1	27.9	2706.6	21.9	5.2
96-04-1450-2-37	293106	0.507	0.007	13.176	0.171	0.188	0.001	0.949	2642.9	70.5	2692.3	27.9	2728.0	17.0	3.8
96-04-1450-2-38	125420	0.485	0.007	12.444	0.181	0.186	0.001	0.939	2549.0	69.7	2638.5	27.8	2711.4	19.0	7.2
96-04-1450-2-39	163354	0.499	0.008	12.782	0.170	0.186	0.001	0.951	2607.3	72.2	2663.7	27.9	2710.3	17.7	4.6
96-04-1450-2-40	223728	0.492	0.007	12.792	0.149	0.188	0.001	0.951	2577.4	70.7	2664.4	27.9	2728.0	17.3	6.7
96-04-1450-2-41	103376	0.491	0.008	12.194	0.176	0.181	0.002	0.923	2574.0	71.3	2619.5	27.8	2663.6	21.7	4.1
96-04-1450-2-42	223806	0.506	0.008	13.068	0.174	0.187	0.001	0.950	2640.7	72.9	2684.6	27.9	2719.2	17.7	3.5
96-04-1450-2-43	121237	0.156	0.002	1.575	0.020	0.074	0.001	0.855	933.9	28.5	960.5	18.5	1033.8	34.7	10.4
96-04-1450-2-44	178335	0.489	0.008	12.757	0.156	0.188	0.001	0.949	2568.4	72.1	2661.9	27.9	2724.9	18.3	7.0
96-04-1450-2-45	302978	0.470	0.012	12.266	0.259	0.189	0.001	0.985	2483.8	80.2	2625.0	27.8	2734.6	17.9	11.0

Uncertainties reported at 1σ (absolute) and are calculated by numerical propagation of all known sources of error

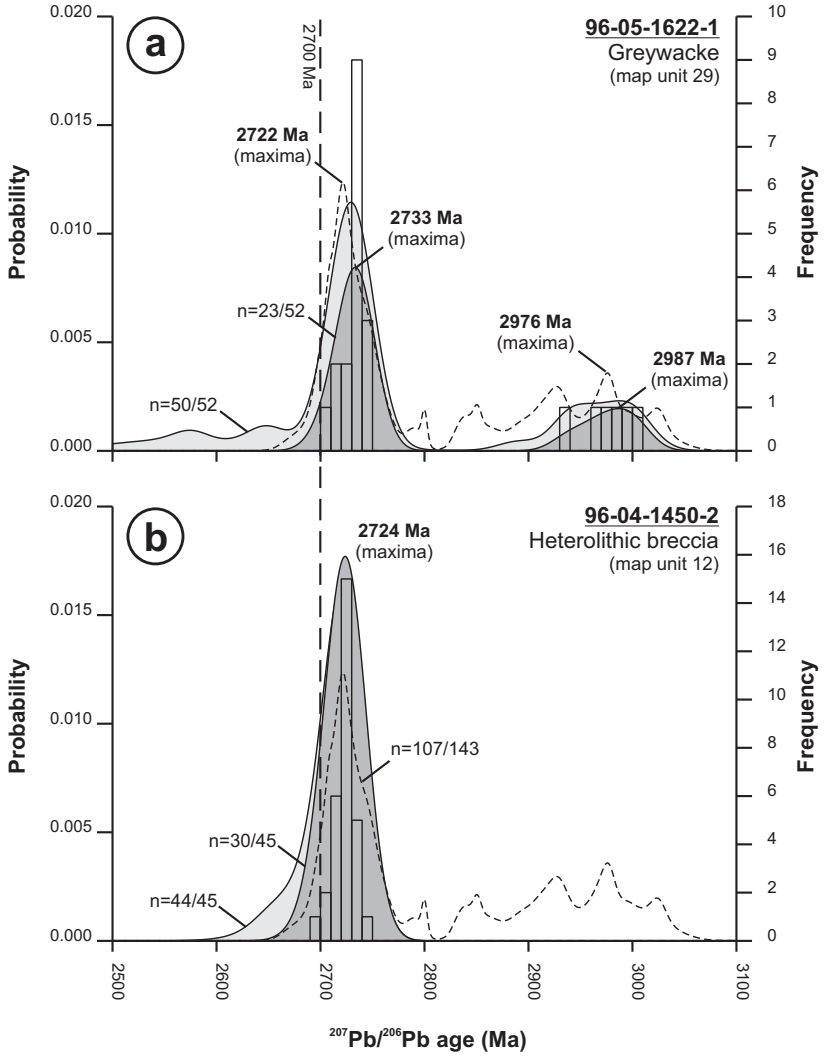

Figure 51: *Combined frequency histograms and probability density distribution (PDD) curves of $^{207}Pb/^{206}Pb$ ages (Ma) for detrital zircons from siliciclastic rock samples in the Rice Lake area:* ***a)*** *sample 96-05-1622-1 (n = 52);* ***b)*** *sample 96-04-1450-2 (n = 45). Light shaded curve indicates PDD for the unfiltered data sets, excluding outlier analyses ($^{207}Pb/^{206}Pb$ ages <2500 Ma). Dark shaded curve indicates PDD for the filtered data sets (analyses ≥90% concordant, with 1σ errors ≤20 Ma). Dashed line shows PDD curve of sensitive high-resolution ion microprobe (SHRIMP) $^{207}Pb/^{206}Pb$ ages for detrital zircons in arkose samples from the Guano Island, Hole River and San Antonio assemblages (data* from *Percival et al., 2006a; filtered to include only those analyses ≥95% concordant, with 1σ errors ≤20 Ma). Bin width on the histograms is 10 Ma. See text for discussion.*

Table 9: Summary of the preferred interpretation and geological significance of the U-Pb zircon analyses from the Rice Lake area.

Sample	Easting (Zone 15, NAD 83)	Northing	Rock type	Assemblage	Lithostratigraphic unit	Preferred interpretation	Geological significance
U-Pb ID-TIMS:							
96-03-1285	319690	5655510	Volcanic pebble conglomerate	Bidou	RLR (unit 8c)	<2727±2 Ma	Max. depositional
96-03-RRP	320712	5647567	Biotite granodiorite	Bidou	RRPS (unit 11a)	2724±1 Ma	Crystallization
96-04-1384	312102	5657942	Rhyolitic quartz-feldspar porphyry	Bidou	RL (unit 21)	2715±2 Ma	Crystallization
U-Pb LA-MC-ICP-MS:							
96-04-1450-2	314678	5654168	Heterolithic breccia	Bidou	TS (unit 12)	<2723 Ma	Max. emplacement
96-05-1622-1	304993	5661211	Greywacke	San Antonio	(unit 29a)	<2732 Ma	Max. depositional

Abbreviations: ID-TIMS, isotope dilution–thermal ionization mass spectrometry; LA-MC-ICP-MS, laser-ablation, multicollector inductively coupled plasma–mass spectrometry; RL, Round Lake unit; RLR, Rainy Lake road unit; RRPS, Ross River plutonic suite; TS, Townsite unit.

Sample 96-03-RRP, biotite granodiorite (unit 11a)

Sample 96-03-RRP is from a massive and homogeneous outcrop of biotite granodiorite along the Rainy Lake logging road in the central portion of the Ross River pluton (~10 km south along the road from PR 304). The granodiorite weathers pale pink-white and is light pinkish grey on fresh surfaces, with a medium-grained, equigranular to sparsely porphyritic texture. The principal minerals are plagioclase (45–60%), quartz (25–35%), K-feldspar (10–15%) and biotite (5–10%). Biotite forms rare, euhedral to subhedral, locally hexagonal phenocrysts that are 5–10 mm across and, in thin section, are observed to contain delicate lattices of rutile needles. Other accessory minerals include zircon, apatite, titanite and pyrite. Alteration is evidenced by weak to moderate saussuritization of feldspar and minor replacement of biotite by epidote and chlorite. In this location, the granodiorite lacks xenoliths, crosscutting veins or dikes, and mesoscopic deformation fabrics.

The sample contained colourless to light pink zircons, which included slender to stubby prismatic grains and equant euhedral grains. The results from the analysis of four single zircon crystals and five multigrain zircon fractions are presented in Table 7 and shown as concordia diagrams in Figure 49b (not included are analyses 6z, 10z and 11z, which failed in the analysis stage or produced spurious results). Analyses 1z through 8z gave results of generally increasing discordance (2.3–28.8%), which prompted the selection of two additional single zircon crystals (9z and 12z) for processing using the thermal annealing–chemical abrasion (TA-CA) method of Mattinson (2005) in an attempt to produce less discordant data. As shown in Figure 49b, a linear regression of the entire data set has a poorly defined upper intercept of 2728 ±10 Ma (MSWD = 20), which is essentially identical to the 2728 ±8 Ma age reported for the Ross River pluton by Turek et al. (1989). One of the TA-CA analyses (z9) yielded a slightly discordant (2.8%) $^{207}Pb/^{206}Pb$ age of 2713.8 ±1.1 Ma that plots significantly off the regression line shown in Figure 49b, possibly as a consequence of ancient Pb loss from domains that were not removed during the TA-CA process. A linear regression that excludes this analysis defines a slightly older upper intercept age of 2733 ±9 Ma (MSWD = 5.1). A slightly better constrained, though essentially identical, upper intercept of 2726 ±7 Ma (MSWD = 4.5) is defined by a linear regression of analyses 1z–5z, all of which were processed using conventional techniques (Figure 49c). Of these analyses, the three least-discordant analyses were obtained from two single zircon crystals (1z, 2z) and one three-grain zircon fraction (4z), and returned overlapping $^{207}Pb/^{206}Pb$ ages of 2723.1 ±2.0 Ma (2.3% discordant), 2724.6 ±0.7 Ma (9.7% discordant) and 2723.3 ±0.8 Ma (9.6% discordant), respectively. A weighted average of these $^{207}Pb/^{206}Pb$ ages yields a date of 2724 ±1 Ma (MSWD = 0.85; probability of fit = 0.43), which is considered to be the best estimate of the age of crystallization of the biotite granodiorite.

Sample 96-04-1384, rhyolitic quartz-feldspar porphyry (QFP; unit 21)

Sample 96-04-1384 is from the discordant body of quartz-feldspar porphyry near the top of the RL unit, which is interpreted to represent a very high level hypabyssal intrusion. The sample was collected from a massive and homogeneous outcrop along the Vanson mine road, approximately 2.0 km northeast of PR 304. The porphyry weathers buff or light grey and exhibits a seriate porphyritic texture defined by phenocrysts of feldspar, quartz and rare hornblende (<10 mm) in an aphanitic to very fine grained matrix of feldspar, quartz, sericite and carbonate. The quartz phenocrysts are slightly blue-grey and include abundant examples of delicate, magmatically embayed crystals.

The sample contained pale pink to tan, stubby prismatic crystals of uniform size (150–200 μm), from which three multigrain fractions of 2–4 zircons each were selected for analysis. Fractions 1z and 2z gave near-concordant analyses (0.6 and 0.7% discordant) with $^{207}Pb/^{206}Pb$ ages of 2715.4 ±1.1 Ma and 2719.4 ±1.3 Ma, respectively, whereas fraction 3z was significantly more discordant (17.2%), with a $^{207}Pb/^{206}Pb$ age of 2729.2 ±1.0 Ma (Table 7; Figure 49d). A reference line through the younger near-concordant analysis (1z) and analysis 3z gives an upper intercept age of 2715 ±2 Ma, with an essentially zero lower intercept (–204 ±39 Ma), which is considered the best estimate of the age of emplacement of the quartz-feldspar porphyry.

Sample 96-05-1622-1, greywacke (unit 29a)

Sample 96-05-1622-1 consists of feldspathic greywacke from the fault-bounded panel of the San Antonio assemblage along the trace of the Wanipigow Shear Zone. The sample was collected from a poorly graded, 30 cm thick bed in a section of rhythmically interbedded greywacke and mudstone turbidites that forms a large outcrop at Silver Falls on the Wanipigow River. The sampled greywacke is medium to very coarse grained and composed of angular to subrounded quartz, feldspar and lithic grains in a sericitic mudstone matrix. Abundant granules composed of blue quartz or coarse-grained aggregates of quartz and feldspar suggest a mainly plutonic source area.

The sample contained zircons of variable size and morphology. Most grains are equant to slightly tabular and euhedral to subhedral. The sample also contained significant populations of relatively small, slender to stubby, euhedral prismatic grains and considerably larger, stubby euhedral prisms. The $^{207}Pb/^{206}Pb$ ages of 52 analyses from 46 zircon grains range from 2387 to 3007 Ma. There does not appear to be any systematic variation between morphology and $^{207}Pb/^{206}Pb$ age. Anomalously young $^{207}Pb/^{206}Pb$ ages (2387–2690 Ma) obtained from nine analyses tend to exhibit higher uncertainties and/or significant discordance. When filtered to exclude those analyses with higher analytical errors (1σ >20 Ma) and/or significant discordance (>10%), the $^{207}Pb/^{206}Pb$ ages define two distinct clusters at 2705–2747 Ma (n = 17) and 2938–3006 Ma (n = 6). The younger cluster of filtered $^{207}Pb/^{206}Pb$ ages defines a unimodal population, the weighted-average age of which is 2731.7 ± 8.0 Ma (MSWD = 0.41; probability of fit = 0.98).

Sample 96-04-1450-2, heterolithic breccia (unit 12)

Sample 96-04-1450-2 consists of matrix material from the dike-like body of heterolithic breccia that discordantly cuts stratified intermediate flows and volcaniclastic rocks in the upper portion of the IL unit (map unit 6), and is interpreted to represent a clastic dike. The sample was collected from the only locality of this rock type, on the north bank of Papineau Creek approximately 750 m east of Rice Lake. The breccia is

unsorted and predominantly matrix supported, and contains a chaotic assortment of very angular to subangular lithic fragments that range in size up to 4.0 m but are typically less than 20 cm in maximum dimension. The matrix material consists of hematitic, fine- to coarse-grained pebbly sandstone, composed of very angular to subrounded feldspar, quartz and lithic grains in a chloritic mudstone matrix. The sampled material contained less than 10% lithic fragments.

The sample contained zircons of variable size and morphology. Most grains are euhedral to subhedral and equant to slightly tabular. The subhedral grains have rounded terminations suggestive of detrital reworking. Also present are a significant population of anhedral subrounded grains and relatively pristine, slender to stubby, euhedral prismatic grains. The $^{207}Pb/^{206}Pb$ ages of 45 analyses from 41 zircon grains range from 2656 to 2744 Ma, with a single near-concordant outlier analysis of uncertain significance at 1034 Ma. When filtered to exclude the outlier analysis and those analyses with higher analytical errors (1σ >20 Ma) and/or significant discordance (>10%), the age range narrows to 2691–2744 Ma (n = 30). The filtered $^{207}Pb/^{206}Pb$ ages define a unimodal population, the weighted-average age of which is 2723 ±7 Ma (MSWD = 0.31; probability of fit = 1.0).

Interpretation of the U-Pb age data

Analyses of zircon from the felsic volcanic conglomerate layer near the top of the medial epiclastic section of the Rainy Lake road (RLR) unit (sample 96-03-1285) indicate a maximum age of 2727 ±2 Ma for the final increments of basin infilling and the associated extrusion of voluminous flows of MORB-like tholeiitic basalt. Slightly older (ca. 2731–2747 Ma) zircons in this sample are in accord with the heterolithic clast population and were most likely sourced from the Independence Lake (IL) unit, either down-section or from the footwall of the synvolcanic subsidence structure located to the west along strike. The epiclastic section of the RLR unit is cut by spherulitic granodiorite dikes and, to the west, is truncated by the northwestern apophysis of the Ross River pluton, which is interpreted to be controlled by a subsidence structure. Igneous zircon from the biotite granodiorite sample (96-03-RRP) collected from the central portion of the pluton indicates a best-estimate emplacement age of 2724 ±1 Ma; this age also indicates a ca. 2724 Ma minimum age for the RLR unit, which is intruded to the west and south by the Ross River pluton. Within the limits of the analytical error, this age overlaps the 2728 ±8 Ma age reported by Turek et al. (1989) for the Ross River pluton.

Igneous zircons from the rhyolitic quartz-feldspar porphyry near the top of the Round Lake (RL) unit (sample 96-04-1384) yielded a best-estimate emplacement age of 2715 ±2 Ma, which represents the youngest volcanic rock type identified to date in the Rice Lake belt. This age is identical to the 2715 ±10 Ma ages reported by Krogh et al. (1974) for quartz diorite and granodiorite in the western portion of the belt at Lake Winnipeg, which appear to approximate the waning stages of volcanic-arc magmatism in the Bidou assemblage.

In keeping with the results of previous studies of detrital zircon populations in the fluvial-alluvial and turbiditic siliciclastic successions that unconformably overlie the Bidou assemblage in the Rice Lake belt (e.g., Davis, 1996; Percival et al., 2006a; Anderson, unpublished data, 2006), detrital zircons in the sample of greywacke from Silver Falls on the Manigotagan River (sample 96-05-1622-1) define two distinct age clusters at 2705–2747 Ma and 2938–3006 Ma. The younger cluster has a weighted-average age of 2732 ±8 Ma, which is a conservative estimate for the maximum depositional age of the greywacke. The maximum depositional age of the San Antonio assemblage as a whole is better constrained by the 2715 ±2 Ma age obtained from the quartz-feldspar porphyry in the RL unit, which is truncated at the basal unconformity. Percival et al. (2006a) reported a 2705 ±5 Ma age for the youngest detrital zircon grain obtained from a sample of arkose near the base of the San Antonio assemblage, north of Red Rice Lake. This age, which is based on six sensitive high-resolution ion microprobe (SHRIMP) analyses of the grain, is considered the best estimate of the maximum depositional age of the assemblage.

Detrital zircons from the texturally immature, quartz-rich, sandstone matrix of the clastic dike in the upper portion of the IL unit form a unimodal population with a weighted-average age of 2723 ±7 Ma (sample 96-04-1450-2). Although potential sources of the matrix sand are found nearby at the base of the Townsite (TS) unit (unit 12) and the San Antonio assemblage (unit 27 or 28), the unimodal aspect of zircon population indicates the former as the most likely source. As noted above, fluvial-alluvial sandstone of the San Antonio assemblage, and its equivalents elsewhere in the Rice Lake belt, is invariably characterized by multimodal zircon populations that include significant numbers of ca. 2.9–3.0 Ga detrital zircons. The base of the TS unit is interpreted to be composed of proximal to medial outwash deposits in a subaerial to shallow-marine fan, As such, it would presumably be highly susceptible to fluid overpressuring and sediment fluidization, given the potential combination of coarse, water-saturated sand and an active extensional tectonic regime.

Very angular to subrounded fragments of sericitic and quartzofeldspathic phyllite in the clastic dike provide evidence of pre-entrainment alteration and ductile deformation, and indicate the nearby presence of exhumed rocks, which were either subaerially exposed during the initial depositional stages of the TS unit or were in a near-surface setting (and were sampled) by the clastic dike during emplacement; the unimodal (ca. 2723 Ma) zircon population implicates exhumed volcanic-arc rocks. As described by Bruhn et al. (1994), phyllic (i.e., sericitic) mineral assemblages and phyllite are observed in the deeper parts of normal faults, where they form as a consequence of high heat flow and hydrothermal circulation during active displacement. In such systems, continued displacement on the controlling faults, coupled with active erosional denudation, may result in rapid exhumation of phyllic footwall rocks. A similar mechanism is envisaged for the Rice Lake area, where exhumed rocks in the immediate footwall of the synvolcanic subsidence structure east of Rice Lake are considered the most likely source of the phyllite fragments. These fragments were likely transported via erosion into the basal portion of the TS unit and subsequently mobilized into the clastic dike via fluidization. Due to such factors as differential uplift and erosion along the strike of the subsidence structure, it is possible that the exhumed source of the fragments is not present at the current level of exposure.

As noted previously, the felsic volcanic sandstone and conglomerate in the TS unit are equivalent to the 'Hares Island formation' of Poulsen et al. (1996), the type locality of which is Hares Island on Rice Lake. It is from this locality that Turek et al. (1989) obtained a U-Pb zircon age of 2729 ± 3 Ma from a sample described simply as 'rhyolite', with no indication of its field relationship or genesis. Although the same sample was described by Poulsen et al. (1996) as consisting of a single subrounded clast of feldspar and quartz-phyric felsic volcanic rock in a volcanic conglomerate, this description appears to be at odds with the weight of the sample (approximately 50 kg; Turek et al., 1989), given that the maximum clast diameter observed on the island is approximately 10 cm (Tirschmann, 1986; Poulsen et al., 1996; this study). As opposed to rhyolite *sensu stricto,* or a single rhyolite clast, it therefore appears likely that this sample consisted of an epiclastic aggregate. As reported by Turek et al. (1989), two near-concordant zircon fractions from this sample gave $^{207}Pb/^{206}Pb$ ages of 2727 and 2729 Ma, whereas one additional, more discordant fraction gave a $^{207}Pb/^{206}Pb$ age of 2723 Ma. A regression line through all three analyses gave an upper intercept age of 2729 ±3 Ma, which is herein conservatively taken to indicate a maximum depositional age. It is perhaps noteworthy that the younger $^{207}Pb/^{206}Pb$ age is identical to the ca. 2723 Ma weighted-average age obtained from zircons in the clastic dike. Moreover, both of these ages are also nearly identical to the 2724 ±1 Ma best-estimate age of the granodiorite sample from the core of the Ross River pluton, which lends support to the inference, from field relationships, that the epiclastic succession at the base of the TS unit records exhumation of the Ross River plutonic suite, or age-equivalent rocks.

The results of the U-Pb zircon dating reported here, coupled with published U-Pb ages (*see* compilation by Bailes et al., 2003), indicate that mafic and felsic magmatism in the central portion of the Rice Lake belt occurred mainly in the ca. 2747–2715 Ma time interval, and thus closely corresponds to the ca. 2.75–2.72 Ga time period documented elsewhere for continental-arc magmatism in the Uchi Subprovince (e.g., Sanborn-Barrie et al., 2001).

Structural geology

In order to gain a better understanding of the structural evolution of the north-central portion of the Rice Lake belt, deformation structures throughout the Rice Lake area were examined in detail. In the field, emphasis was placed on reconstructing the sequence of deformations through the careful examination of overprinting relationships between various generations of mesoscopic deformation fabric. In the laboratory, these data were augmented by petrographic and microstructural examinations of oriented thin-sections.

Deformation structures

Ductile and ductile-brittle deformation structures in the Rice Lake area are subdivided into six generations (G_1–G_6; Table 10) on the basis of overprinting relationships. In areas of poor exposure, the style of deformation structures and their patterns of orientation were also used for correlation. The observed structures include planar fabrics (e.g., foliations, cleavages, shear bands, flattened clasts), linear fabrics (e.g., mineral, stretching, slickenline and intersection lineations) and/or folds, which are denoted in the text and figures by S_x, L_x and F_x, respectively, where 'X' indicates the assigned generation. Intersection lineations are denoted by L^X_Y, where 'X' and 'Y' refer to the generations of intersecting planar fabrics. In any given outcrop, the mesoscopic deformation structure is usually dominated by three distinct generations of planar fabric, which are assigned to the G_3, G_4 and G_5 generations (hence, S_3, S_4 and S_5). Poulsen et al. (1986) described these fabrics as the first, second and third foliations. Figure 52 provides two representative examples of these fabrics and illustrates their overprinting relationships, which are consistent throughout the

Table 10: Summary of ductile and ductile-brittle deformation in the Rice Lake area.

Generation	Shortening direction[1]	Mesoscopic structure	Macroscopic structure	Deformation episode and inferred tectonic significance
G_1	?	Penetrative to finely spaced S_1 foliation in phyllite fragments in clastic dikes	Synvolcanic subsidence structures (normal faults)	D_1 : arc extension; initiation of back-arc spreading?
	?	None observed	Early tilting of the Bidou assemblage	D_2 : arc accretion and back-arc basin inversion?
G_2	?	Local, weak, layer-parallel S_2 foliation in San Antonio assemblage	Thrust fault at top of San Antonio assemblage	D_3 : basin inversion; continued accretion and/or initial crustal thickening
G_3	NNE-SSW	Regional WNW-trending S_3; steep L_3 stretching lineation; upright F_3 folds	Macroscopic folds (HLA, GCS); sinistral-reverse shear in WSZ	D_4 : collisional tectonics; crustal thickening
G_4	NW-SE	Regional, WSW-trending, S_4 crenulation cleavage; F_4 Z-folds		Early D_5 : onset of terminal collision; dextral transpression
G_5	NNW-SSE	Regional S_5 shear-band cleavage; mylonitic S_5 in NW-trending high-strain zones; shallow L_5 lineation; F_5 Z-folds	Main-stage dextral shear in WSZ and subsidiary zones; coaxial flattening in NCSZ	Main D_5 : terminal collision; dextral transpression
G_6	E-W	Open, north-trending F_6 crenulations	Open fold in the Bidou assemblage at Rice Lake	Late D_5 : buttress effect on Ross River pluton; continued dextral transpression

[1] inferred trend of maximum principal far-field stress axis, based on *present* orientation of associated fabric elements
Abbreviations: GCS, Gold Creek syncline; HLA, Horseshoe Lake anticline; NCSZ, Normandy Creek shear zone; WSZ, Wanipigow shear zone

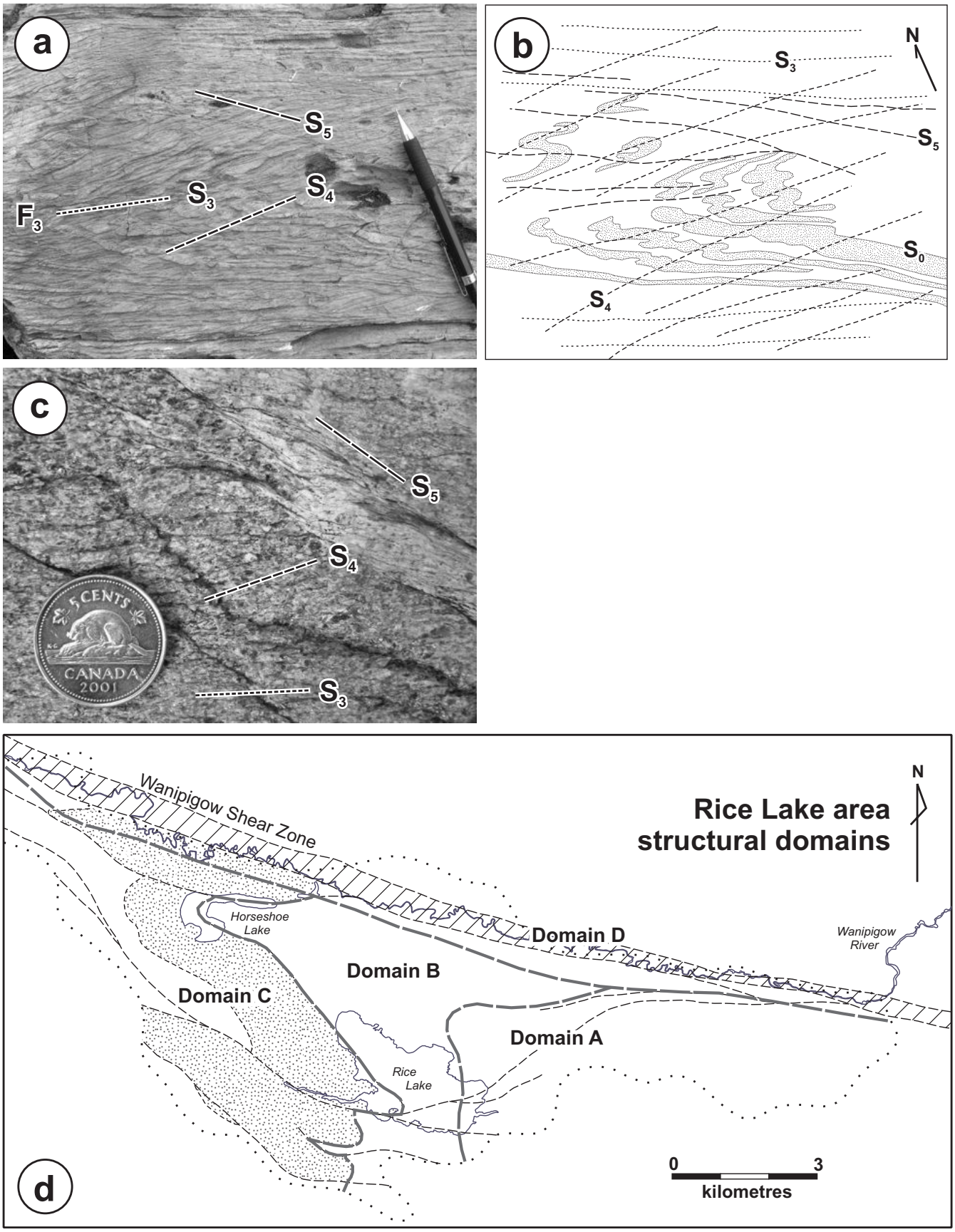

Figure 52: *Outcrop photographs showing the overprinting relationships and typical styles of the S_3, S_4 and S_5 generations of planar deformation fabric, San Antonio assemblage, north of Horseshoe Lake (north is toward the top of both photographs):* ***a)*** *and* ***b)*** *transposed, thin-bedded greywacke and mudstone showing an isoclinal F_3 closure transected by S_4 and S_5;* ***c)*** *massive, coarse-grained arkosic wacke showing continuous S_3 shape fabric, finely spaced S_4 cleavage and discrete S_5 shear-band cleavage;* ***d)*** *sketch map showing the four structural domains in the Rice Lake area.*

study area and thus provide a useful means of structural correlation. These fabrics are pervasive in the San Antonio assemblage, which indicates that penetrative regional deformation occurred after ca. 2705 Ma, the maximum depositional age of these rocks as documented by Percival et al. (2006a).

The following structural descriptions are accompanied by lower-hemisphere, equal-area projections of structural data collected during the bedrock-mapping component of this study. On these diagrams, the data are subdivided into four distinct structural domains (A, B, C and D), based on the prevailing orientations and styles of the constituent deformation structures, as described below. The approximate boundaries of these domains are shown on Figure 52d.

G_1 structure

Meso- and microscopic examples of G_1 deformation structure are identified in very angular to subrounded fragments of sericitic and quartzofeldspathic phyllite in the heterolithic clastic dike near the top of the Independence Lake (IL) unit. The G_1 structure consists of a continuous to finely spaced S_1 foliation defined by very fine grained sericite and chlorite. In some fragments, quartz (±feldspar) exhibits undulose extinction, lattice-preferred orientation, serrated grain margins and a weak shape-preferred orientation, which are indicative of dynamic recrystallization under greenschist-facies metamorphic conditions. The S_1 fabrics show misalignment between fragments, do not extend across the boundaries of individual fragments and are not observed in the generally massive chloritic sandstone matrix of the clastic dike, thereby indicating that they predate fragment entrainment (Figure 22b). The unimodal (ca. 2723 Ga) zircon population in the clastic dike and the delicate shapes of the phyllite fragments suggest a very proximal source for the exhumed volcanic-arc rocks. For these reasons, the S_1 fabrics are interpreted to be broadly synvolcanic and a result of deformational processes within the Bidou volcanic arc. The synvolcanic subsidence structure east of Rice Lake likely represents a macroscopic G_1 structure.

G_2 structure

Structural facing criteria in the Gold Creek (GC) unit of the Bidou assemblage and the younger San Antonio assemblage indicate that both face west on the west-northwest-trending axial-planar S_3 fabric associated with the F_3 Horseshoe Lake anticline (*see* below), and thus describe an older-over-younger structural relationship that must predate regional F_3 folding (Figure 3). For this reason, the upper contact of the San Antonio assemblage is interpreted as a thrust fault, which is assigned to the G_2 generation of deformation structure on the basis of the macroscopic field relationships described above. Due to a combination of poor exposure and a generally intense structural overprint, mesoscale structural or kinematic evidence in support of this hypothesis is generally lacking. In most locations, the contact coincides with a zone of sericitic tectonite that appears to record multiple generations of fabric development, yet fails to provide convincing evidence of a deformation fabric that might correspond to the G_2 generation. Nevertheless, several examples of a G_2 deformation fabric are preserved in bedded arenite of the San Antonio assemblage, in locations immediately below the inferred position of the macroscopic G_2 thrust fault, as well as deeper down-section. This fabric is best preserved in the hinge of the F_3 Gold Creek syncline and comprises a penetrative and continuous shape fabric (S_2) defined by fine-grained foliated sericite and elongate quartz grains. The S_2 fabric roughly parallels bedding and is folded around the hinges of mesoscopic, open to tight folds that are interpreted to be parasitic to the macroscopic F_3 closure (Figure 53a, b); these structures are locally transected by a spaced, northeast-trending crenulation cleavage assigned to the G_4 generation of structure (*see* below).

G_3 structures

The earliest regionally pervasive deformation structure observed in the Rice Lake area is a planar-linear (S-L) shape fabric that is most prominently defined on a mesoscopic scale by flattened and stretched primary features (e.g., feldspar

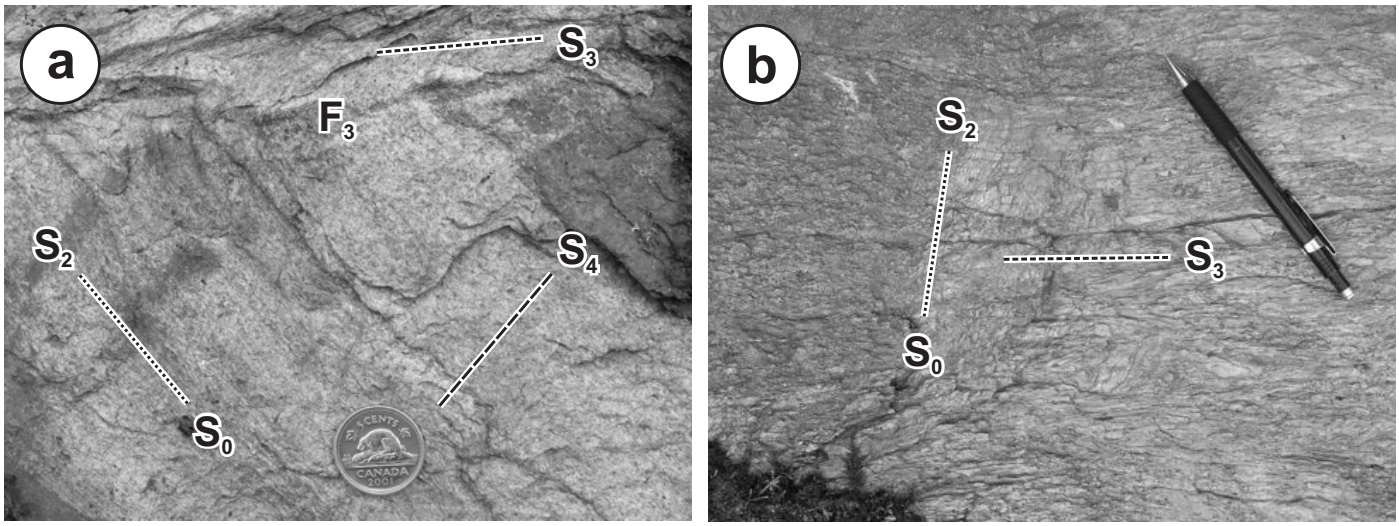

Figure 53: *Outcrop photographs of G_2 deformation structures in the San Antonio assemblage:* ***a)*** *bedding-parallel S_2 shape fabric overprinted by F_3 Z-fold and S_4 cleavage in feldspathic arenite near the upper contact of the assemblage, just north of Gold Creek on the Quesnel Lake road (north is towards the upper left);* ***b)*** *bedding-parallel S_2 shape-fabric overprinted by open F_3 folds and differentiated S_3 crenulation cleavage in tonalitic sandstone near the base of the assemblage, in the hinge of the Gold Creek syncline, west of Red Rice Lake on the Quesnel Lake road (pencil points north).*

phenocrysts, clasts, amygdules, pillows, etc.; Figure 54a; *see also* Figures 23b, 35a, b, 38f). On a meso- to microscopic scale, the shape fabric typically includes a continuous foliation defined by fine-grained chlorite, actinolite and sericite. The planar fabrics, which are assigned to the G_3 generation of deformation structures, generally trend west-northwest and dip steeply to moderately north (Figure 55). In general, the associated L_3 stretching lineation plunges moderately to the northeast in the plane of the S_3 fabric. The axial ratios of stretched and flattened primary features are highly variable but typically in the range 2–5:1 (Y:Z, X:Z and X:Y); finite strain determinations performed by Lau and Brisbin (1996) on porphyritic samples from unit 16 indicate strain ellipsoids that vary from constrictional to flattening type. At depth in the Rice Lake mine, the G_3 shape fabric in the host gabbro sill is locally manifested as a pure L-tectonite, in which the linear fabric element is defined by stretched plagioclase laths (Figure 54b). The G_3 shape fabric is generally symmetric (e.g., Lau and Brisbin, 1996) except where overprinted by later deformation, and is thus interpreted to indicate the predominance of pure shear over simple shear. From north to south across the Rice Lake area, the L_3 lineation exhibits a systematic change in trend and plunge, from steeply or moderately north-northeast plunging in the south to shallowly east plunging in the north (Figure 56). This change is interpreted to result from later reorientation during dextral transcurrent shear on the Wanipigow Shear Zone (e.g., Poulsen et al., 1986).

In the Townsite (TS) and Round Lake (RL) units, the S_3 fabric is consistently oriented at a very shallow, counter-clockwise angle to bedding (which thus faces east on S_3; Figure 54c), and mesoscopic examples of F_3 folds are very rare. Across the Normandy Creek Shear Zone in the Rainy Lake road (RLR) unit, S_3 is consistently oriented clockwise to bedding (which thus faces west on S_3), and is axial planar to open to tight, S-asymmetric folds that plunge shallowly northwest. In both of these areas, S_3 dips more steeply than bedding. Widely separated examples of bedding in the IL unit show both clockwise and counter-clockwise relationships to the S_3 fabric. West of Rice Lake, the S_3 fabric passes continuously into the San Antonio assemblage, where it is most prominently defined

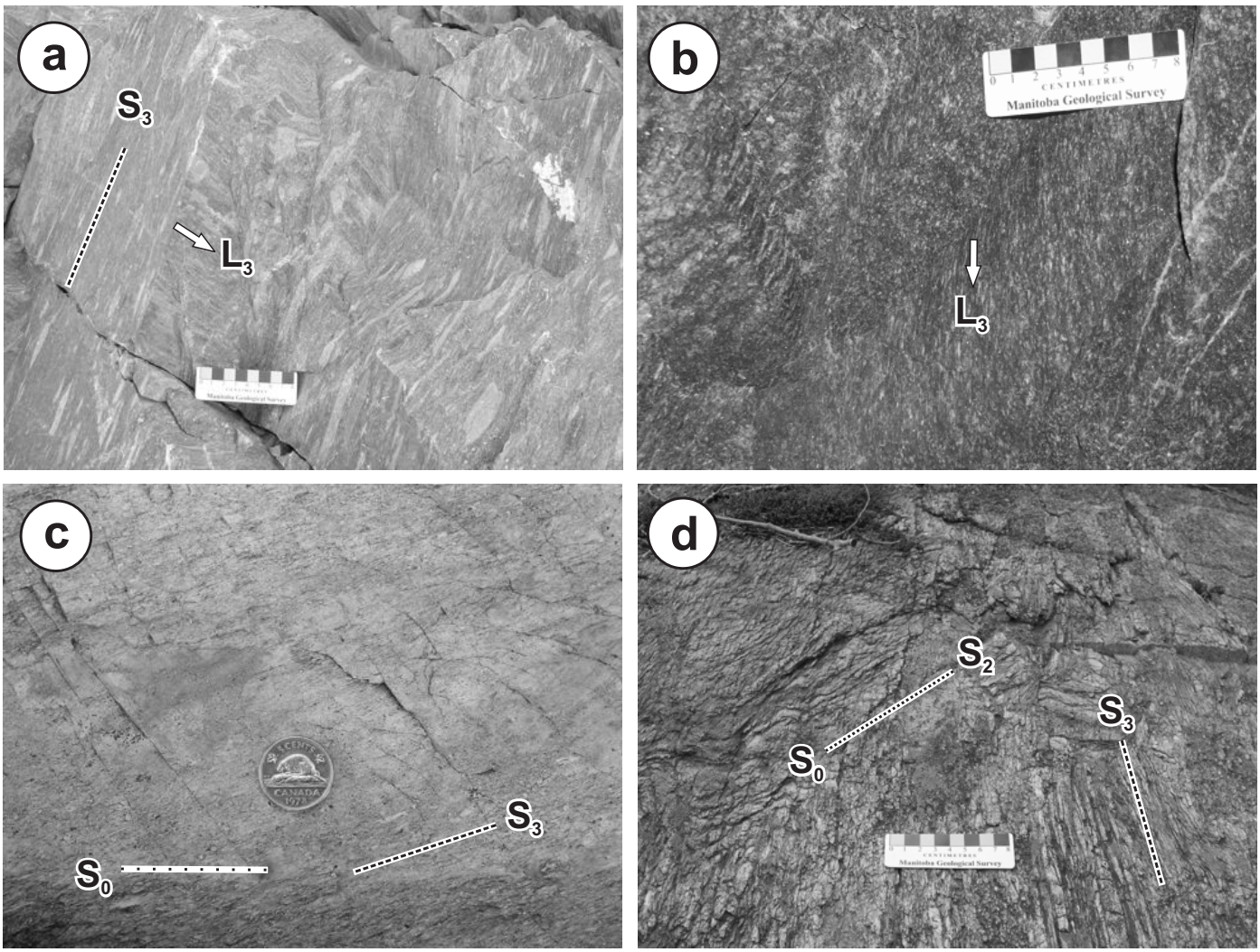

Figure 54: *Outcrop photographs of G_3 structures:* ***a)*** *S-L shape fabric in felsic volcanic conglomerate (unit 20) exposed in the rock quarry ~5 km east of Bissett, on the north side of PR 304 (looking northeast at quarry face);* ***b)*** *penetrative L-tectonite fabric in gabbro (unit 14), 3096E subdrift, level 30, Rice Lake mine (looking southwest);* ***c)*** *angular relationship between bedding (S_0) and S_3 shape fabric (defined by flattened clasts) in felsic epiclastic rocks (unit 20) north of Bissett (north is toward the upper left);* ***d)*** *near-orthogonal angular relationship between S_0-S_2 and a differentiated S_3 crenulation cleavage (note open F_3 folds) in the hinge of the Gold Creek syncline at Red Rice Lake (looking northwest).*

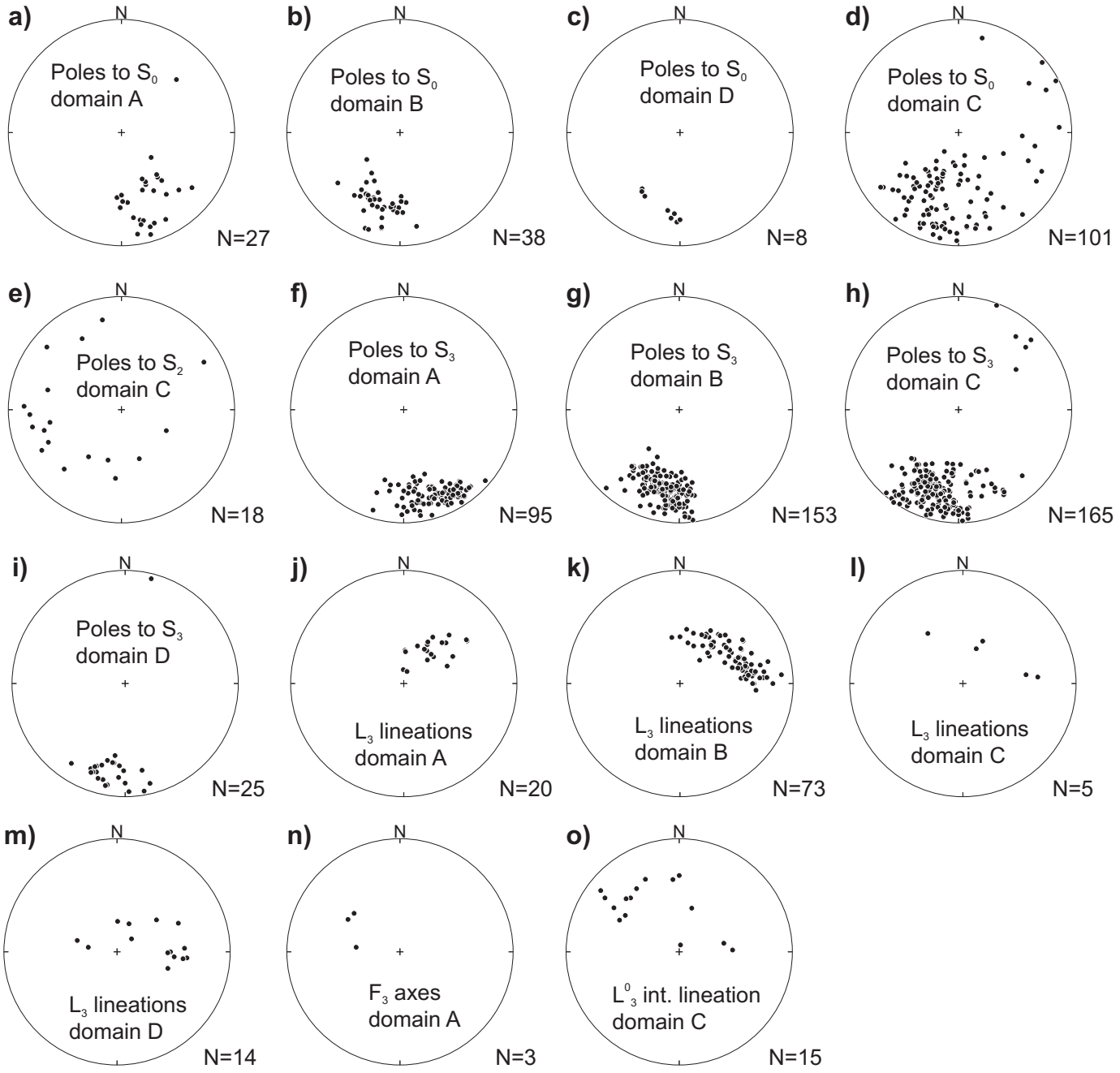

Figure 55: *Lower-hemisphere, equal-area projections of G_3 structural data, separated according to structural domain, where N is the number of data points. Bedding (S_0) and S_2 measurements are included for reference.*

by a preferred alignment of elongate pebbles in conglomerate (Figure 38f) and channel-lag deposits (Figure 39e); the L_3 fabric is generally not well developed in these rocks. In most outcrops, the S_3 clast elongation is significantly oblique to bedding and thus constrains the macroscopic F_3 fold geometry.

In the San Antonio assemblage and GC unit, the S_3 fabric exhibits an axial planar relationship (Figure 54d; *see also* Figure 38f) to the Horseshoe Lake anticline (HLA) and Gold Creek syncline (GCS), which are the most prominent closures in a macroscopic train of folds that trends across the regional structural grain of the belt (Figure 3). These folds are tight, steeply inclined and asymmetric structures that are assigned to the third generation (G_3) of deformation structures on the basis of overprinting and bedding-cleavage (S_0-S_3) relationships. In the San Antonio assemblage, bed forms and ubiquitous younging criteria (trough and tabular-planar crossbeds and graded bedding) indicate that the F_3 folds are overturned to the southwest, with upright limbs that dip moderately to steeply northeast and overturned limbs that dip steeply in the same direction. On the shared limb of the HLA and GCS, south of Horseshoe Lake, the S_3 fabric is refracted toward the west-southwest in the quartz-rich arenitic rocks of the San Antonio assemblage, presumably in response to a higher competence as compared to the adjacent volcanic and volcaniclastic rocks. Map patterns and the absence of S_0-S_3 vergence changes in the TS and RL units of the Bidou assemblage indicate that the macroscopic

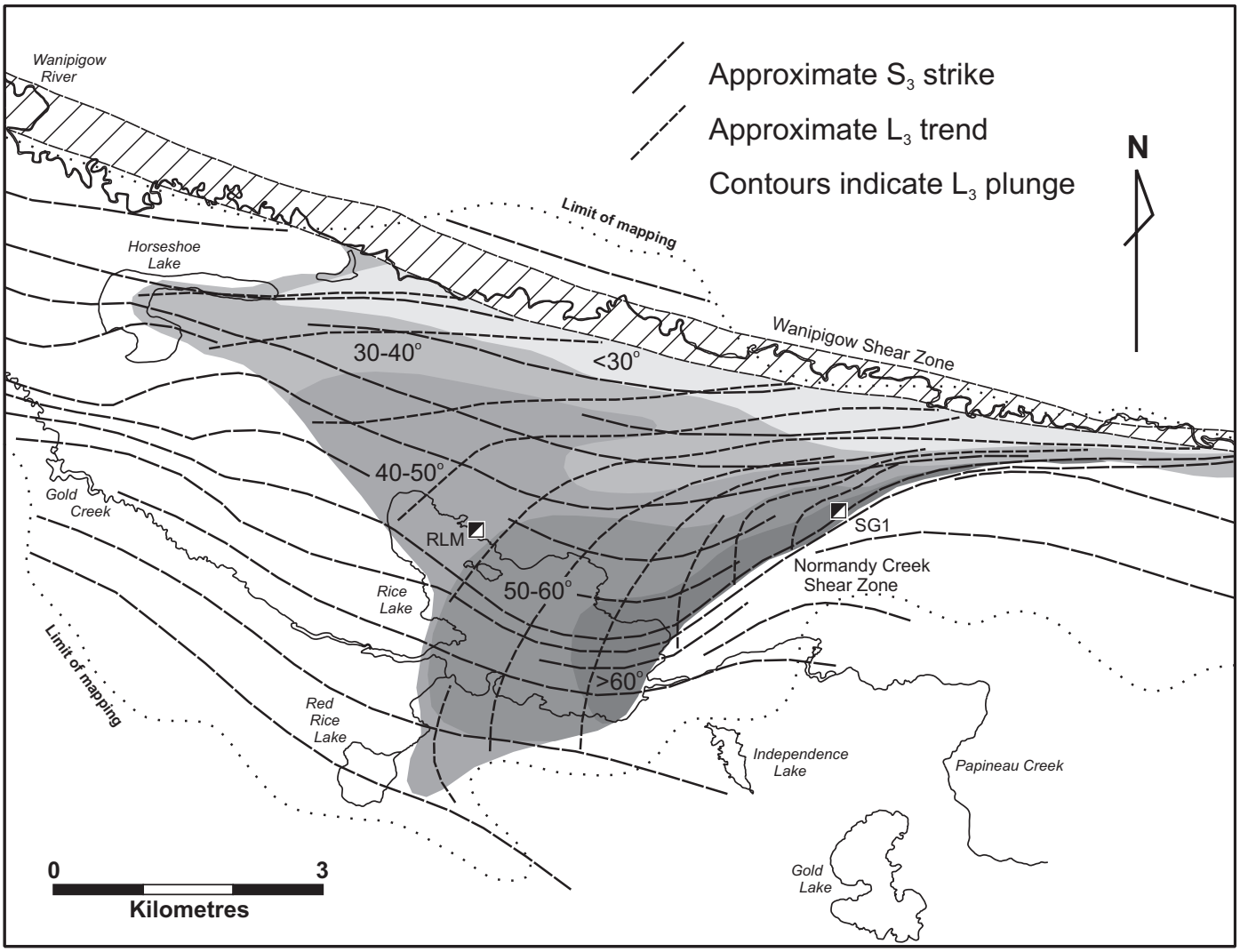

Figure 56: *Schematic map showing the trends of the S_3 and L_3 fabrics (dashed lines) and the plunge of the L_3 lineation (contours) in the Rice Lake area. The systematic change in trend and plunge of the L_3 lineation along the margin of the Wanipigow Shear Zone was originally described by Poulsen et al. (1986). Abbreviations: RLM, Rice Lake mine (A-shaft); SG-1, SG-1 mine portal.*

F_3 fold train terminates at the base of the San Antonio assemblage. As described by Bailes (1998), this relationship is best explained in the context of the pronounced angular unconformity in this location, which must have been configured such that the maximum principal stress during folding was oriented subparallel to the primary anisotropy (i.e., bedding) in the San Antonio assemblage but suborthogonal to that in the underlying units. Hence, the younger rocks accommodated the regional shortening by buckling and folding, whereas the older rocks experienced layer-subparallel flattening without buckling.

In general, minor fold hinges and bedding-cleavage (S_0-S_3) intersection lineations associated with the GCS plunge shallowly northwest or southeast (Figure 57a), whereas those in the HLA plunge more steeply (Figure 57b). In the footwall of the San Antonio assemblage, this change in F_3 plunge is mimicked by the systematic change, from south to north, in the trend and plunge of the L_3 lineation (Figure 57c), which maintains a near-orthogonal angular relationship with the macroscopic hinge in the adjacent segment of the F_3 fold train. From these relationships, the G_3 linear structures are interpreted to have developed contemporaneously within a regional kinematic frame of northeast-southwest shortening. Towards the north, these structures appear to have been reoriented, in a sympathetic manner, in response to dextral transcurrent shear along the south margin of the Wanipigow Shear Zone, as suggested by Poulsen et al. (1986).

On the north margin of the Wanipigow Shear Zone, psammitic and semipelitic rocks of the Little Beaver assemblage exhibit a penetrative and pervasive foliation defined by a preferred alignment of micaceous minerals, quartz segregations and elongate garnet porphyroblasts (Figure 58a). In these rocks, the foliation parallels a locally well-developed gneissosity defined by alternating quartzofeldspathic and micaceous domains. In some outcrops, a weak to moderate stretching and mineral lineation is also developed, and plunges moderately to the northeast in the foliation plane. The foliation is axial planar to tight to isoclinal folds of quartz segregations and the gneissosity. Some of these folds are rootless and markedly noncylindrical (Figure 58b). Kinematic indicators in the quartzofeldspathic layers, which include asymmetric boudins, shear-bands and S-C fabrics, consistently indicate sinistral-reverse oblique-slip shear (Figure 58a, c). In contrast, the same types of kinematic indicators in the more micaceous semipelite layers consistently indicate dextral strike-slip shear (Figure 58d). From this

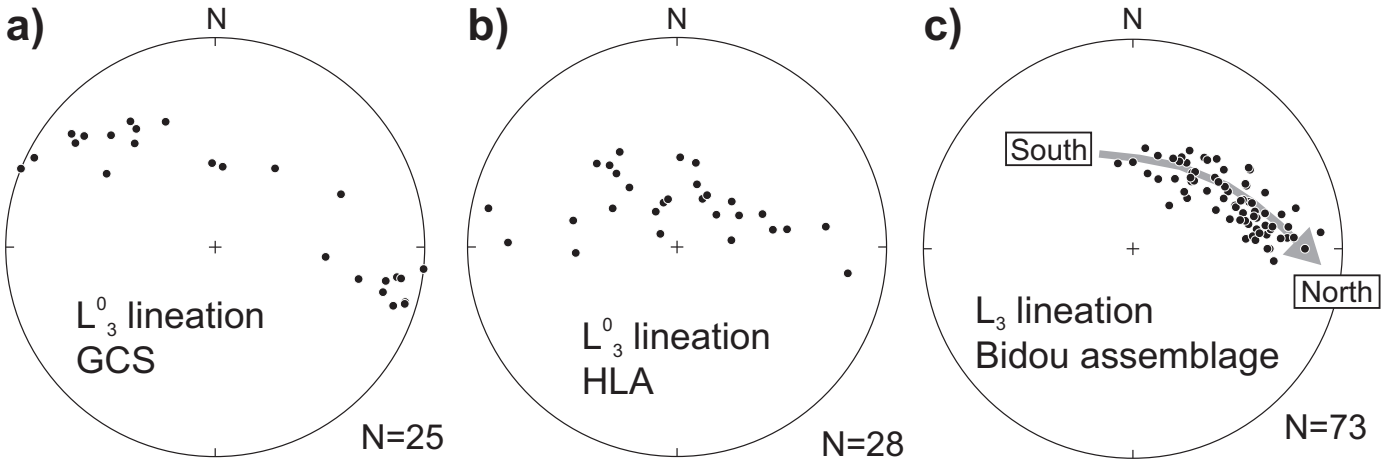

Figure 57: *Lower-hemisphere, equal-area projections of structural data, where N is the number of data points:* ***a)*** *and* ***b)*** *calculated intersection lineations (L^0_3) from pairs of bedding (S_0) and cleavage (S_3) measurements from individual outcrops of the San Antonio assemblage in the Gold Creek syncline (GCS) and Horseshoe Lake anticline (HLA), respectively;* ***c)*** *stretching-lineation measurements in the underlying Bidou assemblage.*

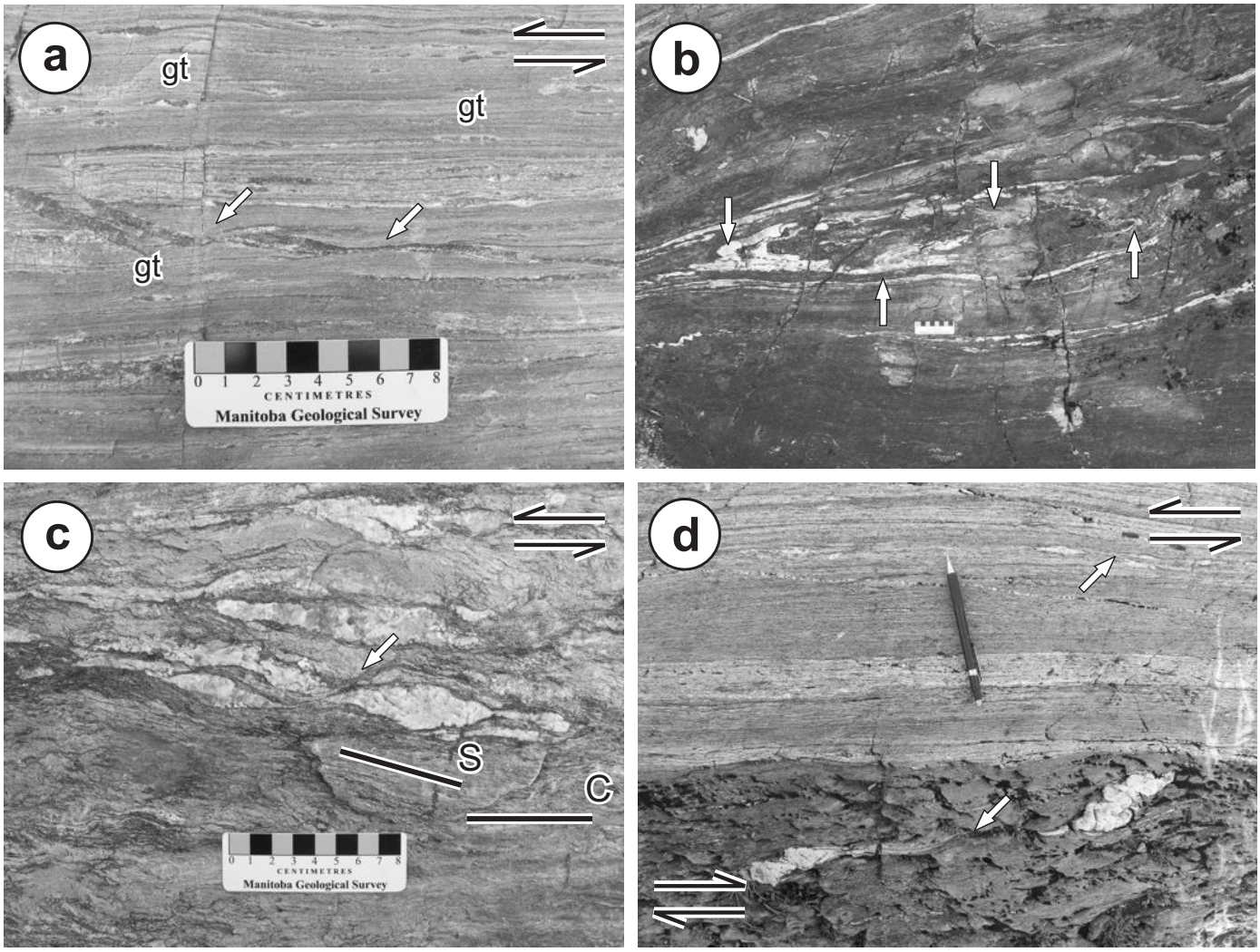

Figure 58: *Outcrop photographs of G_3 deformation structures in the Little Beaver assemblage, northwest of the Vanson mine:* ***a)*** *penetrative foliation defined by aligned garnet (gt) porphyroblasts and fine-scale gneissosity; arrow indicates sinistral offset of quartz veinlet;* ***b)*** *rootless, isoclinal and noncylindrical folds, with closures indicated by arrows;* ***c)*** *sinistral S-C fabric and shear bands (arrow);* ***d)*** *example of antithetic offset of quartz veins (arrows) in quartzofeldspathic (top) and semipelitic (bottom) layers.*

relationship, it is inferred that the quartzofeldspathic (and presumably more competent) layers preserve an earlier generation of deformation structures associated with a sinistral kinematic frame, whereas the semipelitic (and presumably less competent) layers preserve evidence of younger shear deformation within a dextral kinematic frame. Based on their orientation and kinematics, which are consistent with northeast-southwest shortening, the earlier structures are correlated with the G_3 structures south of the Wanipigow Shear Zone in the Rice Lake belt.

The overall geometry of G_3 structure in the Rice Lake area supports a model of regional sinistral transpression in which strongly partitioned northeast-southwest shortening is manifested by three different styles of deformation in three distinct structural domains (Figure 52d): 1) sinistral-oblique noncoaxial shearing within a precursor to the Wanipigow Shear Zone (domain D), 2) upright subhorizontal folding in those rocks structurally above the basal unconformity of the San Antonio assemblage (domain C), and 3) bulk flattening and subvertical stretching in those rocks below (domain B). Structural domain A exhibits a combination of structural styles, with bulk flattening and subvertical stretching northwest of the NCSZ and weak flattening and minor S-asymmetric folding to the southeast.

G_4 structures

Throughout the mapped area, the S_3 shape fabric is overprinted at a shallow counter-clockwise angle by a variably developed crenulation cleavage attributed to G_4 deformation (Figure 59a, b). The S_4 cleavage trends west or southwest, dips steeply north (Figure 60) and is often best preserved as a finely spaced crenulation cleavage within flattened clasts that define the regional G_3 fabric (Figure 59c). In these instances, the S_4 cleavage typically strikes 20–40° counter-clockwise to the intermediate (Y) axes of the flattened clasts. In many cases, this internal S_4 cleavage is sharply truncated at the margins of individual clasts (Figure 59c), suggesting reactivation of S_3 during, or subsequent to, development of S_4. The S_4 cleavage transects meso- and macroscopic F_3 folds in the San Antonio assemblage (Figure 59d), and intersects S_3 to form a prominent and pervasive L^3_4 intersection lineation (Figure 59e) that generally plunges at moderate angles to the northeast (Figure 60). The L^3_4 lineation varies from parallel to slightly oblique to the L_3 stretching lineation (Figure 59f), and likewise exhibits a shallower plunge along the south margin of the Wanipigow Shear Zone. The S_4 fabric is axial planar to rare, open to tight, Z-asymmetric folds that plunge moderately north. No examples of regional-scale F_4 folds are delineated in the Rice Lake area, and the G_4 structures appear to have accommodated weak northwest-southeast shortening of the Rice Lake belt, perhaps during the early increments of regional dextral transpression (*see* below).

G_5 structures

Fifth-generation ductile deformation structures are pervasive in the Rice Lake area, but are only penetrative in a series of discrete high-strain zones, the most notable example of which is the regional-scale Wanipigow Shear Zone (WSZ). This shear zone ranges up to more than 1.5 km thick and defines the interface between the North Caribou Terrane and the Uchi Subprovince, along the northern boundary of the mapped area. Other prominent examples of G_5 high-strain zones, which are generally about 50–100 m thick, include the Gold Creek, Normandy Creek and Red Rice Lake shear zones (Figure 3). South of Rice Lake, subsidiary G_5 high-strain zones splay towards the south off the Gold Creek and Red Rice Lake shear zones, the most prominent example of which is the Pilot–Smuggler Shear Zone described by Bailes (1971).

The G_5 high-strain zones are characterized by penetrative mylonitic foliations (S_5) that are defined by domains of fine-grained, foliated sericite and chlorite that alternate with domains of dynamically recrystallized quartz and feldspar. In coarsely porphyritic rock types, these mylonite zones preserve textural evidence of contemporaneous brittle failure of plagioclase and ductile flow of quartz, suggesting deformation at or near the brittle-ductile transition (Figure 61a). The mylonitic foliation parallels an intense shape fabric defined by highly deformed primary features, including pillows and clasts (Figure 61b, c). In many locations, these features delineate significant variations in apparent finite strain along and across strike in the G_5 high-strain zones. Although it is not possible to quantify the proportion of the accumulated strain that can be attributed to G_5 structure, the highest finite strains are recorded in coarse clastic rocks near the confluence of the Normandy Creek Shear Zone and the WSZ. In general, the S_5 fabrics and their host high-strain zones trend west-northwest to north-northwest and dip subvertically (Figure 62).

The G_5 high-strain zones typically contain a well-developed lineation defined by quartz-filled pressure fringes on porphyroclasts or pyrite cubes, stretched clasts, locally well-developed quartz ribbons (Figure 61d) and ridge-in-groove striations. The mylonitic foliation commonly envelops packets of strongly Z-asymmetric, open to tight, upright, chevron-style F_5 folds (Figure 61e) that exhibit highly variable plunges, from shallowly east to steeply north. Dextral kinematic indicators are well developed on horizontal outcrop surfaces, and typically include S-C fabrics, σ-porphyroclast systems, shear bands and asymmetric boudins (Figure 61b, c, f; Figure 63a). Conjugate shear bands and shear fractures are a common feature of particularly high strain zones in the WSZ, as well as the NCSZ (Figure 63b), consistent with a significant component of zone-normal shortening. The structural geometry of the G_5 structures indicates that they accommodated dextral transcurrent shear deformation in response to north-northwest–south-southeast shortening of the Rice Lake belt. This deformation was strongly partitioned into the discrete high-strain zones, which appear to be controlled by a combination of primary anisotropy and/or pre-existing structures.

South of the WSZ and outside the G_5 high-strain zones, the S_5 fabric is manifested as a regionally pervasive, spaced, fracture or shear-band cleavage (Figures 52a, b, c, 63c, d) that trends northwest or north-northwest and dips subvertically (Figure 62). The S_3 and S_4 fabrics are transposed in a dextral sense along the margins of the S_5 cleavage planes. On the scale of individual outcrops, this fabric is locally observed to intensify into discrete high-strain zones that, like the examples described above, are characterized by shallow-plunging lineations and well-developed dextral kinematic indicators on horizontal outcrop surfaces.

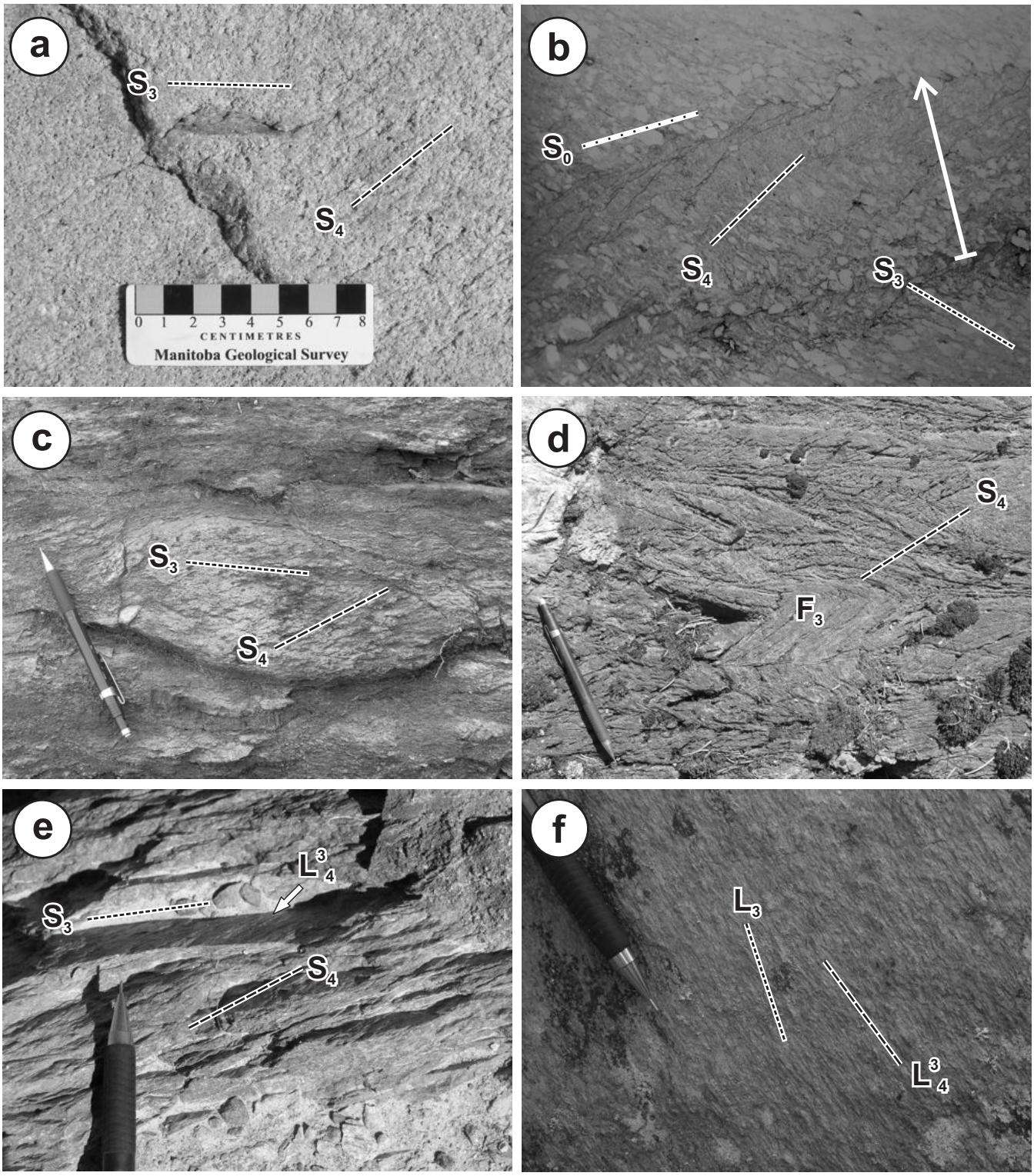

Figure 59: *Outcrop photographs of G_4 deformation structures:* ***a)*** *spaced S_4 cleavage showing overprinting relationship to S_3 shape fabric (indicated by flattened pebble) in arenite (unit 27), southeast of Horseshoe Lake (north is toward upper left);* ***b)*** *thin-section photograph (plane-polarized light) showing bedding (S_0; defined by grain-size and compositional variations) and a continuous S_3 shape fabric (defined by elongate quartz grains and foliated sericite) overprinted by spaced S_4 cleavage in thin-bedded arenite (unit 27) on the south limb of the Gold Creek syncline, northwest of Red Rice Lake (arrow indicates north younging direction in 1 cm thick graded bed);* ***c)*** *spaced S_4 cleavage oblique to the intermediate axis of a flattened cobble (S_3) in heterolithic conglomerate (unit 26) in the hinge of the Gold Creek syncline, south shore of Rice Lake (pencil points north);* ***d)*** *minor F_3 folds transected by spaced S_4 cleavage in thin-bedded arenite (unit 27), northwest of Red Rice Lake (pencil points north);* ***e)*** *intersection lineation (arrow) associated with well-developed S_3 and S_4 fabrics in intermediate volcaniclastic rocks of unit 16 at the Wingold deposit, northeast of Bissett (pencil points north);* ***f)*** *S_3 foliation plane showing slight obliquity between L_3 (stretched phenocrysts to the immediate right of the short-dashed line) and L^3_4 intersection lineation in volcaniclastic rocks of unit 19, northwest of Bissett (looking north at a near-vertical outcrop face).*

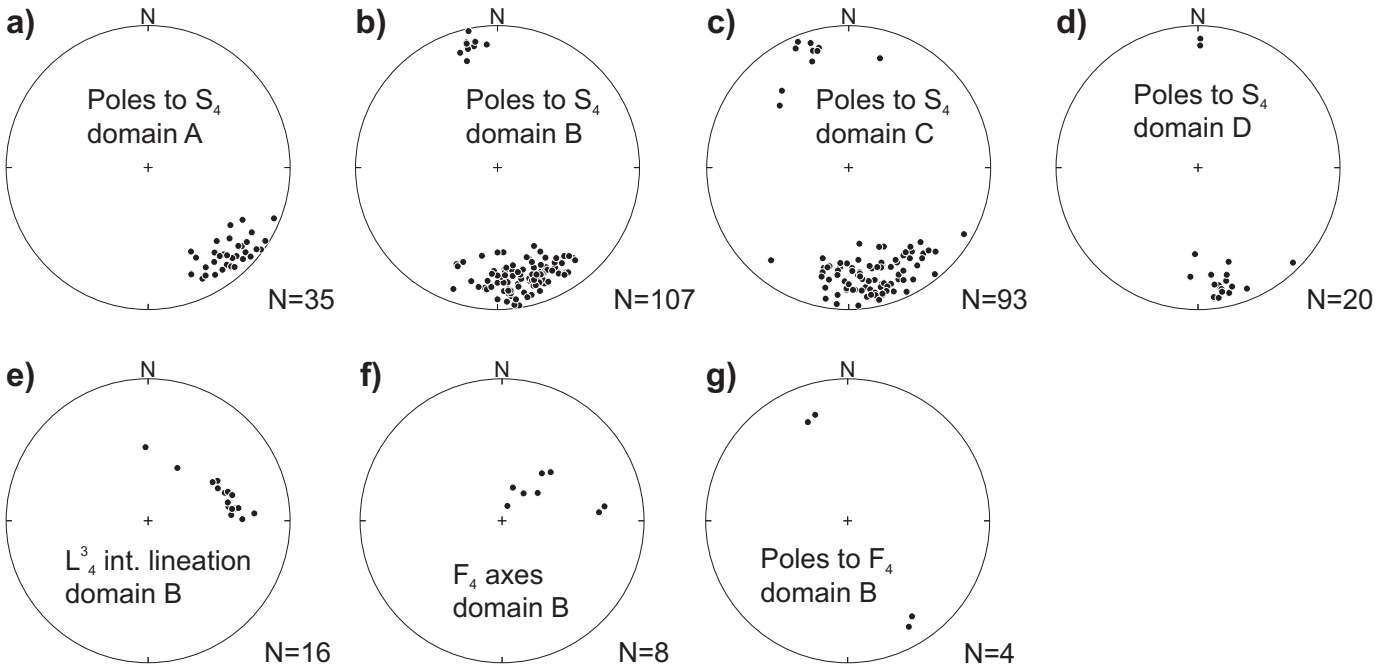

Figure 60: *Lower-hemisphere, equal-area projections of G_4 structural data, separated according to structural domain, where N is the number of data points.*

G_6 structures

The latest generation of ductile deformation, G_6, appears to be associated with an open, north-trending flexure in the Rice Lake area that is best defined by macroscopic map patterns in the TS unit. On a mesoscopic scale, outcrops in the hinge of this fold contain a weak to moderate, typically closely spaced, crenulation cleavage (S_6) that is associated with open, upright, steeply north-plunging, symmetric folds of the earlier generations of planar fabric (Figure 64a, b). The S_6 cleavage generally dips steeply to the east-southeast (Figure 65). The G_6 structures are best developed along the south shoreline of Rice Lake and are also well exposed at the A-shaft station on level 26 of the Rice Lake mine. On the east limb of the macroscopic fold, the early fabrics (S_3, S_4, S_5) maintain their consistent overprinting relationships but have been rotated approximately 50° in a counter-clockwise sense into a more northeasterly trend. The G_6 structures appear to have accommodated east-west shortening of the Rice Lake area, perhaps in response to a buttressing effect along the northwest margin of the Ross River pluton during the late increments of north-northwest–south-southeast shortening of the belt.

Structural evolution

The orientation and style of the deformation structures, coupled with inferences drawn from associated kinematic indicators and macroscopic map patterns, indicate that the deformation history of the Rice Lake area likely involved five distinct episodes of regional deformation (D_1–D_5; Table 10; Figure 66), two of which (D_1 and D_2) predate deposition of the San Antonio assemblage and are interpreted to be broadly synvolcanic. In this scheme, each deformation episode is interpreted to represent a distinct kinematic frame. The distinction between deformation episode (D_X) and generation of deformation structure (G_Y) is used to emphasize the fact that more than one generation of fabric may form during a single episode of progressive deformation (e.g., Tobisch and Paterson, 1988). In the present case, the G_4–G_6 structures are interpreted to record progressive deformation associated with regional northwest-southeast (present co-ordinates) shortening, and are thus assigned to a single, possibly protracted, episode of deformation (D_5).

The predepositional G_1 fabric observed in fragments in the clastic dike near the top of the IL unit is attributed to high heat flow and hydrothermal alteration associated with synvolcanic normal faulting within the Bidou volcanic arc. This faulting likely coincided with the onset of mafic magmatism in the RLR unit, which exhibits a chemical affinity to back-arc basin basalt. In this regard, the G_1 fabric is interpreted to record an episode of arc extension and normal faulting (D_1), possibly associated with the initiation of back-arc spreading along the inboard portion of the Bidou volcanic arc. Continued D_1 normal faulting of the RLR and IL units, prior to deposition of the TS unit, is interpreted to account for the angular discordance at the base of the TS unit.

In the Horseshoe Lake area, the map patterns of the San Antonio and Bidou assemblages indicate the existence, and provide evidence of the nature, of two temporally distinct deformation episodes (D_2 and D_3). The D_2 episode is not associated with any observed meso- or microscale deformation structures, but is indicated by the pronounced angular unconformity at the base of the San Antonio assemblage. In particular, the near-orthogonal orientation of the unconformity with respect to primary stratification in the rocks beneath indicates that the Bidou assemblage must have been tilted into a near-vertical orientation prior to deposition of the San Antonio assemblage (Figure 66; D_2). This tilting is ascribed to the D_2 deformation episode and is inferred to result from accretionary processes along the southern margin of the North Caribou Terrane, perhaps in association with tectonic inversion of the Bidou back arc.

West of Horseshoe Lake, the older-over-younger map

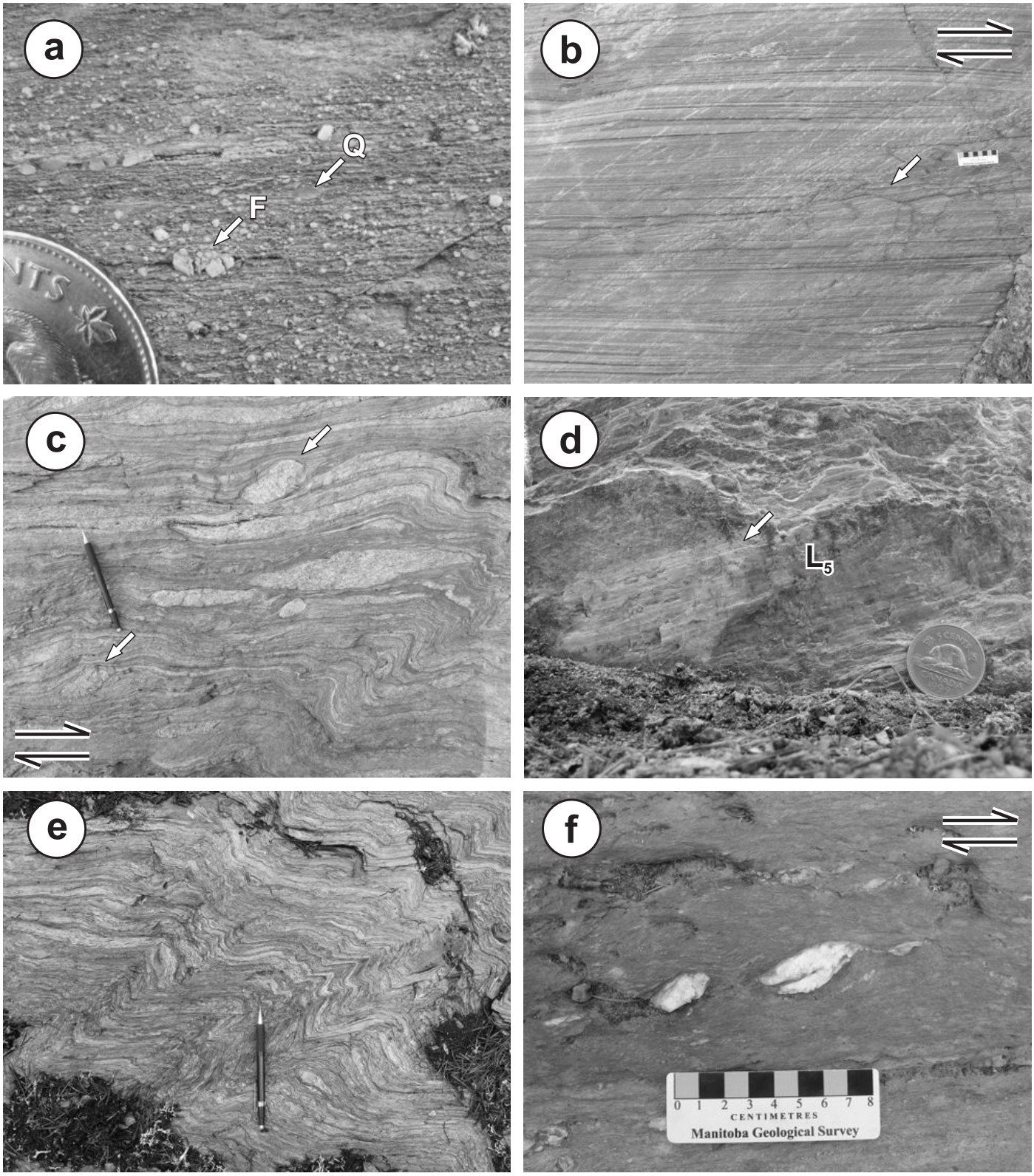

Figure 61: *Outcrop photographs of G_5 structures (in all but d; north is toward the upper left):* ***a)*** *porphyroclastic mylonite along the south margin of the WSZ (unit 20), showing evidence of brittle failure of feldspar (F, light grey blocky grains) and ductile flow of quartz (Q, darker grey wispy grains);* ***b)*** *banded mylonite in volcanic conglomerate (unit 20); aspect ratios of individual clasts in this subhorizontal surface range up to 100:1, or more;* ***c)*** *asymmetric folds and σ-type porphyroclasts (arrows) in polymictic conglomerate (unit 26), north of Silver Falls on the Wanipigow River;* ***d)*** *shallow quartz-ribbon lineation in discrete G_5 shear zone (south of Rice Lake on the Quesnel Lake road; looking northeast at S_5 plane);* ***e)*** *Z-asymmetric chevron folds in volcanic conglomerate (unit 24), south of Silver Falls on the Wanipigow River;* ***f)*** *chloritic mylonite in basalt (unit 10) with well-developed asymmetric quartz boudins.*

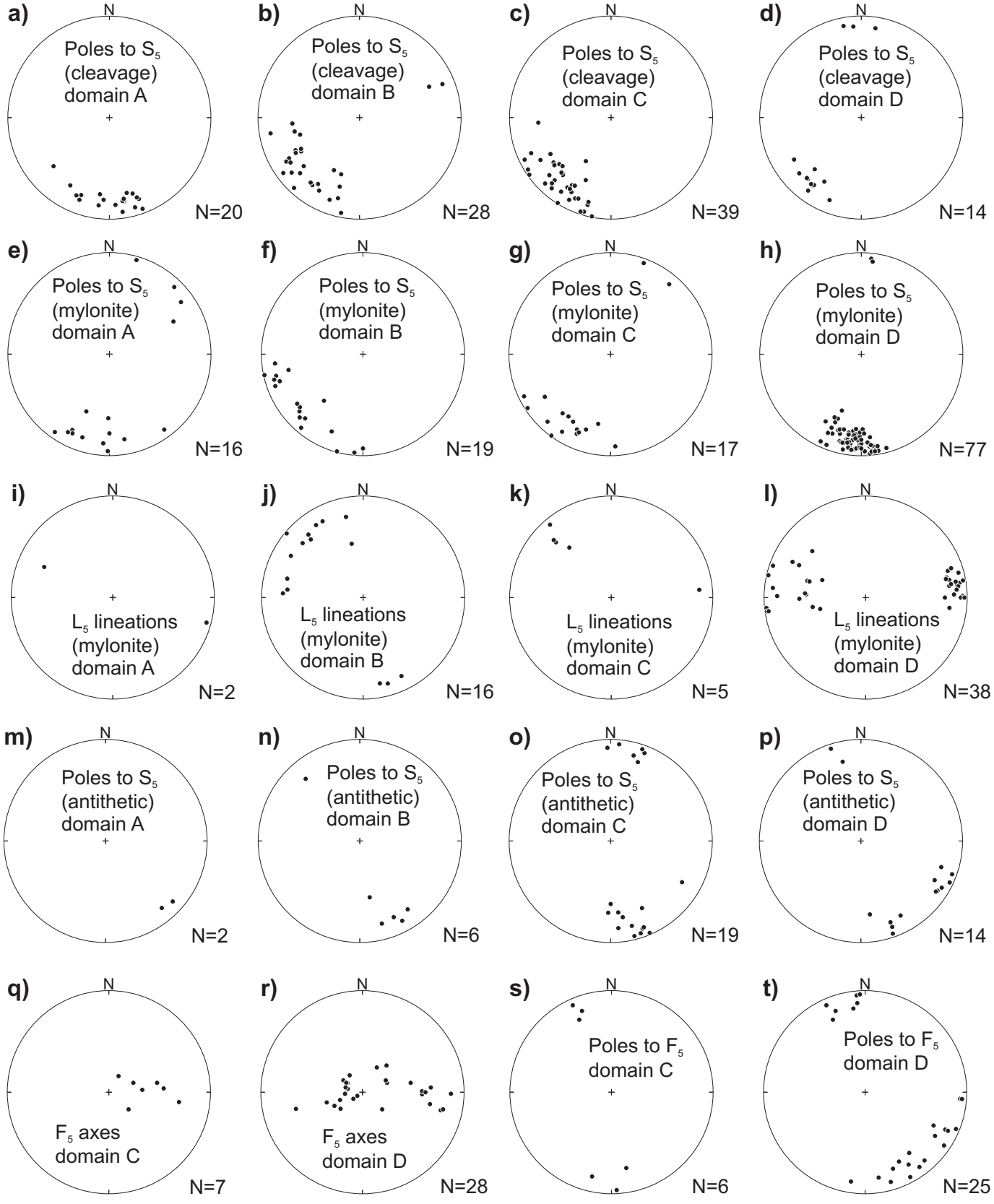

Figure 62: *Lower-hemisphere, equal-area projections of G_5 structural data, separated according to structural domain, where N is the number of data points:* ***a)*** *to* ***d)*** *poles to the regional cleavage, external to high-strain zones;* ***e)*** *to* ***h)*** *poles to mylonitic foliation in high-strain zones;* ***i)*** *to* ***l)*** *lineation associated with mylonitic foliation;* ***m)*** *to* ***p)*** *antithetic shear bands and shear factures in high-strain zones;* ***q)*** *and* ***r)*** *fold axes;* ***s)*** *and* ***t)*** *poles to fold axial planes.*

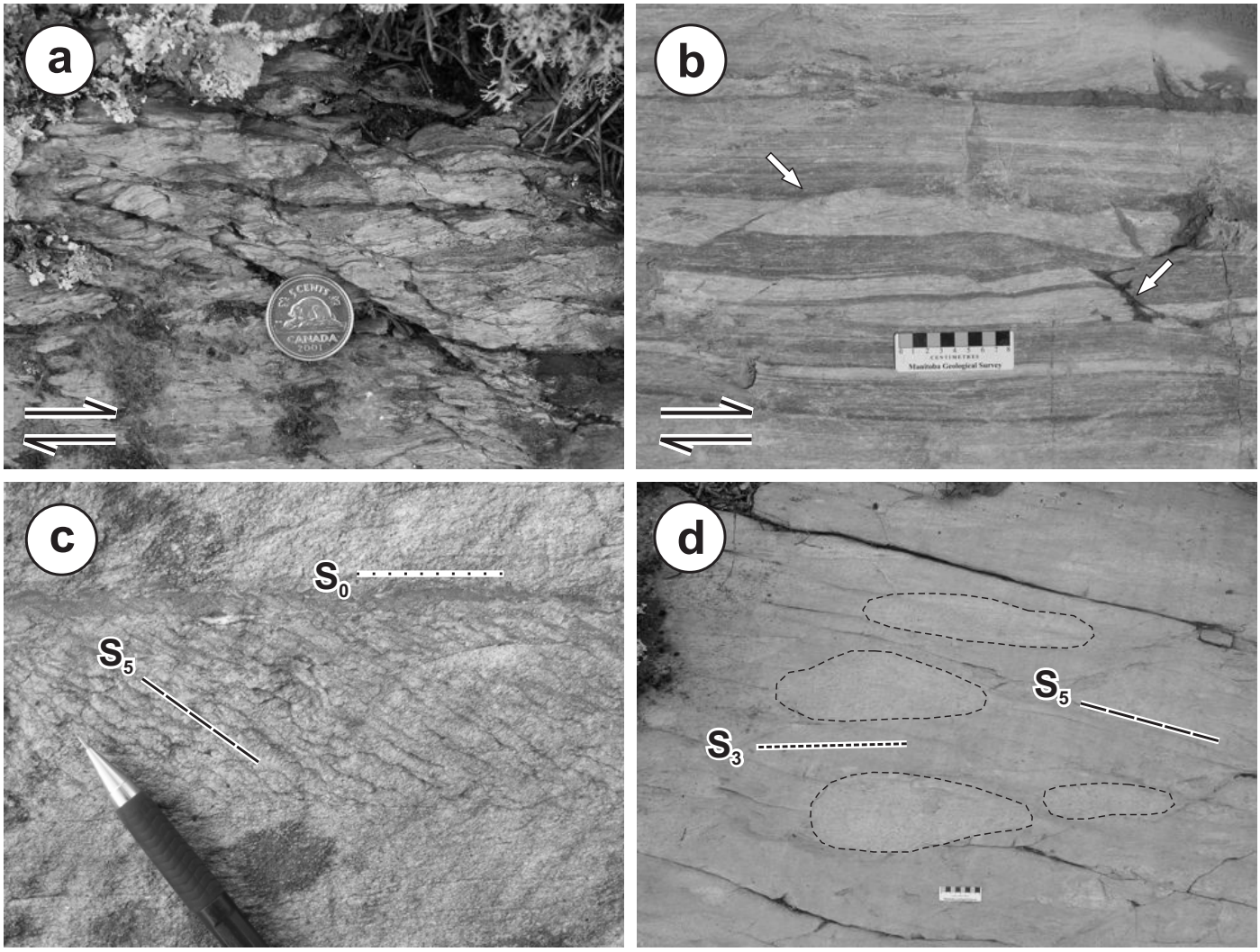

Figure 63: *Outcrop photographs of G_5 structures (north is toward upper left):* ***a)*** *mylonitic fabric and shear bands in discrete G_5 shear zone, south of Rice Lake on the Quesnel Lake road;* ***b)*** *banded mylonite in volcanic conglomerate (unit 20) with synthetic (right) and antithetic (left) shear bands;* ***c)*** *spaced, asymmetric crenulation cleavage in bedded arenite (unit 27), just south of Gold Creek on the Quesnel Lake road;* ***d)*** *widely spaced shear bands in andesite breccia (unit 5), south of Rice Lake; dashed lines show the outlines of flattened clasts that define the S_3 planar fabric.*

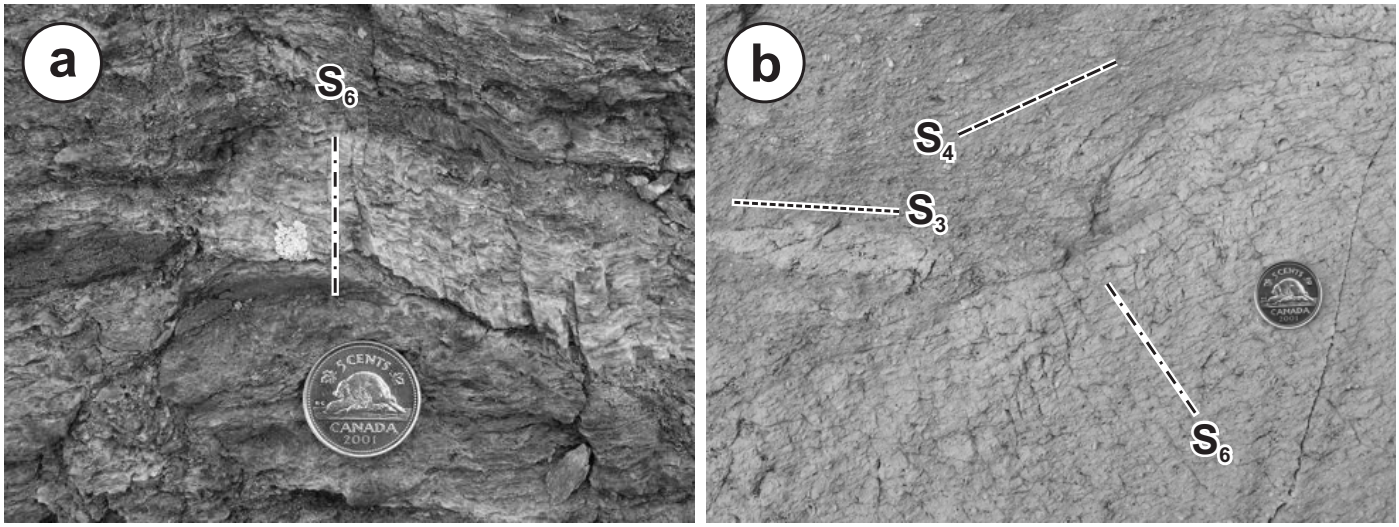

Figure 64: *Outcrop photographs of G_6 deformation structures:* ***a)*** *spaced crenulation cleavage and open crenulations in heterolithic conglomerate (unit 26), south shore of Rice Lake (north is toward top of photo);* ***b)*** *example of weak, spaced S_6 crenulation cleavage showing overprinting relationship to S_3 (flattened clast) and S_4 (finely spaced cleavage) fabrics; S_6 fabric is most pronounced along the margin of an intermediate dike in the lower right portion of the photo (north is toward the upper left).*

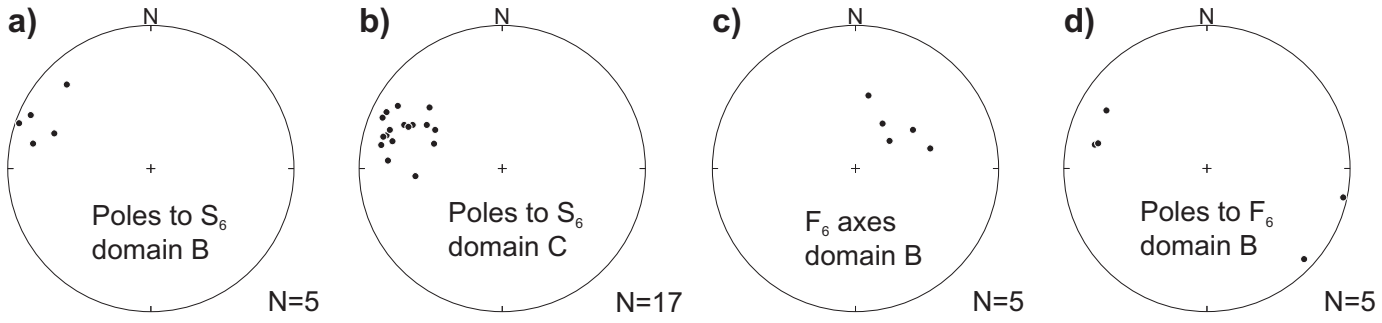

Figure 65: *Lower-hemisphere, equal-area projections of G_6 structural data, separated according to structural domain, where N is the number of data points.*

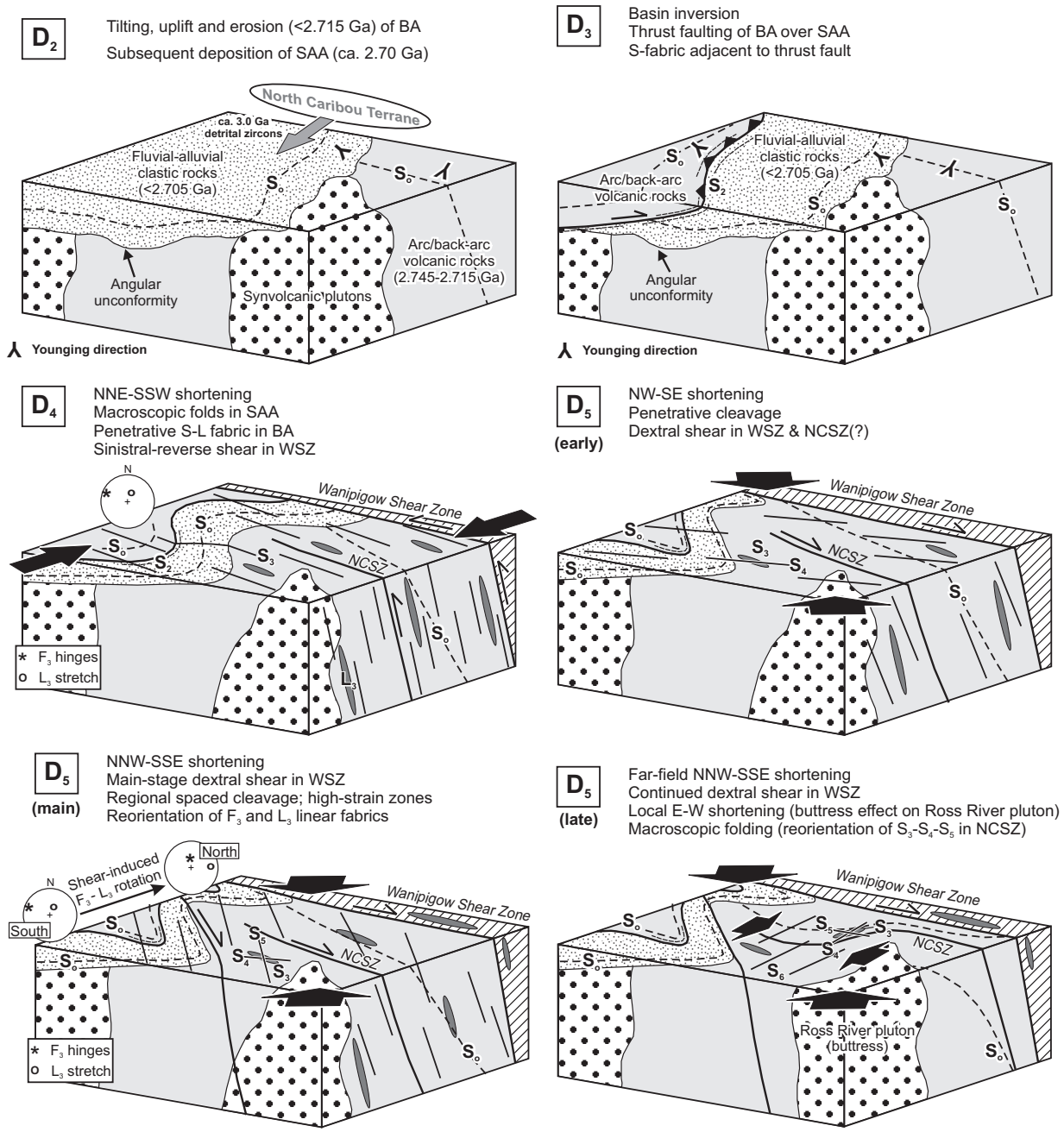

Figure 66: *Schematic block diagrams illustrating the structural evolution of the Rice Lake area. Not depicted is the D_1 deformation, which is interpreted to be associated with extensional faulting in the Bidou assemblage prior to D_2 tilting and uplift and subsequent deposition of the San Antonio assemblage. Abbreviations: BA, Bidou assemblage; NCSZ, Normandy Creek Shear Zone; SAA, San Antonio assemblage; WSZ, Wanipigow Shear Zone.*

pattern of the Bidou and San Antonio assemblages is interpreted to indicate the presence of a G_2 thrust fault, formed during the D_3 deformation episode (Figure 66; D_3). Although the kinematics of the D_3 episode remain unknown, it is interpreted to have accompanied tectonic inversion of the San Antonio basin, perhaps as a consequence of accretionary processes along the North Caribou margin or in the initial stages of crustal thickening associated with terminal collision of the North Caribou and Winnipeg River terranes during the Kenoran Orogeny.

The D_4 deformation episode, as recorded by G_3 deformation structures, was strongly partitioned into macroscopic domains of sinistral-oblique noncoaxial shearing (Wanipigow Shear Zone), bulk flattening and subvertical stretching (Bidou assemblage at Rice Lake), and upright subhorizontal folding (San Antonio assemblage and the GC unit of the Bidou assemblage, west of Rice Lake; Figure 66; D_4). The geometry and kinematics of the G_3 structures indicate a regional regime of sinistral transpression in response to north-northeast–south-southwest shortening (present co-ordinates) of the Rice Lake belt. This deformation likely coincided with major crustal thickening during the main collisional stage of the Kenoran orogeny in the Uchi Subprovince.

The G_4, G_5 and G_6 structures are interpreted to record progressive deformation (D_5) within a regional regime of late-orogenic dextral transpression associated with the terminal phase of the Kenoran Orogeny. The G_4 structures consist of a penetrative to finely spaced crenulation cleavage that transects the macroscopic F_3 folds west of Rice Lake and appears to have accommodated weak northwest–southeast shortening (present co-ordinates) during an early increment of D_5 transpression (Figure 66; early D_5). The G_5 structures include a series of generally west-northwest-trending, ductile>brittle, high-strain zones, as well as a regionally pervasive fracture or shear-band cleavage that trends northwest. The high-strain zones contain mylonitic foliations, shallowly plunging lineations, packets of strongly Z-asymmetric folds and well-developed dextral kinematic indicators on horizontal outcrop surfaces, and are interpreted to have accommodated strongly partitioned north-northwest–south-southeast shortening during main-stage D_5 transpression (Figure 66; main D_5). The G_6 structures are associated with an open, north-trending flexure of the Bidou assemblage in the Rice Lake area that may be related to a local strain perturbation in the hangingwall of the Normandy Creek Shear Zone, perhaps in response to a buttressing effect along the northwestern margin of the RRP during late-stage D_5 transpression (Figure 66; late D_5).

Economic considerations

Lode gold

Since the initial discovery of gold in 1911 on the north shore of Rice Lake, the Rice Lake greenstone belt has been the focus of considerable mining and exploration activity, focused mainly on lode gold. The belt hosts hundreds of gold occurrences, several significant deposits and past-producing mines, and the presently producing Rice Lake and SG-1 mines, which are located at Rice Lake. The geology and metallogeny of lode gold deposits in the belt has been described by numerous previous workers, beginning with the work of Moore (1914) on the initial gold discovery at Rice Lake and culminating with the belt-scale overview of Poulsen et al. (1996). Descriptions of individual deposits or occurrences in the study area, including their exploration history, can be found in the Mineral Deposits Series reports by Theyer and Yamada (1989) and Theyer (1994), and references therein. Particularly useful descriptions of the historical occurrences and deposits have also been provided by Stockwell (1938) and Davies (1953). Various aspects of the Rice Lake (a.k.a. San Antonio or Bissett) deposit are described by Reid (1931), Stockwell (1938, 1940), Bragg (1943), Gibson and Stockwell (1948), Skerl (1955), Stephenson (1972), Ames (1988), Lau (1988), Poulsen (1989), Ames et al. (1991), Lau and Brisbin (1996) and Rhys (2001). A capsule description of lode gold deposits in the study area is provided below.

In the Rice Lake area, gold mineralization is invariably hosted by quartz-carbonate vein systems in discrete brittle-ductile shear zones or complex networks of shear and tensile fractures. Although the hostrocks include a wide variety of rock types, the largest known deposits occur in tholeiitic gabbro sills (map unit 14; Rice Lake and Cartwright/Gabrielle deposits) and Fe-tholeiitic basalt flows (unit 10; SG-1 deposit) within well-stratified sections of felsic epiclastic rocks. In these deposits, significant ore also occurs at the contacts between rock types, in settings that highlight the importance of hostrock chemistry and competency contrasts in localizing ore. Dacitic volcaniclastic rocks in the upper portion of the TS unit (unit 16) host several significant deposits and occurrences (e.g., Wingold, Gold Standard). Auriferous, shear-hosted veins are found in tonalite of the Ross River plutonic suite (unit 11), both east and west of Rice Lake. Shear-hosted veins are also found in the San Antonio assemblage, although none are known to contain significant gold values (Stockwell, 1938; Davies, 1953).

In all deposits, the principal controlling structures are ductile and brittle-ductile shear zones that vary from parallel to transverse to the local anisotropy in the hostrocks and, in general, dip steeply northwest or northeast. As noted by Stockwell (1938), veins exhibit a high degree of structural control and are better developed in more competent rock types. Shear-hosted veins (Figure 67a) include massive, laminated and brecciated varieties, often within the same vein, and typically pinch and swell along strike and down-dip. Thicker veins, or portions of veins, are often associated with inflection points in the host shear zones, suggesting hydrothermal infill of dilational jogs. Most shear zones are associated with fringing arrays of kinematically linked extension and oblique-extension quartz veins (Figure 67b) that locally intensify into complex peripheral stockwork-breccia systems (Figure 67c, d). Coupled with the geometry of the vein arrays, the vein textures are indicative of synkinematic emplacement under brittle-ductile rheological conditions. Most deposits include arrays of sub-horizontal extension veins (Figure 67e), which indicate that emplacement was likely accompanied by transiently supra-lithostatic fluid pressures. In the Rice Lake deposit, the two major vein sets comprise northeast- to east-trending fault-fill veins and northwest-trending stockwork-breccia veins that are arranged in an en échelon manner along the strike and down the dip of the host gabbro sill. Individual shear-hosted veins exhibit multiple generations of fault-fill quartz, planar slip-surfaces, quartz-matrix breccia, extension veins and stylolitic pressure-

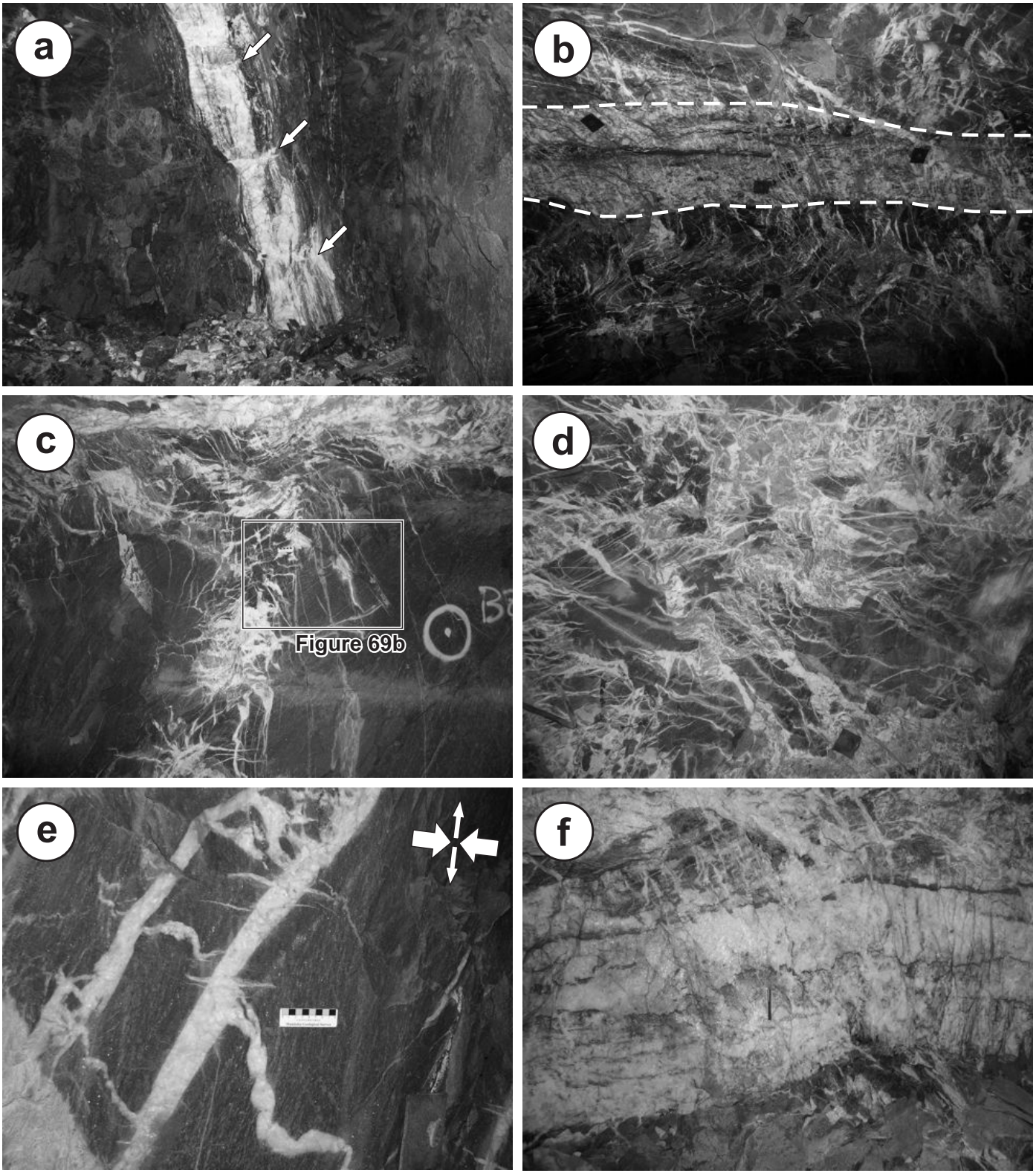

Figure 67: *Underground exposures of auriferous quartz veins in the Rice Lake mine:* ***a)*** *laminated shear-hosted vein showing insipient boudinage (arrows), 3096E subdrift, level 30 (face exposure, looking west; vein is approximately 25 cm thick);* ***b)*** *laminated shear-hosted vein (dashed lines) and complex peripheral arrays of kinematically linked extension veins; 96-vein sill drift, level 4670 (back exposure, facing south; rock-bolt plates are 15 cm square);* ***c)*** *irregular stockwork on the margin of a shear-hosed vein (visible along top edge of photo); 3096E subdrift, level 30 (wall exposure, looking southeast; field of view is approximately 2.5 m);* ***d)*** *stockwork-breccia vein; A-vein sill drift, level 4670 (back exposure, facing southeast; rock-bolt plate at lower right for scale);* ***e)*** *fault-fill quartz vein and variably deformed subhorizontal extension veins; 3098E sill drift, level 30 (wall exposure, looking east); arrows indicate the inferred kinematic frame of subhorizontal shortening and subvertical extension during vein emplacement;* ***f)*** *laminated shear-hosted vein showing multiple generations of slip surfaces, fault-fill veins and stylolitic pressure-solution seams; 2998E subdrift, level 30 (back exposure, facing south; pencil in centre for scale).*

solution seams (Figure 67f), which indicate repeated cycles of stress accumulation, dissolution, fluid-pressure build-up, shear failure, hydraulic fracturing, dilation, fluid ingress and hydrothermal sealing (i.e., fault-valve behaviour; Sibson et al., 1988; Cox, 1995). As described by Lau (1988) and Lau and Brisbin (1996), the geometry and apparent kinematics of the two major vein sets and their controlling structures indicate that the near-field maximum principal stress for each was situated in the northeast quadrant, and plunged shallowly (i.e., roughly northeast-southwest, subhorizontal shortening; present co-ordinates). A similar model was proposed by Davies (1953), based on the geometry and apparent kinematics of auriferous shear zones south of Rice Lake. In some deposits, most notably those along the Normandy Creek Shear Zone (SG-1 and SG-3), gold mineralization was intensely transposed during later ductile deformation (Figure 68a, b).

Auriferous veins in the Rice Lake area are uniformly composed of quartz, with subordinate carbonate (ankerite>calcite); minor albite, chlorite and sericite; and rare tourmaline and fuchsite. Sulphide minerals comprise mostly pyrite, with minor chalcopyrite and rare sphalerite, galena and telluride minerals (*see also* Stephenson, 1972). The pyrite generally accounts for less than 5 vol. % of individual veins and occurs as scattered crystals and irregular blebs within or along the margins of the veins, or is concentrated along planar slip surfaces or stylolitic pressure-solution seams. Gold typically occurs as free grains associated with or as minute inclusions in pyrite (Stephenson, 1972), with a typical concentration of 8–10 grams/tonne; however, gold grades tend to be highly erratic within individual veins. The gold ores are characterized by high Au:Ag ratios (>5:1) and very low concentrations of base metals (Cu, Pb, Zn) and pathfinder elements (e.g., As, Bi, B, Sb, W). Fluid-inclusion studies of vein quartz from the Rice Lake deposit (Diamond et al., 1990) indicate low-salinity aqueous-carbonic fluids. Wallrock alteration varies from negligible to intense and is typically zoned outward, from proximal albite-ankerite-sericite-quartz-pyrite through medial chlorite-ankerite±sericite to distal chlorite-calcite; these assemblages overprint the regional greenschist-facies metamorphic mineral assemblage (e.g., Ames et al., 1991). Most veins exhibit evidence of wallrock sulphidization in the form of distinct haloes of coarse euhedral pyrite (Figure 68c). In the Rice Lake deposit, thick zones of altered and sulphidized wallrock, with negligible vein quartz, locally constitute ore (Bragg, 1943). The largest deposits (Rice Lake and SG-1) exhibit a close spatial association with laterally continuous zones of relatively 'clean' ankerite-sericite phyllite and phyllonite (Figure 68d) that serve as important guides to ore. Deformation structures in the phyllonite preserve evidence of a complex kinematic history, increments of which both pre- and postdate vein emplacement (Figure 68e). In accord with deposits of this type elsewhere, the Rice Lake deposit exhibits a significant vertical extent (>2 km) yet displays negligible variation in vein mineralogy, texture and structure.

The above characteristics identify these deposits as classical 'greenstone-hosted vein' deposits, which are also known as 'mesothermal'- or 'mother lode'–type deposits (Poulsen et al., 2000). Recently, these deposits have also been termed 'orogenic' (Groves et al., 1998), to emphasize their consistent spatial association with accretionary orogens and the synkinematic and synmetamorphic timing of lode emplacement (e.g., Kerrich and Wyman, 1990; Hodgson, 1993; Kerrich and Cassidy, 1994). The preferred model for this type of deposit involves fluids generated by thermal equilibration of accreted sediments during the clockwise P-T-t evolution of accretionary orogens (e.g., Kerrich and Cassidy, 1994; McCuaig and Kerrich, 1998). The resulting fluids are thought to migrate upward along transcrustal fault systems into subsidiary brittle-ductile shear and fracture arrays in the middle to upper crust, where gold is deposited in synkinematic and synmetamorphic quartz-carbonate veins due to physical and/or chemical changes in the ore fluid brought about by pressure fluctuations, wallrock sulphidization reactions, phase separation and/or fluid mixing.

Historically, several authors have invoked nearby arc-magmatic rocks, and particularly the Ross River pluton, as the source of heat and fluids for the generation of auriferous veins at Rice Lake (i.e., syngenetic gold; e.g., Cooke, 1922; Reid, 1931; Wright, 1932; Stockwell, 1940). As described above, however, the structural styles of the veins and their hosting structures, including those within the Ross River pluton, clearly indicate synkinematic emplacement under brittle-ductile rheological conditions. Although the relative ages of individual vein systems and the various generations of regional deformation structure remain to be resolved in detail, the available data also indicate that vein emplacement occurred after a significant amount of ductile strain had accumulated in the hostrocks but prior to at least the latest increments of ductile deformation. Indeed, main-stage veins in both the Wingold and the Rice Lake deposits clearly crosscut the penetrative regional G_3 shape-fabric in the hostrocks (Figure 69a, b) and therefore postdate at least the initial strain increments recorded by this fabric (i.e., the regional D_4 deformation). Rhys (2001) concluded that the vein systems and G_3 shape-fabric (which was referred to as 'D_2' in his report) developed synchronously.

As described in the 'Structural geology' section, the G_3 shape-fabric is pervasive in the Rice Lake area and is thus constrained to postdate the ca. 2.705 Ga maximum depositional age (Percival et al., 2006a) of the San Antonio assemblage. By this constraint, the auriferous veins must postdate arc magmatism (ca. 2.715–2.745 Ga) in the Bidou assemblage by at least 10 Ma and probably considerably more, given the fact that the overlying San Antonio assemblage must have been buried to mid-crustal depths and have accumulated a significant amount of ductile strain prior to the onset of vein emplacement. Indeed, as noted by Ames et al. (1991), proximal wallrock alteration in the Rice Lake deposit overprints the regional greenschist-facies metamorphic assemblage. For these reasons, historical models that invoke fluids exsolved from the Ross River pluton are rejected as untenable; the author favours a wholly epigenetic origin for the auriferous veins in the Rice Lake district (*see also* Bailes, 1971; Stephenson, 1972; Poulsen et al., 1986; Rhys, 2001).

In keeping with epigenetic lode-gold districts elsewhere in the Superior Province, the most important district- to prospect-scale guides to ore in the Rice Lake area include: 1) the presence of chemically and/or rheologically favourable rock types; 2) evidence of structural preparation, in the form of mesoscale brittle-ductile shear zones or fracture arrays; and

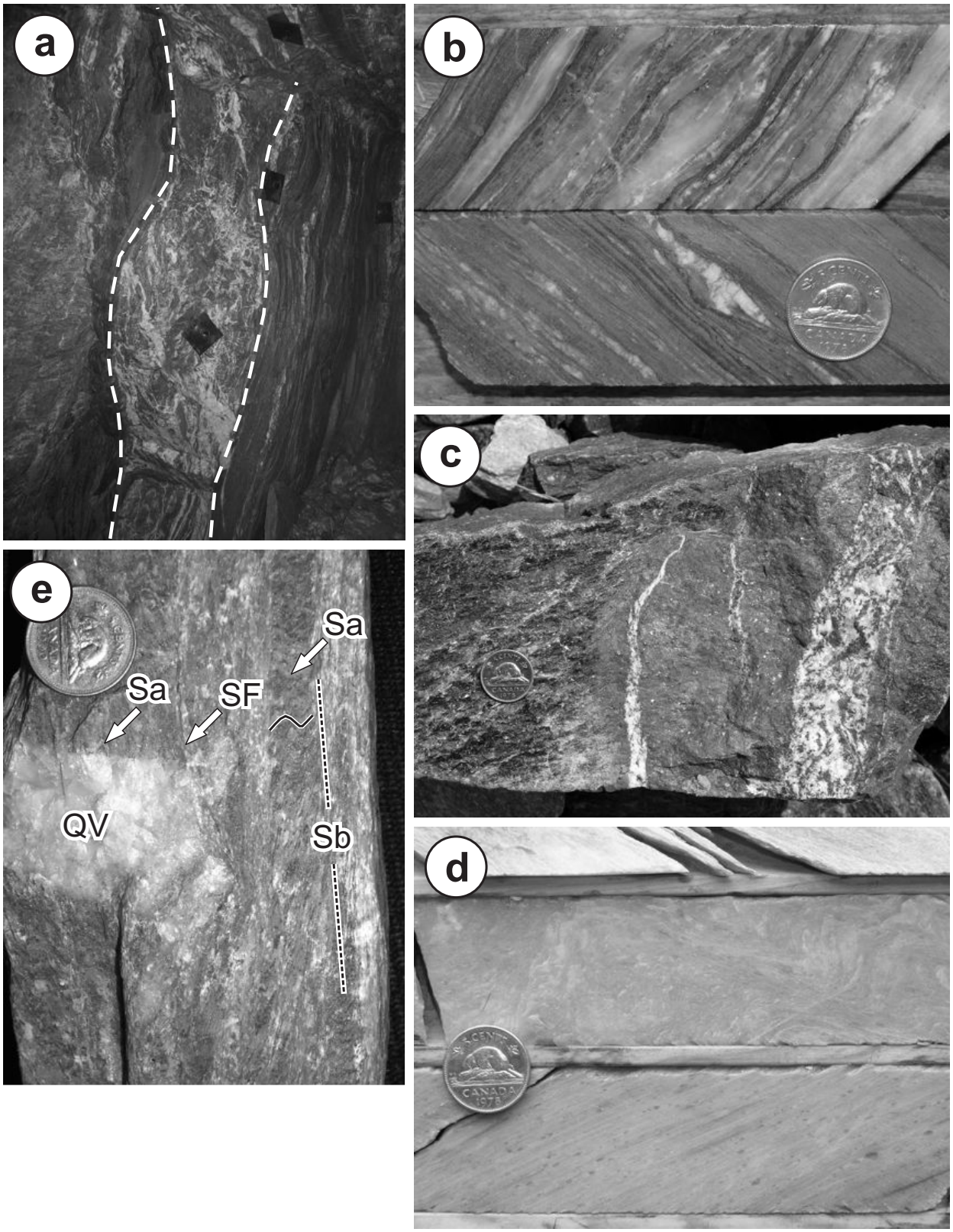

Figure 68: *Examples of gold mineralization and associated alteration in the Rice Lake area:* ***a)*** *strongly transposed and boudinaged stockwork in the SG-1 deposit (level 6E; wall exposure, looking northeast; rock-bolt plates are 15 cm square);* ***b)*** *examples of intensely deformed, high-grade gold mineralization in the SG-3 deposit (top, diamond-drill hole SN-03-11, 40.7 m; bottom, diamond-drill hole SN-03-10, 80.0 m);* ***c)*** *hand specimen from the Rice Lake deposit, showing well-developed albite-ankerite-sericite-pyrite alteration halo on narrow quartz-ankerite-pyrite veins;* ***d)*** *example of 'clean' ankerite-sericite phyllonite in the footwall of the SG-1 deposit (diamond-drill hole SG-04-3, 129–130 m);* ***e)*** *hand specimen from the Rice Lake deposit, showing evidence of a complex sequence of deformation in the footwall ankerite-sericite phyllonite; quartz-filled extension facture (QV) crosscuts early differentiated crenulation cleavage (Sb), formed via transposition of early foliation (Sa), and is crosscut by discrete ductile shear fracture (SF); sequence of events, from oldest to youngest, is as follows: Sa>Sb>QV>SF.*

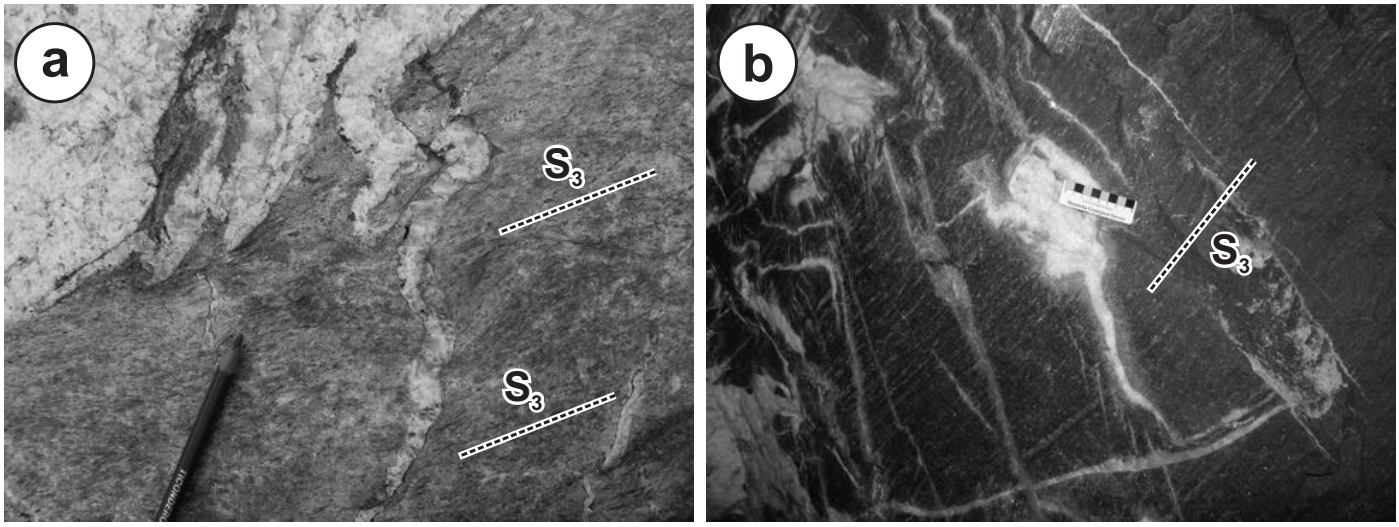

Figure 69: *Photographs of crosscutting relationships between quartz-filled extension fractures and the regional S_3 fabric on the periphery of two auriferous shear-hosted veins:* ***a)*** *Wingold deposit, surface showing (pencil points north);* ***b)*** *Rice Lake deposit, 3096E subdrift, level 30 (wall exposure, looking east; see Figure 67c for structural context). Both photographs highlight the contrast between the intense S_3 flattening fabric in the wallrock and the weakly deformed nature of the quartz-filled extension fractures.*

3) evidence of large-scale hydrothermal-fluid flow, in the form of laterally extensive alteration zones. From this perspective, two areas stand out as having a particularly favourable combination of the above-listed attributes, yet do not appear to have been the focus of previous exploration activity. The first is situated west of Rice Lake, along the wide drift-filled valley of Gold Creek, west of the San Antonio assemblage. Here, moderate to intense sericite-ankerite±pyrite alteration is observed along the northern margin of the Gold Creek Shear Zone, in scattered outcrops of intermediate epiclastic rocks of the Gold Creek (GC) unit on the south limb of the Horseshoe Lake anticline. Similar alteration is also observed 3–4 km to the southeast, along the upper contact of the San Antonio assemblage near the hinge of the Gold Creek syncline. In these locations, the GC unit includes sills and flows of tholeiitic gabbro and basalt that are chemically similar to those hosting the Rice Lake and SG-1 deposits in the Townsite (TS) and Rainy Lake road (RLR) units, respectively. In one location, the gabbro exhibits evidence of structural preparation in the form of complex arrays of chloritic shear fractures. The second target is located just east of Rice Lake in the upper portion of the RLR unit, where moderate to strong sericite-ankerite alteration is developed in a lens of heterolithic conglomerate within a thick succession of Fe-tholeiitic basalt and gabbro. The conglomerate is very highly strained, perhaps suggesting the presence of a subsidiary structure to the Normandy Creek Shear Zone, and thus a potentially analogous setting to the SG-1 deposit. In both these settings, exploration should be focused on chemically and/or rheologically favourable mafic volcanic and plutonic rocks, and particularly their contacts with adjacent volcaniclastic rocks.

Exhalative base metals

Although traditionally considered a 'gold belt', several areas of the Rice Lake greenstone belt exhibit potential for volcanic-hosted massive sulphide (VHMS) deposits. As described by Anderson (2005a), a subaerial to shallow-subaqueous rhyolitic vent complex in the Gem assemblage is composed of quartz-phyric to aphyric, high-silica rhyolite flows, coarse flow-lobe breccia units and hypabyssal intrusions (cryptodomes), with minor pumiceous pyroclastic rocks and derived epiclastic rocks. The rhyolite classifies as FII and FIIIa type in the scheme of Lesher et al. (1986), with high-field-strength-element signatures indicative of extension-related, within-plate volcanism (Anderson, 2005a). Evidence of exhalative activity is widespread, and includes occurrences of stringer-style chlorite alteration, stringer-pyrite mineralization, laminated black-chert horizons, semiconcordant sericite-pyrite alteration and sulphidic clasts in overlying epiclastic units. The Gem assemblage is interpreted to record the initiation of an arc-rift basin on the southern margin of the Bidou volcanic arc (i.e., a possible fore-arc rift; Poulsen et al., 1996) and, as such, represents a very prospective depositional setting for VHMS deposits.

In the Rice Lake area, similar evidence of VHMS potential exists in the medial portion of the RLR unit, which is interpreted to represent a relatively deep water, restricted basin that formed in the hangingwall of a synvolcanic subsidence structure located along strike to the west, in a location now occupied by an apophysis of the synvolcanic Ross River pluton (Figures 3, 5). An overlying succession of Fe-tholeiitic basalt flows and subvolcanic sills exhibits a chemical affinity to modern back-arc basin basalt and, accordingly, the RLR unit is interpreted to record an episode of arc extension associated with the initiation of a back-arc basin on the northern margin of the Bidou volcanic arc. Although chemically favourable (i.e., FII- or FIII-type) rhyolite is apparently lacking in the Rice Lake area, the RLR unit exhibits abundant evidence of exhalative activity in the form of stringer-style chlorite-garnet alteration (Figure 12b), a drill intercept of a faintly layered solid-sulphide lens composed of barren pyrite (Figure 12c; Assessment File 93163), laminated intervals of sulphidic black chert, and solid-sulphide clasts (pyrrhotite-chalcopyrite) in heterolithic debris flows (Figure 13b). These features indicate that basin infilling was at least locally accompanied by hydrothermal circulation, seafloor discharge (exhalation) and sulphide deposition close to a fault-controlled

discharge site. A grab sample of sulphide-rich pebble conglomerate, collected a few metres below the top of unit 8 in an interval of interlayered sulphidic mudstone, feldspathic wacke and heterolithic pebble conglomerate, returned 2.19 % Zn, 337 ppm Cu, 562 ppb Au, 3.5 ppm Ag, 91 ppm Pb and 440 ppm Ba — a chemical signature consistent with a base- and precious-metal–rich exhalative system. A follow-up sample, collected for assay from the reversely graded base of an 80 cm thick pebbly sandstone bed, returned 5.45% Zn and 1940 ppb Au, with negligible Cu, Pb and Ag. Mudstone rip-ups and rounded dacite pebbles in this bed are supported in a coarse-grained sandstone matrix that contains up to 60% sulphide (deep red sphalerite, with subordinate pyrite). Sharp unaltered margins on the mudstone rip-up clasts indicate transported (i.e., clastic), as opposed to *in situ* replacement, sulphide. Given the typical association of VHMS deposits with extensional geodynamic settings (e.g., Lentz, 1998; Syme, 1998; Syme et al., 1999), these data indicate significant VHMS potential in the RLR unit. The style and depositional setting of the sulphide mineralization identified by this study indicate an analogy to the Middle Jurassic Eskay Creek deposit in northwestern British Columbia (*see* Barrett and Sherlock, 1996; Roth et al., 1999).

References

Allen, R.L. 1988: False pyroclastic textures in altered silicic lavas, with implications for volcanic-associated mineralization; Economic Geology, v. 83, p. 1424–1446.

Ames, D.E. 1988: Stratigraphy and alteration of gabbroic rocks near the San Antonio gold mine in the Rice Lake area, southeastern Manitoba; M.Sc. thesis, Carleton University, Ottawa, Ontario, 202 p.

Ames, D.E., Franklin, J.M. and Froese, E. 1991: Zonation of hydrothermal alteration at the San Antonio gold mine, Bissett, Manitoba, Canada; Economic Geology, v. 86, p. 600–619.

Anderson, S.D. 2002: Preliminary report on the geology and structure of the Garner Lake area, southeast Rice Lake greenstone belt (NTS 52L14), Manitoba; *in* Report of Activities 2002, Manitoba Industry, Trade and Mines, Manitoba Geological Survey, p. 234–249.

Anderson, S.D. 2003a: Geology and structure of the Garner Lake area, southeast Rice Lake greenstone belt, Manitoba (NTS 52L14); *in* Report of Activities 2003, Manitoba Industry, Economic Development and Mines, Manitoba Geological Survey, p. 178–195.

Anderson, S.D. 2003b: Geology and structure of the Garner Lake area, southeast Rice Lake greenstone belt, Manitoba (part of NTS 52L14); Manitoba Industry, Economic Development and Mines, Manitoba Geological Survey, Preliminary Map PMAP2003-1, scale 1:20 000.

Anderson, S.D. 2004: Preliminary results and economic significance of geological mapping and structural analysis in the Rice Lake area, central Rice Lake greenstone belt, Manitoba (NTS 52M4 and 52L13); *in* Report of Activities 2004, Manitoba Industry, Economic Development and Mines, Manitoba Geological Survey, p. 216–231.

Anderson, S.D. 2005a: Preliminary results and economic significance of geological mapping in the Gem Lake area, southeastern Rice Lake belt, Manitoba (NTS 52L11 and 14), with emphasis on the Neoarchean Gem assemblage; *in* Report of Activities 2005, Manitoba Industry, Economic Development and Mines, Manitoba Geological Survey, p. 104–116.

Anderson, S.D. 2005b: Geology and structure of the Rice Lake area, Rice Lake greenstone belt, Manitoba (part of NTS 52M04 and 52L13); Manitoba Industry, Economic Development and Mines, Manitoba Geological Survey, Preliminary Map PMAP2005-1, scale 1:20 000.

Anderson, S.D. 2006a: Update and economic significance of geological mapping in the Garner–Gem lakes area, Rice Lake greenstone belt, southeastern Manitoba (NTS 52L11 and 14); *in* Report of Activities 2006, Manitoba Science, Technology, Energy and Mines, Manitoba Geological Survey, p. 155–169.

Anderson, S.D. 2006b: Geology and structure of the Garner–Gem lakes area, Rice Lake greenstone belt, Manitoba (NTS 52L11 and 14); Manitoba Science, Technology, Energy and Mines, Manitoba Geological Survey, Preliminary Map PMAP2006-7, scale 1:20 000.

Anderson, S.D. 2007: Stratigraphic and structural setting of gold mineralization in the Lily Lake area, Rice Lake greenstone belt, Manitoba (NTS 52L11, 14); *in* Report of Activities 2007, Manitoba Science, Technology, Energy and Mines, Manitoba Geological Survey, p. 114–128.

Bailes, A.H. 1971: Geology and geochemistry of the Pilot-Smuggler shear zone, Rice Lake region, southeastern Manitoba; *in* Geology and Geophysics of the Rice Lake Region, Southeastern Manitoba (Project Pioneer), W.D. McRitchie and W. Weber (ed.), Manitoba Department of Mines and Natural Resources, Mines Branch, Publication 71-1, p. 299–312.

Bailes, A.H. 1998: Geochemical sampling of the Bidou Lake subgroup of the Rice Lake greenstone belt; *in* Report of Activities 1998, Manitoba Energy and Mines, Geological Services, p. 144–150.

Bailes, A.H. 1999: Geochemical sampling and geological reconnaissance of the western Rice Lake greenstone belt; *in* Report of Activities 1999, Manitoba Industry, Trade and Mines, Geological Services, p. 102–105.

Bailes, A.H. and Percival, J.A. 2000: Geology and structure of the North Caribou Terrane–Uchi Subprovince boundary in eastern Manitoba, with emphasis on volcanic and volcaniclastic rocks of the Black Island assemblage; *in* Report of Activities 2000, Manitoba Industry, Trade and Mines, Manitoba Geological Survey, p. 161–174.

Bailes, A.H. and Percival, J.A. 2005a: Geology of the Black Island area, Lake Winnipeg, Manitoba (parts of NTS 62P1, 7 and 8); Manitoba Industry, Economic Development and Mines, Manitoba Geological Survey, Geoscientific Report GR2005-2, 33 p.

Bailes, A.H. and Percival, J.A. 2005b: Lithogeochemical and lithological data, Sm-Nd isotopic data and geochronological data for the Black Island area, Lake Winnipeg, Manitoba (parts of NTS 62P1, 7 and 8) and the Rice Lake greenstone belt (parts of NTS 62P, 52M and 52L); Manitoba Industry, Economic Development and Mines, Manitoba Geological Survey, Data Repository Item DRI2005004, http://www.gov.mb.ca/stem/mrd/info/libmin/DRI2005004.xls, Microsoft® Excel® file.

Bailes, A.H. and Syme, E.C. 1989: Geology of the Flin Flon–White Lake area; Manitoba Energy and Mines, Geological Services, Geological Report GR87-1, 313 p.

Bailes, A.H., Percival, J.A., Corkery, M.T., McNicoll, V.J., Tomlinson, K.Y., Sasseville, C., Rogers, N., Whalen, J.B. and Stone, D. 2003: Geology and tectonostratigraphic assemblages, West Uchi map area, Manitoba and Ontario; Manitoba Geological Survey, Open File Report OF2003-1, 1:250 000 scale with marginal notes.

Barrett, T.J. and MacLean, W.H. 1994: Chemostratigraphy and hydrothermal alteration in exploration for VHMS deposits in greenstones and younger volcanic rocks; *in* Alteration and Alteration Processes Associated with Ore-Forming Systems, D.R. Lentz (ed.), Geological Association of Canada, Short Course Notes, v. 11, p. 433–467.

Barrett, T.J. and Sherlock, R.L. 1996: Geology, lithogeochemistry and volcanic setting of the Eskay Creek Au-Ag-Cu-Zn deposit, northwestern British Columbia; Exploration and Mining Geology, v. 5, p. 339–368.

Barrie, C.T., Ludden, J.M. and Green, T.H. 1993: Geochemistry of volcanic rocks associated with Cu-Zn and Ni-Cu deposits in the Abitibi Subprovince; Economic Geology, v. 88, p. 1341–1358.

Beacom, L.E., Anderson, T.B. and Holdsworth, R.E. 1999: Using basement-hosted clastic dykes as syn-rifting palaeostress indicators: an example from the basal Stoer Group, northwest Scotland; Geological Magazine, v. 136, p. 301–310.

Bragg, J.G. 1943: Rock alteration at the San Antonio mine; Canadian Mining Journal, v. 64, p. 553–556.

Brommecker, R., Scoates, R.F.J. and Poulsen, K.H. 1993: Komatiites in the Garner Lake–Beresford Lake area: implications for tectonics and gold metallogeny of the Rice Lake greenstone belt, southeast Manitoba; *in* Current Research, Part C, Geological Survey of Canada, Paper 93-1C, p. 259–264.

Brown, M. 2006: Duality of thermal regimes is the distinctive characteristic of plate tectonics since the Neoarchean; Geology, v. 34, p. 961–964.

Bruhn, R.L., Parry, W.T., Yonkee, W.A. and Thompson, T. 1994: Fracturing and hydrothermal alteration in normal fault zones; Pure and Applied Geophysics, v. 142, p. 609–644.

Cabanis, B. and Lecolle, M. 1989: Le diagramme La/10-Y/15-Nb/8: un outil pour la discrimination des series volcaniques et la mise en evidence des processus de mélange et/ou de contamination crustale; Comptes Rendus de l'Academie des Sciences, v. 309, p. 2023–2029.

Campbell, F.H.A. 1971: Stratigraphy and sedimentation of part of the Rice Lake Group, Manitoba; *in* Geology and Geophysics of the Rice Lake Region, Southeastern Manitoba (Project Pioneer), W.D. McRitchie and W. Weber (ed.), Manitoba Department of Mines and Natural Resources, Mines Branch, Publication 71-1, p. 135–188.

Card, K.D. 1990: A review of the Superior Province of the Canadian Shield, a product of Archean accretion; Precambrian Research, v. 48, p. 99–156.

Card, K.D. and Ciesielski, A. 1986: Subdivisions of the Superior Province of the Canadian Shield; Geoscience Canada, v. 13, p. 5–13.

Cas, R.A.F. 1979: Mass-flow arenites from a Palaeozoic interarc basin, New South Wales, Australia: mode and environment of emplacement; Journal of Sedimentary Petrology, v. 49, p. 29–44.

Cas, R.A.F. 1983: Submarine 'crystal tuffs': their origin using a Lower Devonian example from southeastern Australia; Geological Magazine, v. 120, p. 471–486.

Cas, R.A.F. and Wright, J.V. 1987: Volcanic successions, modern and ancient: a geological approach to processes, products and successions; Unwin Hyman Ltd., London, United Kingdom, 528 p.

Cooke, H.C. 1922: Geology and mineral resources of Rice Lake and Oiseau River areas, Manitoba; Canada Department of Mines, Geological Survey, Summary Report, 1921, Part C, 36 p.

Corfu, F., Stott, G.M. and Breaks, F.W. 1995: U-Pb geochronology and evolution of the English River Subprovince, an Archean low P-high T metasedimentary belt in the Superior Province; Tectonics, v. 14, p. 1220–1233.

Cox, S.F. 1995: Faulting processes at high fluid pressures: an example of fault valve behaviour from the Wattle Gully Fault, Victoria, Australia; Journal of Geophysical Research, v. 100, p. 12 841–12 859.

Davies, J.F. 1949: Geology of the Wanipigow Lake area, Rice Lake Mining Division, Manitoba; Manitoba Department of Mines and Natural Resources, Mines Branch, Publication 48-2, 14 p.

Davies, J.F. 1950: Geology of the Wanipigow River area, Rice Lake Mining Division, Manitoba; Manitoba Department of Mines and Natural Resources, Mines Branch, Publication 49-3, 21 p.

Davies, J.F. 1953: Geology and gold deposits of southern Rice Lake area; Manitoba Department of Mines and Natural Resources, Mines Branch, Publication 52-1, 41 p.

Davies, J.F. 1963: Geology and gold deposits of the Rice Lake–Wanipigow River area, Manitoba; Ph.D. thesis, University of Toronto, Ontario, 142 p.

Davis, D.W. 1994: Report on the geochronology of rocks from the Rice Lake belt, Manitoba; Royal Ontario Museum, Geology Department, Toronto, Ontario, unpublished report.

Davis, D.W. 1996: Provenance and depositional age constraints on sedimentation in the Western Superior Transect area from U-Pb ages of zircons; *in* LITHOPROBE Western Superior Transect, Report of Second Annual Workshop, R.M. Harrap and H. Helmstaedt (ed.), LITHOPROBE Secretariat, University of British Columbia, Report 53, p. 18–23.

Defant, M.J. and Drummond, M.S. 1990: Derivation of some modern arc magmas by melting of young subducted lithosphere; Nature, v. 347, p. 662–665.

De Lury, J.S. 1927: The mineral resources of southeastern Manitoba, Rice Lake District, Oiseau River District, Boundary District; Industrial Development Board of Manitoba, Winnipeg, Manitoba, 55 p.

de Wit, M.J. 1998: On Archean granites, greenstones, cratons and tectonics: does the evidence demand a verdict?; Precambrian Research, v. 91, p. 181–226.

Diamond, L.W., Marshall, D.D., Jackman, J.A. and Skippen, G.B. 1990: Elemental analysis of individual fluid inclusions in minerals by secondary ion mass spectrometry (SIMS): application to cation ratios of fluid inclusions in an Archaean mesothermal gold-quartz vein; Geochimica et Cosmochimica Acta, v. 54, p. 545–552.

Dimroth, E., Cousineau, P., Leduc, M. and Sanschagrin, Y. 1978: Structure and organization of Archean subaqueous basalt flows, Rouyn-Noranda area, Quebec, Canada; Canadian Journal of Earth Sciences, v. 15, p. 902–918.

Dresser, J.A. 1917: Gold-bearing district of southeastern Manitoba; *in* Summary Report of the Geological Survey, Department of Mines, for the calendar year 1916, Sessional Paper No. 26, p. 169–175.

Drummond, M.S. and Defant, M.J. 1990: A model for trondhjemite-tonalite-dacite genesis and crustal growth via slab melting: Archean to modern comparisons; Journal of Geophysical Research, v. 95, p. 21 503–21 521.

Fedikow, M.A.F. 1983: Geochemical studies at the San Antonio gold mine, Bissett, Manitoba; *in* Report of Field Activities 1983, Manitoba Department of Energy and Mines, Mineral Resources Division, p. 107–109.

Fisher, R.V. 1961: Proposed classification of volcaniclastic sediments and rocks; Geological Society of America Bulletin, v. 72, p. 1409–1414.

Fisher, R.V. 1966: Rocks composed of volcanic fragments and their classification; Earth-Science Reviews, v. 1, p. 287–298.

Furnes, H., de Wit, M., Staudigel, H., Rosing, M. and Muehlenbachs, K. 2007: A vestige of Earth's oldest ophiolite; Science, v. 315, p. 1704–1707.

Geological Survey of Canada 1986: Manitoba (Flin Flon) – Area 300 Bisset, aeromagnetic survey; Geological Survey of Canada, Geoscience Data Repository (available on-line at http://gdrdap.agg.nrcan.gc.ca/geodap/index_e.html).

George, P.T. 2006: Mineral resource and mineral reserve estimates as of December 1, 2006, Rice Lake project, Rice Lake greenstone belt, Bissett, Manitoba, Canada, for San Gold Corporation; A.C.A. Howe International Ltd., Report 902, 160 p.

Gibson, H.L., Morton, R.L. and Hudak, G.J. 1999: Submarine volcanic processes, deposits, and environments favourable for the location of volcanic-associated massive sulphide deposits; *in* Volcanic Associated Massive Sulphide Deposits: Processes and Examples in Modern and Ancient Settings; C.T. Barrie and M.D. Hannington (ed.), Reviews in Economic Geology, Volume 8, p. 13–51.

Gibson, J.C. and Stockwell, C.H. 1948: San Antonio mine; *in* Structural Geology of Canadian Ore Deposits, Canadian Institute of Mining and Metallurgy, Geology Division, Symposium Volume, p. 315–321.

Goldstein, S.L., O'Nions, R.K. and Hamilton, P.J. 1984: A Sm–Nd study of atmospheric dusts and particulates from major river systems; Earth and Planetary Science Letters, v. 70, p. 221–236.

Groves, D.I., Goldfarb, R.J., Gebre-Mariam, M., Hagemann, S.G. and Robert, F. 1998: Orogenic gold deposits: a proposed classification in the context of their crustal distribution and relationship to other gold deposit types; Ore Geology Reviews, v. 13, p. 7–27.

Hamilton, W.B. 1998: Archean magmatism and deformation were not products of plate tectonics; Precambrian Research, v. 91, p. 143–179.

Hamilton, W.B. 2003: An alternative Earth; GSA Today, v. 13, no. 11, p. 4–12.

Hart, T.R., Gibson, H.L. and Lesher, C.M. 2004: Trace element geochemistry and petrogenesis of felsic volcanic rocks associated with volcanogenic massive Cu-Zn-Pb sulphide deposits; Economic Geology, v. 99, p. 1003–1013.

Heaman, L.M., Erdmer, E. and Owen, J.V. 2002: U-Pb geochronologic constraints on the crustal evolution of the Long Range Inlier, Newfoundland; Canadian Journal of Earth Sciences, v. 39, p. 845–865.

Henderson, P.J. 1994: Surficial geology and drift composition of the Bissett–English Brook area, Rice Lake greenstone belt, southeastern Manitoba; Geological Survey of Canada, Open File 2910, 190 p.

Hodgson, C.J. 1993: Mesothermal lode-gold deposits; *in* Mineral Deposit Modeling, R.V. Kirkham, W.D. Sinclair, R.I. Thorpe and J.M. Duke (ed.), Geological Association of Canada, Special Paper 40, p. 635–678.

Hollings, P. and Kerrich, R. 2000: An Archean arc basalt–Nb-enriched basalt–adakite association: the 2.7 Ga Confederation assemblage of the Birch-Uchi greenstone belt, Superior Province; Contributions to Mineralogy and Petrology, v. 139, p. 208–226.

Hollings, P., Wyman, D. and Kerrich, R. 1999: Komatiite-basalt-rhyolite volcanic associations in northern Superior Province greenstone belts: significance of plume-arc interaction in the generation of the proto continental Superior Province; Lithos, v. 46, p. 137–161.

Irvine, T.N. and Baragar, W.R.A. 1971: A guide to the chemical classification of the common volcanic rocks; Canadian Journal of Earth Sciences, v. 8, p. 523–548.

Jensen, L.S. 1976: A new cation plot for classifying subalkaline volcanic rocks; Ontario Geological Survey, Miscellaneous Paper 66, 22 p.

Jolly, R.J.H. and Lonergan, L. 2002: Mechanisms and controls on the formation of sand intrusions; Journal of the Geological Society, v. 159, p. 605–617.

Jonk, R., Kelly, J. and Parnell, J. 2004: The origin and tectonic significance of Lewisian- and Torridonian-hosted clastic dykes near Gairloch, NW Scotland; Scottish Journal of Geology, v. 40, p. 123–130.

Kay, R.W. 1978: Aleutian magnesian andesites: melts from subducted Pacific Ocean crust; Journal of Volcanology and Geothermal Research, v. 4, p. 177–132.

Kerrich, R. and Cassidy, K.F. 1994: Temporal relationships of lode gold mineralization to accretion, magmatism, metamorphism and deformation — Archean to present: a review; Ore Geology Reviews, v. 9, p. 263–310.

Kerrich, R. and Wyman, D. 1990: Geodynamic setting of mesothermal gold deposits: an association with accretionary tectonic regimes; Geology, v. 18, p. 882–885.

Kremer, P.D. 2004: An Archean unconformity at the base of the San Antonio formation: implications for gold mineralization in the Rice Lake greenstone belt, southeastern Manitoba; B.Sc. thesis, University of Manitoba, Winnipeg, Manitoba, 44 p.

Krogh, T.E., Ermanovics, I.F. and Davis, G.L. 1974: Two episodes of metamorphism and deformation in the Archean rocks of the Canadian shield; *in* Carnegie Institution of Washington, Geophysical Laboratory Yearbook, p. 573–575.

Langford, F.F. and Morin, J.A. 1976: The development of the Superior Province of northwestern Ontario by merging island arcs; American Journal of Science, v. 276, p. 1023–1034.

Lau, M.H.S. 1988: Structural geology of the vein system in the San Antonio gold mine, Bissett, Manitoba, Canada; M.Sc. thesis, University of Manitoba, Winnipeg, Manitoba, 154 p.

Lau, M.H.S. and Brisbin, W.C. 1996: Structural geology of the San Antonio mine, Bissett, Manitoba; Geological Survey of Canada, Open File 1699, 65 p.

Le Bas, M.J., Le Maitre, R.W., Streckeisen, A. and Zanettin, B. 1986: A chemical classification of volcanic rocks based on the total alkali-silica diagram; Journal of Petrology, v. 27, p. 745–750.

Lemkow, D.R., Sanborn-Barrie, M., Bailes, A.H., Percival, J.A., Rogers, N., Skulski, T., Anderson, S.D., Tomlinson, K.Y., McNicoll, V., Parker, J.R., Whalen, J.B., Hollings, P. and Young, M. 2006: GIS compilation of geology and tectonostratigraphic assemblages, western Uchi Subprovince, western Superior Province, Ontario and Manitoba; Manitoba Geological Survey, Open File Report OF2006-30, CD-ROM.

Lentz, D.R. 1998: Petrogenetic evolution of felsic volcanic sequences associated with Phanerozoic volcanic-hosted massive sulphide systems: the role of extensional geodynamics; Ore Geology Reviews, v. 12, p. 289–327.

Lesher, C.M., Goodwin, A.M., Campbell, I.H. and Gorton, M.P. 1986: Trace-element geochemistry of ore-associated and barren, felsic metavolcanic rocks in the Superior Province, Canada; Canadian Journal of Earth Sciences, v. 23, p. 222–237.

Ludwig, K.R. 2003: Isoplot 3.00: a geochronological toolkit for Microsoft® Excel®; Berkeley Geochronological Center, Special Publication No. 4, 71 p.

Martin, H. 1999: Adakitic magmas: modern analogues of Archaean granitoids; Lithos, v. 46, p. 411–429.

Martin, H., Smithies, R.H., Rapp, R., Moyen, J-F. and Champion, D. 2005: An overview of adakite, tonalite-trondhjemite-granodiorite (TTG), and sanukitoid: relationships and some implications for crustal evolution; Lithos, v. 79, p. 1–24.

Mattinson, J.M. 2005: Zircon U-Pb chemical abrasion ('CA-TIMS') method: combined annealing and multi-step partial dissolution analysis for improved precision and accuracy of zircon ages; Chemical Geology, v. 220, p. 47–66.

McCall, G.J.H. 2003: A critique of the analogy between Archean and Phanerozoic tectonics based on regional mapping of the Mesozoic-Cenozoic plate convergent zone in the Makran, Iran; Precambrian Research, v. 127, p. 5–17.

McCuaig, T.C. and Kerrich, R. 1998: P–T–t–deformation–fluid characteristics of lode gold deposits: evidence from alteration systematics; Ore Geology Reviews, v. 12, p. 381–453.

McPhie, J., Doyle, M. and Allen, R. 1993: Volcanic Textures: A Guide to the Interpretation of Textures in Volcanic Rocks; Centre for Ore Deposit and Exploration Studies, University of Tasmania, 198 p.

McRitchie, W.D. 1971: Geology of the Wallace Lake–Siderock Lake area: a reappraisal; *in* Geology and Geophysics of the Rice Lake Region, Southeastern Manitoba (Project Pioneer), W.D. McRitchie and W. Weber (ed.), Manitoba Department of Mines and Natural Resources, Mines Branch, Publication 71-1, p. 107–125.

McRitchie, W.D. and Weber, W. 1971a: Geology and geophysics of the Rice Lake region, southeastern Manitoba (Project Pioneer), W.D. McRitchie and W. Weber (ed.), Manitoba Department of Mines and Natural Resources, Mines Branch, Publication 71-1, 430 p.

McRitchie, W.D. and Weber, W. 1971b: Metamorphism and deformation in the Manigotagan Gneissic Belt, south-eastern Manitoba; *in* Geology and Geophysics of the Rice Lake Region, Southeastern Manitoba (Project Pioneer), W.D. McRitchie and W. Weber (ed.), Manitoba Department of Mines and Natural Resources, Mines Branch, Publication 71-1, p. 235–284.

Moore, E.S. 1914: Region east of the south end of Lake Winnipeg; *in* Summary Report of the Geological Survey, Department of Mines, for the calendar year 1912, Sessional Paper No. 26, p. 262–270.

Paulus, G.E. and Turnock, A.C. 1971: Petrography of the Ross River pluton, Manitoba; *in* Geology and Geophysics of the Rice Lake Region, Southeastern Manitoba (Project Pioneer), W.D. McRitchie and W. Weber (ed.), Manitoba Department of Mines and Natural Resources, Mines Branch, Publication 71-1, p. 215–225.

Pearce, J.A. 1996: A user's guide to basalt discrimination diagrams; *in* Trace Element Geochemistry of Volcanic Rocks: Applications for Massive Sulphide Exploration, D.A. Wyman, (ed.), Geological Association of Canada, Short Course Notes, v. 12, p. 79–113.

Pearce, J.A. and Peate, D.W. 1995: Tectonic implications of the composition of volcanic arc magmas; Annual Review of Earth and Planetary Sciences, v. 23, p. 251–285.

Pearce, J.A., Harris, N.B.W. and Tindle, A.G. 1984: Trace element discrimination diagrams for the tectonic interpretation of granitic rocks; Journal of Petrology, v. 25, p. 956–983.

Percival, J.A., Bailes, A. and McNicoll, V. 2002: Mesoarchean breakup, Neoarchean accretion in the western Superior craton, Lake Winnipeg, Canada; Geological Association of Canada–Mineralogical Association of Canada, Joint Annual Meeting, May 30–June 2, 2002, Saskatoon, Saskatchewan, Field Trip B3 Guidebook, 42 p.

Percival, J.A., McNicoll, V. and Bailes, A.H. 2006a: Strike-slip juxtaposition of ca. 2.72 Ga juvenile arc and >2.98 Ga continent margin sequences and its implications for Archean terrane accretion, western Superior Province, Canada; Canadian Journal of Earth Sciences, v. 43, p. 895–927.

Percival, J.A., Sanborn-Barrie, M., Skulski, T., Stott, G.M., Helmstaedt, H. and White, D.J. 2006b: Tectonic evolution of the western Superior Province from NATMAP and LITHOPROBE studies; Canadian Journal of Earth Sciences, v. 43, p. 1085–1117.

Pettijohn, F.J. 1975: Sedimentary Rocks, Third Edition; Harper & Row, 628 p.

Polat, A. and Kerrich, R. 2001: Magnesian andesites, Nb-enriched basalt-andesites, and adakites from late-Archean 2.7 Ga Wawa greenstone belts, Superior Province, Canada: implications for late Archean subduction zone petrogenetic processes; Contributions to Mineralogy and Petrology, v. 141, p. 36–52.

Poulsen, K.H. 1987: Structural and alteration studies, Bissett area; *in* Report of Field Activities 1987, Manitoba Energy and Mines, Minerals Division, p. 169–170.

Poulsen, K.H. 1989: Structure and hydrothermal alteration, Rice Lake gold district, southeastern Manitoba; *in* Investigations by the Geological Survey of Canada in Manitoba and Saskatchewan during the 1984-1989 Mineral Development Agreements, A.G. Galley (comp.), Geological Survey of Canada, Open File 2133, p. 42–49.

Poulsen, K.H., Ames, D.E., Lau, S. and Brisbin, W.C. 1986: Preliminary report on the structural setting of gold in the Rice Lake area, Uchi Subprovince, southeastern Manitoba; *in* Current Research, Part B, Geological Survey of Canada, Paper 86-1B, p. 213–221.

Poulsen, K.H., Robert, F. and Dubé, B. 2000: Geological classification of Canadian gold deposits; Geological Survey of Canada, Bulletin 540, 106 p.

Poulsen, K.H., Weber, W., Brommecker, R. and Seneshen, D.N. 1996: Lithostratigraphic assembly and structural setting of gold mineralization in the eastern Rice Lake greenstone belt, Manitoba; Geological Association of Canada–Mineralogical Association of Canada, Joint Annual Meeting, May 27–29, 1996, Winnipeg, Manitoba, Field Trip A4 Guidebook, 106 p.

Poulsen, K.H., Weber, W., Garson, D.F. and Scoates, R.F.J. 1994: New geological observations in the Rice Lake belt, southeastern Manitoba; *in* Report of Activities 1994, Manitoba Energy and Mines, Geological Services, p. 163–166.

Reid, J.A. 1931: The geology of the San Antonio gold mine, Rice Lake, Manitoba; Economic Geology, v. 26, p. 644–661.

Rhys, D.A. 2001: Report on a structural geology study of the San Antonio mine, Bissett, Manitoba; Harmony Gold (Canada) Inc., internal company report, 74 p.

Richards, J.P. and Kerrich, R. 2007: Adakite-like rocks: their diverse origins and questionable role in metallogenesis; Economic Geology, v. 102, p. 537–576.

Rogers, N. 2001: Preliminary report on the stratigraphy and structure of the Bee Lake greenstone belt, Superior Province, northwestern Ontario; Geological Survey of Canada, Current Research 2001-C17, 17 p.

Rogers, N. 2003: Geology, Bee Lake greenstone belt, Ontario-Manitoba; Geological Survey of Canada, Open File 4315, scale 1:50 000.

Roth, T., Thompson, J.F.H. and Barrett, T.J. 1999: The precious metal–rich Eskay Creek deposit, northwestern British Columbia; *in* Volcanic Associated Massive Sulphide Deposits: Processes and Examples in Modern and Ancient Settings; C.T. Barrie and M.D. Hannington (ed.), Reviews in Economic Geology, v. 8, p. 357–373.

Sanborn-Barrie, M., Skulski, T. and Parker, J. 2001: Three hundred million years of tectonic history recorded by the Red Lake greenstone belt, Ontario; Geological Survey of Canada, Current Research 2001-C19, 19 p.

Sasseville, C., Tomlinson, K.Y., Hynes, A. and McNicoll, V. 2006: Stratigraphy, structure, and geochronology of the 3.0–2.7 Ga Wallace Lake greenstone belt, western Superior Province, southeast Manitoba, Canada; Canadian Journal of Earth Sciences, v. 43, p. 929–945.

Schmidberger, SS., Heaman, L.M., Simonetti, A., Creaser, R.A. and Whiteford, S. 2007: Lu-Hf, *in-situ* Sr and Pb isotope and trace element systematics for mantle eclogites from the Diavik diamond mine: evidence for Paleoproterozoic subduction beneath the Slave craton, Canada; Earth and Planetary Science Letters, v. 254, p. 55–68.

Schmidtke, R.H. 1984: Mineral deposit documentation in the Bissett area; *in* Report of Field Activities 1984, Manitoba Energy and Mines, Mineral Resources, p. 92–99.

Selley, R.C. 1988: Applied Sedimentology; Academic Press Ltd., London, United Kingdom, 446 p.

Seneshen, D.M. and Owens, D.J. 1985: Geological investigations in the Stormy Lake area; *in* Report of Field Activities 1985, Manitoba Energy and Mines, Geological Services/Mines Branch, p. 112–119.

Shirey, S.B. and Hanson, G.N. 1984: Mantle derived Archaean monzodiorites and trachyandesites; Nature, v. 310, p. 222–224.

Sibson, R.H., Robert, F. and Poulsen, K.H. 1988: High-angle reverse faults, fluid-pressure cycling, and mesothermal gold-quartz deposits; Geology, v. 16, p. 551–555.

Simonetti, A., Heaman, L.M., Hartlaub, R.P., Creaser, R.A., MacHattie, T.G. and Böhm, C. 2005: U-Pb zircon dating by laser ablation-MC-ICP-MS using a new multiple ion counting Faraday collector array; Journal of Analytical Atomic Spectrometry, v. 20, p. 677–686.

Sinton, J.M. and Fryer, P. 1987: Mariana Trough lavas from 18°N: implications for the origin of back arc basin basalts; Journal of Geophysical Research, v. 92, no. B12, p. 12782–12802.

Sircombe, K.N. 2004: AgeDisplay: an EXCEL workbook to evaluate and display univariate geochronological data using binned frequency histograms and probability density distributions; Computers and Geosciences, v. 30, p. 21–31.

Skerl, A.C. 1955: A study of the structural setting of the San Antonio gold mine; San Antonio Gold Mines Ltd., internal company report, 45 p.

Skulski, T., Corkery, M.T., Stone, D., Whalen, J.B. and Stern, R.A. 2000: Geological and geochronological investigations in the Stull Lake–Edmund Lake greenstone belt and granitoid rocks of the northwestern Superior Province; *in* Report of Activities 2000, Manitoba Industry, Trade and Mines, Manitoba Geological Survey, p. 117–128.

Smithies, R.H. and Champion, D.C. 2000: The Archean high-Mg diorite suite: links to tonalite-trondhjemite-granodiorite magmatism and implications for Early Archaean crustal growth; Journal of Petrology, v. 41, p. 1653–1671.

Stacey, J.S. and Kramers, J.D. 1975: Approximation of terrestrial lead isotope evolution by a two-stage model; Earth and Planetary Science Letters, v. 26, p. 207–221.

Stephenson, J.F. 1972: Gold deposits of the Rice Lake–Beresford Lake area, southeastern Manitoba; Ph.D. thesis, University of Manitoba, Winnipeg, 294 p.

Stern, R. 1989: Petrogenesis of the Archaean Sanukitoid Suite; State University at Stony Brook, New York, 275 p.

Stern, R.A., Hanson, G.N. and Shirey, S.B. 1989: Petrogenesis of mantle-derived, LILE-enriched Archean monzodiorites and trachyandesites (sanukitoids) in southwestern Superior Province; Canadian Journal of Earth Sciences, v. 26, p. 1688–1712.

Stern, R.J. 2005: Evidence from ophiolites, blueschists, and ultrahigh-pressure metamorphic terranes that the modern episode of subduction tectonics began in Neoarchean time; Geology, v. 33, p. 557–560.

Stockwell, C.H. 1938: Rice Lake–Gold Lake area, southern Manitoba; Canada Department of Mines and Resources, Geological Survey, Memoir 210, 79 p.

Stockwell, C.H. 1940: Gold mines and prospects in Rice Lake–Beresford Lake area, Manitoba; Transactions of the Canadian Institute of Mining and Metallurgy, v. 43, p. 613–626.

Stockwell, C.H. 1945: Rice Lake; Geological Survey of Canada, Map 810A, scale 1:63 360.

Stott, G.M. and Corfu, F. 1991: Uchi Subprovince; *in* Geology of Ontario, P.C. Thurston, H.R. Williams, R.H. Sutcliffe and G.M. Stott, (ed.), Ontario Geological Survey, Special Volume 4, Part 1, p. 145–236.

Sun, S.-S. and McDonough, W.F. 1989: Chemical and isotopic systematics of oceanic basalts: implications for mantle composition and processes; *in* Magmatism in the Ocean Basins, A.D. Saunders and M.J. Norry, (ed.), Geological Society of London, Special Publication 42, p. 313–345.

Syme, E.C. 1998: Ore-associated and barren rhyolites in the central Flin Flon belt: case study of the Flin Flon mine sequence; Manitoba Energy and Mines, Geological Services, Open File Report OF98-9, 26 p.

Syme, E.C., Lucas, S.B., Bailes, A.H. and Stern, R.A. 1999: Contrasting arc and MORB-like assemblages in the Paleoproterozoic Flin Flon Belt, Manitoba, and the role of intra-arc extension in localizing volcanic-hosted massive sulphide deposits; Canadian Journal of Earth Sciences, v. 36, p. 1767–1788.

Theyer, P. 1983: Geology of gold environments in the Bissett/Wallace Lake portion of the Rice Lake greenstone belt; *in* Report of Field Activities 1983, Manitoba Department of Energy and Mines, Mineral Resources Division, p. 101–106.

Theyer, P. 1984: Mineral deposit investigations in the Rice Lake greenstone belt; *in* Report of Field Activities 1984, Manitoba Energy and Mines, Mineral Resources, p. 87–91.

Theyer, P. 1994: Mineral deposits and occurrences in the Bissett area, NTS 52M/4; Manitoba Energy and Mines, Geological Services, Mineral Deposit Series, Report 18, 101 p.

Theyer, P. and Yamada, P.H. 1989: Mineral deposits and occurrences in the Manigotagan Lake area, NTS 52L/13; Manitoba Energy and Mines, Geological Services, Mineral Deposit Series, Report 4, 108 p.

Thurston, P.C., Osmani, I.A. and Stone, D. 1991: Northwestern Superior Province: review and terrane analysis; *in* Geology of Ontario, P.C. Thurston, H.R. Williams, R.H. Sutcliffe and G.M. Stott (ed.), Ontario Geological Survey, Special Volume 4, Part 1, p. 81–142.

Tirschmann, P.A. 1986: Physical volcanology and sedimentology of part of the Archean Rice Lake Group, Rice Lake greenstone belt, southeastern Manitoba; B.Sc. thesis, University of Manitoba, Winnipeg, Manitoba, 99 p.

Tobisch, O.T. and Paterson, S.R. 1988: Analysis and interpretation of composite foliations in areas of progressive deformation; Journal of Structural Geology, v. 10, p. 745–754.

Turek, A. and Weber, W. 1991: New U-Pb zircon ages from the Rice Lake area: evidence for 3 Ga crust; *in* Manitoba Energy and Mines, Minerals Division, Report of Activities, 1991, p. 53–55.

Turek, A., Keller, R., Van Schmus, W.R. and Weber, W. 1989: U-Pb zircon ages for the Rice Lake area, southeastern Manitoba; Canadian Journal of Earth Sciences, v. 26, p. 23–30.

Unterschutz, J.L.E., Creaser, R.A., Erdmer, P., Thompson, R.I. and Daughtry, K.L. 2002: North American margin origin of Quesnel terrane strata in the southern Canadian Cordillera: inferences from geochemical and Nd isotopic characteristics of Triassic metasedimentary rocks; Geological Society of America Bulletin, v. 114, p. 462–475.

Wall, G.R.T. and Jenkyns, H.C. 2004: The age, origin and tectonic significance of Mesozoic sediment-filled fissures in the Mendip Hills (SW England): implications for extension models and Jurassic sea-level curve; Geological Magazine, v. 141, p. 471–504.

Weber, W. 1969: Project Pioneer; *in* Summary of Geological Fieldwork 1969, Manitoba Mines and Natural Resources, Mines Branch, Geological Paper 4/69, p. 102–106.

Weber, W. 1971a: Geology of the Long Lake–Gem Lake area, southeastern Manitoba; *in* Geology and Geophysics of the Rice Lake Region, Southeastern Manitoba (Project Pioneer), W.D. McRitchie and W. Weber (ed.), Manitoba Department of Mines and Natural Resources, Mines Branch, Publication 71-1, p. 63–106.

Weber, W. 1971b: Geology of the Wanipigow River–Manigotagan River region; *in* Geology and Geophysics of the Rice Lake Region, Southeastern Manitoba (Project Pioneer), W.D. McRitchie and W. Weber (ed.), Manitoba Department of Mines and Natural Resources, Mines Branch, Publication 71-1, Map 71-1/4.

Weber, W. 1987: Geological investigations in the Lily Lake area; *in* Report of Field Activities 1987, Manitoba Energy and Mines, Minerals Division, p. 108–109.

Wentworth, C.K. 1922: A scale of grade and class terms for clastic sediments; The Journal of Geology, v. 30, p. 377–392.

Whalen, J.B., Percival, J.A., McNicoll, V.J. and Longstaffe, F.J. 2003: Intra-oceanic production of continental crust in a Th-depleted ca. 3.0 Ga arc complex, western Superior Province, Canada; Contributions to Mineralogy and Petrology, v. 146, p. 78–99.

White, J.D.L. and Houghton, B.F. 2006: Primary volcaniclastic rocks; Geology, v. 34, p. 677–680.

Whiting, B.H. 1989: The lithology and lithogeochemistry of the San Antonio gold mine, Bissett, Manitoba; M.Sc. thesis, University of British Columbia, Vancouver, British Columbia, 250 p.

Winchester, J.A. and Floyd, P.A. 1977: Geochemical discrimination of different magma series and their differentiation products using immobile elements; Chemical Geology, v. 20, p. 325–343.

Williams, H.R., Stott, G.M., Thurston, P.C., Sutcliffe, R.H., Bennett, G., Easton, R.M. and Armstrong, D.K. 1992: Tectonic evolution of Ontario: summary and synthesis; *in* Geology of Ontario, P.C. Thurston, H.R. Williams, R.H. Sutcliffe and G.M. Stott (ed.), Ontario Geological Survey, Special Volume 4, Part 2, p. 1255–1332.

Wood, D.A. 1980: The application of a Th-Hf-Ta diagram to problems of tectonomagmatic classification and to establishing the nature of crustal contamination of basaltic lavas of the British Tertiary Volcanic Province; Earth and Planetary Science Letters, v. 50, p. 11–30.

Wright, J.F. 1923: Rice Lake map-area, southeastern Manitoba; Canada Department of Mines, Geological Survey, Summary Report, 1922, Part C, p. 45–88.

Wright, J.F. 1932: Geology and mineral deposits of a part of southeastern Manitoba; Canada Department of Mines, Geological Survey, Memoir 169, 150 p.